# Form-Finding structures for spatial structures applications

**Politecnico di Torino**

Architecture for Sustainability

**Supervisor:**

Assoc. Prof. Amedeo Domenico Manuello Bertetto

**Co-Advisers:**

Visiting Prof. Valentina Sumini

Assoc. Prof. Matteo Pavese

**Author:**

Michele Barone S314994

July 2026



# Summary


**Acknowledgements** ..... 4

**Introduction** ..... 6

**CHAPTER 1 – The Moon** ..... 8

**1.1 Overview of the Moon** ..... 8

**1.2 Origin and evolution** ..... 12

**1.3 Geology and regolith** ..... 17

**1.4 Atmosphere** ..... 23

**1.5 Water resources** ..... 28

**1.6 Lunar radiation environment** ..... 33

**CHAPTER 2 – Lunar Exploration and Extraterrestrial Habitats** ..... 40

**2.1 The history and evolution of Lunar exploration** ..... 40

**2.2 Apollo missions** ..... 41

**2.3 Other relevant missions** ..... 44

**2.4 Contemporary Lunar exploration and future perspectives** ..... 48

**2.5 Artemis missions** ..... 53

**2.6 Extraterrestrial habitats** ..... 56

**CHAPTER 3 – Nature Inspires** ..... 67

**3.1 Biomimetics** ..... 67

**3.2 Biomimetics in Architecture and Engineering** ..... 74

**3.3 Inspiration** ..... 79

**CHAPTER 4 – The process** ..... 89

**4.1 Shell Structures** ..... 89

**4.2 Form-finding** ..... 110

**4.3 The first form-finding process** ..... 121

**4.4 The second form-finding process** ..... 125

**CHAPTER 5 – Resource-Based Design Strategies** ..... 134

**5.1 In-Situ Resource Utilization (ISRU)** ..... 134

**5.2 Construction material** ..... 140

**5.3 Preliminary experimental campaign** ..... 145

**5.4 Radiation shielding and life-support system** ..... 150

**CHAPTER 6 – Structural analysis** ..... 159

**6.1 Load definition** ..... 159

**6.2 Cross-section optimization and geometric smoothing** ..... 163

**6.3 Results of the structural analysis** ..... 164

**Conclusions** ..... 179
**Bibliography** ..... 184

## Acknowledgements

I would like to express my sincere gratitude to Professor Amedeo Domenico Manuello Bertetto, from the Department of Structural, Building and Geotechnical Engineering (DISEG) at Politecnico di Torino, who served as the principal supervisor of this thesis. He first proposed the research topic and provided the conceptual framework to develop this research. His guidance was particularly important during the initial stages of the thesis, helping me define its direction and establish a coherent methodological approach. His contribution was especially valuable in relation to the engineering principles underlying the project, the structural interpretation of the proposed system and the development of the form-finding process.

I am deeply grateful to Professor Valentina Sumini, Visiting Professor at Politecnico di Torino and affiliated with the Space Exploration Initiative at the MIT Media Lab, whose expertise was fundamental in shaping the space architecture aspects of this research. Her guidance contributed significantly to framing the project within the broader context of extraterrestrial habitat design. She also provided essential support in the development of the parametric and computational workflow, particularly in the use of Grasshopper and of tools such as Kangaroo, Raven, and Karamba3D.

I would also like to sincerely thank Professor Matteo Pavese, from the Department of Applied Science and Technology (DISAT) at Politecnico di Torino, for his guidance concerning lunar regolith and its possible use as a construction material. His support was essential throughout the experimental campaign, during which he introduced me to the procedures required for preparing the specimens and carrying out the mechanical tests. This experience allowed me to gain a clearer understanding of the practical and methodological challenges involved in material experimentation and in the mechanical characterization of regolith-based compounds.

More broadly, I would like to thank all the professors who contributed to the development of this research through their knowledge, advice, and availability. I am also grateful to Politecnico di Torino for providing access to the spaces, equipment, and facilities required to conduct the experimental activities, including the laboratories used for specimen preparation and mechanical testing. These resources allowed me to carry out a preliminary experimental study alongside the theoretical, computational and design aspects developed in this research.

*Declaration on the Use of Artificial Intelligence*

Artificial intelligence tools were used during the preparation of this thesis as supplementary instruments supporting the revision, translation, visual communication, and organization of the document.

In particular, AI-assisted tools were employed to identify spelling mistakes, typographical errors, omissions, and minor grammatical inconsistencies. They also supported the translation of parts of the text from Italian into English. To improve linguistic reliability and avoid dependence on a single system, the proposed translations were frequently compared across different tools, including *ChatGPT* and *Gemini*, and subsequently checked using language-support platforms such as *Reverso*, *Grammarly* and other online dictionaries.

AI tools were also used to explore synonyms and alternative expressions, mainly to reduce unnecessary lexical repetition and improve the fluency of the text. These suggestions were

generally cross-checked through multiple AI systems and online dictionaries before being incorporated into the final document.

Within the visual development of the thesis, generative AI was employed for the production of selected rendered images and for the graphic enhancement, refinement, or quality improvement of other visual materials. These images were used for illustrative and communicative purposes and should not be interpreted as experimental evidence or as substitutes for the computational and structural models developed during the research.

Artificial intelligence also assisted in the organization and generation of selected summary tables derived from data processed within the thesis. This does not apply to tables reproduced or adapted directly from external sources, which are identified and cited accordingly.

AI was also used as a technical support tool during the development of the computational workflow. It served primarily as an interactive reference for understanding the operation of software and plug-ins such as Grasshopper, Kangaroo, and Karamba3D, as well as for diagnosing errors and identifying possible solutions when problems arose in the workflow. Raven, in particular, was used mainly to obtain guidance on troubleshooting and on the interpretation of specific components and operations. Only on limited occasions it was used to suggest the initial setup of individual workflow steps, which were subsequently tested, revised, and validated.

Finally, AI-supported procedures were used as an additional cross-check for bibliographic information, references, and the correspondence between citations and bibliography entries. However, these checks were verified against the original publications and official sources.

All suggestions and outputs produced through these tools were critically reviewed, selected, modified, or rejected during the review of the thesis. The research questions, scientific interpretation, design methodology, computational workflow, structural analyses, conclusions, and overall intellectual responsibility for the thesis remain entirely those of the author.

## Introduction

This thesis originates from an architectural background while intentionally extending toward a more interdisciplinary approach. It provided an opportunity to explore the emerging field of space architecture, which is predominantly shaped by engineering, aerospace, structural and material-science perspectives. Adopting an interdisciplinary approach, the research investigates how architectural design can contribute to this domain by bringing together geometrical, structural, material, technological and environmental considerations within the same design process.

The development of sustained human presence on the Moon requires habitats capable of ensuring safety, habitability, and reduced dependence on materials transported from Earth. Among the principal design challenges is the containment of internal pressure in an external near-vacuum environment. This condition generates significant tensile stresses, whereas lunar regolith, considered one of the main resources available for in-situ construction, is expected to exhibit predominantly ceramic-like and quasi-brittle behavior, generally more suitable for compression than for tension.

Research on lunar habitats has extensively investigated pressure vessels, inflatable structures, regolith-based construction, radiation protection, biomimetic design, and computational form-finding. These topics, however, are often addressed separately. A gap therefore remains in the development of integrated design methods capable of relating pressure-generated geometry, structural differentiation, local material use, and environmental performance within a single architectural system.

Starting from this gap, the research addresses the following question:

How can a bioinspired and materially differentiated shell contribute to the design of a pressurized lunar habitat while reducing dependence on materials transported from Earth?

The main objective is to develop a preliminary design methodology in which internal pressure is considered not only as a load to be resisted, but also as a parameter capable of generating and organizing architectural form. The study investigates whether a lobed shell geometry can produce a recognizable distribution of structural demand, support the localized use of reinforcement, and generate an interstitial space capable of accommodating complementary protective and life-support functions.

The research adopts the cellular organization of Arabidopsis thaliana as a biological reference. The intention is not to reproduce its morphology literally, but to translate the relationship among internal pressure, resistant cell walls, shared interfaces, and differentiated material organization into an architectural and structural strategy.

The methodology combines literature review, research through design, computational form-finding, preliminary structural analysis, and experimental investigation. The environmental and operational conditions of lunar habitation are first defined, followed by the study of biomimetics, plant-cell mechanics, shell structures, and form-finding methods. These principles are subsequently translated into a parametric workflow developed in Grasshopper. The material component is addressed through the study of regolith-based construction and through a preliminary experimental campaign intended to establish a repeatable protocol for future testing of extraterrestrial simulants.

The research is situated at a preliminary conceptual and methodological stage. It does not present a fully engineered lunar habitat or a construction-ready structural system. The structural analyses are based on simplified loading, restraint, and material assumptions, while the properties of the final regolith-based compound still require experimental characterization. Construction processes, airtightness, foundations, thermal actions, instability phenomena and the complete interaction between the two shells remain outside the present scope. The results must therefore be interpreted as a basis for subsequent investigation rather than as a definitive structural validation.

The thesis is organized into six chapters. Chapter 1 defines the lunar environmental and geological context. Chapter 2 examines the evolution of lunar exploration and the principal types of extraterrestrial habitats. Chapter 3 introduces biomimetics and the biological reference adopted in the research. Chapter 4 presents the theoretical and computational development of the shell geometry. Chapter 5 investigates resource-based construction strategies, the preliminary experimental campaign, and the multifunctional role of the interstitial layer. Chapter 6 presents the structural analysis and the evaluation of the proposed system. The Conclusions summarize the contribution of the research, its limitations, and the directions for future development.

# CHAPTER 1 – The Moon

## 1.1 Overview of the Moon

The Moon is Earth's only natural satellite and is the celestial body closest to our planet, as well as one of the most extensively studied objects in the Solar System (Vidmachenko, 2026; Burke, 2026). Its scientific importance derives from the fact that the lunar surface, lacking a dense atmosphere, a hydrosphere, and erosional processes comparable to those occurring on Earth, preserves extremely ancient traces of the history of the inner Solar System (Vidmachenko, 2026b)[1]. Unlike Earth, which is continuously reshaped by plate tectonics, erosion, and biological activity, the Moon retains on its surface the effects of meteoritic bombardment, space weathering, and ancient volcanic activity (Vidmachenko, 2026; Vidmachenko, 2026b). For this reason, the study of the Moon makes it possible not only to reconstruct its evolution, but also to gain a better understanding of the earliest stages in the formation of Earth and the other terrestrial planets (Vidmachenko, 2026).

From a morphological and physical standpoint, the Moon is a rocky body of approximately spherical shape, with a mean radius of about 1,737 km. Its diameter is approximately 3,474 km, about one quarter of that of Earth, a characteristic that makes it a relatively large satellite in relation to the planet around which it orbits (Jaumann, et al., 2012; Burke, 2026; Vidmachenko, 2026). The Moon's total surface area is approximately 38 million $km^2$, corresponding to roughly one fourteenth of Earth's surface area (Vidmachenko, 2026; Burke, 2026). In comparative terms, the Moon is the fifth largest natural satellite in the Solar System and, in relation to the mass of its host planet, represents a particularly significant case among planet–satellite systems (Jaumann, et al., 2012; Sossi, et al., 2025).

The Moon's mass is approximately $7.3477 \times 10^{22}$ kg, corresponding to about 1.2% of Earth's mass, or approximately 1/81 of it (Jaumann, et al., 2012; Sossi, et al., 2025; Burke, 2026; Vidmachenko, 2026). The Moon's mean density is approximately 3.34 $g/cm^3$, lower than Earth's mean density of about 5.51 $g/cm^3$, but comparable to that of the Earth's crust, which is approximately 3.35 $g/cm^3$. This relatively low density suggests a composition dominated by silicate materials and a lower abundance of iron than on Earth (Sossi, et al., 2025; Burke, 2026; Vidmachenko, 2026). This configuration is consistent with the presence of a relatively small metallic core, estimated to have a radius of approximately 300 to 400 km, whose mass would represent only 1–4% of the Moon's total mass. Furthermore, the value of its moment of inertia, which is very close to that of a homogeneous sphere, indicates that its mass is distributed in an approximately uniform manner and that the concentration of dense material within the core is limited compared with Earth (Sossi, et al., 2025). The lower density of the Moon compared with Earth also constitutes one of the arguments supporting the giant impact hypothesis, according to which the Moon formed predominantly from lighter materials originating from the mantle of the proto-Earth and of the impacting body (Vidmachenko, 2026). The Moon's surface gravity is approximately 1.62 $m/s^2$, or about one sixth of Earth's gravity (Jaumann, et al., 2012; Burke, 2026; Vidmachenko, 2026). This reduced gravitational acceleration is a direct consequence of the smaller size and lower mass of the lunar body (Burke, 2026). Low gravity affects surface processes, since materials ejected by impacts can be dispersed over greater distances than on Earth, while volcanic landforms may assume different morphologies (Vidmachenko, 2026). The Moon's escape velocity, the minimum velocity required for an object to escape the Moon's gravitational attraction, is approximately 2.38 km/s, far lower than Earth's value of 11.2 km/s.

[1] *The citation refers to the source: Physical characteristics and relief of the surface of the Moon* (Vidmachenko, 2026b).

This condition contributes to the almost complete absence of a stable atmosphere around the Moon (Burke, 2026; Vidmachenko, 2026). The lunar environment is characterized by an extremely rarefied exosphere, with a surface pressure reported to be around $3 \times 10^{-15}$ bar and a very low molecular density. Under such conditions, the gas molecules present near the surface move with almost no mutual collisions, confirming the extremely tenuous nature of the lunar environment (Burke, 2026). The absence of a dense atmosphere directly exposes the surface to cosmic radiation, the solar wind, and the bombardment of meteorites and micrometeorites. Over billions of years, these processes have fragmented and transformed the surface layer of the bedrock, giving rise to the lunar regolith (Vidmachenko, 2026b).

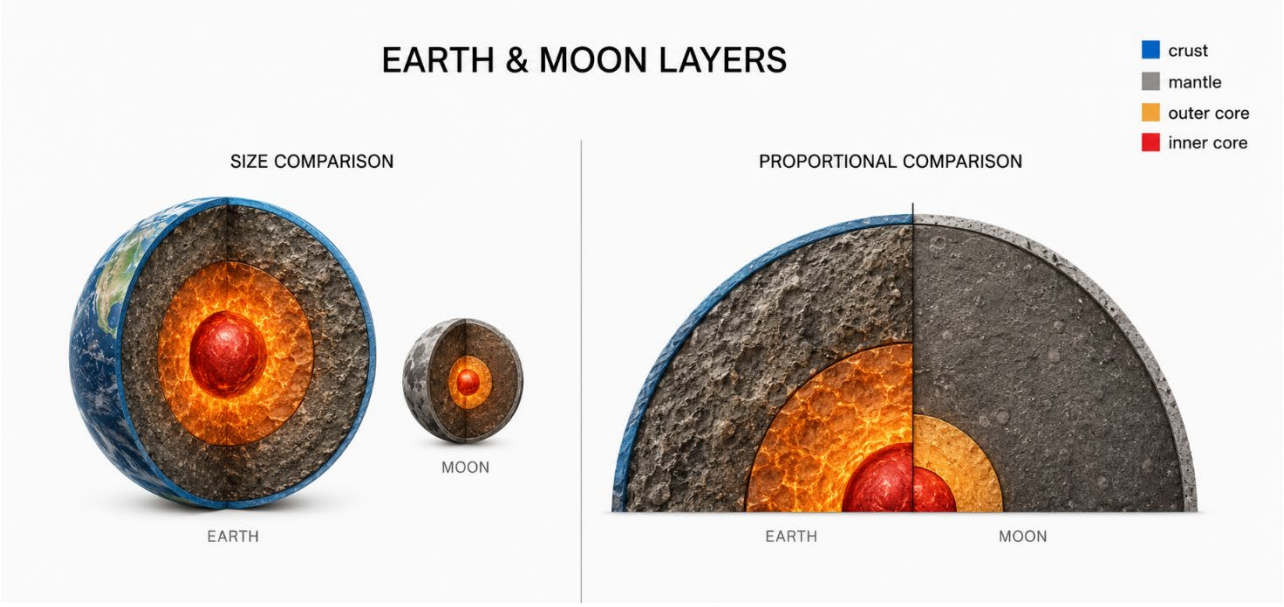



***Figure 1.1**: Schematic comparison of the internal layered structure of the Earth and the Moon. The image illustrates both the difference in size between the two bodies and a proportional comparison of their main internal layers, distinguishing crust, mantle, outer core, and inner core. Adapted from: NASA/Vi Nguyen.*

The Moon orbits the Earth along an elliptical trajectory, with a mean distance between the centers of the two bodies of approximately 384,400 km. Owing to its orbital eccentricity, equal to approximately 0.0549, the Earth–Moon distance varies throughout the orbit (Burke, 2026; Vidmachenko, 2026). Perigee, namely the point in the orbit closest to the Earth, is generally reported at around 363,300 km, whereas apogee, namely the farthest point, is generally reported at around 405,500 km (Vidmachenko, 2026). According to the data provided by Burke, perigee may vary approximately between 356,500 and 370,400 km, while apogee may vary between about 404,000 and 406,700 km (Burke, 2026). This variation in distance affects the apparent size of the Moon in the sky and is one of the factors contributing to terrestrial tides (Burke, 2026; Vidmachenko, 2026).

The Earth–Moon system may be interpreted as a gravitational system in which both bodies orbit around a common center of mass, known as the barycenter. This point is located within the Earth, approximately 4,700 km from its center, and serves as the dynamic reference point for the mutual motion of the two bodies (Burke, 2026). The relatively high mass of the Moon in relation to that of the Earth makes the Earth–Moon system distinctive compared with most planet–satellite systems in the Solar System (Jaumann, et al., 2012; Burke, 2026). Tidal

interactions between the Earth and the Moon also cause the satellite to recede gradually from the planet, at an estimated rate of approximately 3.8 cm per year. The conservation of the system's angular momentum implies that the slowing of the Earth's rotation is accompanied by the progressive increase in the lunar distance and in the duration of the lunar month (Burke, 2026).

The Moon's sidereal orbital period, namely the time required to complete one full orbit around the Earth relative to the fixed stars, is approximately 27.3 Earth days. Its synodic period, namely the time interval between two equivalent lunar phases, such as two successive full moons, is instead approximately 29.5 days (Jaumann, et al., 2012; Burke, 2026; Vidmachenko, 2026). The difference between the sidereal and synodic periods results from the fact that, while the Moon orbits the Earth, the Earth–Moon system itself moves around the Sun, thereby modifying the illumination geometry observed from the Earth (Burke, 2026; Vidmachenko, 2026).

The Moon's rotation is synchronous with its orbital motion, as it rotates about its own axis in the same interval of time required to complete one revolution around the Earth (Jaumann, et al., 2012; Burke, 2026; Vidmachenko, 2026). This condition, known as t*idal locking* or *tidal capture*, is the result of the prolonged action of tidal forces between the Earth and the Moon (Burke, 2026; Vidmachenko, 2026). Consequently, the Moon always presents the same hemisphere toward the Earth (Jaumann, et al., 2012; Vidmachenko, 2026). However, owing to libration[2], more than 59% of the lunar surface can be observed from the Earth over time (Burke, 2026). The lunar orbit is inclined by approximately 5.145° with respect to the plane of the ecliptic, namely the plane of the Earth's orbit around the Sun. The inclination of the orbit with respect to the plane of the Earth's equator varies between 18.28° and 28.58°, while the Moon's rotational axis is inclined by approximately 6.68° with respect to the plane of its orbit (Vidmachenko, 2026). This orbital inclination explains why solar and lunar eclipses do not occur at every new moon or every full moon, but only when the Moon crosses the plane of the ecliptic in a favorable configuration (Burke, 2026; Vidmachenko, 2026). Lunar phases, by contrast, result from the changing geometry between the Sun, the Earth, and the Moon, which determines the illuminated portion of the lunar disc visible from the Earth (Jaumann, et al., 2012; Burke, 2026). The Moon has an overall low reflectivity, with an albedo of approximately 0.11–0.12. This means that the lunar surface reflects only 11–12% of the incident solar radiation. Despite this low reflectivity, the Moon appears as the brightest object in the night sky after the Sun, owing to its proximity to the Earth (Vidmachenko, 2026b). The progressive darkening of the surface is associated with space weathering processes, produced by the action of the solar wind and micrometeoritic bombardment on rocks and regolith (Vidmachenko, 2026; Vidmachenko, 2026b).

The lunar thermal environment is characterized by extreme temperature variations, due to the near absence of an atmosphere and the slow alternation between solar illumination and darkness (Burke, 2026; Vidmachenko, 2026). At the equator, during the lunar day, temperatures can reach approximately +120/+130 °C, while during the long lunar night they can fall to approximately −160/−170 °C (Vidmachenko, 2026). Other data indicate a mean surface temperature of approximately 380 K during the day, corresponding to 107 °C, and approximately 120 K during the night, corresponding to −153 °C. Extreme temperatures may range from approximately 396 K, namely 123 °C, to approximately 40 K, namely −233 °C (Burke, 2026). In

[2] *Phenomenon resulting from the Moon's rotational and orbital motions, whereby, to an observer on Earth, the Moon does not always show exactly the same hemisphere. The portion of the Moon visible from the Earth is slightly more than half (circa 59/100) of its total surface area* (Treccani, n.d.).

permanently shadowed regions near the poles, temperatures may fall to approximately −240 °C, creating cold traps potentially capable of preserving volatile substances (Vidmachenko, 2026b).

The Moon does not possess a global magnetic field comparable to that of the Earth, although certain lunar rocks and samples display weak residual magnetism (Burke, 2026; Vidmachenko, 2026b). This residual magnetism suggests that, during the early stages of its history, the Moon may have possessed an ancient magnetic field, which subsequently disappeared (Vidmachenko, 2026b). At present, lunar internal activity appears to be very limited, as indicated by weak seismic activity and low heat flow, averaging approximately 29 $mW/m^2$ compared with 63 $mW/m^2$ on Earth (Burke, 2026). Nevertheless, the presence of moonquakes indicates that the Moon is not a completely static body but continues to undergo slow processes of contraction and crustal adjustment (Vidmachenko, 2026b).

Overall, the Moon may be interpreted as a celestial body of limited size compared with the Earth, yet of exceptional scientific value for understanding planetary evolution (Jaumann, et al., 2012; Sossi, et al., 2025; Vidmachenko, 2026). The combination of low gravity, absence of a dense atmosphere, extreme temperature variations, a regolith-covered surface, and the preservation of ancient morphologies makes the Moon a privileged geological archive of the history of the inner Solar System (Vidmachenko, 2026; Vidmachenko, 2026b). Current knowledge of the satellite derives from the integration of telescopic observations, orbital missions, data collected *in situ*, seismic experiments, and analyses of samples returned by the Apollo, Luna, and Chang'e missions (Jaumann, et al., 2012; Vidmachenko, 2026b). For a thesis focused on lunar exploration and habitat design, these characteristics constitute the environmental and geological framework from which the principal design conditions arise (Vidmachenko, 2026b).




***Figure 1.2**: The Moon's near side and far side. Source: NASA LRO / Jatan Mehta.*

***Table 1.1:*** *Main physical, orbital, and environmental parameters of the Moon.*

| Parameter | Value |
|---|---|
| Mean radius | approximately 1,737–1,737.4 km |
| Diameter | approximately 3,474–3,475 km |
| Surface area | approximately 37.9–38 million $km^2$ |
| Mass | $7.3477 \times 10^{22}$ kg |
| Mean density | approximately 3.34–3.346 $g/cm^3$ |
| Surface gravity | approximately 1.62–1.622 $m/s^2$ |
| Escape velocity | approximately 2.38 km/s |
| Mean distance from the Earth | approximately 384,400 km |
| Orbital eccentricity | approximately 0.0549 |
| Mean perigee | approximately 363,300 km |
| Mean apogee | approximately 405,500 km |
| Sidereal period | approximately 27.3 days |
| Synodic period | approximately 29.5 days |
| Rotation | synchronous, approximately 27.3 days |
| Orbital inclination with respect to the ecliptic | approximately 5.145° |
| Bond albedo | approximately 0.11 |
| Geometric albedo | approximately 0.12 |
| Extreme surface temperature | approximately from +120/+130 °C to −160/−170 °C |
| Atmosphere | extremely tenuous exosphere / near-vacuum |
| Atmospheric pressure | $3 \times 10^{-15}$ bar |
| Global magnetic field | absent, with weak local residual magnetism |

*Adapted from:* (Jaumann, et al., 2012; Sossi, et al., 2025; Burke, 2026; Vidmachenko, 2026; Vidmachenko, 2026b).

Rather than representing only a list of data, these parameters define the environmental background that any lunar habitat design must take into account. Conditions such as reduced gravity, thermal fluctuations, radiation exposure and many others directly influence the strategies required to support a stable human presence on the Moon.

## 1.2 Origin and evolution

The Moon constitutes a geological archive of exceptional importance for understanding the origin and evolution of the Earth–Moon system, as it preserves evidence of planetary differentiation processes and the formation of a magma ocean that, on Earth and on other bodies characterized by greater geological activity, have been largely erased or profoundly reworked over time. Its exploration therefore makes it possible not only to reconstruct the evolutionary history of the satellite, but also to obtain essential geochemical and geophysical constraints for interpreting the earliest stages of Earth's evolution and, more broadly, those of the rocky planets of the inner Solar System (Crawford & Joy, 2014). Understanding the origin of the Moon plays a fundamental role in planetary science, since it enables investigation of the conditions that characterized the earliest stages of the Earth–Moon system and reconstruction of the thermal, magmatic, and geological processes that subsequently shaped its evolution (Jaumann, et al., 2012).

Scientific interest in the origin of the Moon predates the era of space missions and has its roots in astronomical observations and dynamic analyses progressively developed from the Renaissance onwards and consolidated between the seventeenth, eighteenth, and nineteenth

centuries (Burke, 2026). Observations accumulated over time have shown that, as a result of tidal interactions, the rotation of both the Earth and the Moon is gradually slowing, while the distance between the two bodies is progressively increasing (Burke, 2026; Vogel, 2026). The Moon is currently receding from the Earth at a rate of approximately 3.8 cm per year, a value measured by means of the reflectors installed on the lunar surface during the *Apollo* missions. This evidence indicates that, during the early stages of their evolution, the Earth and the Moon must have been in a much closer configuration and that the rotation of the primordial Earth must have been significantly faster than it is today. Consequently, any model concerning the formation of the Moon must be capable of explaining not only the composition of the satellite, but also its current distance from the Earth, the progressive variation of its orbit, its orbital inclination, and the tidal evolution of the Earth–Moon system over billions of years (Vogel, 2026).

Prior to the acquisition of data and samples from the Apollo program, the principal hypotheses formulated to explain the origin of the Moon could be traced back to three models: co-accretion, fission, and gravitational capture. The co-accretion model proposed that the Earth and the Moon formed simultaneously, within the same region of the solar nebula, as components of a double planetary system. However, this interpretation cannot satisfactorily explain either the high angular momentum of the Earth–Moon system or the different densities of the two bodies. The fission hypothesis instead proposed that the Moon was expelled from a rapidly rotating proto-Earth, but this scenario is not compatible with the observed orbital dynamics and would require unrealistically high tidal forces to separate from the Earth enough material to form the satellite. Finally, the gravitational capture model suggested that the Moon formed elsewhere in the Solar System and was subsequently captured by the Earth's gravitational field (Jaumann, et al., 2012; Burke, 2026). This hypothesis presents significant limitations, since it would imply a cold, relatively undifferentiated Moon that was chemically similar to chondritic meteorites, whereas analyses of the samples collected by the Apollo and Luna missions demonstrated that the satellite is not a primitive body and cannot be regarded as the source of chondrites (Jaumann, et al., 2012). Furthermore, the celestial-mechanical conditions required to slow down a passing body and insert it permanently into Earth orbit are highly improbable, further weakening the capture model (Burke, 2026).

During the twentieth century, the expansion of knowledge concerning the Moon introduced increasingly stringent constraints for the evaluation of the various formation theories. The Moon's lower density compared with that of the Earth, together with its relatively iron-poor composition, highlighted the difficulty of attributing the two bodies to a simple common origin without subsequent transformations or compositional separation (Burke, 2026). Indeed, among the principal constraints that a model of lunar formation must explain are the Moon's depletion in metallic iron, the small size of its core, its scarcity of volatile elements, and the high angular momentum of the Earth–Moon system (Jaumann, et al., 2012). These aspects are compounded by the question of the chemical and isotopic composition of lunar and terrestrial materials, whose comparison represents one of the fundamental tools for reconstructing the origin of the satellite. Although the overall composition of the silicate Earth is relatively well known through the study of mantle xenoliths and the modeling of lavas produced by partial melting, the bulk composition of the silicate Moon remains far less constrained, partly because no direct samples of the lunar mantle have yet been identified and current reconstructions are based on a limited set of samples obtained from the Apollo and Luna missions (Crawford & Joy, 2014).

In light of this evidence, the model currently most widely accepted for explaining the origin of the Moon is the giant impact hypothesis, which became established particularly from the 1980s onwards. According to this interpretation, the Moon formed following the collision between the proto-Earth and a planetary body comparable in size to Mars, commonly referred to as *Theia*. The event would have occurred during the earliest stages of the history of the Solar System, approximately 4.5 billion years ago according to the reconstruction proposed by NASA, or shortly after the formation of the proto-Earth from the solar nebula, dated to around 4.6 billion years ago according to other reconstructions (Burke, 2026; Vogel, 2026). Dating of lunar samples also indicates that the Moon may have formed approximately 60 million years after the beginning of the formation of the Solar System, providing an important chronological reference for situating the impact within primordial planetary evolution (Vogel, 2026).

In the giant impact scenario, both the proto-Earth and Theia were already differentiated into metallic cores and rocky mantles. During the collision, the denser core material was largely retained by Earth, while debris from the outer layers of both bodies was ejected into orbit and later accreted to form the proto-Moon. This mantle-derived origin helps explain the Moon's relative depletion in iron and siderophile elements. (Jaumann, et al., 2012; Burke, 2026). The Apollo missions were crucial in assessing this model, returning 382 kg of lunar samples that transformed the understanding of the Moon's origin. Their analysis revealed strong chemical and isotopic similarities between lunar and terrestrial rocks, suggesting a direct material link between the Moon and the early Earth. The scarcity of volatile elements in the samples also supports formation through an extremely high-energy event. The distribution of iron also supports the giant impact hypothesis. Earth's core accounts for about 30% of the planet's mass, whereas the lunar core represents only 1.6–1.8% of the Moon's mass. This difference suggests that most of the denser metallic material remained within Earth, while the debris that formed the Moon was relatively poor in iron. The combination of isotopic similarity between terrestrial and lunar rocks, the scarcity of volatile elements, and the small size of the lunar core therefore is a fundamental body of evidence for reconstructing the origin of the Moon (Vogel, 2026).

The energy released by the collision would have generated extremely intense heating and large-scale melting of the materials involved, leading to the formation of a deep and persistent lunar magma ocean, probably maintained for tens or hundreds of millions of years (Jaumann, et al., 2012; Vogel, 2026). Evidence from the Apollo samples suggests that the Moon's rapid accretion produced a vast magma ocean. As it cooled, a thin crust formed at the surface, while denser minerals such as olivine and pyroxene crystallized and sank, gradually contributing to the formation of the lunar mantle (Crawford & Joy, 2014).

At a more advanced stage in the evolution of the magma ocean, after approximately 80% of the molten material had already crystallized, plagioclase would have become a dominant crystallizing phase, initiating the processes associated with the formation of the lunar feldspathic crust (Crawford & Joy, 2014). During this phase, the segregation of crystals from the melt would have favored the development of a low-density primitive crust rich in plagioclase (Jaumann, et al., 2012; Burke, 2026). The widespread presence of anorthosite on the lunar surface reinforces this interpretation, since this igneous rock forms through the crystallization of magma and, owing to its lower density, tends to rise toward the surface, contributing to the construction of the earliest lunar crust (Vogel, 2026b).

Despite the central role attributed to the magma ocean, the formation of the lunar crust remains a subject of debate and may be interpreted through different evolutionary models.

According to the traditional model, the plagioclase formed within the magma ocean would have risen toward the surface, creating a global layer of anorthosite. A second model hypothesizes that plagioclase rose during several phases, contributing to the formation of the crust or modifying a pre-existing crust. The third model attributes a significant role to primordial bombardment, hypothesizing that major impacts generated regional magma seas that subsequently differentiated, producing crustal terrains characterized by different compositions (Crawford & Joy, 2014).

The interpretation of lunar crust formation is affected by the limited representativeness of the available samples. Those returned by the Apollo missions largely originate from the Procellarum KREEP Terrain, a geochemically anomalous region, whereas lunar meteorites reveal greater compositional heterogeneity than the highland anorthosites of the near side. The lunar crust may therefore derive from differentiated evolutionary processes in different regions, which cannot be traced back to a single uniform model of a global magma ocean (Crawford & Joy, 2014).

Recent geochronological evidence suggests that lunar crust formation was more complex than traditional models proposed. The overlap between crust formation and later magmatic activity around 4.3–4.2 Ga, together with the presence of distinct geochemical source regions, indicates that the crust may not have formed through a single global flotation event. Instead, it may have developed through a combination of regional magma oceans, successive magmatic episodes and differentiated impact melt sheets (Crawford & Joy, 2014). The complexity of crustal formation is compounded by the marked differences observable between the near side and the far side of the Moon, with the far-side crust being generally thicker than the near-side crust. The two regions also display differences in geological composition, in the distribution of radioactive elements, and in their respective volcanic histories. These differences constitute one of the unresolved questions in the study of lunar evolution and make it necessary to expand knowledge of regions that are poorly represented by the available samples (Vogel, 2026).

The early lunar surface underwent intense bombardment, followed by a gradual decline in impacts over about 100 million years. Once cooled and solidified, it preserved the major basins created by large impact events, including the Imbrium Basin around 3.9 billion years ago. These depressions were later filled by basaltic lava flows over several hundred million years. The chemical and mineralogical diversity of mare basalts reflects variations in the lunar mantle and different processes of partial melting and magmatic differentiation (Burke, 2026).

Despite being the most consistent model with the available evidence, the giant impact hypothesis still leaves several questions unresolved. Simulations suggest that only a limited proportion of the ejected material contributed to the Moon's formation, requiring the impact to have produced a debris disc significantly more massive than the present Moon. Discrepancies also remain between the low orbital inclination predicted by accretion models and the higher values inferred from orbital reconstructions. Further uncertainties concern the distribution of material within the circumterrestrial disc and the time required for it to evolve before lunar accretion began (Jaumann, et al., 2012).

A more complete understanding of the Moon's origin and early evolution will require new geophysical data and samples from a wider range of well-defined geological contexts. Measurements obtained through seismometers, heat-flow probes and magnetometers could clarify the Moon's initial thermal conditions and the evolution of its magma ocean. Samples from the mantle, the polar regions, the far side and highland areas beyond the Apollo sites

would also help reveal the true compositional and chronological diversity of the lunar crust (Crawford & Joy, 2014). The discrepancies between simulations and orbital reconstructions, the uncertainties relating to accretion efficiency, and the geological differences observed between the near side and the far side also indicate the need for further investigations, new samples, and increasingly detailed numerical models (Jaumann, et al., 2012; Vogel, 2026b).

Overall, the formation of the Moon emerges as the result of a complex sequence of physical, dynamic, and geological processes, for which the giant impact hypothesis currently provides the most convincing explanatory framework. The collision between the proto-Earth and Theia, the formation of a circumterrestrial disc of debris, and the subsequent reaggregation of the proto-Moon explain the satellite's relative depletion in iron and siderophile elements (Jaumann, et al., 2012; Burke, 2026). The isotopic similarity between terrestrial and lunar rocks, the scarcity of volatile elements in the Apollo samples, the small size of the lunar core, and the dynamic evolution of the Earth–Moon system constitute further evidence consistent with this interpretation (Vogel, 2026). The subsequent formation of a magma ocean, the crystallization of mafic cumulates, the development of the mantle, and the progressive formation of an anorthositic crust rich in plagioclase describe the principal stages of the Moon's primordial internal evolution, while leaving open several interpretations concerning the specific processes through which the crust was actually formed. It is precisely the preservation of traces of these processes that makes the Moon an indispensable geological archive for reconstructing its own evolutionary history, that of the Earth–Moon system, and the earliest transformations that affected the rocky planets of the inner Solar System (Crawford & Joy, 2014).

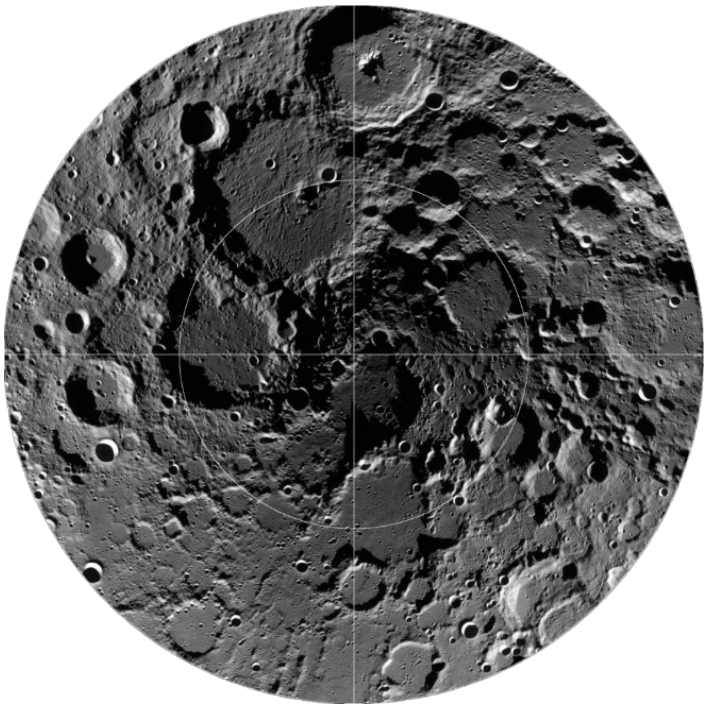


**Figure 1.3**: The lunar north pole, captured by the Lunar Reconnaissance Orbiter Camera, is dappled with craters highlighted in a stark display of sunlight and shadow. Source: NASA/GSFC/Arizona State University.

### 1.3 Geology and regolith

Lunar geology is the result of a long evolution dominated by the satellite's internal differentiation, meteoritic bombardment, basaltic volcanism, and the continuous reworking of surface material. At a macroscopic scale, the surface of the Moon has been shaped primarily by impacts, volcanic phenomena, and tectonic processes, although the latter do not occur through plate tectonics comparable to those of the Earth (Jaumann, et al., 2012). As a first approximation, the lunar surface can be divided into two principal geological units: the highlands, which are older and characterized by lighter tones, and the maria, darker regions occupying large impact basins, particularly on the near side of the Moon. This morphological and compositional distinction constitutes an essential reference both for interpreting the geological evolution of the Moon and for assessing the distribution and potential use of its resources from an ISRU perspective (Crawford, 2015). From the standpoint of its internal structure, the Moon is a differentiated body, composed of crust, mantle, and core, according to a general organization comparable to that of the Earth, although characterized by profoundly different proportions. The lunar crust displays a marked asymmetry between the two hemispheres. According to NASA, the thickness of the crust on the near side is approximately 40 km, whereas on the opposite side it reaches approximately 60 km (Vogel, 2026b)[3].

The lunar crust is predominantly composed of minerals containing oxygen, silicon, magnesium, iron, calcium, and aluminum, together with smaller amounts of titanium, uranium, thorium, potassium, and hydrogen. The color differences observable across the surface reflect significant variations in material composition. Indeed, the lighter highlands are relatively rich in calcium and aluminum, whereas the darker maria contain greater abundances of iron and titanium (Vogel, 2026b). The lunar highlands are generally interpreted as the expression of the Moon's original crust and are composed predominantly of anorthositic rocks, characterized by more than 90% plagioclase feldspar. Lunar plagioclase is calcium-rich, and the dominant mineralogy of the highlands can be approximated to anorthite, $CaAl_2Si_2O_8$. Consequently, these regions are relatively rich in Ca, Al, Si, and O, while containing more limited quantities of Mg and Fe, mainly associated with the presence of minerals such as pyroxene and olivine (Heiken, et al., 1991; Jaumann, et al., 2012). The more reflective highlands also include rocks belonging to the magnesian suite, also characterized by abundant plagioclase (Jaumann, et al., 2012).

The traditional distinction between anorthositic highlands and basaltic maria does not fully reflect the geological complexity of the lunar surface. Data from the *Lunar Prospector* mission identified two main terranes with distinct geological, geochemical and geophysical characteristics: the Feldspathic Highlands Terrane (FHT) and the Procellarum KREEP Terrane (PKT). The FHT covers about 60% of the lunar surface and consists mainly of ancient anorthositic rocks associated with the ferroan anorthosite suite (Jaumann, et al., 2012).

The Procellarum KREEP Terrane is located mainly in the *Oceanus Procellarum* and *Mare Imbrium* regions and is characterized by significantly higher thorium concentrations. This terrane also displays a high abundance of mare basalt flows, whose eruptive activity appears to have extended from at least 4.2 Ga until approximately 1 Ga. The high concentrations of heat-producing elements present in the Procellarum KREEP Terrane are considered a possible cause of the extensive magmatic productivity and prolonged volcanic activity observed in this region. Indeed, the concentration of radioactive elements such as K, U, and Th would have favored the

[3] *The citation refers to the source: Moon Composition & Structure* (Vogel, 2026b).

partial melting of ultramafic mantle materials at depths ranging from 60 to 500 km, producing basaltic magmas and contributing to the greater volcanic activity of the near side of the Moon compared with the far side (Jaumann, et al., 2012).

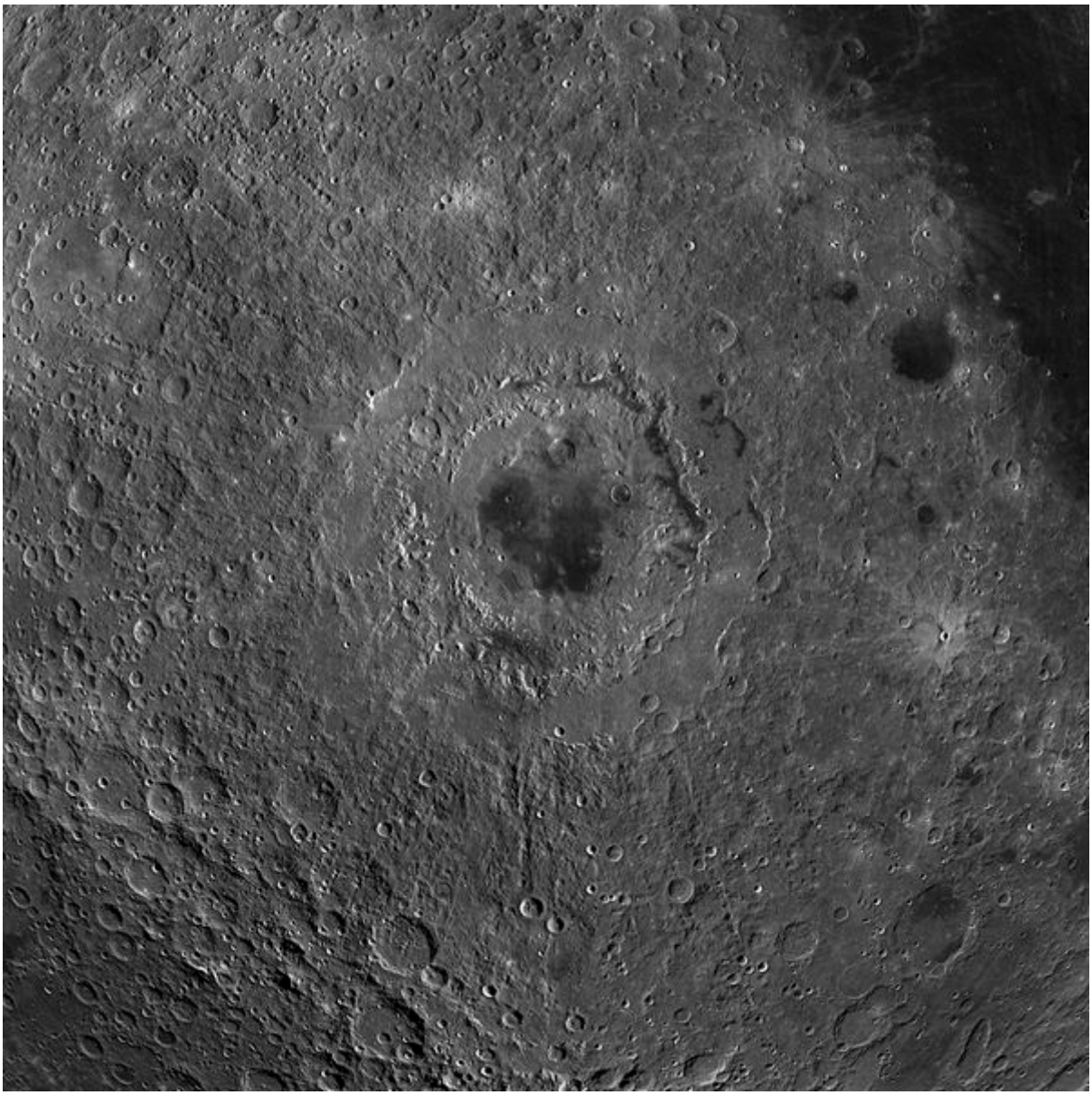


***Figure 1.4**: Orientale Basin is the youngest of the large lunar basins, thought to have formed about 3.8 billion years ago. The distinct outer ring is about 590 miles (950 km) from east-to-west. Source: NASA/GSFC/Arizona State University.*

The lunar maria consist of extensive basaltic lava flows that filled topographically depressed impact basins, reshaping large portions of the surface through lavas characterized by high temperatures and low viscosity. These deposits are concentrated predominantly on the near side of the Moon and cover approximately 17% of the satellite's total surface, although they account for only about 1% of the overall volume of the lunar crust. Approximately 30% of the near-side hemisphere is covered by dark mare deposits, formed through the eruption of large volumes of basaltic lava within impact basins (Jaumann, et al., 2012).

From a mineralogical perspective, lunar mare basalts mainly comprise plagioclase, orthopyroxene, clinopyroxene, olivine, and ilmenite. Compared with highland rocks, they are generally richer in Mg, Fe, and Ti and poorer in Ca and Al, while still retaining a significant presence of plagioclase (Crawford, 2015). Similarly, Jaumann et al. describe mare basalts as materials enriched in FeO and $TiO_2$, depleted in $Al_2O_3$, and characterized by higher $CaO/Al_2O_3$ ratios than highland rocks; from a mineralogical standpoint, they also contain greater quantities of olivine and pyroxene and smaller quantities of plagioclase (Jaumann, et al., 2012).

In addition to the basaltic flows of the maria, a particularly relevant group of surface materials is represented by pyroclastic deposits, interpreted as volcanic ash produced by eruptions occurring in certain mare regions (Heiken, et al., 1991; Gaddis, et al., 2003). Samples collected at the Apollo 15 and Apollo 17 sites show that these deposits may consist of small glass spheres or partially crystallized material, with diameters in the order of tens of micrometers and an essentially basaltic composition. From a resource perspective, pyroclastic deposits are of particular interest because they may contain higher concentrations of volatiles than ordinary regolith, because their glassy component may be more easily decomposed in processes intended for oxygen extraction, and because the material appears potentially more homogeneous than common regolith (Crawford, 2015).

The geological evolution of the lunar surface was strongly shaped by impacts. Both hemispheres preserve large basins, including the *South Pole–Aitken Basin*, the largest known impact structure in the Solar System. During the early period of intense bombardment, major impacts fractured and mixed the crust to depths of several kilometers, producing a widespread layer of debris. After about 3.8–3.9 Ga, smaller impactors became more common and gradually formed the loose, fine-grained and poorly sorted material known as lunar regolith (Jaumann, et al., 2012).

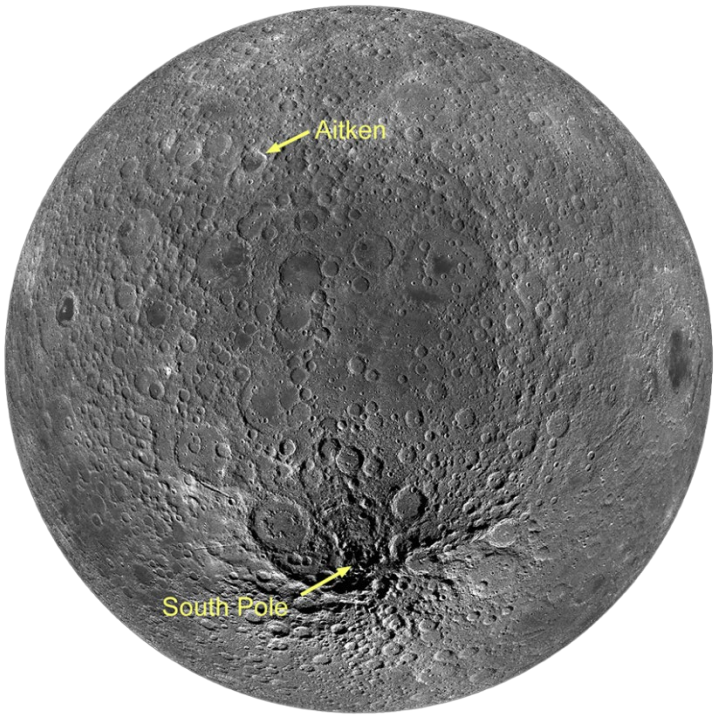



***Figure 1.5**: The Moon's largest impact feature, the South Pole–Aitken basin, is so named because it stretches between Aitken crater and the south pole. Source: NASA/GSFC/Arizona State University.*

Thus, regolith constitutes the unconsolidated surface layer that covers almost the entire Moon and represents the result of billions of years of meteoritic and micrometeoritic impacts, solar irradiation, and space weathering processes *(Jaumann, et al., 2012; Vogel, 2026b)*. The term lunar soil generally refers to the sub-centimeter fraction of the regolith, consisting of the finer material within the unconsolidated surface cover *(Heiken, et al., 1991)*. Similarly, Jaumann uses the expression lunar regolith or lunar soil with reference to the fine-grained fraction, predominantly smaller than 1 cm, of the loose surface material *(Jaumann, et al., 2012)*. According to NASA, regolith may be described as a dusty and rocky substance produced by the continuous bombardment of the lunar surface by meteorites of different sizes and by charged particles originating from the Sun *(Vogel, 2026b)*.

The composition of the regolith largely reflects that of the underlying rocks, thus varying from predominantly basaltic materials in mare regions to predominantly anorthositic materials in highland areas. This local component is supplemented by a meteoritic fraction generally less than or equal to 2% (Jaumann, et al., 2012; Crawford, 2015). Regolith comprises materials derived from the anorthositic crust, extrusive volcanic products of variable composition, materials excavated from depth by impacts, extra-lunar components, meteorites, solar particles, and products generated by the impacts themselves. Its constituent particles include mineral fragments, fragments of original crystalline rocks, breccia fragments, impact and volcanic glasses, agglutinates, and blocks of varying dimensions. Agglutinates are aggregates of smaller particles welded together by glasses produced by micrometeorite impacts and represent a particularly significant component of mature soils (Jaumann, et al., 2012).

The average grain size ranges between 60 and 80 μm (Jaumann, et al., 2012), while, according to NASA sources, the finer particles of lunar dust may be smaller than 10–20 μm and are therefore significantly thinner than the width of a human hair (Vogel, 2026b). These grain-size characteristics are relevant not only to the geological description of the material, but also to understanding its mobility, compaction, interaction with equipment, and possible processing methods.

The thickness of the regolith varies significantly according to the age and geological nature of the surface on which it developed. Crawford indicates that the regolith layer reaches several meters in mare regions and may reach, or perhaps exceed, 10 m in the older highland areas (Crawford, 2015). NASA describes values of a few meters in the younger mare areas, where bedrock may occasionally be exposed, and thicknesses of up to approximately 20 m in the older highland regions (Vogel, 2026b). The analysis reported by Jaumann, obtained through the inversion of the size-frequency distributions of small impact craters, indicates typical values of a few meters in mare regions and almost 10 m in the highlands. A study by Fa and Wieczorek, based on Earth-based radar data, obtained similar results, although radar estimates of regolith thickness are more dependent on the model employed (Jaumann, et al., 2012).

The surface regolith should be distinguished from the deeper megaregolith formed by earlier and larger impacts. Estimates suggest that ejecta deposits extend for several kilometers, while structural disturbance and fracturing may reach depths greater than 10 km and locally approach 25 km. The shallower regolith developed later through the continuous action of smaller impacts, which repeatedly mixed the upper soil layers and brought fresh material to the surface. This process, known as *impact gardening*, is one of the main mechanisms shaping the lunar regolith (Jaumann, et al., 2012).

Although the uppermost centimeters of the lunar regolith are relatively loose and disturbed, the material rapidly becomes denser with increasing depth. In situ relative density of lunar soil is approximately 65% within the upper 15 cm and exceeds 90% below a depth of 30 cm. This variation indicates that the regolith cannot be considered a uniformly loose deposit throughout its thickness but must instead be understood as a granular medium whose density and compaction change significantly with depth. These properties are particularly relevant for operations involving excavation, transport, placement and compaction, since the handling and manipulation of lunar soil would loosen the material and prevent it from being restored to its original undisturbed density (Heiken, et al., 1991).

Regolith also constitutes the primary interface between the Moon and the space environment. From a scientific perspective, it preserves information relating to the interaction of the surface with solar wind particles, galactic cosmic rays, interplanetary dust, meteorites, and materials originating from other regions of the Solar System. Studies conducted on Apollo samples have shown that solar wind particles are effectively implanted within the regolith, enabling the lunar soil to preserve traces of the composition and evolution of the Sun. Regolith may also contain terrestrial meteorites, evidence of the primordial Earth's atmosphere, and records of ancient fluxes of galactic cosmic rays or interstellar dust, thereby constituting a scientific archive that would be difficult to access through other planetary bodies (Crawford & Joy, 2014).

According to Wang et al., lunar regolith consists mainly of mineral grains such as pyroxene, ilmenite, plagioclase and olivine, together with fragments of basalt, breccia and glass. Unlike the generally smoother particles found in terrestrial soils, lunar grains are mostly angular and elongated, with irregular edges and rough surfaces. Their morphology is gradually altered by impacts, abrasion, agglutination, sputtering, thermal fatigue and radiation damage (Wang, et al., 2026).

Finally, regolith is also important as a potential lunar resource. Although the Moon lacks the hydrothermal and biological processes that form many mineral deposits on Earth, its geological history involved extensive melting and magmatic differentiation. Processes such as magma-ocean crystallization, impact melting and mare volcanism may therefore have produced localized concentrations of useful materials, despite the absence of Earth-like geological conditions (Crawford, 2015).



***Figure 1.6**: Astronaut boot prints mark the lunar regolith in this Apollo 15 photograph, taken by astronaut David Scott during a 1971 moonwalk. The grid of black crosses in each Apollo image can be used to calculate distances and heights on the lunar landscape. Source: NASA.*

Within this framework, regolith does not constitute merely a surface cover, but simultaneously serves as a geological archive, the product of prolonged interaction between the Moon and the space environment, and a potential raw material for future in situ resource utilization strategies (Crawford & Joy, 2014; Crawford, 2015; Wang, et al., 2026). Its composition depends on the nature of the local rocky substrate, the presence of meteoritic materials, the impact history, soil maturity, and the space weathering processes that continuously transform its physical and morphological properties. For research focused on the design and construction of lunar habitats, regolith cannot therefore be considered a uniform and undifferentiated material, but must be assessed as a local, stratified, and variable resource, whose properties depend on the geological context and the specific evolutionary history of the site under consideration

(Jaumann, et al., 2012; Vogel, 2026b; Wang, et al., 2026). Understanding lunar geology and the characteristics of regolith therefore represents an essential prerequisite for defining reliable strategies for the extraction, transformation, and construction-oriented use of the materials available on the surface of the Moon (Crawford, 2015; Wang, et al., 2026).

### 1.4 Atmosphere

The traditional image of the Moon as a body entirely devoid of an atmosphere requires scientific clarification, since our satellite does not possess a dense and stratified atmosphere such as that of the Earth, but is nevertheless surrounded by an extremely rarefied gaseous envelope. The difficulty in recognizing this atmosphere derives from the fact that it does not produce evident optical phenomena, such as hazes, clouds, or refraction, which is why the Moon was long considered to be essentially "without an atmosphere". According to Stern, the Moon is enveloped by a tenuous layer of particles, with extremely low density and surface pressure, more comparable to those of a cometary coma than to those of an ordinary planetary atmosphere (Stern, 1999).

NASA confirms this interpretation, emphasizing that the Moon possesses a *"barely perceptible"* atmosphere, profoundly different from that of the Earth and primarily identifiable with its exosphere (Barry, 2026).

The fundamental characteristic of the lunar atmosphere is therefore its exospheric nature, namely the condition whereby its constituent particles are so distant from one another that they travel long distances without colliding with each other. This condition radically distinguishes the Moon from the Earth, where the atmosphere is collisional and air molecules continuously interact with one another, mutually affecting their motion (Barry, 2026). In the lunar case, by contrast, the almost complete absence of collisions makes it possible to consider each chemical species as an almost dynamically autonomous component, characterized by its own cycles of release, migration, adsorption, and loss (Stern, 1999; Barry, 2026).

Indeed, Stern describes the different compositional components of the lunar exosphere as *"independent atmospheres"* occupying the same space, precisely because their weak collisional interaction prevents them from behaving as a single continuous atmospheric fluid (Stern, 1999).

The rarefaction of the lunar exosphere is extreme also in quantitative terms, since NASA indicates that it contains approximately one million billion ($10^{15}$) fewer molecules per cubic centimeter than the Earth's atmosphere. This difference is primarily related to the lower mass of the Moon, which results in a far more limited gravitational capacity to retain gases around the celestial body. This is compounded by the absence of active atmospheric sources comparable to those found on Earth, such as persistent volcanism or geological systems capable of sustaining a dense atmosphere over time (Barry, 2026). The absence of global magnetic protection also contributes to the vulnerability of the lunar environment, since solar wind and energetic particles can interact directly with the surface and with exospheric species (Crawford, 2015; Barry, 2026).

From a planetary science perspective, the Moon is a key example of a surface-bounded exosphere, in which the exobase effectively coincides with the ground. The lunar surface therefore plays a central role in the production, transformation and loss of atmospheric

particles. The Moon's proximity to Earth makes it an ideal laboratory for studying the interaction between rarefied gases, regolith and the space environment (Farrell, et al., 2023).

The composition of the lunar exosphere is dominated by extremely dilute species, including helium, neon, and argon, accompanied by smaller quantities of other elements and molecules. Molecular hydrogen is present only in small fractions but is of considerable scientific interest because hydrogen is one of the chemical components associated with the processes of water formation and transformation on the Moon. Sodium is another minor but extensively studied species, since it possesses a spectral signature that is relatively easy to detect remotely through Earth-based telescopes or orbital instruments (Barry, 2026). Earth-based observations of sodium and potassium, conducted after the Apollo phase, represented an important moment in the resumption of studies on the lunar atmosphere, since they demonstrated that even species present in minimal quantities can be detected and studied through suitable spectroscopic techniques (Stern, 1999).



***Figure 1.7**: Left: Earth as seen by Apollo 8 astronauts circling the Moon (1968). Right: the Moon as seen by astronauts orbiting Earth on the International Space Station (2024). Source: NASA/Vi Nguyen.*

The first direct detections of the lunar atmosphere nevertheless date back to the Apollo era, when instruments placed on the surface and in orbit made it possible to measure neutral and ionized components of the circumlunar environment (Stern, 1999). The CCGE (*Cold Cathode Gage Experiment)* instruments, installed during Apollo 12, 14, and 15 missions, were designed to measure the density of neutral particles and determine the quantity of gas present near the surface (Barry, 2026). These instruments confirmed the presence of an extremely rarefied atmosphere, although the measurements were strongly affected by problems of contamination and outgassing from Apollo equipment (Stern, 1999).

The Apollo 17 mission made a decisive further contribution through LACE, the *Lunar Atmosphere Composition Experiment*, a mass spectrometer designed to identify the chemical composition of the lunar atmosphere (Stern, 1999; Barry, 2026). The data obtained demonstrate that the lunar atmosphere is supplied both by external sources, such as the solar wind, and by internal sources, such as outgassing and the radioactive decay of elements present in the crust (Stern, 1999; Farrell, et al., 2023).

The modern lunar environment is understood as an interaction between rarefied gas, plasma and dust, rather than as a purely neutral exosphere. According to Farrell et al., meteoroid

impacts and incident plasma continuously disturb the surface, releasing atoms and fine particles into circumlunar space. The lunar surface is therefore not inactive but constantly altered at the microscopic scale by processes that reshape the regolith and influence the surrounding environment. The lunar exosphere is sustained by several surface processes, including thermal and photon-stimulated desorption, sputtering, solar-wind interactions and micrometeoroid impacts. Ultraviolet radiation can release volatile elements such as sodium and potassium, while heating of the regolith promotes the desorption of surface-bound species. High-velocity micrometeoroid impacts also vaporize part of the surface, producing ejecta and releasing neutral atoms into the exosphere. Micrometeoroid bombardment is especially significant because the Moon lacks a dense atmosphere capable of shielding its surface. Each impact can eject a mass of material far greater than that of the incoming particle and contributes to regolith gardening, the continuous mixing of the upper soil layers. By exposing fresh material and releasing particles and neutral atoms, these impacts connect the physical evolution of the regolith with the dynamics of the lunar exosphere (Farrell, et al., 2023).

The solar wind also represents a fundamental source of the lunar exospheric environment, since it transports protons, electrons, alpha particles, and ionic species that directly reach the surface (Crawford, 2015; Farrell, et al., 2023). Crawford observes that, since the Moon possesses neither a dense atmosphere nor a global magnetic field, solar wind particles are implanted directly into the lunar regolith. This interaction contributes to the presence of implanted volatiles, including hydrogen and helium, which can accumulate in the regolith over very long periods and subsequently be released through thermal or energetic processes (Crawford, 2015). Farrell further emphasizes that the lunar surface does not behave simply as an absorbing boundary, but as a conversion surface, capable of re-emitting solar hydrogen and helium in different forms and over different characteristic timescales (Farrell, et al., 2023).

The ionized component of the lunar environment largely derives from processes of ionization of neutral species and their subsequent interaction with the electric and magnetic fields of interplanetary space. The SIDE (*Suprathermal Ion Detector Experiment*) instruments of the Apollo missions showed that the lunar ionosphere is directly coupled with the interplanetary electric field, with non-thermal, highly directional, and variable ionic fluxes. The same instruments measured near-surface electric potentials of +5/+10 V on the dayside and negative values ranging from tens to hundreds of volts on the nightside (Stern, 1999). These results indicate that the lunar surface and the environment immediately above it are electrically active, and that the rarefaction of the atmosphere does not imply the absence of plasma–surface phenomena (Stern, 1999; Farrell, et al., 2023).

The lunar atmosphere is controlled not only by its sources, but also by highly efficient loss processes. Stern identifies an overall atmospheric loss rate of approximately 10 g/s, a high value when compared with the extremely low total mass of the lunar atmosphere. This relationship between low mass and continuous loss implies that the abundances of exospheric species are regulated by a dynamic balance between replenishment and removal (Stern, 1999). The principal loss processes include gravitational escape, photoionization, charge exchange, electron-impact ionization, molecular dissociation, and interaction with the solar wind (Stern, 1999; Farrell, et al., 2023).

Gravitational escape is particularly relevant for light species, since atoms or molecules reaching velocities greater than the lunar escape velocity can leave the exosphere directly without undergoing significant collisions (Stern, 1999). Photoionization instead transforms neutral species into ions, which may subsequently be carried away by the electric field of the

solar wind and removed from the lunar environment. Implantation into the surface and cold trapping represent additional pathways of temporary or permanent removal, particularly for species that can be adsorbed by the regolith or trapped in cold regions (Farrell, et al., 2023). The lunar exosphere must therefore be understood as a transient system, continuously regenerated and continuously dispersed, rather than as a stable atmospheric structure (Stern, 1999; Farrell, et al., 2023).

A particularly interesting aspect of the lunar atmospheric environment concerns the presence of suspended or mobilized dust above the surface (Stern, 1999). The question of exospheric dust is complex. The LADEE (*Lunar Atmosphere and Dust Environment Explorer*) mission confirmed the existence of an ejecta cloud produced by the impacts of interplanetary dust but did not conclusively confirm the presence of a stable population of electrostatically lofted dust at high altitudes. LDEX (*Lunar Dust Experiment*) measurements established upper limits for the density of submicrometric dust in the terminator region, suggesting that electrostatic mechanisms are inefficient or incapable of lofting fine particles to high altitudes. At the same time, Farrell et al. acknowledge that charging, mobilization, and electrostatic transport processes may be effective very close to the surface, contributing to the local distribution of fine lunar particles (Farrell, et al., 2023).

The lunar atmosphere is also relevant because it preserves information concerning near-surface volatiles and the interactions between regolith, solar wind, and the space environment. Stern emphasizes that, although the entire native atmospheric envelope has an extremely low mass, its scientific value is considerable because it can provide indications concerning the distribution of volatiles, including water. The atmosphere itself may act as a temporary reservoir for gases released from the lunar interior, offering indirect information concerning outgassing phenomena and residual endogenous activity. Furthermore, certain atmospheric species may reflect the composition of specific surface mineralogical units, making the exosphere an indirect tool for interpreting processes and materials on the lunar surface (Stern, 1999). The missions following Apollo, analyzed in the subsequent chapter, greatly expanded knowledge of the lunar atmosphere by introducing more sensitive instruments and more detailed orbital observations (Farrell, et al., 2023; Barry, 2026).

According to Stern, the replenishment rate of gases in the native lunar atmosphere is of the order of 10 g/s, while the total mass of the atmosphere is extremely small of the order of $10^7$ g. This low mass makes the lunar atmosphere particularly susceptible to human activities, since even limited gas releases can temporarily alter its natural state. Stern observes that each Apollo landing mission deposited exhaust gases and effluents equivalent to approximately 0.2 masses of the native lunar atmosphere, interfering with measurements of the atmospheric environment conducted by the ALSEP instruments (*Apollo Lunar Surface Experiments Package*) (Stern, 1999). NASA confirms that human and robotic activity can also modify the lunar exosphere, since the exhaust gases from a single lander can temporarily dominate the surrounding space. This alteration is particularly critical because spacecraft exhaust may contain water and other compounds that also occur naturally on the Moon, making it more difficult to distinguish between natural signals and contamination caused by exploration activities (Barry, 2026). For this reason, the study of the lunar exosphere is not only a scientific matter, but also a prerequisite for assessing the environmental impact of future missions, repeated landings, and prospecting or construction activities on the surface (Farrell, et al., 2023; Barry, 2026).

Indeed, Farrell indicates that the LADEE mission was also conceived to obtain an inventory of the Moon's dusty exosphere before a more extensive human presence could alter its fragile nature (Farrell, et al., 2023).

In conclusion, the lunar atmosphere cannot be interpreted as a simple vacuum devoid of phenomena, but rather as an extremely tenuous, dynamic exospheric system that is sensitive to interactions between surface and space. Its composition and variability depend on an unstable balance between external sources, internal sources, interactions with the regolith, and loss processes toward space. It is precisely this fragility that makes the lunar exosphere an essential subject of study for understanding the Moon as an active environment, but also a parameter to be considered in future strategies for exploration, settlement, and resource utilization.

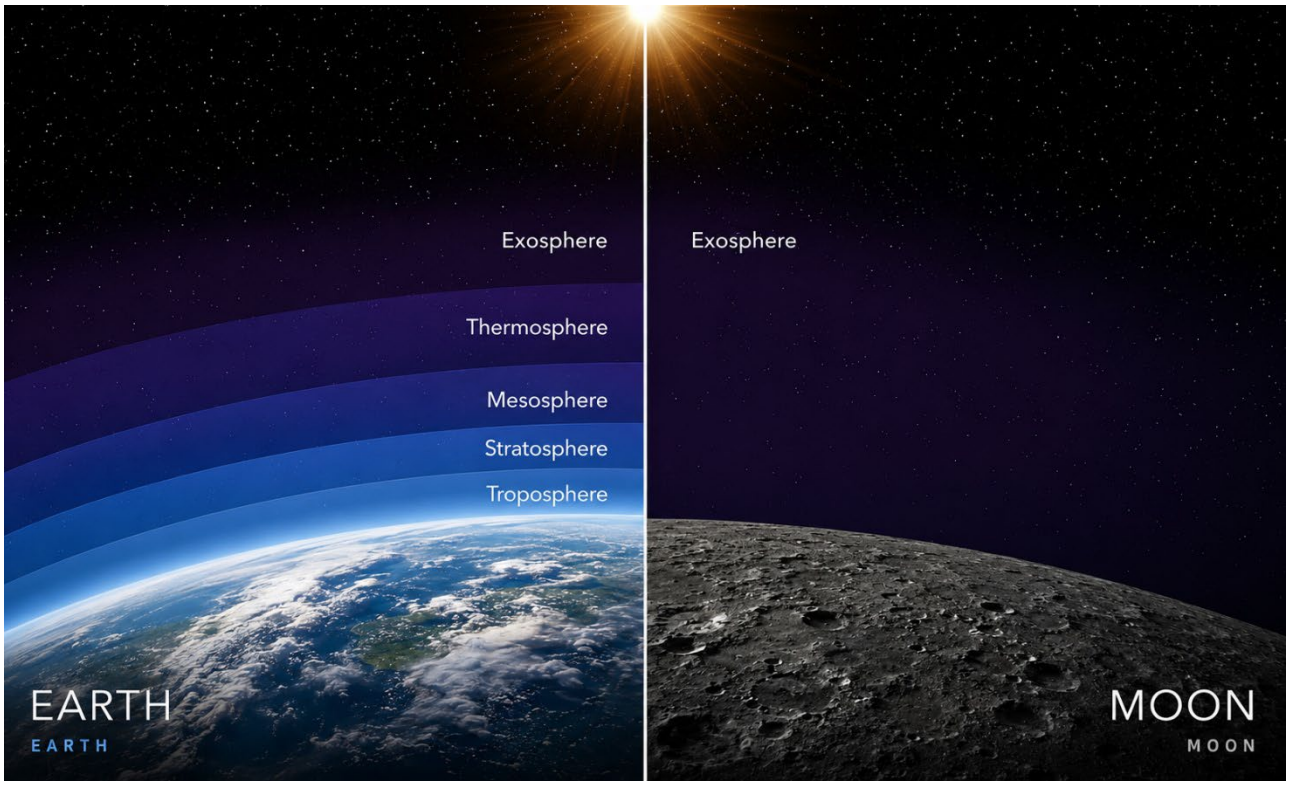
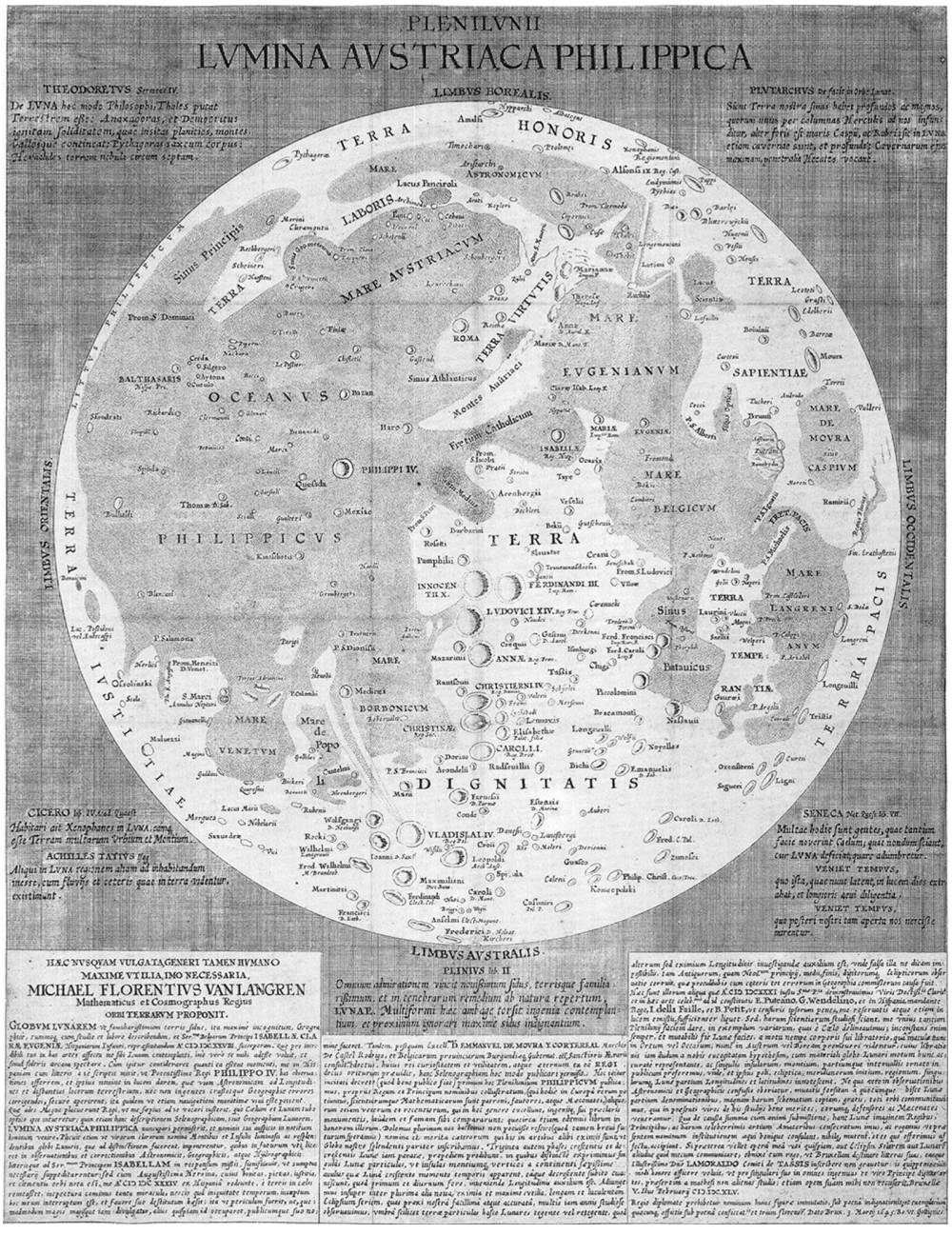



***Figure 1.8**: A comparison between Earth's atmospheric layers and Moon's exosphere. Adapted from: NASA.*

## 1.5 Water resources

For a long time, the Moon was described as an essentially arid body, devoid of any significant atmosphere and therefore incapable of preserving stable water on its surface (Gasparini & Wasser, 2026). This interpretation derived from the assumption that, in the absence of sufficient atmospheric pressure, any exposed surface water would have rapidly evaporated or sublimated into space (Liu, 2022; Gasparini & Wasser, 2026). Initial analyses of Apollo samples reinforced this view, since they revealed no immediate evidence of water and led the lunar surface to be considered completely dry for decades (Liu, 2022).


PLENILVNII
LVMINA AVSTRIACA PHILIPPICA
LIMBVS BOREALIS
LIMBVS AVSTRALIS
LIMBVS OCCIDENTALIS
TERRA HONORIS
MARE AVSTRIACVM
OCEANVS
PHILIPPICVS
TERRA
MARE
EVGENIANVM
SAPIENTIAE
CASPIVM
BELGICVM
DIGNITATIS
Sinus Principis
Sinus Aestuum
Sinus Iridum
Sinus Roris
Sinus Lauri
Sinus Amoris
Sinus Medii
Sinus Aestatis
Mare de Popo
MARE VENETVM
Montes Carpatus
Montes Taurus
Montes Pyrenaei
Montes Apenninus
Montes Alpes
Montes Caucasus
Montes Rhodopus
Montes Riphaeus
Montes Taygetus
Montes Olympus
Montes Haemus
Montes Pindus
Montes Atlas
Montes Caucasus
Montes Altaicus
Montes Imaus
Montes Hyperboreus
Montes Ceraunius
Montes Taurus
Montes Cordillera
Montes Andes
Montes Altaic

Over the last few decades, however, a series of orbital missions, spectroscopic observations, and new analyses of lunar samples has progressively altered this framework, demonstrating that lunar water exists in different forms, with different distributions and potentially multiple origins *(Reiss, 2024)*.

The presence of water on the Moon must be understood by distinguishing among different chemical and physical forms, namely molecular water ($H_2O$), hydroxyl groups OH, water ice, and hydrated species bound to or trapped within the regolith. These forms may be adsorbed onto grain surfaces, incorporated within minerals or glasses, trapped in pores and fractures, or mixed with the regolith in cold regions (Reiss, 2024). It is therefore inappropriate to imagine lunar water as a single homogeneous reservoir, since it instead constitutes a set of discontinuous occurrences controlled by temperature, solar exposure, surface composition, grain size, depth, and local geological history (Parkinson, et al., 2023; Reiss, 2024).

The conception of the Moon as a completely arid body changed thanks to orbital observations, spectroscopic measurements and new analyses of lunar samples. In 1961, Kenneth Watson proposed that water ice could survive on the floors of lunar craters that never receive sunlight, anticipating the concept of permanently shadowed regions as potential cold traps for volatiles (Gasparini & Wasser, 2026). This hypothesis was consistent with the fact that, while Sun-illuminated areas reach temperatures incompatible with the stability of exposed water, some polar depressions remain sufficiently cold to limit sublimation losses (Hayne, et al., 2015; Gasparini & Wasser, 2026). The possibility of frozen water in permanently shadowed craters was subsequently strengthened by data from the *Clementine* mission in 1994 and the *Lunar Prospector* mission in 1998, which indicated possible ice signatures and elevated hydrogen concentrations near the lunar poles, respectively (Parkinson, et al., 2023; Gasparini & Wasser, 2026). A decisive development occurred in 2008, when the re-examination of Apollo samples by researchers at Brown University identified hydrogen within small volcanic glass beads (Gasparini & Wasser, 2026). Since these glasses derive from ancient volcanic eruptions, the presence of hydrogen within them suggested that water or hydrogen-bearing components were present in the lunar interior at the time of volcanic activity (Gasparini & Wasser, 2026; Hauri, et al., 2015). In 2009, the *Chandrayaan-1*, *Cassini*, and *Deep Impact* missions detected signs of hydration in illuminated areas of the lunar surface, interpreted as the presence of OH and/or $H_2O$ (Reiss, 2024), (Gasparini & Wasser, 2026). These results demonstrated that lunar hydration was not restricted exclusively to the colder polar regions but could also affect surfaces exposed to solar radiation (Gasparini & Wasser, 2026). The LCROSS (*Lunar Crater Observation and Sensing Satellite)* mission provided further direct evidence when, in 2009, an impactor was directed toward *Cabeus* crater, in a permanently shadowed region of the south pole, making it possible to analyze the ejected material (Parkinson, et al., 2023; Gasparini & Wasser, 2026). Observations of the LCROSS impact plume revealed the presence of water ice and other volatiles, confirming that certain polar cold traps preserve hydrogen-bearing and icy materials (Parkinson, et al., 2023). In 2020, SOFIA (*Stratospheric Observatory for Infrared Astronomy*) data confirmed the presence of molecular water on the Sun-illuminated lunar surface, particularly in Clavius crater, demonstrating that water is not confined exclusively to cold and dark areas. According to NASA's synthesis, the concentration detected by SOFIA in Clavius crater was reported as equivalent to approximately 355 ml per cubic meter of lunar soil. In 2023, a large-area map based on SOFIA data provided further indications of the distribution of water and the possible movement of molecules across the lunar surface, extending attention toward the south pole and future areas of interest for the Artemis and *VIPER* mission (Gasparini & Wasser, 2026).

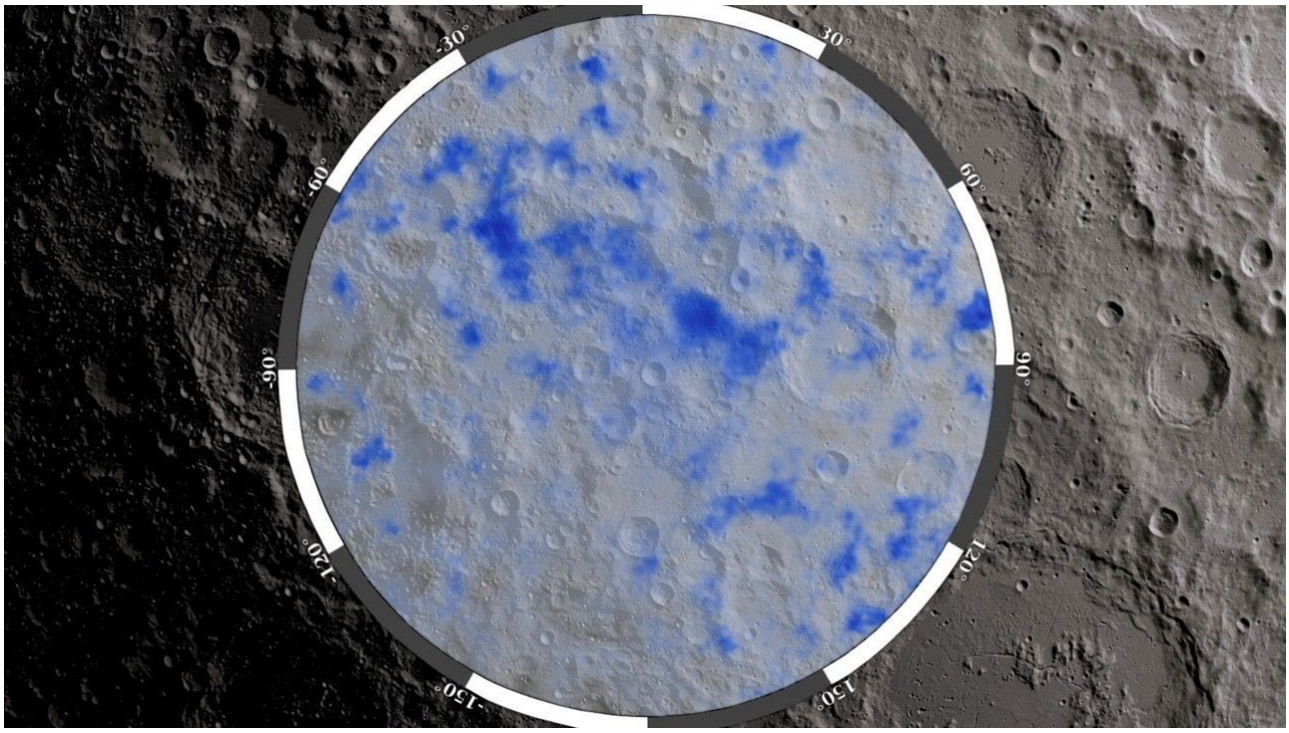



***Figure 1.10:*** *Areas of the Moon's south pole with possible deposits of water ice, shown in blue. The map is based on data taken by NASA's Lunar Reconnaissance Orbiter. Source: NASA.*

Lunar water should not be interpreted as a static resource, but rather as part of an extremely weak, discontinuous volatile cycle regulated by mechanisms of production, transformation, migration, and loss. As a body devoid of a dense atmosphere, the Moon directly records, over geological timescales, its interaction with the solar wind, radiation, and impact bombardment, which cause a continuous supply, release, and remixing of volatile components. Among the weak but continuous sources is the solar wind, whose protons can react with oxygen bonds present in regolith minerals, forming OH groups and $H_2O$ molecules. In the Moon's early history, however, impact bombardment by hydrated and icy material would have constituted a far more intense source, up to four orders of magnitude greater than solar-wind-induced production (Reiss, 2024).

Internal outgassing from the primordial Moon may also have contributed to water accumulation, although the extent to which volcanic activity supplied the polar deposits remains uncertain. The principal accumulation mechanisms include cold trapping through molecular adsorption, entrapment within melts or glasses, and burial of icy deposits by regolith. The main processes of loss or conversion include impact vaporization, thermal release, photolysis, photon-stimulated desorption, photodissociation, atomic sputtering, and thermal escape of free molecules (Reiss, 2024).

Water migration occurs through ballistic hops in the lunar exosphere and through interaction with electromagnetic fields, while in the subsurface molecular mobility is controlled by desorption, adsorption, and diffusion (Reiss, 2024). This mobility enables volatile species to be transferred from warmer regions toward colder areas, where molecules may be temporarily or permanently trapped (Hayne, et al., 2015; Reiss, 2024). Permanently shadowed polar regions therefore constitute particularly significant reservoirs, since low temperatures reduce

sublimation and favor the preservation of volatiles over very long timescales (Hayne, et al., 2015; Parkinson, et al., 2023).

Permanently shadowed regions (PSR) are lunar areas that receive extremely limited solar radiation over long geological periods, particularly at high polar latitudes. According to Parkinson, PSRs located beyond 80° latitude receive little solar radiation owing to the low inclination of the lunar axis, equal to approximately 1.5°. The combination of limited insolation and a tenuous exosphere enables these regions to maintain temperatures below approximately 120 K, generating particularly effective cold traps in topographic depressions such as craters (Parkinson, et al., 2023).

The distribution of lunar ice must be understood in three dimensions, distinguishing between surface ice, near-surface ice, and possible deeper deposits. Chakraborty's study integrates data from the Lunar Reconnaissance Orbiter mission and suggests that ice may occur as surface frost, icy horizons interlayered with regolith at depths of approximately 50 cm or several meters, or thicker slabs at depths of tens of meters. The authors distinguish surface and near-surface deposits, extending down to approximately 1 m, from subsurface deposits located approximately between 1 and 3 m. The estimated extent of ice at the north pole is approximately 1,100 $km^2$, and about 562 $km^2$ at the south pole. This vertical organization is relevant not only to reconstructing the history of volatiles, but also to the accessibility of the deposits for future robotic and human missions (Chakraborty, et al., 2024). Consequently, the possibility of reaching ice depends on the combination of location, depth, temperature, topographic accessibility, and the ability of instruments to distinguish between ice, hydrogen, and hydrated regolith (Chakraborty, et al., 2024; Reiss, 2024).

Confirmation of molecular water on the Sun-illuminated surface significantly broadens the understanding of the distribution of lunar water. SOFIA data show values far lower than the concentrations estimated in certain polar cold traps but demonstrate that the illuminated surface may nevertheless contain $H_2O$ in protected, bound, or trapped forms (Reiss, 2024; Gasparini & Wasser, 2026). Liu nevertheless adopts a more cautious position, arguing that "bare" water or ice should not be physically stable on the lunar surface and proposing that $H_2$, OH, and $H_2O$ may respectively be associated with the solar wind, surface hydrated minerals, or inclusions in impact glasses (Liu, 2022). This caution does not negate the observational evidence, but emphasizes the importance of distinguishing among free water, exposed ice, chemical hydration, adsorbed water, and water trapped in glassy or mineral materials (Liu, 2022; Reiss, 2024). For this reason, the current scientific framework requires *in situ* measurements, new samples, analogue studies, and more refined models to constrain the abundance, distribution, temporality, and origin of lunar water (Reiss, 2024).

Recent measurements of hydrogen content in certain lunar samples indicate that part of the Moon's water may be indigenous and related to its magmatic history. Hauri's research suggests that volatile components were not entirely lost during lunar formation and that water may have been accreted or retained within the satellite's interior. Although reconstructing the original water content remains complex, the presence of water in the lunar mantle cannot be treated as an isolated anomaly, challenging the models that interpret the Moon as strongly depleted in volatiles (Hauri, et al., 2015).

This evidence places an important constraint on models of lunar formation, since many giant impact scenarios predict extensive melting and vaporization of protolunar material, conditions that make it difficult to explain the preservation of water within the interior. According to

Gorkavyi, the mega-impact theory implies a largely desiccated Moon, in which residual water should derive from exogenous contributions, such as comets, solar wind, or transfer from the Earth's atmosphere (Gorkavyi, 2023). However, the origin of lunar water remains one of the most complex issues, since the available data indicate potentially different contributions that have not yet been fully quantified (Chakraborty, et al., 2024; Reiss, 2024).

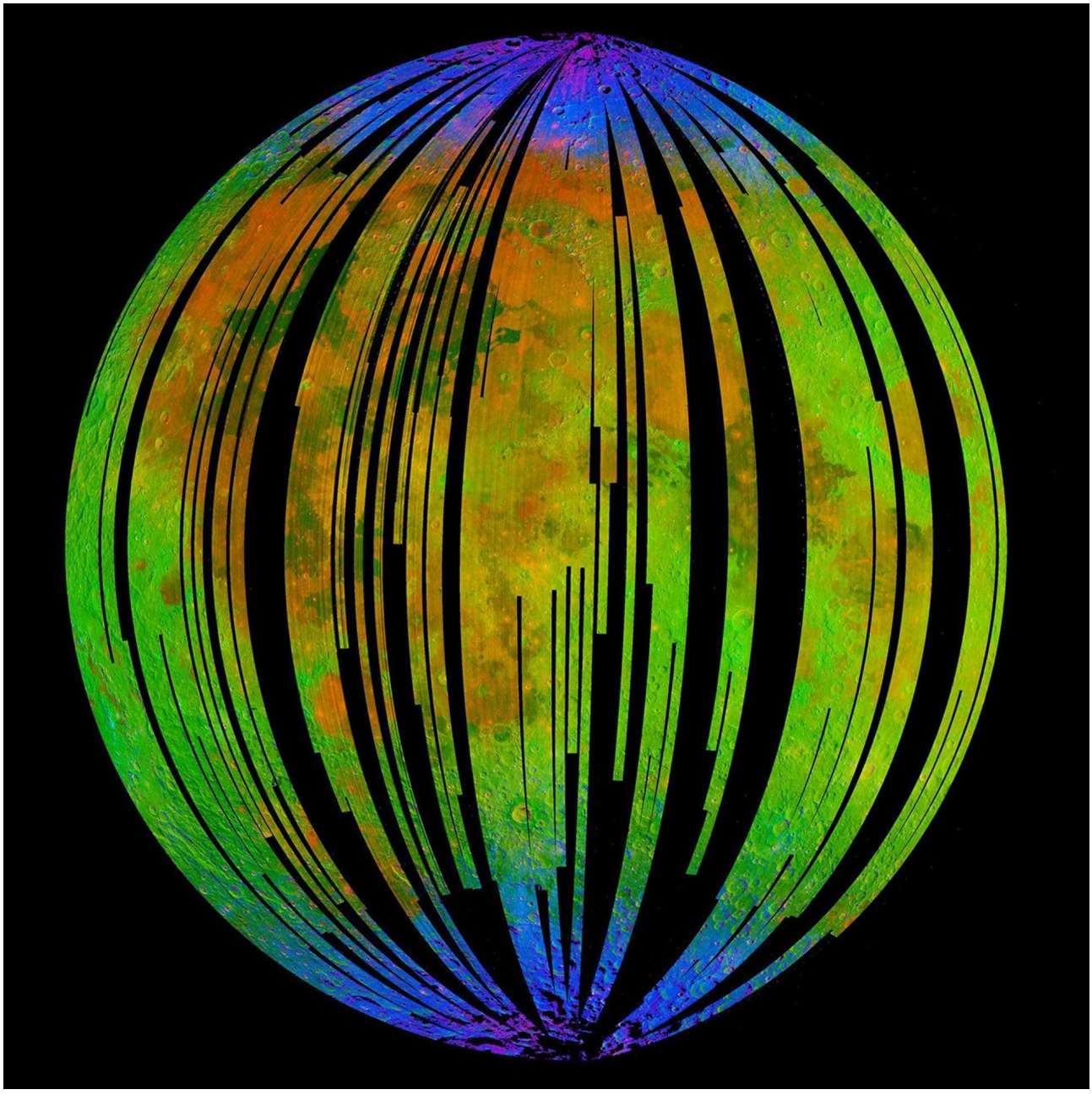


***Figure 1.11:*** *A composite image using data from NASA's Moon Mineralogy Mapper. The blue shows areas of confirmed water ice on the lunar surface. Source: ISRO/NASA/JPL-Caltech/Brown University/USGS.*

Interest in lunar water is not merely scientific, but also operational, since it constitutes a resource for life support, propellant production, and the sustainability of future exploration missions (Parkinson, et al., 2023; Reiss, 2024). According to Reiss, water is particularly relevant because its form, abundance, and variability are closely linked to the evolution of the Moon and

its interaction with the space environment (Reiss, 2024). From an ISRU perspective, the possibility of locating and characterizing accessible deposits influences the planning of settlements, energy systems, surface architectures, and extraction strategies (Parkinson, et al., 2023; Chakraborty, et al., 2024). Crawford instead emphasizes that the lunar poles are particularly important because water and other volatiles may remain trapped in permanently shadowed craters, making these areas relevant for the assessment of lunar resources (Crawford, 2015).

At the same time, lunar water represents an archive of processes of interaction between surface and space. The analysis of hydrogen and water concentrations at different depths may contribute to reconstructing the evolution of the solar wind, the degree of soil maturity, and the intensity of mixing produced by impacts. However, the preservation or loss of volatiles is extremely sensitive to surface activities, since heat, mechanical disturbance, and gases released by landers can alter or mobilize molecules weakly bound to the regolith. For this reason, Reiss highlights the need for new *in situ* investigations, analyses of returned samples, analogue experiments, and integrated models capable of connecting sources, reservoirs, loss processes, and transformations (Reiss, 2024).

In conclusion, the presence of water on the Moon cannot be reduced to the simple question of whether the satellite is “dry” or “wet”, since the evidence indicates a complex system of molecular water, hydroxyl, surface ice, subsurface ice, and internal water preserved in magmatic materials (Hauri, et al., 2015; Hayne, et al., 2015; Reiss, 2024). Permanently shadowed polar regions constitute the most promising reservoirs for stable ice, but widespread hydration and evidence of water on the illuminated surface demonstrate that the lunar water cycle also concerns broader and more dynamic environments (Chakraborty, et al., 2024; Gasparini & Wasser, 2026). Understanding lunar water therefore requires the integration of orbital data, spectroscopic measurements, thermophysical models, geochemical analyses, and future *in situ* verification, since only this combination makes it possible to distinguish the origin, form, abundance, depth, and actual accessibility of the deposits (Parkinson, et al., 2023; Chakraborty, et al., 2024; Reiss, 2024).

### 1.6 Lunar radiation environment

Radiation is one of the principal environmental factors to be considered in the design of human missions and permanent infrastructure on the Moon, since the satellite possesses neither a significant atmosphere nor a global magnetic field capable of effectively shielding energetic particles originating from space. In the absence of these two natural protection systems, particles of galactic and solar origin can reach the lunar surface almost without attenuation, generating a radiation environment profoundly different from that of the Earth (Reitz, et al., 2012). Lunar radiation must therefore be interpreted as a complex system, consisting of primary radiation originating from space, secondary radiation produced through interaction with the soil and shielding materials, direct solar radiation incident upon the surface, and transient radiative phenomena associated with meteoritic impacts (Bouley, et al., 2012; Dobynde & Guo, 2021; Lin, et al., 2025).

In the context of human radiation protection, the most relevant sources are Galactic Cosmic Rays (GCR) and solar particle events, identified as Solar Particle Events or Solar Energetic Particles (SPE or SEP), since both can contribute significantly to the dose absorbed by astronauts (Adams, et al., 2007; Reitz, et al., 2012). These primary components are

supplemented by albedo particles, particularly neutrons, produced when GCR and SEP interact with the lunar crust and regolith (Adams, et al., 2007; Isolan, et al., 2024). This distinction is fundamental because the radiation environment of the Moon does not simply coincide with the flux incident from space but also includes the physical response of the lunar soil, which transforms a portion of the primary radiation into secondary particles capable of contributing to the biological dose (Denisov, et al., 2011; Dobynde & Guo, 2021).

The Earth's surface is protected by the atmosphere and the magnetosphere, whereas the lunar surface is directly exposed to energetic particles originating from the interplanetary environment (Isolan, et al., 2024). This difference explains why, on Earth, cosmic radiation contributes only approximately one sixth of the annual natural dose of 2.4 mSv, whereas on the lunar surface annual exposure due to GCR is estimated at approximately 380 mSv during solar minimum and approximately 110 mSv during solar maximum (Reitz, et al., 2012). The relationship between solar activity and GCR is in fact anticorrelated because, during solar minimum, the flux of galactic cosmic rays increases, whereas during solar maximum, the greater intensity of the solar wind reduces the penetration of lower-energy galactic components (Reitz, et al., 2012; Rizzo, et al., 2023).

The Moon does not possess a global radiation belt analogous to the Earth's Van Allen belts[4], although local surface magnetic anomalies have been detected (Reitz, et al., 2012). This absence of a global magnetosphere implies that the natural protection available on the lunar surface is essentially geometric and material in nature, namely related to the shielding provided by the lunar body itself, by topography, by the regolith, and by any habitat structures (Adams, et al., 2007; Dobynde & Guo, 2021). According to Adams et al., the flux and therefore the dose rate from GCR and SEP on the Moon are approximately half those in deep space, since the lunar body geometrically blocks a portion of the incident sky (Adams, et al., 2007). However, this partial protection does not eliminate the risk, because the primary radiation reaching the ground in turn generates a secondary component, also directed toward the surface, which contributes to the radiation field experienced by astronauts (Dobynde & Guo, 2021).

*Galactic Cosmic Rays (GCR)*

Galactic Cosmic Rays are high-energy charged particles originating from sources external to the Solar System and represent a continuous, penetrating, and omnidirectional component of the lunar radiation environment (Dachev, et al., 2011; NASA OCHMO, 2025). The nuclear component of GCR consists mainly of protons, accounting for approximately 87% of the flux, helium ions, accounting for approximately 12%, and a smaller fraction of heavier nuclei, often referred to as HZE[5] particles (Dachev, et al., 2011; Reitz, et al., 2012; Isolan, et al., 2024). Despite their lower abundance, heavy ions are of particular radiobiological significance because they are characterized by high Linear Energy Transfer (LET) and a greater capacity to produce concentrated biological damage (Dachev, et al., 2011; Rizzo, et al., 2023).

From a biological perspective, the hazard posed by space radiation fields derives from their capacity to deposit energy over very short distances, increasing the probability of DNA damage and making high-LET radiation more effective, for the same absorbed dose, than low-LET radiation such as X-rays. This aspect is also expressed through the concept of Relative Biological Effectiveness, which compares the absorbed doses required to produce the same

[4] *Regions rich in high-energy particles (plasma), primarily protons and electrons, trapped by the Earth's magnetic field at a fixed distance from the planet* (Cappelli, 2008).

[5] *HZE stands for High-Z and Energy or, in its extended form, High Atomic Number and High Energy.*

biological effect for different types of radiation. Consequently, measuring absorbed dose alone is insufficient to describe the actual biological severity of the lunar environment, since radiation quality, particle composition, and the production of secondary particles alter the real risk to the human body (Rizzo, et al., 2023).

GCR constitute a persistent and unavoidable source within the lunar environment, although their flux varies over time according to the solar cycle (Reitz, et al., 2012; Rizzo, et al., 2023). During solar maximum, the models cited by Rizzo et al. indicate a reduction in GCR fluence by as much as one order of magnitude, accompanied, however, by a hardening of the spectrum, namely a relative shift toward higher energies. This dynamic makes the temporal planning of missions a matter of compromise, since solar maximum may reduce the GCR component while increasing the probability of energetic solar events (Rizzo, et al., 2023; NASA OCHMO, 2025).

*Solar Particle Events (SPE)*

Alongside the continuous GCR component, the lunar surface is exposed to sudden solar events in which the Sun releases energetic particles, primarily protons, associated with solar flares and Coronal Mass Ejections (CME) (Reitz, et al., 2012; Rizzo, et al., 2023).

Reitz, Berger and Matthiae emphasize that SPE display considerable variability in both flux and energy spectrum and may expose the crew to doses that are potentially life-threatening. According to the same study, extreme SPE scenarios may result in exposures in the order of 1 Sv, whereas in worst-case scenarios the dose to blood-forming organs may reach approximately 900 mSv under conditions of minimal or absent shielding (Reitz, et al., 2012).

SPE are generally more likely during phases of increased solar activity, although precise predictions of their occurrence remain limited. For this reason, the NASA Office of the Chief Health and Medical Officer (OCHMO) emphasizes the need for monitoring, accurate event determination, dosimetry, and timely warning systems that enable the crew to reach a shielded refuge. Within the NASA-STD-3001[6] framework, exposure to a reference SPE, based on the proton spectrum derived from the sum of the October 1989 events, must be maintained below an effective dose of 250 mSv. Shielding is more effective against SPE than against GCR, since SPE are dominated by low- or medium-energy protons, which can be attenuated more readily by shielding materials than high-energy galactic ions. NASA indicates that, for SPE, shielding in the order of 5–20 g/cm$^2$ in aluminum and polyethylene can be effective, although optimization is still required to limit mass (NASA OCHMO, 2025). The authors also show that, in the case of severe SPE, increased shielding can drastically reduce exposure, with values at 25 g/cm$^2$ ranging from approximately 25 mSv for liquid hydrogen to 150 mSv for aluminum, and values at 100 g/cm$^2$ decreasing to almost 0 mSv for liquid hydrogen and approximately 40 mSv for aluminum (Reitz, et al., 2012).

*Secondary radiation and albedo neutrons*

Lunar radiation does not consist solely of incident primary particles, since the impact of GCR and SEP with the regolith produces secondary particles such as protons, neutrons, mesons, muons, electrons, gamma rays, and nuclear fragments (Reitz, et al., 2012; Dobynde & Guo, 2021). Among these components, neutrons play a particularly relevant role because, being

[6] *It refers to the system of technical requirements and safety limits established by NASA to protect astronauts' health and performance during human spaceflight missions. More specifically, NASA-STD-3001 is the NASA Spaceflight Human-System Standard, developed by the Office of the Chief Health and Medical Officer (OCHMO).*

electrically neutral, they do not interact through Coulomb forces and can penetrate deeply into materials and tissues (Dribi & Ounoughi, 2024). Rizzo notes that neutrons are not a stable primary component of free space but are generated as secondary particles through the fragmentation and ablation of heavier nuclei (Rizzo, et al., 2023).

Adams et al. define the lunar ionizing radiation environment as the result of three principal contributions: galactic cosmic rays, solar energetic particles, and albedo particles, mainly neutrons, originating from the lunar surface. However, Adams et al. conclude that thermal and epithermal neutrons respectively contribute only 0.14% and 0.77% of the total effective neutron dose and are therefore of little significance in estimating human radiation risk (Adams, et al., 2007).

*Radiation in the lunar subsurface and the role of regolith*

Lunar regolith can function as a shielding material, but its interaction with GCR also generates hadronic cascades[7] and secondary particles, making it necessary to accurately evaluate the distribution of radiation with depth (Denisov, et al., 2011; Dobynde & Guo, 2021).

According to Dobynde and Guo, most particle fluxes within the soil reach a maximum at depths between 0.5 and 1 m, with variations depending on particle type and energy. This information is of decisive importance for design, since it indicates that an incorrectly dimensioned thickness of regolith could locally increase the production of secondary radiation rather than immediately reducing risk. The same authors observe that particles heavier than protons, such as alpha particles, fragment efficiently within the soil and become difficult to detect below a depth of 1 m. The REDMoon model also shows that albedo radiation at the surface is largely isotropic within the upward-facing hemisphere for protons, neutrons, and light particles, whereas in the subsurface primary particles and high-energy secondary particles propagate predominantly downwards (Dobynde & Guo, 2021).

Denisov likewise confirms that interaction with the lunar soil produces a hadronic cascade with a maximum intensity at a depth of approximately 0.8 m. In their model, neutron fluxes generated by GCR and SEP at a depth of approximately 80 cm are greater than the neutron fluxes present at the surface across the entire energy interval considered. The same authors demonstrate that, at depths greater than approximately 0.5 m, the contribution of secondary neutrons to absorbed and equivalent doses exceeds that of protons, particularly in the case of equivalent dose. They also conclude that including GCR nuclei in the calculation increases the dose by approximately 1.5 times compared with the dose produced by GCR protons alone. By contrast, the contribution of SEP nuclei to the dose is limited to only a few percentage points compared with the SEP proton component (Denisov, et al., 2011).

The Chandrayaan-1 mission provided important data through the RADOM instrument, designed to measure total absorbed dose, energetic particle flux, and the spectrum of deposited energy during transfer toward the Moon and in lunar orbit (Dachev, et al., 2011). During its circular lunar orbit at an altitude of 100 km, RADOM measured an average dose rate of 0.227 mGy/day between November 2008 and May 2009. At an altitude of approximately 200 km during the final months of the mission, the measured dose rate increased to 0.257 mGy/day, owing to the reduction in the shielding effect of the lunar body and the increase in GCR flux associated with

[7] *A hadronic cascade is a sequence of nuclear interactions produced when a high-energy particle, such as a proton or a heavy nucleus from galactic cosmic rays (GCRs), strikes the atomic nuclei of a material. The adjective hadronic derives from hadron, a category of particles subject to the strong nuclear interaction, including protons, neutrons, and pions* (Simonsen & Slaba, 2025).

declining solar activity (Reitz, et al., 2012). Dachev et al. also report that, during the lunar transfer trajectory between 308,000 and 20,000 km from the Moon, RADOM measured an average dose rate of approximately 12.76 μGy/h, with actual values ranging between 3.34 and 41.34 μGy/h. Once it entered lunar orbit at approximately 100 km, the average dose rate decreased to approximately 8.8 μGy/h as a result of the shielding provided by the lunar body (Dachev, et al., 2011).

CRaTER (Cosmic Ray Telescope for the Effects of Radiation), aboard the Lunar Reconnaissance Orbiter, also contributed to the characterization of the lunar radiation environment through measurements of dose and LET spectra. CRaTER consists of six silicon detectors and includes tissue-equivalent plastics to assess the radiation field under conditions more closely resembling the human biological response. CRaTER measurements in lunar orbit indicate radiation exposure of approximately 0.22–0.27 mGy/day (Reitz, et al., 2012).

The doses predicted for lunar missions must be evaluated not only in physical terms, but also in relation to biological effects and the operational limits established for astronauts. NASA OCHMO reports that the total effective career dose limit for a crew member, according to NASA-STD-3001, must be less than 600 mSv, a universal value for all ages and sexes. The same document associates this limit with the concept of Risk of Exposure-Induced Death (REID), adopting an average cancer mortality risk threshold of 3%. For habitable systems intended to support crews for more than 60 days, NASA-STD-3001 further requires that exposure to GCR remain below 1.3 mSv/day for systems in free space and below 0.9 mSv/day for systems on planetary surfaces (NASA OCHMO, 2025).

The health risk associated with radiation includes long-term effects, such as increased cancer morbidity or mortality, as well as potential cognitive, motor, behavioral, or neurological alterations. SPE, by contrast, may produce acute risks during a mission, such as nausea, vomiting, fatigue, skin lesions, and impairment of blood-forming organs. This distinction between chronic risk from GCR and acute risk from SPE is essential for the design of lunar habitats, since it requires both a reduction in cumulative dose and the availability of rapidly accessible shelters in the event of a solar event (Reitz, et al., 2012; NASA OCHMO, 2025).

Rizzo emphasizes that space radiation protection cannot be treated as a simple extension of terrestrial radiation protection, because space radiation fields are dominated by high-LET particles and by secondary particles produced within habitat materials. The terrestrial paradigm, based primarily on exposures to photons, alpha and beta particles, and lower-energy neutrons, does not adequately represent the complexity of the ionic fields present in deep space. For this reason, managing radiation risk for lunar missions requires a multidisciplinary approach integrating mission planning, passive shielding, possible active shielding, space weather monitoring, dosimetry, biology, pharmacology, and physiology (Rizzo, et al., 2023; Isolan, et al., 2024).

Shielding is one of the principal means of reducing radiation exposure, but its effectiveness depends strongly on the type of radiation under consideration (Rizzo, et al., 2023; NASA OCHMO, 2025). According to NASA, shielding against GCR is not fully effective because interactions among high-energy particles, shielding materials, and tissues can generate secondary radiation (NASA OCHMO, 2025). Rizzo specifies that nuclear fragmentation processes can increase the equivalent dose downstream of the shield, because they produce charged fragments and neutrons with high radiobiological quality factors (Rizzo, et al., 2023). An effective shielding material for the space environment must therefore not only attenuate

incident radiation but also limit the development of hadronic showers and secondary neutrons (Rizzo, et al., 2023; Dribi & Ounoughi, 2024). Aluminum is frequently used for space structures because of its balance between mechanical properties and low density, but it provides only modest attenuation against high-energy GCR. Hydrogen-rich materials, such as polyethylene, are considered more effective than aluminum for certain shielding functions, because they reduce the production and penetration of secondary neutrons. Dribi and Ounoughi show that a configuration consisting of 15 g/cm$^2$ of aluminum followed by 5 g/cm$^2$ of polyethylene reduces the secondary neutron flux by approximately 30% compared with a shield composed of 30 g/cm$^2$ of aluminum alone. The same authors observe that the multilayer subdivision of polyethylene can reduce the secondary neutron flux by approximately 10%, whereas aluminum layering does not produce the same benefit (Dribi & Ounoughi, 2024).

For a lunar base, regolith represents a particularly relevant shielding resource because it is available *in situ* and can contribute to reducing the mass that must be transported from the Earth (Reitz, et al., 2012; Dobynde & Guo, 2021). However, the results of Dobynde, Guo and Denisov indicate that the use of regolith as shielding must be optimized in relation to depth, since the secondary field may increase within the first decimeters and reach a maximum between approximately 0.5 and 1 m (Denisov, et al., 2011; Dobynde & Guo, 2021).

This condition is particularly significant for lunar architecture, because it suggests that effective protection cannot be defined solely in terms of “more mass”, but requires an integrated evaluation of thickness, composition, geometry, and the distribution of crew-occupied areas (Dobynde & Guo, 2021; Rizzo, et al., 2023).

Direct solar radiation constitutes a fundamental environmental variable for the lunar surface, since it influences the availability of solar energy, the thermal behavior of the soil and habitats, as well as the presence and preservation of volatiles in permanently shadowed regions. In the absence of a significant atmosphere, attenuation of solar radiation on the Moon can be regarded as negligible; its distribution therefore depends primarily on orbital geometry and the local morphology of the terrain. In particular, at high latitudes, low solar elevation angles accentuate the effects of topographic shadowing, resulting in a more uneven distribution of illumination and favoring the formation of permanently shadowed regions. Although it does not constitute a radiobiological risk comparable to that posed by GCR or SPE, direct solar radiation therefore forms an essential parameter for site selection and the energy and thermal design of a lunar habitat (Lin, et al., 2025).

Overall, the lunar radiation environment results from the interaction between continuous galactic radiation, impulsive solar events, the production of secondary particles within the regolith, the topographic distribution of direct solar radiation, and transient impact-related radiative phenomena (Bouley, et al., 2012; Reitz, et al., 2012; Dobynde & Guo, 2021; Lin, et al., 2025). For human habitability, GCR represent a chronic and penetrating source, whereas SPE constitute episodic but potentially acute events, requiring different mitigation strategies (Reitz, et al., 2012; NASA OCHMO, 2025). Regolith offers a concrete possibility for *in situ* shielding but must be carefully designed because the production of secondary particles may generate maxima in flux and dose within the first meters of the subsurface (Denisov, et al., 2011; Dobynde & Guo, 2021). The design of lunar habitats must therefore integrate shielding thicknesses, hydrogen-rich materials, the possible use of regolith, shelter areas for SPE, continuous radiation monitoring, and careful site selection in relation to illumination, topography, and thermal conditions (Dribi & Ounoughi, 2024; Lin, et al., 2025; NASA OCHMO, 2025). From this perspective, radiation is not merely an environmental constraint to be

mitigated, but a structuring parameter of lunar design, capable of influencing location, morphological configuration, construction technologies, the functional organization of inhabited spaces, and crew protection strategies (Dobynde & Guo, 2021; Rizzo, et al., 2023; NASA OCHMO, 2025).

# CHAPTER 2 – Lunar Exploration and Extraterrestrial Habitats

## 2.1 The history and evolution of Lunar exploration

Having defined the Moon, this chapter examines how it became an object of exploration, technological experimentation and architectural design. Furthermore, the characteristics discussed in Chapter 1 outline the environmental context and the boundary conditions of the project.

The desire to understand the cosmos has accompanied humankind since its origins. The Sun, the stars, and the planets have raised questions that ancient civilizations initially interpreted through symbolic and mythological frameworks. With the gradual consolidation of scientific inquiry, the observation of the sky evolved into a means of understanding celestial bodies and the phenomena that characterize them (Sah, 2025). Within this trajectory, the Moon has played a privileged role, becoming deeply rooted in human experience and imagination due to its dominant presence in the night sky. Its proximity to Earth also made it a particularly favorable destination for observation and, subsequently, for the direct exploration of extraterrestrial space (Benaroya, 2010).

Early observations were initially shaped by religious beliefs, but the decisive turning point came with the introduction of telescopic observation. In 1610, Galileo Galilei identified the presence of craters and irregularities on the lunar surface, contributing to the overcoming of the idea of a perfect and immutable sky and to the emergence of a physical interpretation of celestial bodies (Sah, 2025).

In the following centuries, the evolution of observational instruments progressively expanded the possibility of recording and interpreting the lunar surface. In 1840, John William Draper produced one of the first clear photographs of the Moon obtained through a telescope, introducing photographic documentation into astronomical observation and paving the way for a form of knowledge no longer entrusted solely to drawings or to the observer's written descriptions (Sah, 2025).

With the twentieth century, the observation of the Moon gradually evolved into direct exploration, made possible by the development of space launch vehicles and robotic missions. According to NASA, lunar exploration in the proper sense began in the 1950s, when the United States and the Soviet Union started developing probes designed to reach Earth's natural satellite. In 1959, the Soviet Luna 1 mission performed the first flyby of the Moon, while Luna 3, in the same year, returned the first images of the far side, making visible a region that until then had remained beyond any direct observation from Earth (Sah, 2025; NASA, 2026a)[8].

Robotic exploration thus made it possible to move from remote observation to the collection of data directly in the vicinity of the lunar surface. In 1966, Luna 9 achieved the first soft landing on the Moon and transmitted the first photographs taken from the lunar surface. In the same year, Luna 10 entered orbit around the Moon, carrying instruments intended to study its magnetic field, radiation environment, micrometeorites, and surface composition. In parallel, the American Lunar Orbiter missions produced increasingly extensive photographic documentation of the surface. In particular, Lunar Orbiter I photographed Earth from the lunar region, while Lunar Orbiter IV contributed to the mapping of large portions of both the near side and the far side of the Moon (Sah, 2025; NASA, 2026a).

[8] *The citation refers to the source NASA: Moon Exploration* (NASA, 2026a).

This progressive acquisition of images and measurements did not merely represent a sequence of technological milestones but also prepared the conditions for a human presence on the Moon. In December 1968, Apollo 8 became the first crewed mission to orbit the Moon, testing the operations, communications, and procedures required for the subsequent lunar landing missions. During the journey, the crew also captured the famous Earthrise photograph, in which Earth appears beyond the lunar horizon—an image that profoundly transformed the cultural perception of the relationship between the home planet and extraterrestrial space. In July 1969, Apollo 11 achieved the first human landing on the Moon (Sah, 2025; NASA, 2026a).

### 2.2 Apollo missions

Between 1969 and 1972, the Apollo 11, 12, 14, 15, 16, and 17 missions brought a total of twelve astronauts to operate on the lunar surface, constituting the first and, to date, only phase of direct human exploration of the Moon (NASA, 2026a; NASA, 2026b)[9]. The program's primary objective was to achieve a human lunar landing and ensure the safe return of the crews to Earth; however, it also included the development of space technologies, the verification of the human ability to work in the lunar environment, the achievement of United States pre-eminence in space, and the implementation of a scientific exploration program of the satellite (NASA, 2026b). From an operational perspective, the lunar missions adopted the lunar orbit rendezvous mode, whereby the Command and Service Module remained in orbit, while the Lunar Module transported two astronauts to the surface and subsequently returned them to the main spacecraft. As already discussed in Section 1.2, the crews brought back to Earth 382 kg of lunar rocks and soil intended for scientific study (NASA, 2026a). The analysis of these samples provided fundamental data for reconstructing the formation, evolution, and composition of the Moon.

*Apollo 11*

Launched on 16 July 1969, Apollo 11 achieved the first human lunar landing on 20 July, when Neil Armstrong and Edwin Aldrin reached *Mare Tranquillitatis* aboard the Lunar Module *Eagle* (Loff, 2015; NASA, 2026b). During the extravehicular activity, which lasted more than two and a half hours, the astronauts collected samples and installed the *Early Apollo Scientific Experiments Package* (EASEP), which included instruments for the analysis of the solar wind, seismic monitoring, and laser measurement of the Earth–Moon distance, thereby initiating the direct scientific exploration of the lunar surface (Loff, 2015).

[9] *The citations refers to the sources NASA: The Apollo Program* (NASA, 2026b).

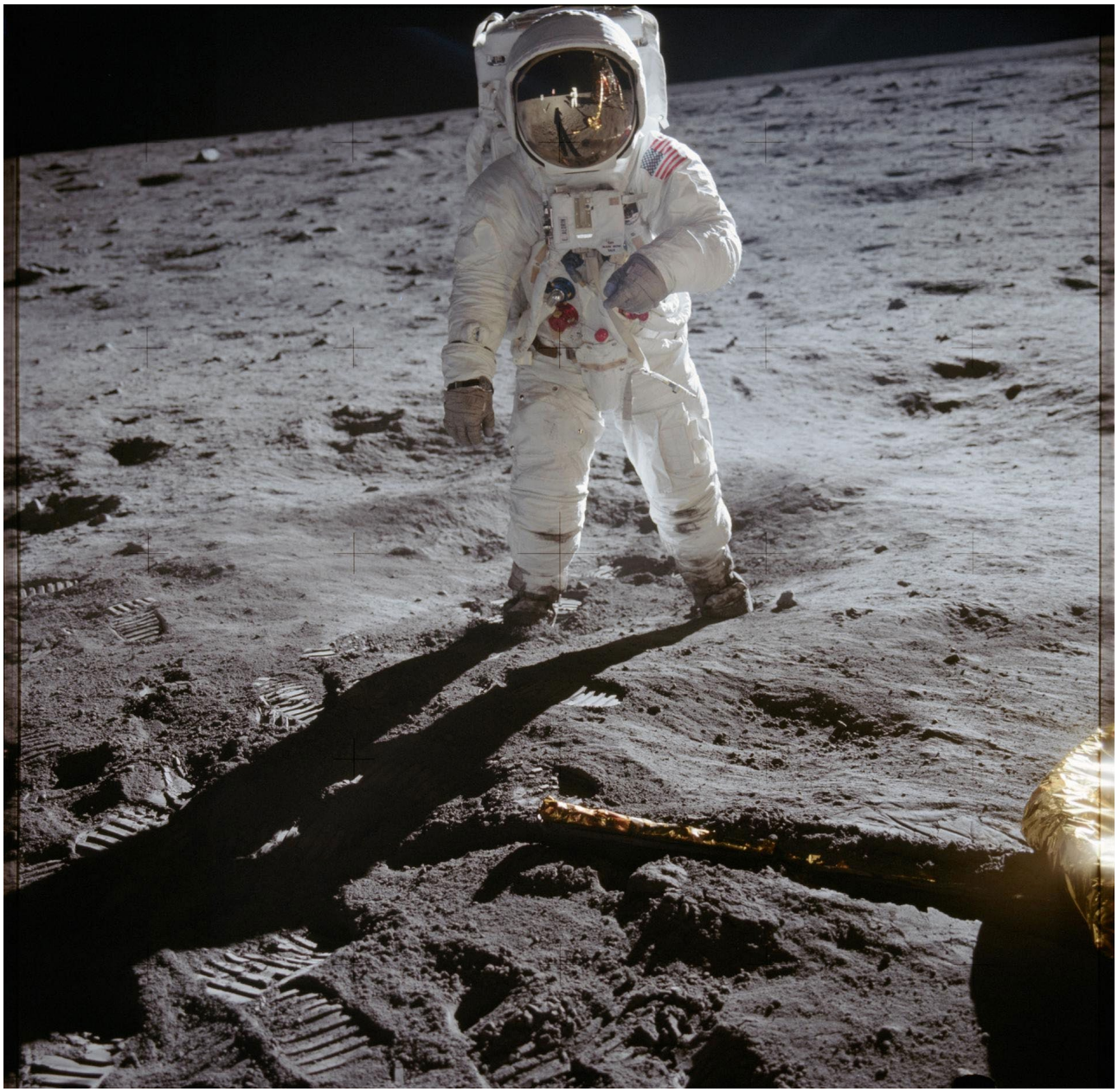


***Figure 2.1:*** *Astronaut Buzz Aldrin stands on the Moon facing a U.S. flag during the Apollo 11 mission in July 1969. Source: NASA.*

*Apollo 12*

With Apollo 12, lunar exploration achieved greater operational precision. The *Intrepid* module landed in *Oceanus Procellarum* near the *Surveyor III* probe, components of which were recovered in order to analyze the effects of exposure to the lunar environment. The mission also installed the *Apollo Lunar Surface Experiments Package* (ALSEP) and, through the controlled impact of the ascent stage, produced data useful for the seismic study of the Moon (NASA, 2009a)[10].

[10] *The citation refers to the source NASA: Apollo 12, The Pinpoint Mission* (NASA, 2009a).

*Apollo 14*

Conducted between January and February 1971, Apollo 14 explored the *Fra Mauro* region, reached by the Lunar Module *Antares* with the most precise landing achieved up to that time (NASA, 2009b; NASA, 2026b)[11]. During two extravehicular activities, Alan Shepard and Edgar Mitchell installed the ALSEP, carried out geological investigations, and collected approximately 43 kg of samples, contributing to the scientific study of the site and to the documentation of possible areas for subsequent missions (NASA, 2009b).

*Apollo 15*

With Apollo 15, launched in July 1971, the so-called "J" missions began, characterized by a longer stay on the surface and enhanced scientific capabilities (NASA, 2009c)[12]. In the *Hadley–Apennine* region, Scott and Irwin used the Lunar Roving Vehicle (LRV) for the first time, expanding the range of geological reconnaissance, and collected more than 77 kg of lunar samples (NASA, 2009c; NASA, 2026b). The mission also included the installation of the ALSEP, soil coring operations, and orbital observation activities conducted through the Scientific Instrument Module (SIM), extending scientific investigation from the surface to lunar orbit (NASA, 2009c).



***Figure 2.2**: Apollo 15 astronaut Jim Irwin uses a scoop to collect soil samples on the lunar surface. Source: NASA.*

[11] *The citation refers to the source NASA: Apollo 14, Mission Details* (NASA, 2009b).

[12] *The citation refers to the source NASA: Apollo 15, Mission Details* (NASA, 2009c).

*Apollo 16*

Launched in April 1972, Apollo 16 explored the *Descartes* highlands, combining surface operations with orbital observations and experiments conducted during the journey (Uri, 2022; NASA, 2026b). These included the study of the behavior of particles in flight and the analysis of light flashes perceived by the astronauts. In addition, the controlled impact of the Saturn V third stage produced a signal useful to the seismometers previously installed on the Moon (Uri, 2022).

*Apollo 17*

Apollo 17, conducted in December 1972 in the *Taurus–Littrow* valley, concluded the Apollo program of human lunar exploration and represented the highest development of the "J" missions (NASA, 2011). The presence of geologist Harrison H. Schmitt strengthened the scientific character of the mission, during which the crew travelled 30.5 km with the rover and collected 110.4 kg of samples, the largest quantity returned by a single Apollo mission (NASA, 2011; NASA, 2026b). The experimental program included instruments for the seismic, thermal, gravitational, and atmospheric study of the lunar environment, consolidating the scientific value of the last human mission to the surface of the Moon (NASA, 2011).

Taken as a whole, the Apollo missions marked the transition from the first human lunar landing to an increasingly articulated scientific exploration of the Moon. Apollo 11 inaugurated human and experimental activities on the lunar surface, while Apollo 12 and Apollo 14 refined landing precision and expanded instrumental and geological investigations (Loff, 2015; NASA, 2009a; NASA, 2009b). With Apollo 15 and Apollo 16, the use of the rover, the extension of surface activities, and observations conducted from orbit increased both the range and the quality of scientific exploration (NASA, 2009c; Uri, 2022). Apollo 17 ultimately represented the operational and scientific culmination of the program, owing to the presence of a geologist, the largest quantity of samples collected, and an extensive program for analyzing the lunar environment (NASA, 2011). The Apollo program thus transformed the Moon from a symbolic objective of the space race into an environment directly accessible to human scientific investigation (NASA, 2026a; NASA, 2026b).

### 2.3 Other relevant missions

United States lunar missions came to a halt with Apollo 17 in 1972, before resuming in the 1990s with *Clementine* (1994) and *Lunar Prospector* (1998). In the meantime, the USSR continued the *Luna* missions until 1976. After a long pause at the global level, January 1990 marked the first Japanese mission to the Moon, *Hiten*.

The following section presents, in chronological order, a selection of missions particularly relevant to the framework of this thesis.

*Clementine* (January 1994)

Launched on 25 January 1994, Clementine was the first United States mission directed toward the Moon in more than twenty years. It originated from a collaboration between the *Ballistic Missile Defense Organization* and NASA, with the dual objective of testing lightweight components and sensors for future low-cost missions and conducting scientific observations of the Moon. Inserted into lunar polar orbit on 19 February 1994, the spacecraft completed 297 orbits and transmitted approximately 1.6 million digital images of the surface, enabling the first

comprehensive observation of the lunar landscape, including the polar regions. Its scientific payload included ultraviolet, visible, and infrared cameras, a LIDAR system (*Light Detection and Ranging*), a high-resolution camera, a bistatic radar experiment, and instruments for gravitational and charged-particle analysis, making the mission significant both for surface mapping and for the physical characterization of the lunar environment. Among its most important results, the collected data indicated the possible presence of ice at the bottom of a permanently shadowed crater near the lunar south pole, although with considerable uncertainty regarding the estimated size of the deposit. Clementine fully achieved its intended objectives and contributed to renewing exploratory interest in the Moon, demonstrating the value of scientific missions carried out through lighter and more cost-effective technologies (NASA, 2023a)[13].

*Lunar Prospector* (January 1998)

Launched in January 1998, *Lunar Prospector* was the third mission of NASA's *Discovery Program*, designed to carry out the first complete mapping of the Moon's surface composition and gravitational field, as well as to further investigate the search for ice in the polar regions. During nearly nineteen months of activity in polar orbit, the spacecraft employed spectrometers, a magnetometer, an electron reflectometer, and gravitational experiments to characterize the lunar surface and environment. The most significant result was the detection of hydrogen at both poles by means of the neutron spectrometer, interpreted as evidence of the possible presence of water ice mixed with the polar regolith. The mission also identified intense localized magnetic fields, contributed to the global mapping of the main rock types, and detected evidence suggesting the existence of an iron-rich core, with an estimated diameter of approximately 600 km. Concluded in July 1999 through a controlled impact in the permanently shadowed *Shoemaker* crater, Lunar Prospector significantly expanded knowledge of the Moon's composition, internal structure, and potential resources, reinforcing the scientific and exploratory value of the polar regions for subsequent missions (NASA, 2026c)[14].

*LCROSS – Lunar Crater Observation and Sensing Satellite* (June 2009)

Launched on 18 June 2009 together with the Lunar Reconnaissance Orbiter (LRO), LCROSS was designed to verify the presence of water ice in a permanently shadowed crater near the lunar south pole. The mission adopted an investigation strategy based on the controlled impact of the *Centaur* upper stage into *Cabeus* crater. On 9 October 2009, the impact raised a plume of material, which LCROSS flew through a few minutes later, collecting data through visible and infrared cameras, spectrometers, and a photometer before itself impacting the surface. The acquired data confirmed the presence of water in the southern polar regions and indicated that, in some areas, it existed in the form of predominantly pure ice crystals. The mission also detected useful materials, including mercury, magnesium, calcium, silver, and sodium, contributing to the description of the Moon as a chemically active body characterized by a water cycle. LCROSS therefore had significant exploration value, as it demonstrated the importance of permanently shadowed regions as potential resource deposits for future lunar exploration (NASA, 2024a)[15].

[13] *The citation refers to the source NASA: Clementine* (NASA, 2023a).

[14] *The citation refers to the source NASA: Lunar Prospector* (NASA, 2026c).

[15] *The citation refers to the source NASA: LCROSS* (NASA, 2024a).

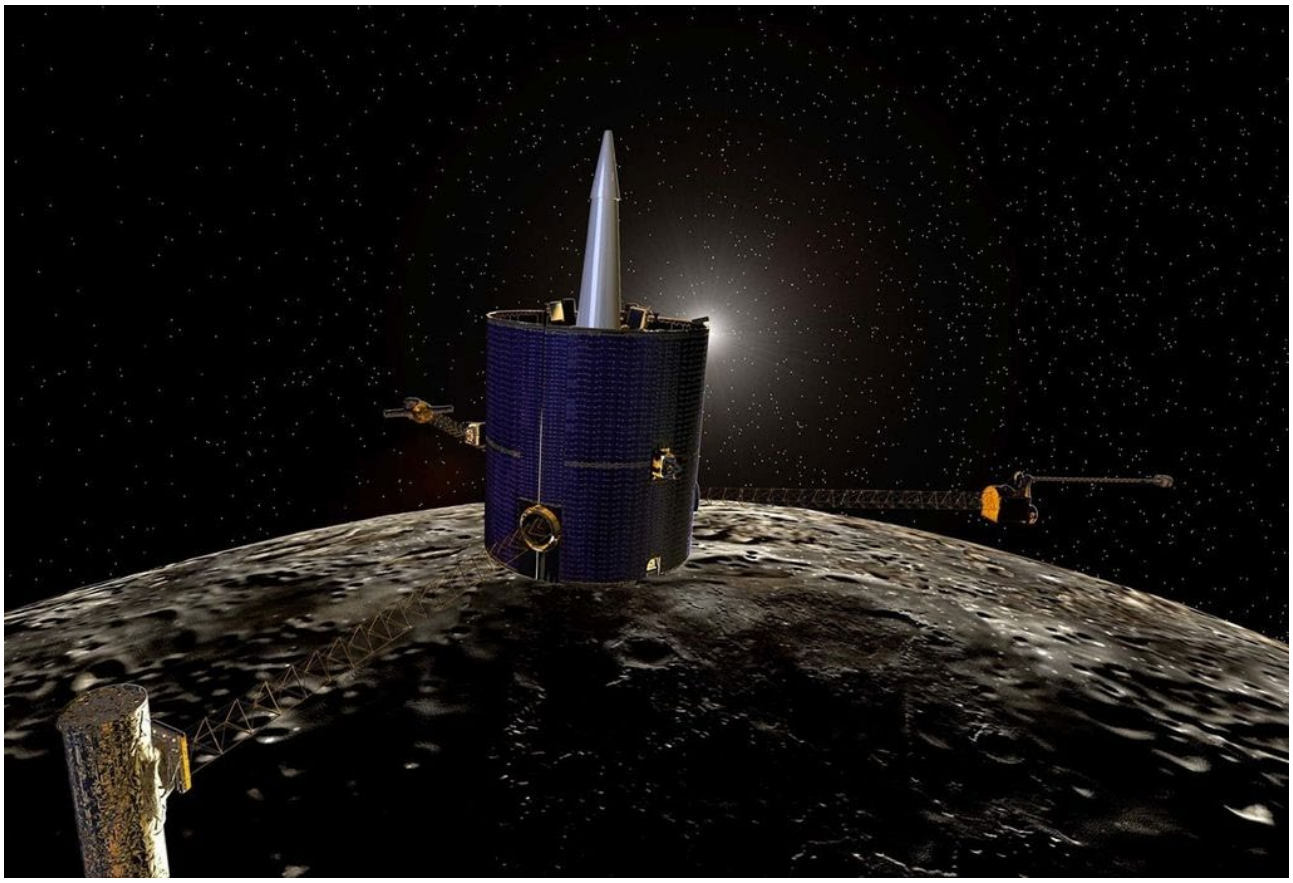


***Figure 2.3:*** *An artist's concept of the Lunar Prospector spacecraft just before impact on the Moon. Source: NASA/Ames.*

*LRO – Lunar Reconnaissance Orbiter* (June 2009)

Launched on 18 June 2009 and still operational, LRO is an orbital mission dedicated to the close study of the Moon and to the preparation of future robotic and human exploration. Over the course of its activity, which has become the longest ever conducted by a spacecraft in lunar orbit, LRO has mapped the surface of the satellite and measured its temperature, composition, and radiation environment with unprecedented detail. Among its seven scientific instruments, the *Lunar Orbiter Laser Altimeter* (LOLA) measures the altimetric profile of the surface, allowing three-dimensional representations of the lunar terrain to be constructed, including areas near the south pole. The mission data also make it possible to analyze the alternation between light and shadow in the polar regions and to identify areas characterized by the presence of fundamental resources, such as water, as well as by prolonged periods of solar illumination, which are useful for energy production and exploration activities. LRO therefore plays a central role in the scientific understanding of the Moon and in the selection of landing and operational sites (NASA, 2026d)[16].

CRaTER is one of the scientific instruments on board LRO, designed to measure radiation in the lunar space environment, particularly galactic cosmic rays and solar energetic particles. Its value is closely related to future human presence on the Moon, as it allows radiation exposure to be estimated through materials analogous to human tissue and different shielding

[16] *The citation refers to the source NASA: Lunar Reconnaissance Orbiter* (NASA, 2026d).

thicknesses. The data collected therefore contribute to assessing risks for astronauts and, at the same time, to studying the effects of radiation on the lunar environment, including ice deposits in permanently shadowed regions, where prolonged irradiation may alter their chemical composition (NASA, 2023b)[17].

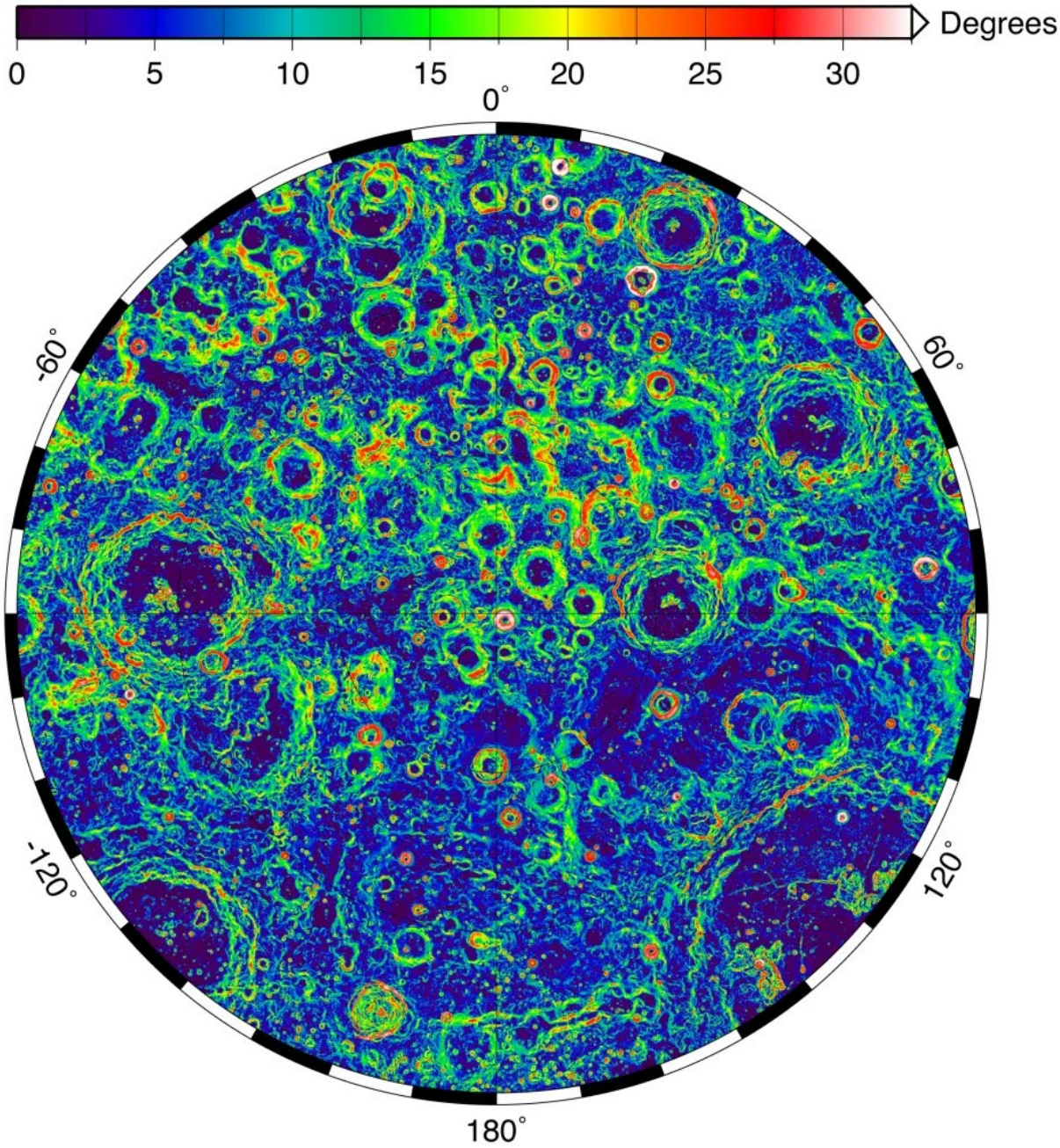



***Figure 2.4:*** *The Lunar Orbiter Laser Altimeter (LOLA) maps the lunar surface morphology, measuring variations in elevation and slope. Source: NASA.*

[17] *The citation refers to the source NASA: CRaTER, Exploring Space Radiation at the Moon* (NASA, 2023b).

*THEMIS–ARTEMIS* (2007–2010)

The THEMIS–ARTEMIS mission originated from the repurposing of two probes from the THEMIS mission (*Time History of Events and Macroscale Interactions during Substorms*), launched in 2007 to study the magnetic processes associated with terrestrial auroras. Renamed ARTEMIS-P1 and ARTEMIS-P2 (*Acceleration, Reconnection, Turbulence and Electrodynamics of the Moon's Interaction with the Sun*), the two probes were redirected toward the Moon to analyze the interaction among the solar wind, plasma, Earth's magnetosphere, and the Moon's weak magnetism. Between 2010 and 2011, they were the first spacecraft to orbit the Earth–Moon Lagrange points[18] before being inserted into lunar orbit. Through simultaneous measurements of electric and magnetic fields and energetic particles, ARTEMIS provided three-dimensional data on the lunar space environment, the plasma wake generated by the Moon, and local deformations of the interplanetary magnetic field. The mission therefore contributed significantly to the understanding of dynamic relationships among the Moon, Earth, and the Sun, providing data useful for characterizing the environment in which future lunar exploration activities will take place (NASA, 2026e)[19].

*GRAIL – Gravity Recovery and Interior Laboratory* (September 2011)

Launched on 10 September 2011, GRAIL was a mission composed of two twin spacecraft, later named *Ebb* and *Flow*, placed in lunar orbit to map variations in the Moon's gravitational field and derive information about its internal structure. During formation flight, variations in gravity slightly altered the relative distance between the two spacecraft. These changes, measured by the *Lunar Gravity Ranging System* (LGRS), made it possible to produce the highest-resolution gravitational map ever obtained for a celestial body up to that time. Over nine months of observations, GRAIL deepened knowledge of the composition and internal organization of the Moon and located the large mass concentrations, or *mascons*, present beneath the surface and formed as a result of impacts by large asteroids or comets when the lunar interior was warmer. The mission also included the *MoonKAM* imaging system, intended for educational and outreach activities, and ended on 17 December 2012 with the controlled impact of both spacecraft on the lunar surface. Owing to the precision of its gravitational mapping and its contribution to reconstructing the internal evolution of the Moon, GRAIL represented a fundamental mission in advancing geophysical knowledge of Earth's satellite (NASA, 2024b)[20].

### 2.4 Contemporary Lunar exploration and future perspectives

Contemporary lunar exploration is situated within a substantial shift in perspective. The Moon is no longer regarded solely as the destination of isolated missions aimed at sample collection or the demonstration of technical supremacy, but rather as the first extraterrestrial environment in which to test a progressively more stable and autonomous human and robotic presence, supported by dedicated lunar infrastructure. According to the *Moon to Mars* strategy, NASA identifies the Moon as the place where the procedures, technologies, and operational

[18] *In the Earth-Moon system, Lagrange points are regions of space where gravitational relations between the two bodies allow an object to maintain a relatively stable position relative to the Earth and the Moon with theoretically low energy expenditure. Among the five identifiable points, L1, L2 and L3 are unstable, while L4 and L5, also called Trojan libration points, assume particular importance because they correspond to equilibrium configurations placed at the vertices of an equilateral triangle built on the Earth-Moon line* (Di Feo, 2016).

[19] *The citation refers to the source NASA: THEMIS-ARTEMIS* (NASA, 2026e).

[20] *The citation refers to the source NASA: GRAIL (Ebb and Flow)* (NASA, 2024b).

systems required for human presence in deep space can be consolidated, while maintaining future crewed missions to Mars as the long-term objective. This approach is not based on a rigid and definitive architecture, but on an evolutionary process that can be updated in relation to the technological maturation of systems, the development of international and commercial collaborations, and the acquisition of new scientific and operational data (NASA, 2025).

The vision of the Moon as an operational element in the future expansion of human activity beyond Earth does not arise exclusively from current programs but has significant precedents in the design studies of the second half of the twentieth century. As early as the volume *NASA Space Settlements: A Design Study*, published in 1977 and edited by R. D. Johnson and C. Holbrow, the Moon was interpreted as a strategic resource for the development of space infrastructure, due to the shallower depth of its gravitational well compared with that of Earth and to the presence of materials potentially usable for the production of oxygen, metals, glass, and protective shielding. In the model described, a lunar base would not have served a purely scientific function but could also have supported the extraction and processing of regolith, the transfer of materials to other space infrastructures, and the protection of crews through the use of lunar soil as shielding against radiation, thermal extremes, and micrometeorites. Although this was an experimental study rather than an operational program, it anticipated several themes that are central today, including in-situ resource utilization, the design of protected habitats, and the transformation of the Moon from a mere exploratory destination into an enabling platform for long-duration human activities in space (Johnson & Holbrow, 1977).

The centrality of the Moon in future strategies derives, first and foremost, from its position in relation to Earth and Mars. In his volume, *Building Habitats on the Moon: Engineering Approaches to Lunar Settlements*, H. Benaroya emphasizes that the Moon can be reached in approximately three days and allows almost immediate communication with Earth, whereas a mission to Mars involves significantly longer transfer times, communication delays, and more severe operational, medical, and logistical challenges. For this reason, the Moon is interpreted as the first coherent location in which to test technologies, habitats, construction procedures, life-support systems, and the working conditions of humans and robots beyond Earth orbit, before undertaking more complex interplanetary missions (Benaroya, 2018). The author formulates the same approach in his earlier volume *Turning Dust to Gold*, in which the Moon-first strategy assigns lunar permanence the role of a testing ground for evaluating habitat reliability, maintenance processes, construction technologies, and the physiological and psychological responses of crews in a low-gravity environment that remains relatively accessible from Earth (Benaroya, 2010).

The initial phase of NASA's contemporary architecture is defined as Human Lunar Return and includes the Artemis missions aimed at re-establishing human presence on the Moon after the Apollo program. However, the return of astronauts is not understood as a repetition of twentieth century missions but is instead associated with the verification of crew and cargo transportation systems, the development of communications in lunar orbit, the progressive activation of support infrastructures, and the execution of scientific activities directly on the surface. The privileged region for these activities is the lunar south pole, considered particularly significant both for understanding the chronology and composition of the Moon and for investigating the volatiles potentially present in permanently shadowed regions, as well as the information preserved in the regolith concerning the interaction between the lunar surface and the Sun (NASA, 2025).

Within the same phase, human exploration is closely integrated with robotic missions. The *Commercial Lunar Payload Services* (CLPS) program enables NASA to acquire transportation services to the lunar surface from commercial operators for scientific instruments and technology demonstrators. These missions do not constitute a separate sector from crewed missions, but rather a fundamental preparatory and complementary tool. Indeed, they make it possible to collect data, validate technologies, characterize sites of interest, and progressively reduce the uncertainty of subsequent human operations (NASA, 2025).

A fundamental element of this architecture is the *Gateway*, an orbital outpost planned in a *Near-Rectilinear Halo Orbit* around the Moon and conceived as an infrastructure that can be progressively expanded through modules supplied by NASA and its international partners. In its initial configuration, the Gateway is expected to provide pressurized volumes, power, propulsion, communications, life support, docking capabilities, and opportunities for scientific experiments. In later phases, it may be extended through external robotic systems, airlocks, refueling capabilities, and enhanced telecommunications. Its value lies not only in supporting surface missions, but also in the possibility of testing, in the lunar environment, technologies and operational modes relevant to future missions in deep space and toward Mars (NASA, 2025).

The phase of human return is followed by the phase known as *Foundational Exploration*, oriented toward longer-duration missions, broader mobility, and the geographical expansion of activities in the lunar south polar region. In this phase, surface and orbital operations also function as operational analogues for Mars, as they allow systems, procedures, and human adaptations to be tested in a remote and hostile environment, while maintaining greater proximity to Earth than a Martian mission would allow. The scientific objectives include a deeper understanding of the Moon's geological history and evolution, the characterization of volatiles, the study of space weather, the analysis of the effects of partial gravity and the deep-space environment on living organisms, and the performance of physics experiments made possible by the specific conditions of the lunar surface (NASA, 2025).

The development of longer missions requires dedicated systems for habitation, mobility, power generation, and cargo transport. The *Initial Surface Habitat*, introduced in the Foundational Exploration phase, is conceived to accommodate two crew members for stays ranging from seven to thirty-three days, supporting extravehicular activities, scientific experiments, technology demonstrations, and environmental control and life-support functions, with the possibility of logistical resupply. Surface exploration capability is expanded by the *Lunar Terrain Vehicle,* an unpressurized rover intended for the transport of astronauts and cargo and also usable as a relay for communications and navigation, and by the *Lunar Utility Rover*, a robotic vehicle capable of moving payloads, supporting extravehicular activities, operating autonomously or remotely, and contributing to the maintenance of surface assets. The *Pressurized Rover*, by contrast, introduces the possibility of mobile habitability, associated with the conduct of scientific activities and the testing of procedures transferable to future Martian missions (NASA, 2025).

The issue of energy constitutes a determining condition for extending the duration and complexity of lunar activities. NASA introduces into the architecture a power-generation system based on nuclear fission, intended to complement the solar systems of habitats and vehicles, support operations under unfavorable illumination conditions, and enable technology demonstrations characterized by high energy demand, including those connected to in-situ resource utilization. The testing of this technology on the Moon also has preparatory

value for Mars, as it would make it possible to develop operational expertise and reduce the risks associated with the use of nuclear systems in future crewed architectures on other planetary bodies (NASA, 2025).

The most advanced perspective within NASA's architecture is represented by the *Sustained Lunar Evolution* segment, in which exploration is expected to evolve toward a more regular human and robotic presence, greater scientific capability, and the progressive use of lunar resources in productive and economic activities. In this scenario, the increase in both the number and duration of human stays depends on the ability to progressively reduce dependence on terrestrial resupply, using local resources to obtain water, support food production, and build infrastructure. NASA connects this development to *In-Situ Resource Utilization* (ISRU), initially through technology demonstrations and limited uses of regolith, subsequently through the production of propellants, and, in a broader perspective, through industrial processes capable of generating goods and services from lunar resources (NASA, 2025). The theme of ISRU is crucial for lunar settlements and for future human missions on Mars, as it emerges as the most sustainable strategy for habitat self-sufficiency and for the success of long-duration missions.

Alongside the United States strategy, the landscape of lunar exploration also includes the Sino-Russian initiative of the *International Lunar Research Station* (ILRS), defined in 2021 by the *China National Space* Administration (CNSA) and *Roscosmos* as a set of scientific infrastructures to be developed on the lunar surface and in orbit, with the possibility of involving international partners. The station is conceived to carry out activities related to the exploration and utilization of the Moon, astronomical and Earth observations from the surface, fundamental research experiments, technology verification, and studies concerning the use of in-situ resources. Initial operations are planned in robotic mode, while a later phase contemplates the possibility of human presence (CNSA & Roscosmos, 2021).

The original ILRS roadmap organizes the development of the station into three phases. The first is a reconnaissance phase, oriented toward site selection and the verification of technologies required for precision lunar landings. The second is a construction phase, aimed at developing energy, communication, logistical, and scientific systems, as well as testing ISRU. The third is a utilization phase, planned for 2036, directed toward scientific research, the expansion of infrastructure, and support for future human missions to the Moon. In this architecture as well, therefore, the return to the Moon is not reduced to a sequence of episodic missions, but rather to the progressive construction of robotic and scientific infrastructures capable of preparing a more stable human presence and a broader operational horizon for the lunar environment (CNSA & Roscosmos, 2021).

The NASA and CNSA–Roscosmos architectures present programmatic and institutional differences, yet they share a fundamental transformation in the meaning of lunar exploration. The Moon is no longer considered exclusively as an object of investigation, but as an environment in which to establish infrastructures, test technologies, and prepare future strategies for human permanence (CNSA & Roscosmos, 2021; NASA, 2025).

Within this broader framework, the question of habitation becomes one of the central conditions for transforming lunar exploration from a sequence of isolated missions into a more durable human presence. However, habitat design does not concern only the provision of pressurized volumes for crew survival; it also involves protection from the lunar environment, integration with mobility and robotic systems, the possible use of local resources, and the

progressive reduction of dependence on terrestrial resupply (Sumini, et al., 2018). For this reason, the architectural and constructional implications of extraterrestrial habitats are examined separately in Section 2.6, where different habitat classes and operational typologies are analyzed in relation to lunar and Martian settlement strategies.

*Scientific, strategic, and economic significance of Lunar exploration*

Future lunar exploration is not aimed exclusively at the construction of habitats but also retains significant scientific value. In addition to geological investigations, resource characterization, and the study of the effects of the lunar environment on living organisms, Benaroya also draws attention to the possible use of the Moon for long-duration astronomical observations. In particular, the far side could offer favorable conditions for radio telescopes and interferometric systems, owing to its shielding from the radio noise produced by Earth. The stability of the surface and the possibility of constructing extensive installations would also make the Moon of interest for optical telescopes and other scientific systems. The author specifies, however, that the convenience of placing astronomical structures on the surface must be critically assessed in relation to the alternative represented by observatories in free space or in orbit (Benaroya, 2018).

Alongside the scientific dimension, Benaroya highlights the growing economic importance of lunar development. Unlike the Apollo program, which was essentially sustained by a governmental initiative, the contemporary framework described by the author shows the progressive emergence of commercial interests associated with launch systems, space tourism, privately funded research, sample collection, and the potential exploitation of extraterrestrial resources. A future lunar base could therefore assume the role not only of a scientific and medical laboratory, but also of a logistical and economic node in cislunar space, capable of supporting local production, space transportation, and missions directed toward more distant destinations. The author nevertheless emphasizes that infrastructures of such scale could hardly be financed by private capital alone, making models of collaboration between the public sector and private enterprises necessary (Benaroya, 2018).

The development of productive and residential activities on the Moon also raises legal and ethical questions. Benaroya points to the need to define credible rules for the use of resources, operational safety, the responsibility of the actors involved, and the protection of the lunar environment, emphasizing how uncertainty regarding rights and authorizations may directly affect the capacity to invest in space infrastructure (Benaroya, 2018). A stable human presence therefore cannot be considered solely as a technical or construction-related problem, but requires long-term planning, international cooperation, environmental responsibility, and economic models capable of ensuring the continuity of activities.

In conclusion, contemporary lunar exploration and its future perspectives outline a transition from episodic visits to the construction of a progressively more stable, scientifically productive, and operationally autonomous presence. The Artemis missions and the Moon to Mars architecture place the Moon, particularly the south polar region, at the center of a program that integrates human missions, robotic activities, orbital and surface infrastructures, mobility, energy systems, and the use of local resources (NASA, 2025). In parallel, the International Lunar Research Station highlights how the construction of robotic and scientific infrastructures for a future human presence is also a shared objective among international programs distinct from the United States program (CNSA & Roscosmos, 2021).

From this perspective, the Moon assumes a dual value. On the one hand, it constitutes a scientifically relevant environment in which to advance knowledge of its geological history, volatiles, surface resources, and the effects of deep space on organisms and materials. On the other hand, it serves as the first testing ground for verifying protected habitats, ISRU technologies, energy systems, robotic procedures, and safety strategies required for human permanence beyond Earth (Benaroya, 2018; NASA, 2025). The future of lunar exploration therefore does not simply consist in the return of astronauts to the surface, but in the capacity to transform that return into the beginning of a durable and sustainable presence, increasingly capable of supporting new phases in the exploration of deep space.

### 2.5 Artemis missions

The Artemis program defines NASA's strategy for re-establishing human exploration of the Moon and progressively developing the capabilities required for future crewed missions to Mars. Unlike the Apollo program, which was primarily oriented toward the achievement of individual lunar landing missions, Artemis is conceived as a sequence of missions of increasing complexity, based on the integration of the *Space Launch System* (SLS), the *Orion* capsule, commercial lunar landing systems, and the infrastructures required to support longer-duration activities in cislunar space and on the lunar surface (Warner, 2026; NASA, 2026f)[21]. In the architecture update published in March 2026, NASA introduced an additional demonstration mission before the human return to the surface, with the aim of more accurately verifying transportation and landing systems and of proceeding, after the first surface mission, toward an indicative cadence of one lunar mission per year (Warner, 2026).

*Artemis I* (November 2022)

Launched on 16 November 2022 and concluded with splashdown on 11 December of the same year, Artemis I constituted the first uncrewed integrated test of the systems intended for human exploration of deep space, namely the SLS rocket, the Orion spacecraft, and the Exploration Ground Systems. During a 25-day mission, Orion travelled a total of approximately 2.25 million km and re-entered Earth's atmosphere at a speed of almost 40,000 km/h (NASA, 2026f). The innovative value of the mission lies above all in the operational verification of the new lunar transportation system. SLS was used in flight together with Orion for the first time, while the high-speed re-entry made it possible to assess the capsule's performance under the conditions expected for return from deep space. Artemis I therefore had a predominantly technological and preparatory function, as it enabled the acquisition of the data necessary to support the subsequent use of the spacecraft with astronauts on board (Warner, 2026; NASA, 2026f).

[21] *The citation refers to the source NASA: Artemis I* (NASA, 2026f).

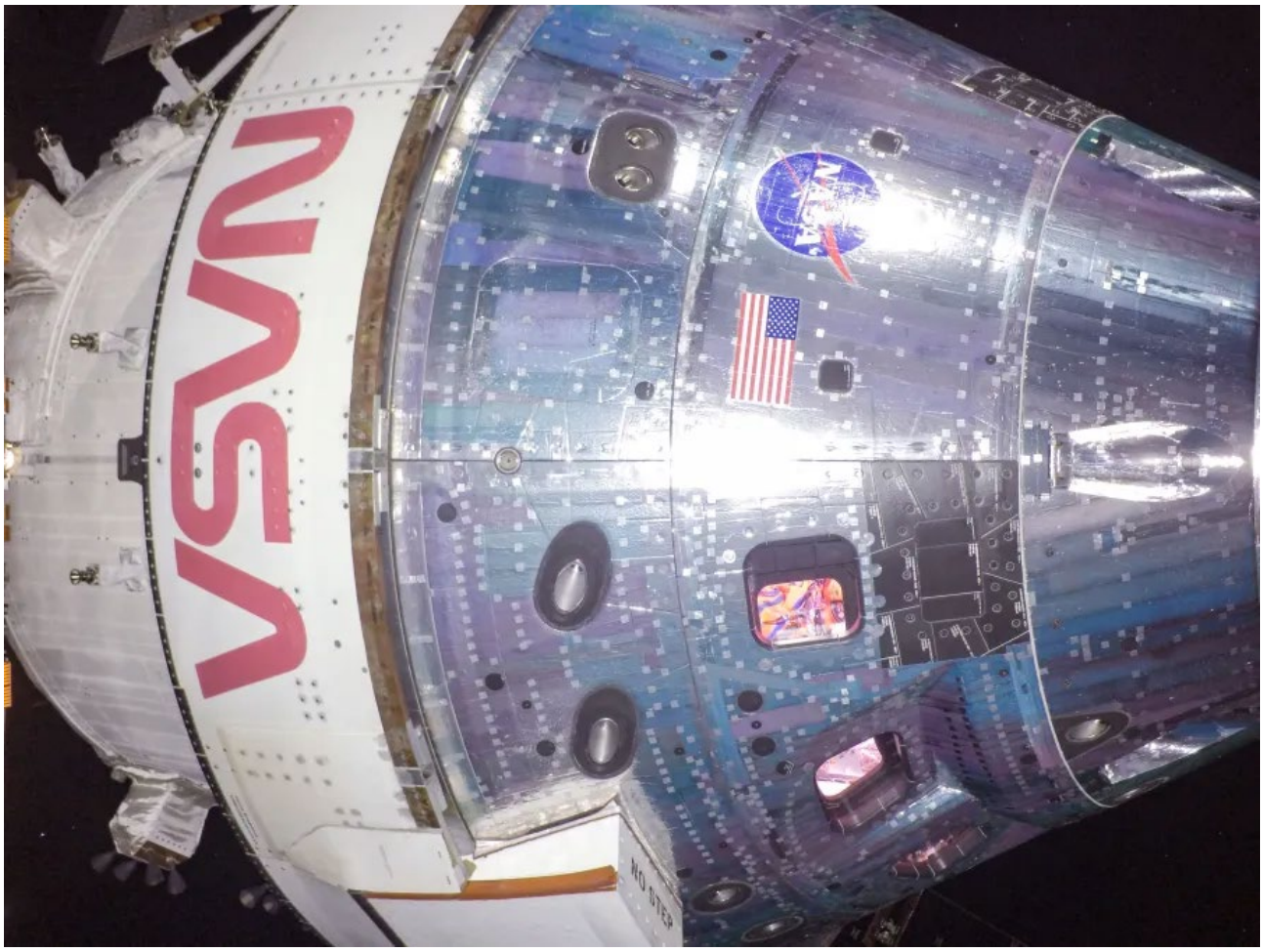



***Figure 2.5:*** *The image shows the crew module as photographed by a camera mounted on one of Orion's solar array wings. Source: NASA.*

*Artemis II* (April 2026)

Artemis II was the first crewed mission of the program and the first human flight aboard the system formed by SLS and Orion. Launch took place on April 1, 2026 and the mission involved a journey of approximately ten days around the Moon and the return of four astronauts to Earth. The exploratory value of the mission lay in verifying the transportation system with a crew present during a deep-space flight, an essential step before conducting rendezvous, docking, and subsequent descent operations toward the lunar surface (Warner, 2026).



***Figure 2.6:*** *The lunar surface dominates the image in sharp detail during the Artemis II lunar flyby, with Earth setting in the distance. Captured at 6:41 p.m. EDT on April 6, 2026, the image shows part of Earth in darkness, while clouds are visible over Australia and the Oceania region on the sunlit side. Source: NASA.*

*Artemis III* (2027)

Artemis III is designed as a new demonstration mission planned for 2027 in low Earth orbit (Warner, 2026; NASA, 2026g)[22]. The mission will launch a crew aboard Orion on SLS and will be aimed at verifying the integrated rendezvous and docking operations between Orion and one or both of the commercial landers developed respectively by *SpaceX* and *Blue Origin* (NASA, 2026g). The main innovative contribution of Artemis III therefore lies in validating the integration between a public human transportation infrastructure, consisting of SLS and Orion, and commercial systems intended to provide access to the lunar surface (Warner, 2026; NASA, 2026g).

*Artemis IV* (2028)

Planned for 2028, Artemis IV is identified by NASA as the mission intended to return humans to the surface of the Moon after more than fifty years, exploring the lunar south polar region (Warner, 2026; NASA, 2026h)[23]. The mission will transport four astronauts to lunar orbit aboard Orion, and two crew members will transfer to a commercial *Human Landing System* to reach the surface, where they will spend approximately one week before returning to orbit and rejoining the rest of the crew for the journey back to Earth. During extravehicular activities, the astronauts will wear advanced suits developed by *Axiom Space*, designed to protect them from

[22] *The citation refers to the source NASA: Artemis III* (NASA, 2026g).

[23] *The citation refers to the source NASA: Artemis IV* (NASA, 2026h).

the extreme environment of the lunar surface and to enable the planned scientific operations to be carried out (NASA, 2026h).

The scientific value of Artemis IV is linked to the possibility of conducting direct field observations, sample collection, and experiments in the southern polar region, a central area for the new phase of lunar exploration. Nine candidate landing regions have been identified near the south pole, each including different potential sites for the first human descent of the Artemis program. The planned scientific activity includes field geology, sample collection and return, and the deployment of experiments, with the aim of expanding understanding of the planetary processes that have shaped the Moon and, more broadly, the evolution of the Solar System. In this sense, Artemis IV does not represent merely the symbolic return of humans to the Moon, but the beginning of a new phase of research conducted directly in an area of the satellite never before explored by human crews (NASA, 2026h).

*Artemis V*

The Artemis architecture update envisages Artemis V as a further surface mission, associated with the beginning of the construction of a lunar base and followed, according to NASA's intentions, by missions at an approximately annual cadence (Warner, 2026). The program therefore assumes a progressive character, expressed first through the uncrewed test flight of Artemis I, then through the crewed circumlunar flight of Artemis II, the verification of commercial landers in Artemis III, and finally the return to the surface with Artemis IV and the prospect of more durable infrastructures introduced by Artemis V (Warner, 2026; NASA, 2026f; NASA, 2026g; NASA, 2026h). Overall, the Artemis program interprets the Moon not only as an exploratory destination, but as a true laboratory for research, technological experimentation, and operational development, aimed at acquiring the knowledge and capabilities required to make the extension of human exploration toward Mars possible in the future (Warner, 2026; NASA, 2026f).

### 2.6 Extraterrestrial habitats

In the field of space architecture, the habitat is an artificial environment designed to enable human presence under external conditions incompatible with terrestrial life, integrating protection, survival, operability, and the quality of the living experience (Sherwood, 2009; Häuplik-Meusburger & Bannova, 2016).

Space architecture has been defined as the theory and practice of designing and constructing inhabited environments in outer space, placing at the center of the design not only the technical system, but also the activities, physiological needs, and psychological conditions of the crew (Sherwood, 2009; Häuplik-Meusburger & Bannova, 2016; Pataranutaporn, et al., 2021). An extraterrestrial habitat is therefore not merely a confined volume, but rather a system in which the load-bearing envelope, pressure containment, life support, thermal control, radiation protection, management of extravehicular activities, and interior organization must jointly contribute to the safety and effectiveness of the mission (Kennedy, 2009; Häuplik-Meusburger & Bannova, 2016; Sumini & Mueller, 2017; Petrov, et al., 2019). In this perspective, the development of extraterrestrial habitats also opens a field for interactive systems, smart environments, human-robot interaction, telepresence, wearable technologies and computer-supported cooperative work, all of which may contribute to supporting human performance and daily life in space (Pataranutaporn, et al., 2021).

Beyond Earth's atmosphere, every human habitat must ensure a pressurized and stable internal environment, since crew survival depends on the capacity of the envelope to maintain a breathable atmosphere, temperature and humidity compatible with life, and reliable support systems. For this reason, pressurized habitation structures generally adopt geometries characterized by curved, cylindrical, spherical, or toroidal sections, while windows, hatches, connections between modules, system interfaces, and docking mechanisms constitute design-sensitive points for the tightness and safety of the system (Häuplik-Meusburger & Bannova, 2016).

The management of internal pressurization was indeed one of the central design issues addressed in the development of this thesis, since it directly influences many aspects of the structure, such as geometry, structural behavior, materials and construction strategies as well as life support systems.

Habitat design changes profoundly according to the destination environment. Orbital habitats operate predominantly in microgravity, are constrained by transportation into orbit, by the need to connect modules and external systems, and require an internal organization that is functional in relation to the absence of a gravitational regime comparable to that of Earth (Kennedy, 2009; Häuplik-Meusburger & Bannova, 2016). Planetary habitats, intended for the Moon or Mars, must instead address partial gravity, interaction with the ground, dust, landing operations, surface mobility, radiation protection through local materials and, in more advanced perspectives, in-situ construction (Häuplik-Meusburger & Bannova, 2016; Kalapodis, et al., 2020). Mobile habitats, finally, introduce an additional operational dimension, as they allow the habitable environment to move together with the crew, the instrumentation, and the resources required for scientific exploration (Cohen, 2003).

The Moon and Mars present different environmental conditions, yet both impose architectural design requirements that are far more severe than those found on Earth. In both cases, it is essential to take into account the near-total absence of atmosphere, extreme thermal variations, exposure to radiation and micrometeoroids, the presence of abrasive dust, and reduced gravity (Cohen, 2002; Kalapodis, et al., 2020).

The progression from orbital habitats to lunar and Martian settlements does not concern only the temporal extension of missions, but also the transition from structures essentially transported from Earth to systems capable of being expanded, protected and, in perspective, constructed through local resources (Cohen, 2002; Cowley, et al., 2016; Sumini, et al., 2018; Kessler & Johnson, 2024). Within this framework, the classification of habitats into Class I, Class II, and Class III provides an essential criterion for understanding the degree of dependence on Earth, the mode of installation, and the level of autonomy achievable by an extraterrestrial settlement (Cohen, 2002; Häuplik-Meusburger & Bannova, 2016; Kessler & Johnson, 2024).

The distinction between orbital, lunar, and Martian habitats concerns the operational location and the environmental conditions to which architecture must respond, whereas the distinction between Class I, Class II, and Class III primarily concerns the process of production, transportation, deployment, and construction of the habitat (Cohen, 2002; Häuplik-Meusburger & Bannova, 2016), and represents a classification that is far more relevant to the context of this research. A lunar or Martian habitat may therefore belong to one of the three classes, or combine elements from different classes, depending on the quantity of

components supplied from Earth and the proportion of construction carried out directly on site (Cohen, 2002; Cohen & Benaroya, 2009).

This classification derives from NASA's 1997 *Habitats and Surface Construction Roadmap*, later discussed by Marc M. Cohen in the study *Selected Precepts in Lunar Architecture*, in which the author introduces the definition of three fundamental categories: Class I, consisting of pre-integrated habitats delivered complete to the destination; Class II, consisting of elements prefabricated on Earth but assembled, deployed, erected, or inflated once they have reached the surface; and Class III, consisting of structures built using in-situ resources and the physical characteristics of the site (Cohen, 2002).

This classification, however, should not be interpreted as a rigid separation between self-contained categories. Cohen emphasizes that a realistic lunar or Martian base would hardly belong exclusively to a single class, since pre-integrated modules, deployable tunnels, mobile systems, airlocks, regolith shielding, and infrastructures produced in situ tend to interact within the same settlement (Cohen, 2002). Häuplik-Meusburger and Bannova also introduce a Class IV, understood as a combination of components belonging to the first three classes, in which conventional rigid modules may be expanded through deployable volumes and externally protected by structures made with regolith (Häuplik-Meusburger & Bannova, 2016).

The progression between classes may also be interpreted as a process of maturation in extraterrestrial human presence. Class I is more compatible with the earliest exploratory missions, as it prioritizes reliability and rapid use; Class II makes it possible to increase habitable volume and support longer stays; Class III opens the possibility of larger, more protected infrastructures that are progressively less dependent on terrestrial resupply (Cohen, 2002; Kessler & Johnson, 2024). NASA itself frames the future evolution of lunar habitation as an integrated transition from initial Class I and Class II modules toward Class III capabilities, without necessarily assuming the abandonment of previous technologies (Kessler & Johnson, 2024).

*Class I Habitat*

Class I habitats consist of modules manufactured and integrated before departure, generally in the form of rigid metallic or composite envelopes, designed to be delivered to the destination in already operational conditions or requiring only minimal activation. Their main advantage lies in the high level of control over the production and verification process on Earth, since the structure, systems, internal fittings, and interfaces can be tested before launch and rapidly used by the crew once the destination has been reached (Cohen, 2002; Häuplik-Meusburger & Bannova, 2016).

This initial reliability, however, entails a significant limitation. The configuration of the habitat remains strictly conditioned by the mass and volume allowed by the launcher, the transfer vehicle and, in the case of planetary bases, the landing system (Kennedy, 2009; Häuplik-Meusburger & Bannova, 2016). Rigid modules are therefore particularly suitable for early missions, critical functions, or relatively limited stays, whereas they may become less convenient when the mission requires extensive habitable areas, greater privacy, specialized laboratories, or prolonged permanence over time (Cohen, 2002; Kessler & Johnson, 2024).

The most direct and documented planetary example of a Class I habitat is the Lunar Module of the Apollo program (Figure 2.1) (Häuplik-Meusburger & Bannova, 2016). It was designed to transport two astronauts from lunar orbit to the surface, support their temporary stay on the

Moon, and enable their return to the Command and Service Module, which remained in orbit. From a configurational point of view, the Lunar Module was divided into a descent stage and an ascent stage: the former housed the descent propulsion system, tanks, and scientific equipment, while the latter contained the habitable volume, the environmental control system, communication equipment, and the instruments required for rendezvous with the vehicle in lunar orbit. The habitable volume was extremely limited, amounting to approximately 6.6 $m^3$ for two astronauts, and the internal organization reflected the limited duration and strongly operational nature of the Apollo missions (Häuplik-Meusburger, 2011). Daily activities, in fact, were not distributed across specialized spaces, but tended to overlap within the same reduced environment (Häuplik-Meusburger & Bannova, 2016). This precedent highlights both the fundamental advantage and limitation of Class I: the possibility of immediately having a functioning shelter is achieved at the cost of reduced volume and limited potential for expansion (Cohen, 2002; Häuplik-Meusburger & Bannova, 2016).

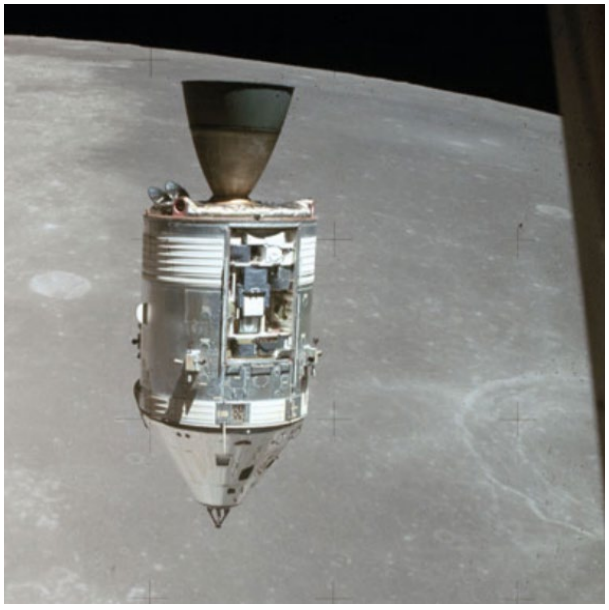




***Figure 2.7 (left):*** *The Command and Service Module of the Apollo System* (Häuplik-Meusburger, 2011).

***Figure 2.8 (right):*** *The Lunar Module of the Apollo System* (Häuplik-Meusburger, 2011).

In the orbital context, the International Space Station (ISS) may be associated with the logic of Class I when considering the individual rigid modules that compose it, since they were manufactured, outfitted, and verified on Earth before being launched and connected in orbit (Kessler & Johnson, 2024; Caiazzo, et al., 2026). However, the ISS as a whole is not a single pre-integrated module, but rather a modular station progressively assembled in orbit, organized around a central truss structure capable of supporting different pressurized elements, solar panels, radiators, and technical infrastructures (Häuplik-Meusburger & Bannova, 2016).

The internal organization of the ISS illustrates the evolution of the habitat from the multifunctional compactness of the Apollo missions toward an articulated system of specialized spaces. Indeed, the station distributes the functions of sleeping, hygiene, eating, work, and leisure across distinct environments, making evident the transition from a short-

duration vehicle to an infrastructure intended for continuous permanence in orbit (Häuplik-Meusburger, 2011; Häuplik-Meusburger & Bannova, 2016).



***Figure 2.9:*** *International Space Station* (Häuplik-Meusburger, 2011).

*Class II Habitat*

Class II habitats consist of elements manufactured on Earth and transported in a compact configuration, but they require assembly, deployment, extension, or inflation operations once they have reached space or the planetary surface (Cohen, 2002; Häuplik-Meusburger & Bannova, 2016). The fundamental characteristic of this typology is the possibility of overcoming, at least in part, the volumetric limits imposed by transportation, obtaining, after deployment, a habitable environment larger than that compatible with a pre-integrated rigid envelope (Cohen, 2002; de la Fuente, et al., 2000).

This typology includes inflatable habitats, telescopic modules, and complex deployable systems obtained through the assembly of prefabricated components on the surface (Cohen, 2002). They allow greater spatial flexibility, improved habitability conditions, and more manageable settlement growth, but they also require reliable deployment systems, sealed connections, robotic or human activation operations, and verification procedures after arrival (Cohen, 2002; Häuplik-Meusburger & Bannova, 2016; Petrov, et al., 2019).

Caiazzo confirms the importance of inflatable pressurized habitats for future lunar and Martian missions, while also highlighting how their lightness and compactness at launch are accompanied by critical issues concerning folding, deployment, equipment installation, material layering, the integration of hatches and windows, and maintenance beneath regolith shielding. Furthermore, the *Genesis I* and *Genesis II* prototypes and the *BEAM* module installed on the ISS have demonstrated in orbit the feasibility of multilayer expandable envelopes, whereas surface applications require further investigation due to the presence of gravity, local shielding, and long-term maintenance requirements (Caiazzo, et al., 2026).

One of the main examples of inflatable architecture for orbital use is *TransHab*, developed by NASA as an expandable habitation module initially intended for interplanetary missions and later evaluated as a possible addition to the International Space Station. The module consisted of a rigid central core made of graphite composite, surrounded by an inflatable envelope capable of being folded during launch and deployed once in orbit, thus providing a larger habitable volume than traditional rigid modules. The interior was organized on three levels, respectively intended for communal spaces, crew quarters with life-support systems, and functions related to physical exercise, hygiene, and medical care. Around the crew cabins, a water-based storm shelter was also planned to provide protection against intense solar events. The multilayer envelope ensured pressure containment, insulation, and protection against micrometeoroids and orbital debris, characteristics that were verified through pressure tests, vacuum deployment tests, and impact tests (de la Fuente, et al., 2000; Häuplik-Meusburger & Bannova, 2016).

In the lunar context, Cohen describes the Lunar Return Habitat designed by Kriss Kennedy[24] as a system that, once landed, autonomously or remotely deploys a pressurized bellows-like volume, as well as an antenna and an access ladder. This example shows that, in Class II, all components originate from Earth, but the final habitable configuration is achieved only through operations carried out after landing and therefore performed on the planetary surface (Cohen, 2002).

More articulated is the concept of the *Lacus Veris Lunar Outpost*, based on a large inflatable lunar dome approximately sixteen meters in diameter, integrated with an inflatable longitudinal module and designed to accommodate a crew of twelve people (Cohen, 2002). The internal section of the habitat included a lower level dedicated to environmental control and life-support systems, three intermediate levels intended for habitation and operational functions, and an upper level mainly dedicated to crew health and recreation. Although the main volume of Lacus Veris belongs to Class II, the project demonstrates the inevitably hybrid nature of advanced planetary architectures. The airlock and pressurized rovers constitute pre-integrated components attributable to Class I, the inflatable connecting tunnels belong to Class II, while the protective rings filled with lunar regolith introduce a Class III component aimed at radiation shielding and envelope protection (Cohen, 2002; Cohen & Benaroya, 2009).

[24] *Kriss J. Kennedy is one of the most renowned and experienced American "space architects", with a 30-year career at NASA Johnson Space Center. He is a pioneering figure in the field of deep-space habitat design, known for having led the development of habitation concepts for the Moon and Mars* (Kennedy, 2023).



***Figure 2.10:*** *The interiors of Lacus Veris Lunar Outpost* (Cohen, 2002).

*Class III Habitat*

Class III habitats are structures constructed, expanded, or protected through the use of local resources and the physical characteristics of the destination site (Cohen, 2002; Häuplik-Meusburger & Bannova, 2016). Their design logic is closely connected to In-Situ Resource Utilization (ISRU), since the use of regolith, sands, rocks, or natural cavities makes it possible to reduce the amount of material that must be transported from Earth and to create infrastructures more extensive than those achievable solely through the launch of prefabricated modules (Cohen, 2002; Cowley, et al., 2016; Kalapodis, et al., 2020).

This category does not necessarily imply that the entire pressurized habitat is produced using local material. Many of the proposals analyzed, in fact, envisage a hybrid system in which the pressurized and technologically more complex part continues to be supplied from Earth, while external structures, radiation protection, foundations, secondary spaces, or extensions are built on site by exploiting local resources (Cohen, 2002; Cowley, et al., 2016; Häuplik-Meusburger & Bannova, 2016). This approach allows atmospheric tightness to be entrusted to initially more controllable components, while using ISRU to progressively reduce logistical dependence on Earth and increase the resilience of the settlement (Cohen & Benaroya, 2009; Kessler & Johnson, 2024).

Class III architectures may be divided into two broad families: structures obtained through the transformation of regolith, and structures that directly use natural features of the terrain. The first family includes shielding made of loose or bagged regolith, masonry, sintered elements,

in-situ vitrified structures, concretes, or analogous materials produced using locally available components. The second family instead includes the use of crater floors or walls, topographic reliefs, cavities, excavated tunnels, and lava tubes as protective elements or as locations for the installation of pressurized modules supplied from Earth (Cohen, 2002; Cohen & Benaroya, 2009).

The use of regolith is particularly relevant for radiation and micrometeoroid protection, since a material already present on the surface can be accumulated above or around rigid and inflatable modules without requiring the entire shielding mass to be transported from Earth (Cohen, 2002; Häuplik-Meusburger & Bannova, 2016). From this perspective, regolith assumes both a constructional and a performance-related role, becoming part of the protective envelope of hybrid habitats (Cohen & Benaroya, 2009; ESA, 2020).

The use of lava tubes, natural cavities, or excavated tunnels introduces a different strategy, in which the site itself becomes part of protective architecture. Cohen observes, however, that the integration between natural cavities and pre-integrated or inflatable habitable liners raises issues of dimensional and configurational adaptation, since it is necessary to determine whether the habitable envelope should be designed according to the available cavity or whether the site should be modified to accommodate the pressurized structure (Cohen, 2002).

In the Martian context, the Lava Hive project constitutes an explicit example of a Class III habitat based on the use of local resources. The concept is based on a hybrid approach in which the central core of the habitat, intended for the crew's main spaces and critical systems, is transported from Earth, while additional environments are produced in situ using Martian sands and regolith. The Lava Hive strategy envisages the reuse of elements from the vehicle's entry, descent, and landing system, particularly the rear protection of the aeroshell, as a cover for the central core and as an additional barrier against radiation and micrometeorites. Around this core, satellite structures are produced through additive manufacturing processes, combining thermal sintering with a process referred to as lava casting, aimed at producing solid basaltic elements. The system is organized according to a modular and expandable logic, characterized by a central habitat connected to subordinate structures produced in situ. The central component maintains the most delicate habitation and technological functions, while the spaces constructed in situ expand the operational capabilities of the base and represent a concrete demonstration of the transition toward structures less dependent on Earth. However, the authors emphasize that ISRU technologies still require development, validation through simulants, and experimental demonstrations capable of confirming the properties of the materials produced and the reliability of the construction process (Cowley, et al., 2016). Class III therefore represents a strategy oriented toward long-term permanence, but depends on energy, robotic, logistical, and quality-control systems that are far more advanced than those required by initial pre-integrated modules (Cowley, et al., 2016; Kalapodis, et al., 2020).

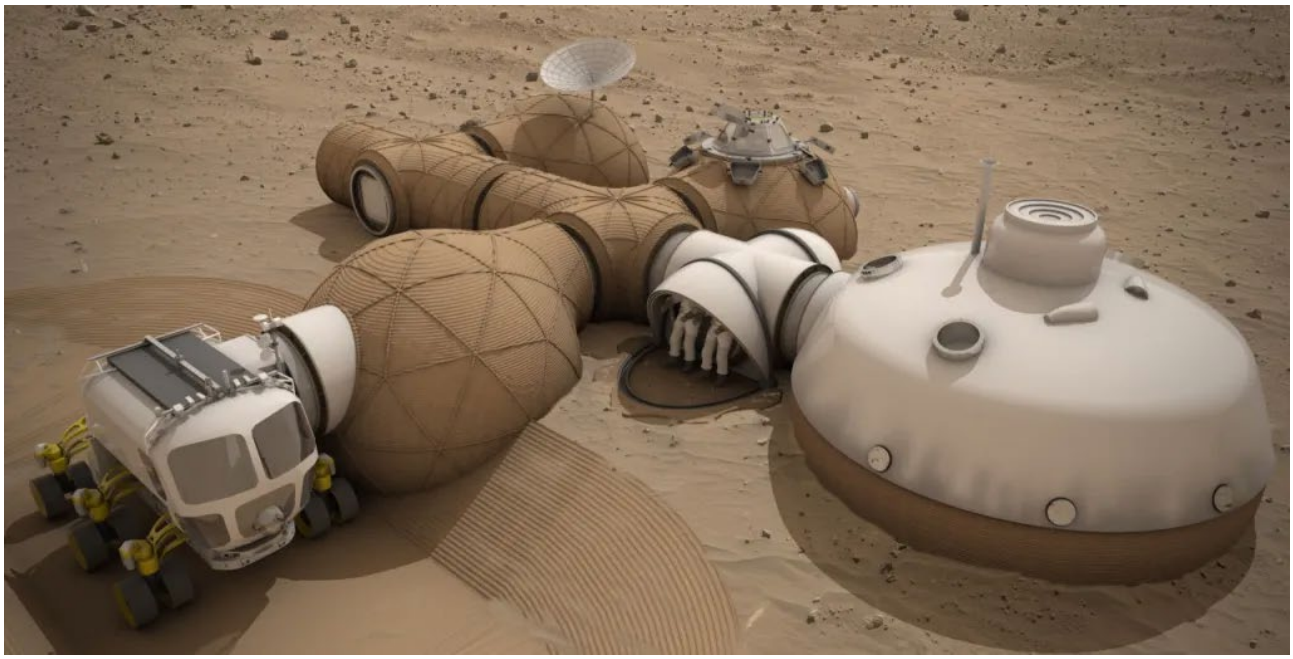


***Figure 2.11:*** *Render of the Lava Hive concept in its linear configuration* (Cowley, et al., 2016).

*Mobile Habitats*

Mobile habitats do not necessarily constitute an autonomous fourth construction class, since they can be realized through pre-integrated modules, deployable systems, or combinations of different construction strategies (Cohen, 2002; Cohen, 2003). Rather, they represent a fundamental operational typology for surface settlements, especially in relation to landing-zone safety, scientific mobility, and the redundancy of habitation systems (Cohen, 2003).

Cohen highlights how a static base makes it possible to concentrate infrastructures, resources, and services on a single site, but requires the transfer of modules and cargo away from the landing zone because of the risks generated by ejecta or by possible accidents during subsequent landing operations. Mobile habitats respond to this critical issue by allowing modules to move autonomously away from the descent area and, at the same time, accompany the crew toward areas of scientific interest, integrating pressurized shelter, laboratories, supplies, and support systems within an itinerant habitation system. This solution expands the operational possibilities of exploration, but introduces specific requirements related to modular connections, automatic or robotic assembly, locomotion reliability, redundancy, and environmental protection (Cohen, 2003). Within the framework of NASA's classification, these aspects confirm how real habitats often tend to combine multiple construction classes, integrating rigid modules, deployable systems, inflatable connections, and protections obtained from local materials (Cohen, 2002; Cohen & Benaroya, 2009).

The three classes of habitat describe a possible evolutionary trajectory of human presence beyond Earth, but they do not imply a clear replacement of one technology by the next. Class I modules guarantee the immediate availability of verified and operational environments; Class II structures expand volume, flexibility, and habitability quality; while Class III structures introduce the use of the site and local resources as the basis for a more autonomous permanence (Cohen, 2002; Häuplik-Meusburger & Bannova, 2016).

NASA considers the evolution of lunar habitation as a progression from an initial condition comprising a small Class I metallic module and a hybrid Class II surface habitat toward a sustainability phase in which it becomes necessary to evaluate the integration of Class III habitats and the reduction of dependence on terrestrial resupply. The same evolutionary architecture includes considerations of livability and psychological well-being, recognizing that the extension of permanence requires a transition from the mere satisfaction of functional needs to the introduction of social spaces, privacy, comfort, and a higher quality of the internal environment (Kessler & Johnson, 2024).

The Moon Village, designed in collaboration between ESA, the architecture firm Skidmore, Owings & Merrill (SOM) and MIT, defines an incremental process for lunar presence, where an initial habitation core must be compatible with available transportation capabilities, while the growth of the base may occur through additional modules, specialized spaces and, subsequently, protective or construction components derived from ISRU (Petrov, et al., 2019; ESA, 2020; Gollins, et al., 2021). The objective is therefore not to immediately create a complex and self-sufficient settlement, but to build a progressively expandable infrastructure, capable of learning from operational experience and incorporating more advanced technologies over time (Gollins, et al., 2021; Kessler & Johnson, 2024).

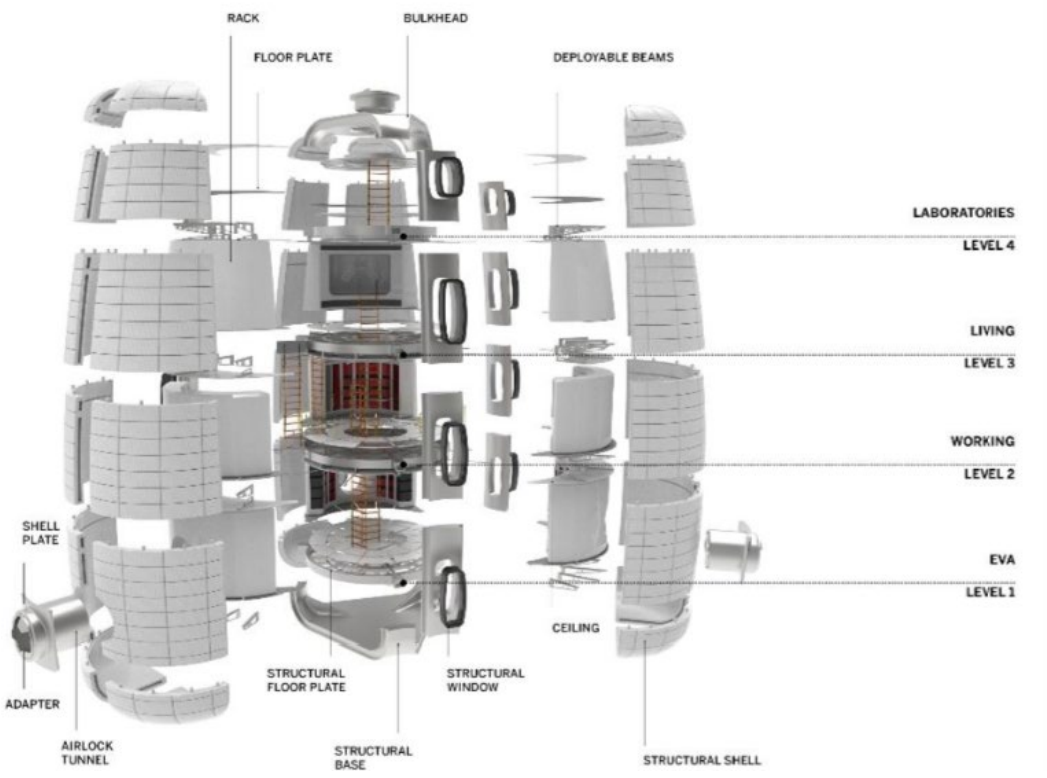



***Figure 2.12:*** *Exploded view of the Moon Village Habitat* (ESA, 2020).



***Figure 2.13:*** *Rendering of the Moon Village Habitat's interior* (ESA, 2020).

In this perspective, the Moon constitutes a privileged environment for testing this progression, since it allows habitation modules, inflatable systems, regolith protections, robotic processes, and ISRU strategies to be verified in an extraterrestrial context that is relatively more accessible than Mars (Benaroya, 2018; Kessler & Johnson, 2024; Petrov, et al., 2019). Martian proposals, such as Lava Hive, instead show how the same logics can be further developed in a more distant environment, where the use of local resources becomes even more decisive for mission sustainability (Cowley, et al., 2016; Kalapodis, et al., 2020).

The distinction into Class I, Class II, and Class III therefore makes it possible to interpret space architectures in relation to their degree of integration with launch, transportation, assembly, volumetric expansion, and construction autonomy. From essential solutions strictly constrained by mission requirements, such as the Apollo Lunar Module, to the modular architectures assembled in orbit of the ISS, and finally to inflatable habitats such as TransHab and lunar and Martian configurations based on the use of regolith and in-situ construction, a progressive transformation of the extraterrestrial habitat emerges: from a temporary shelter highly dependent on Earth to a complex habitation infrastructure capable of supporting more extensive and durable forms of human permanence beyond Earth orbit (de la Fuente, et al., 2000; Häuplik-Meusburger & Bannova, 2016; Cowley, et al., 2016; ESA, 2020).

# CHAPTER 3 – Nature Inspires

## 3.1 Biomimetics

The term *Biomimetics* derives from the Greek word *Biomimesis* (βιομίμησις) and can literally be translated as imitation of Nature. It is composed of the words *bíos* (βίος), meaning life, and *mímēsis* (μίμησις), meaning imitation. Over the years, numerous terms were coined to indicate the same concept, for example bio-inspiration, bio-design, biomimicry, or biomimetics, the latter coined by the scholar Otto Schmitt in 1957. In Europe and Asia, however, the term bionics, coined by Jack Steele in 1960, is common, referring to the concepts of biology and technology, which is why today it is more associated with the field of robotics or bioengineering (Bhushan, 2016). For convenience, from now on the term biomimetics will be used to indicate the conceptual framework where this thesis is situated.

An interesting aspect of biomimetics is its interdisciplinarity; indeed, it entails the understanding of structures and organisms, principles and biological functions, at the cellular scale, at the scale of tissues and organs, or of the whole organism. These concepts must be interpreted from a biological, chemical, physical, and engineering perspective in order to grasp natural strategies and adapt them to human systems, in this case within the context of architecture and engineering. At present, there is a great quantity of materials, structures, devices, or objects with the most varied purposes available on the market and in some way inspired by nature (Bhushan, 2016).

The literature on biomimetics has highlighted two different approaches in the search for bio-inspired design. The first is defined as top-down (*technology pull* or *problem-driven*), whereas the second is referred to as bottom-up (*biology push* or *solution-driven*). The top-down approach involves starting from a specific technical problem for which a solution is found in Nature. As a matter of fact, it is interesting to note that many of the solutions invented by humans, in various fields of application, have a natural counterpart, resulting from millions of years of highly sophisticated evolutionary processes. In this first scenario, although the initial condition is predetermined, it is possible to draw upon different biological systems, perhaps combining several together and arriving at hybrid solutions. The second case, bottom-up, is defined as solution-driven because the starting point is a biological system that is recognized as a possible solution to be applied to a technical product. In this approach, designers are instead more likely to limit their analyses to a single biological system, studying it in a very in-depth manner (Hashemi Farzaneh & Lindemann, 2019).

It is estimated that life on Earth is more than 4 billion years old; however, the organisms on which most biomimetic efforts focus are complex multicellular organisms, which developed less than 1 billion years ago. In the design process, one does not usually draw upon organisms as a whole; on the contrary, specific evolutionary characteristics are sought by analyzing every aspect of the individual model, such as genetics, physiology, internal and external morphology, and behavior. The organisms that constitute these sources of inspiration are the result of highly sophisticated and ongoing processes of adaptation and evolution spanning millions of years. In these processes, it is essential to exploit the available resources in the most efficient way possible, in order to guarantee the survival of the organism itself. This includes drawing upon resources available in their immediate surroundings, developing biological structures composed of limited chemical elements and simple molecular units. Living organisms therefore form tissues, organs, and structures organized according to hierarchies and highly differentiated, in order to respond to multiple interconnected and often contradictory

functional requirements. Knowledge and in-depth analyses in the biological field reveal, in fact, that the solutions adopted by Nature can be described by the expression “good enough,” in the sense that they are sufficiently functional to adapt to surrounding conditions, ensure evolution, proliferation, and the overcoming of rival species, adopting a strategy of economical but sufficiently good solutions. This has led to highly complex organs, such as the vertebrate eye (Knippers, et al., 2016). The logic is to do the best with what is available, because in Nature everything that can make the difference between life and death is not taken for granted and must be gained, making waste impossible. Biological solutions are, consequently, refined to perform multiple objective functions, unlike what happens with technical products.

This is a substantial difference between Nature and what is anthropic, in this particular case architecture and construction in the broad sense. Characteristics such as adaptability and multifunctionality are ubiquitous in Nature, yet scarcely widespread in construction. We design and build structures made with a wide range of different materials that compose individual units specifically designed to perform their role in the best possible way. These artefacts are the product of energy-intensive and polluting industrial processes, are often transported over long distances, and subsequently require maintenance and disposal (Knippers, et al., 2016). The aim of biomimetic architecture is certainly more than mere morphological imitation; true biomimesis should absorb the lessons that biology teaches us at the methodological level. In a context such as the current one, in which ecologically oriented solutions are increasingly widespread and necessary, the artificial product inspired by nature should more than ever take into account energy efficiency, durability, maintenance, recyclability, and resource use.

Frei Otto, the brilliant twentieth-century designer whose work greatly inspired this research, appreciated the lightness of structures, seen as synonymous with efficiency in the use of materials and as energetically advantageous. He is remembered for the realization of works such as the German Pavilion at EXPO 1967 in Montréal, the roofs for the 1972 Munich Olympic Games stadium, and the *Multihalle* in Mannheim in 1975. According to the designer, the understanding and realization of minimal and lightweight systems had to develop from the context of architecture and engineering, and then transfer this knowledge to the natural world, and not vice versa. This is a process that Knippers, Nickel, and Speck define as “*reverse biomimetics”,* in which simulation technologies assume a crucial role, enabling the analysis of biological models and their transposition and implementation in architecture. Information is therefore exchanged bidirectionally between disciplines (architecture and natural sciences) previously unconnected, as an essential part of the research process. For Frei Otto, lightness represented the sustainable future of construction, but today we know that this is not necessarily the case. A lightweight structure, which therefore uses construction material in an optimized and efficient way, cannot be considered sustainable if the materials involved are non-recyclable, energy-intensive, and have a high carbon footprint. In the current context, it appears clear that the two concepts are not necessarily consequential: if a structure is lightweight, then it is also sustainable. A particularly interesting aspect of Frei Otto’s work is form finding, an indispensable element of his design process, which is based on the equilibrium of physical forces. Today, this remains a valid process, but it must combine themes that go far beyond lightness, such as social and ecological aspects, using computational technologies to materialize this evolution (Knippers, et al., 2016).

Natural and artificial structures have various aspects in common, even when the artificial structure has been designed without taking direct inspiration from Nature; this happens because in both domains the same physical laws apply, those of statics, dynamics, and so on. For example, a concrete shell structure may present a series of similarities with the shell of a marine mollusk, given its limited thickness and high mechanical strength, and this is not necessarily a symptom of bio-inspiration, since in both cases the same laws of equilibrium and structural mechanics underlying the functioning of shell structures and marine shells are employed. From the point of view of environmental impact, as seen previously, artificial structures certainly have much to learn from natural ones. In particular, natural structures are the result of evolutionary processes that have taken place over thousands of generations, and the development of changes or new materials requires equally long periods of time. They are often capable of self-repair and regeneration, do not contemplate a safety factor and generally do not resist fire, allow large deformations, and, finally, their ultimate purpose is the survival of the species; consequently, the loss of some specimens is contemplated and accepted (Knippers, et al., 2016).

*Types of Bio-Approaches*

The book *Biomimetic Research for Architecture and Building Construction: Biological Design and Integrative Structures* by J. Knippers proposes an interesting classification of the levels of bio-inspiration.

First, there is what is defined as *Biologically Inspired Design* (BID), which has by now become very popular both in the scientific field and in marketing or fashion. This term, often abbreviated as bioinspiration or biodesign, refers to biology in general, that is, everything that presents a design inspired by and referring to "life." The meaning is deliberately vague and includes within it a series of very different approaches. Examples within this framework are various, ranging from floral applications on a dress, to aromas used in food supply chains, to buildings such as the Soma-Building at EXPO 2012 in South Korea (Knippers, et al., 2016).

The text continues by highlighting a subdivision of the concept of bio-inspiration into several categories: *Biodecoration*, *biotechnology* (including bioengineering), *bionics* (including biomimetics), and *parabionics* (Knippers, et al., 2016).

*Biodecoration*

This term refers to elements with a design inspired by Nature which, however, being decorative objects, often with an attractive aesthetic, do not have a technical functionality that simulates natural mechanisms. An interesting example in this context is the legendary Trojan horse, whose aesthetic is clearly inspired by nature, but whose function has nothing to do with the biological processes and structures of an animal such as the horse. Given the fascination that the natural world has always exerted on humankind, the examples are innumerable: Jewelry, fashion, architecture, product design, and automotive design. The works of Antoni Gaudí also fall within this category, in particular the Sagrada Familia in Barcelona, presenting sinuous and organic forms that give the structure the appearance of an organism developed through natural processes, rather than that of a building made of stone and concrete (Bhushan, 2016; Knippers, et al., 2016).

*Biotechnology and Bioengineering*

The two terms are nowadays used as synonyms. The term biotechnology was coined in 1919 by Karl Ereky, whereas bioengineering was coined in 1939 within MIT. They are currently used to indicate the use of living organisms (cells, enzymes, and biological systems) to obtain products or processes useful to humankind; that is, the mechanisms of biology are exploited for scientific or industrial purposes (Knippers, et al., 2016).

*Bionics and Biomimetics*

Although the two terms are often regarded as synonyms, bionics is generally employed more frequently in the context of mechanical construction, whereas the term biomimetics is more often used with reference to materials and systems. In both cases, nonetheless, they refer to a discipline that studies the structural and functional analogies between living organisms and electronic devices, especially with the aim of developing solutions that transfer into the technical and industrial field functions proper to living organisms.

Despite such definitions, it nevertheless remains complex to establish precisely when a product can actually be considered truly bionic. Biological species, in fact, throughout their evolutionary processes, do not merely develop efficient forms or optimized performances, but intrinsically incorporate principles of sustainability, adaptation, and parsimonious use of resources. From this perspective, a product can be defined as truly bionic not only when it formally recalls a natural element, but also when it assumes its deeper logics of functioning and of relationship with the environment. This implies taking into consideration aspects such as adaptability, multifunctionality, durability, maintenance, efficiency in the use of matter and energy, as well as end-of-life management, reuse, and disposal. Only solutions that integrate these dimensions as well, and not simply a formal or superficial analogy with nature, can therefore be considered fully consistent with an authentic bionic approach (Knippers, et al., 2016).

*Parabionics*

A final category includes products and processes presented as bionic primarily for marketing purposes, even though an estimated 80% of them show no meaningful connection to structures or processes found in nature (Knippers, et al., 2016).

*Nature's Models*

According to some estimates, approximately 10 million different species inhabit the Earth; among these, only 1.7 million have been discovered, highlighting how about 83% would still be a mystery to humankind. Within this multitude, a very large number of organisms are the subject of studies aimed at understanding and adopting one or more of their characteristics of interest in scientific or industrial fields. The most common examples are bacteria, spiders and insects, lizards, frogs, aquatic animals, birds, spider webs, lotus leaves, and an unbounded variety of plant species (Mora, et al., 2011).

In particular, plant organisms have always fascinated humankind because of their morphological variety and their functional characteristics; this includes *Arabidopsis thaliana*. The genus *Nepenthes*, a species of carnivorous plants, captures prey thanks to slippery and highly wettable surfaces consisting of microstructures with radial ridges. These form a film of

water that causes the prey to slip inward, allowing the nourishment of the plant. Leaf surfaces represent another field of great interest, thanks to extremely useful properties in industrial fields such as superhydrophobicity, self-cleaning capability, or antifouling[25]. Plants such as *Nelumbo nucifera*, also known as the lotus, are known to have leaves characterized by a hydrophobic waxy coating. Thanks to the ability of the nanostructures composing the leaves to trap air bubbles, water droplets rest on the top of the surface and slide away, thereby determining the characteristic of water repellency (Neinhuis & Barthlott, 1997; Bhushan & Jung, 2010).

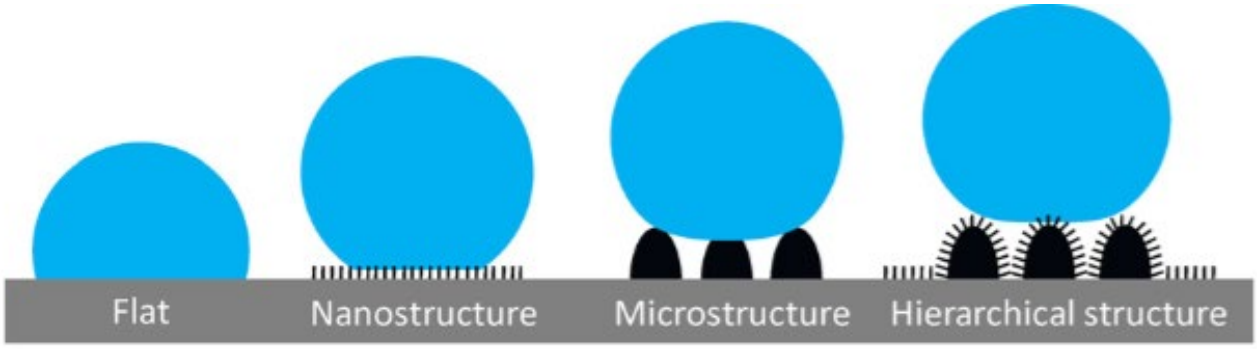



***Figure 3.1:*** *Schematic comparison of droplet wetting on four surface topographies. Flat and microstructured surfaces exhibit the largest solid–liquid contact area, while nanostructuring reduces this interaction and hierarchical structuring minimizes it further* (Bhushan & Jung, 2010).

The animal world also constitutes an immense reservoir of models from which to draw in order to develop innovative and efficient bio-solutions to technical problems. For example, it has been observed that many bacteria are equipped with a motor, similar to an electric one, composed of a starter and a drive shaft, capable of reaching 100,000 revolutions per minute, thus allowing the movement of the organism through space. Shark skin is also an interesting example. It is made up of thousands of serrated scales, called dermal denticles, with longitudinal grooves, riblets, which control vortex motion, keep the skin protected from microorganisms, and ensure antifouling (Bhushan & Jung, 2010), easily flexing together with the body of the animal (Bhushan, 2016).

As has already been pointed out, in biomimetics (or bionics) the aim is to seek a specific intrinsic function or evolutionary characteristic which, according to the designer, may constitute the solution to a given technical question, rather than observing the organism as a whole. This is the case with properties such as hydrophobicity, crucial for the reduction of resistance in fluid flows, for energy saving, and for energy conversion; or again, self-cleaning surfaces, versatile for a series of industrial applications such as solar panels, windows, fabrics, or windshields. Butterfly wings, for example, are studied because they combine superhydrophobicity, self-cleaning, and low aerodynamic resistance, as a result of a hierarchical structure of overlapping scales. A peculiar characteristic is also the phenomenon

[25] *Antifouling properties are the characteristics of a material or surface that prevent, reduce, or hinder the adhesion and accumulation of unwanted organisms, particles, or deposits on its surface. Therefore, a surface endowed with antifouling properties is designed to remain clean for longer, limiting biological or material contamination* (Nir & Reches, 2016).

known as structural coloration, due to the diffusion of light on the nanostructures that compose the wings (Sun, et al., 2013; Bhushan, 2016).

The gecko is one of the most studied and recurrent bionic reference models. More specifically, what arouses interest are its adhesive pads, which allow it to support its weight "dry" (Knippers, et al., 2016). The pads are characterized by a complex structural organization consisting of about 3 million hairs, called *setae*, which branch into 3 billion spatulae, producing an adhesion force equal to 20 N, thanks to which they can climb on almost any surface, even vertical ones, at speeds exceeding 1 m/s (Bhushan, 2016).

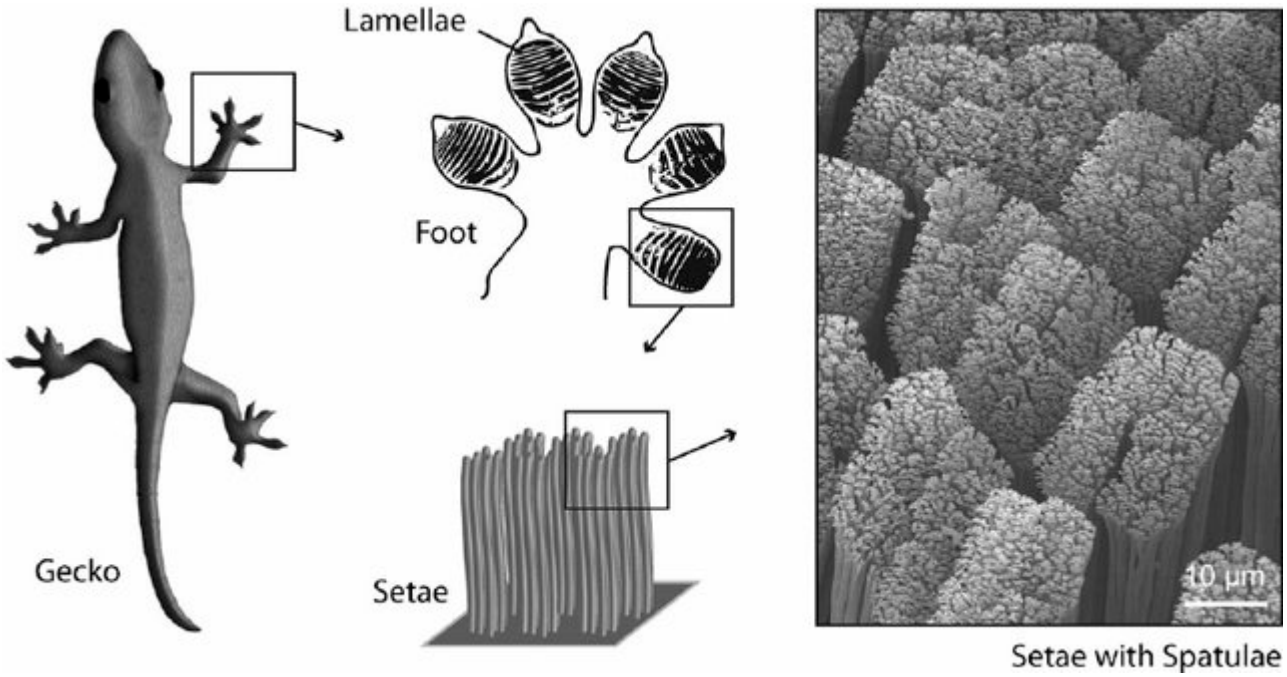



***Figure 3.2:*** *Structural organization of setae and spatulae in gecko's feet* (Heim, et al., 2010).

The ability to fly has always exerted a profound attraction on human beings, arousing wonder and the desire to understand its principles. In this regard, birds represent a privileged reference for observation and study, since their flight is made possible by the integration of highly specialized biological, structural, physical, and morphological characteristics. It is precisely this complexity that has made them among the most investigated organisms in scientific and biomimetic research. It is for these very reasons that the earliest approaches to biomimetics concerned flight. As early as the ninth and eleventh centuries, the first attempts were made by flapping wing prototypes attached to the arms. The most famous studies are probably those of Leonardo da Vinci, who realized, by studying the flight of birds, that human beings are too heavy and not strong enough to emulate their flight by repeatedly flapping their arms. These considerations led to the design of aircraft equipped with wings made of light membranes, manual levers, pedals, and pulleys, of whose actual functioning, however, we have no concrete evidence. It was the German engineer Otto Lilienthal who succeeded in the undertaking for the first time at the end of the nineteenth century, whose repeated flights are well documented. Lilienthal's prototype was improved by the Wright brothers, fascinated by his experiments and by the flight of birds (Primrose, 2020). Bird wings are structures optimized for optimal aerodynamic properties; indeed, in addition to shape, the skeleton is also structurally

organized to enable flight. The bones are strong but light, consisting of a hollow structure comparable to a honeycomb (Gruber, 2011). Birds do not constitute a model only for flying vehicles; on the contrary, their physical and biological characteristics are also highly useful in the naval and railway fields. The *Shinkansen*, famous Japanese bullet trains, are inspired by the kingfisher, a bird that can dive into water at high speeds producing an extremely small amount of splash. By analyzing its anatomy, the front of the train was designed to be 15 m long, respecting the proportions observed on the body of the animal. This strategy addressed the problem of the tunnel boom produced by the air compression as the train entered tunnels at high speed. This design choice also made it possible to reduce air resistance by 30% and energy consumption by 13%, while improving the travel experience (Primrose, 2020).

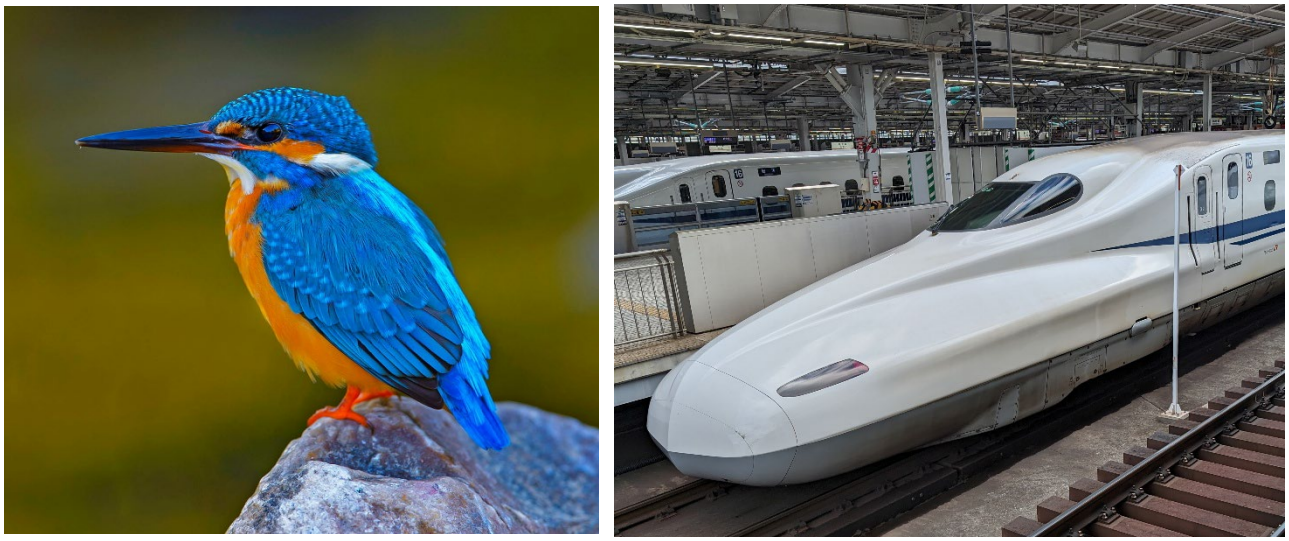


***Figure 3.3:*** *A kingfisher (left) and the Shinkansen train (right)* (Primrose, 2020).

Insects and spiders represent further case studies of considerable interest and with broad application possibilities. Spiders constitute a model of interest especially for their ability to create webs and cocoons, extremely resistant, light, and flexible structures, which have inspired research in material science and engineering. In addition, honeycomb structures, produced by social insects such as bees or wasps, constitute one of the most studied cases of the animal kingdom. They are generally made of wax and represent the geometrically densest packing possible in a two-dimensional space. Insects number over one million species and exhibit a vast series of structures and characteristics. These include compound eyes, chemoreceptors, mechanoreceptors, infrared (IR) receptors, together with their relatively compact brain and, obviously, the exoskeleton (Knippers, et al., 2016).

Another of the most studied and significant systems is represented by the inner layer of the abalone shell, namely mother of pearl (*nacre*), produced by edible marine gastropod mollusks belonging to the *Haliotidae* family. Beyond its aesthetic and commercial interest, however, nacre plays an essential biological role, since it guarantees protection of the animal's soft body thanks to exceptional mechanical properties that combine high hardness, stiffness, strength, and remarkable fracture toughness (Meyers, et al., 2006; Meyers & Chawla, 2008; Meyers, et al., 2011; Sun, et al., 2013). These performances derive from its sophisticated hierarchical organization, a laminated composite consisting of rigid aragonite platelets, a crystalline

polymorph of calcium carbonate, arranged according to a typical "*brick-and-mortar*" configuration, in which mineral platelets act as "bricks", while the thin organic layers act as "mortar". Although this organic matrix is only about 5% by weight of the material, it makes it possible to overcome the brittle behavior typical of monolithic ceramics, thanks to the thin organic interfaces that deflect and hinder crack propagation, preventing sudden failures and favoring dissipative mechanisms that significantly increase the toughness of the system. Overall, it has been observed that, thanks to a multiscale hierarchical organization, the mechanical properties of nacre clearly surpass those of the individual components. Thus, although it is made of a brittle material such as calcium carbonate, it succeeds in combining strength, hardness, and toughness (Bhushan, 2016).

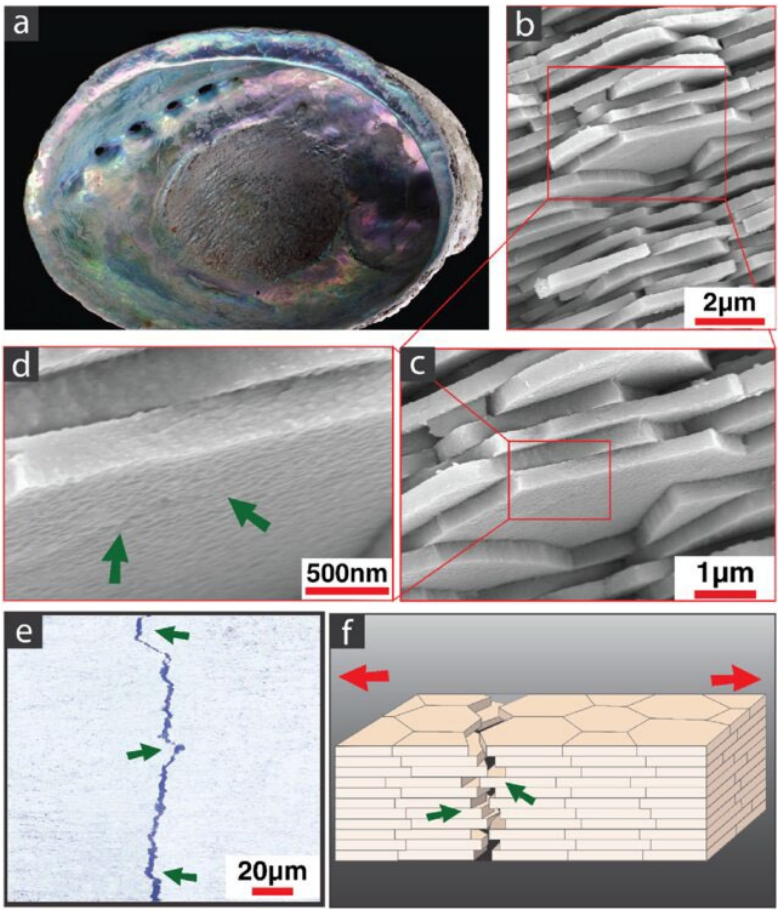



***Figure 3.4:*** *The structure of Nacre in Abalone shell* (Tiu, et al., 2023).

### 3.2 Biomimetics in Architecture and Engineering

Since the 1990s, the great interest and innovations in the field of nanoscience and nanotechnologies have led to the reproduction of natural principles through nanofabrication, generating broad and profitable commercial applications. Within the design landscape, biomimetic architecture is configured as a complex and interdisciplinary field in continuous evolution, in which the relationship with nature is not exhausted in simple formal imitation, but is articulated in a range of approaches extending from the mimesis of biological morphologies to the application of performance-based, organizational, and constructive principles derived from living systems. While scientists and engineers, by emulating biological principles, are directed toward purposes and applications that are mostly commercial, in the field of art and

architecture inspiration has both aesthetic and design-related and functional reasons, materializing biomimetics in an ornamental and structural light (Bhushan, 2016).

Up to the present day, the dialogue between architecture and science has not fully expressed its potential, especially in relation to biomimetics. This distance has been fostered by a reciprocal disciplinary separation, which has often kept the scientific sphere distinct from the design, artistic, and architectural one. Although significant cases of contamination between these worlds are not lacking, they still remain isolated experiences, situated at the margins of current practice. From this derives the need for a cultural and methodological advancement capable of bringing scientific research and design into a more structured proximity, thus making possible a full integration of bio-inspired principles and opening the way to a more mature conception of bio-architecture (Ripley & Bhushan, 2016).

In this context, the analysis of case studies assumes a fundamental role, since it makes it possible to understand in what way architects and designers have interpreted nature at different levels of depth, distinguishing between solutions that merely translate its image and strategies that, instead, assimilate its structural, environmental, material, or adaptive logics. The present chapter therefore aims to construct an analytical framework of such experiences, highlighting the different stages of biomimetic inspiration, the criteria by which the processes of transfer from the biological domain to design have been addressed, and the limits that still separate many built examples from a fully bio-inspired integration. Through this survey, the aim is to bring out not only the state of the art of the topic, but also the potential of future developments, directed toward an architecture capable of integrating the principles of nature within the design process in a more coherent and conscious way.

As can be inferred from the framework outlined so far about biomimetics, the approaches are innumerable; buildings such as the *Royal Saltworks* of Arc-et-Senans, the *Atomium* in Brussels, or the *London Aquatic Centre* constitute examples of architectures inspired by non-living nature (Ripley & Bhushan, 2016). So far, natural reference models ranging from plant organisms to innumerable animal species have been described; however, the following architectures constitute another possible perspective on biomimetics.

*Case Studies*

The *Royal Saltworks* of Arc-et-Senans were designed by Claude-Nicolas Ledoux, commissioned by Louis XVI around 1775. They constitute an interesting example of industrial architecture both for their architectural style and for their location. The project was carried out not near the point of salt extraction, but rather in the vicinity of a forest, that is, the source of the fuel that enabled its distillation. From an architectural point of view, they belong to a cultural context in which a rustic aesthetic was appreciated, mainly as a rejection of classical styles. The columns of the main building are composed of an alternation of cylinders and parallelepipeds, giving a massive and imposing appearance that recalls the salt crystals freshly extracted from the saltworks, thus constituting a symbolic link between form and function. The inspiration is therefore of natural origin; however, it does not concern living nature (Ripley & Bhushan, 2016).

The same principle applies to the *Atomium* in Brussels, created for the 1958 World Expo, and to the *London Aquatic Centre*, built on the occasion of the 2012 Olympics. In the first case, the morphology of the structure takes the cubic iron crystal as its reference model; in the second,

a wave (Ripley & Bhushan, 2016; Bhushan, 2016). These case studies cannot be regarded as bio-architecture, as it has been defined so far, but they represent the extent to which nature can fascinate and influence the design process, without concretely entering the field of bio-architecture.



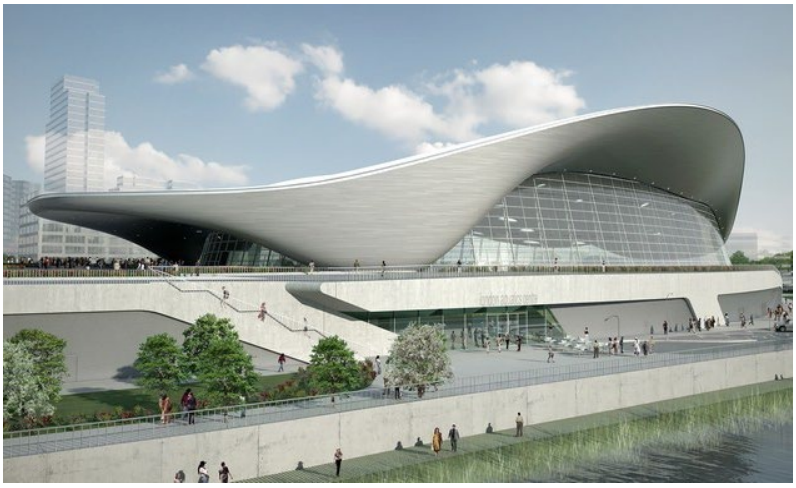


***Figure 3.5 (left):*** *The Atomium in Brussels (1958)* (Ripley & Bhushan, 2016), (Bhushan, 2016).

***Figure 3.6 (right):*** *The London Aquatic Centre (2012)* (Ripley & Bhushan, 2016), (Bhushan, 2016).

Durham Cathedral, in England, dating back to approximately the twelfth century, is interesting because it represents an example of bio-inspiration that is still embryonic and not yet fully accomplished. It does not imitate the form of an organism but can be read as an attempt to transfer into architecture a structural logic observable in nature, namely the relationship between support, load distribution, and the lightening of secondary parts. The stone roof is no longer only a weight to be supported but becomes an organized system of ribs and arches that prefigures Gothic constructive logic, imitating the structural functioning of the trunk and branches of a tree that support its crown (Ripley & Bhushan, 2016; Bhushan, 2016).

The *Sagrada Familia* by Antoni Gaudí in Barcelona was cited in paragraph 3.1.2 *Types of Bio-Approaches*, with reference to bio-decoration. Although it is true that, from an aesthetic point of view, it may fall within this sphere, it is also true that a rigid categorization of these examples is not possible. In this case as well, the logic of the load-bearing structure, particularly of the interior columns, is derived from the functioning of tree branches. Gaudí observed that the structure of tall and slender trees is not rigidly straight; on the contrary, it appears to be flexible and curves in order to support loads efficiently. In the same way, the columns of the cathedral are slender and branched to distribute the load of the roof that must be supported, but without excessively thickening their section (Ripley & Bhushan, 2016; Knippers, et al., 2016).

Following the same structural logic, an interesting case, and certainly a more recent one, is *Stuttgart Airport* (1991). Here too, the pillars supporting the roof of Terminal 1 are modulated by imitating the morphology of trees, following a structural hierarchy subdivided into trunk (composed of four tubular piles), main branches, and secondary ramifications. In this way, the overhead deck is divided into smaller portions, distributing the loads hierarchically among the various components of the pillar and producing minimal bending moments (Primrose, 2020).





***Figure 3.7 (left):*** *The interiors of Stuttgart airport (1991)* (Primrose, 2020).

***Figure 3.8 (right):*** *Detail of the vault in Exeter Cathedral (thirteenth–fifteenth century)* (Ripley & Bhushan, 2016).

A less obvious case of a bio-inspired approach is the *Nakagin Capsule Tower* in Tokyo, a work of the Japanese Metabolist movement. This current was fascinated by the cellular and metabolic organizations observed under the electron microscope, which led to considerations of organization, replication, and functional efficiency in the field of architecture. The building was in fact conceived as an aggregate of individual components, namely minimal housing units that were almost identical, which could be added following the structural framework of the building, complete their life cycle, and once this was concluded be replaced with new units, as happens with the cells of organisms. From this perspective, the main structure remained intact, while the individual units could complete a full life cycle (Ripley & Bhushan, 2016; Bhushan, 2016).

*Exeter Cathedral* (England, thirteenth–fifteenth century) constitutes a step forward in the process that is biomimetics. Here too, the weight of the roof was a considerable structural problem, given the vertical development of the building, the thickness of the perimeter walls, and the presence of large stained-glass windows. The roof is therefore subdivided into ribs, with a structural function, and infill elements built in lighter materials. The principle recalls that of ribs and intercostal spaces, constituted by muscles. This approach made it possible to reduce the loads exerted by the roof and to achieve greater heights, without compromising the static equilibrium of the building (Ripley & Bhushan, 2016).

Two more recent examples concern the *Eiffel Tower* (1889) and the *Institut du Monde Arabe* (1987), both located in Paris. The Eiffel Tower, an engineering avant-garde of its time, owes its structural organization to the force diagrams observable in long bones such as the femur. The strategy is to place greater quantities of material only where structurally necessary, thereby allowing an efficient distribution of material. Representing a completely natural optimized model, the force diagrams in these bones are still studied today in schools of architecture and engineering. As for the Institut du Monde Arabe, designed by Jean Nouvel, the architect was inspired by the human iris, in an attempt to combine technology, cultural representation, and environmental control. The south façade of the building is in fact characterized by an envelope into which artificial irises are incorporated, opening and closing automatically according to the

detected levels of light and heat. Although fascinating, the bio-reference is not the only one. The artificial irises mimic the biological structure in function and purpose, but in their aesthetics, they recall the *moucharabieh*, that is, perforated screens traditionally made of wood, typical of architecture in the Arab-Islamic world, applied to windows, balconies, or façades. They serve to filter light, encourage the passage of air, improve climatic control, and ensure a sense of privacy (Ripley & Bhushan, 2016).

The slime mould *Physarum polycephalum* is a large unicellular amoeboid organism that grows as an interconnected network in order to reach resources distributed in space. It develops a network of connections between food sources, organized hierarchically into direct and intermediate links, which serve to reduce the overall length of the network, and occasional transverse connections that improve structural efficiency. The reason for its interest in the context of this thesis work is the research by Atsushi Tero et al., *Rules for Biologically Inspired Adaptive Network Design*, which involves the mould and the design of the railway system of the Tokyo metropolitan area. The study involved the positioning of 36 food sources corresponding, in location and scale, to the cities surrounding Tokyo that constitute its metropolitan area. Territorial constraints such as bodies of water or mountainous areas were also included, imposing them on the organism through variations in light intensity, given its repulsion to intense light. The study showed that the networks developed by *Physarum* mould displayed characteristics similar to those of the Tokyo railway network, even though it acted in a self-organized manner. The study concludes that organisms such as this have probably reached a biological balance between cost, transport efficiency, fault tolerance and resilience, allowing them to act in the most functional way possible also in relation to the conditions of the substrate and the surrounding environment (Tero, et al., 2010).

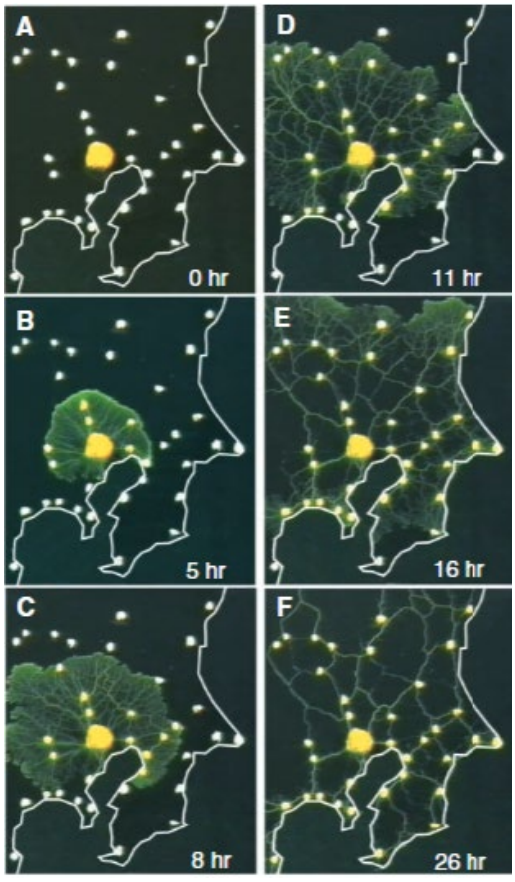



***Figure 3.9:*** *Network development in Physarum polycephalum. (A) At t = 0, a small Physarum plasmodium was positioned at the point corresponding to Tokyo within an experimental area defined by the Pacific coastline, shown by the white boundary. Additional food sources, indicated by white dots, were placed at the locations of the principal cities in the region. Each panel has a horizontal width of 17 cm. (B–F) The plasmodium expanded outward from the initial food source, maintaining a continuous advancing front and gradually reaching the other food locations. As the organism spread, the region behind the growth front reorganized into a tubular network connecting the different food sources* (Tero, et al., 2010).

The objective is not merely to identify examples in which nature has suggested formal or performance-based solutions, but to understand in what way architecture can fully express the biomimetic paradigm. The case studies indeed show different outcomes. In some experiences, the effectiveness of the functional principle emerges above all; in others, by contrast, the evocative and aesthetic value of natural forms prevails. However, none of these dimensions, taken in isolation, is sufficient to define biomimetic architecture in a complete way. For this to occur, a truly integrated and interdisciplinary approach is necessary, in which the reference to nature is exhausted neither in performance nor in image, but simultaneously involves functional logic, formal configuration, constructive processes, structural organization, energy efficiency and the use of resources, extending as far as questions of maintenance and disposal.

### 3.3 Inspiration

Conceiving structures in extraterrestrial environments entails taking into consideration a series of stringent constraints that must be central to the design process, together with the ultimate purpose that the structure is required to fulfil. Given the profound diversity of conditions compared to design on Earth, it is crucial that each of these aspects be resolved appropriately. Otherwise, the consequences may be extremely serious, with repercussions for the life of the crew and the success of the related missions.

As discussed in Chapter 1, the Moon represents a hostile and particularly complex design site, characterized by extreme temperature fluctuations, reduced atmospheric pressure, reduced gravity, radiation exposure, a rarefied atmosphere and micrometeoroid impacts (Sumini & Mueller, 2017). In light of this, any design proposal must necessarily adapt to these constraints by adopting ingenious solutions. Against this background Biomimetic design is situated.

In Section 3.1 it was discussed how, in Nature, living beings, from the animal kingdom to the plant kingdom, from multicellular to unicellular organisms, must face challenges of survival, adaptation and evolution.

Nature, as we know it today, is the result of interconnected evolutionary processes that have endured for about 4 billion years, that is, since the estimated appearance of life on Earth. Over this long span of time, the various species have had the opportunity to adapt and evolve, developing performances that would allow them to overcome the challenges imposed by Nature (Bhushan, 2016). Operating in the most efficient possible way is not only optimal but makes the difference between the survival of the individual, or of the entire species, and death. It is necessary to consider how living beings have at their disposal, in the natural context, a limited quantity of resources, subordinate to the amount available in the habitat of which they are an integral part, or to the capacity of the organism in question to access such resources. This aspect is particularly inherent to the context of this research, since in parallel the realization of lunar (or Martian) habitats presupposes the extremely scarce availability of local resources, but at the same time the need to satisfy as effectively as possible all the design requirements widely discussed so far.

Within this thesis work, the most critical design constraint is certainly that of internal pressurization. In fact, in order to allow the long-term, or in some way stable, human presence on the Moon or on Mars, it is essential to provide structures that have within them levels of pressurization comparable to terrestrial atmospheric pressure (101 kPa) (Sumini & Mueller, 2017). The most intuitive solution would be that of an inflatable, namely a structure consisting

of an extremely elastic and deformable membrane that inflates like a balloon. Membranes of this type are generally made of highly evolved and technological polymeric materials, which are obviously not present on the Moon and which, in any case, would require infrastructures for material extraction and processing up to the stage of finished product. As has already been analyzed in Section 2.6[26], the only alternative, in order to proceed in this direction, is the transport of such structures from Earth, assembled and configured *ad hoc* on the Moon to satisfy the design conditions.

The strategy proposed in this research is headed in a different direction. The intention was to attempt a well-defined approach, namely, to depend as little as possible on Earth as a source of materials, technologies, and processes for the realization of the structure. The focus is on the use of materials available *in situ* (primarily lunar regolith), capable of resisting the stresses generated by internal pressurization, mainly by virtue of its structural morphology, and of providing a protected environment in which the crew may carry out vital and operational functions safely from the radiation and extreme temperatures present outside.

Among the biological systems discussed so far, plant cells are relevant to the matter of this thesis since they combine a condition of internal pressurization, resistant envelopes, anisotropic material behavior, and a morphological configuration driven by growth. These characteristics served as meaningful references for the design of the structure.

*Arabidopsis thaliana as a Design Reference*

The question that led to considering, and then choosing, *Arabidopsis thaliana* as a design reference is the following: *How can we conceive a structure that is built using in-situ material, yet adequately withstands the tensile stresses generated by internal pressurization?*

The question is not trivial, first of all because relying, in the choice of construction material, solely on *in-situ* resources enormously limits the domain of possibilities. What the current literature explores in this context is the use of lunar, or Martian, regolith as a construction material. The possibilities for structural reinforcement range from glass or basalt fibers to carbon or hemp, depending on the case and on the "degree" of ISRU one intends to implement. Generally, the envisaged technique is that of laser sintering or, as within this study, microwave sintering, a process that involves melting regolith at extremely high temperatures until it forms a compact and resistant ceramic-like compound. Here, the issue of pressurization becomes crucial; indeed, a material such as concrete (or similar materials) exhibits very good mechanical performance in compression but is certainly not the most suitable for containing such significant tensile stresses. How, then, can two aspects that appear so contradictory be reconciled?

The answer is not immediate. Part of the solution to the question lies precisely in *Arabidopsis thaliana*, the biological reference that inspires the structure; another part of the solution lies instead in the structural morphology and in the process necessary to achieve it, which are the subject of analysis in Chapter 4[27].

[26] *Chapter 2, Section 2.6 – Class II habitats.*

[27] *Chapter 4, Sections 4.3 – The first form-finding process, and 4.4 – The second form-finding process.*

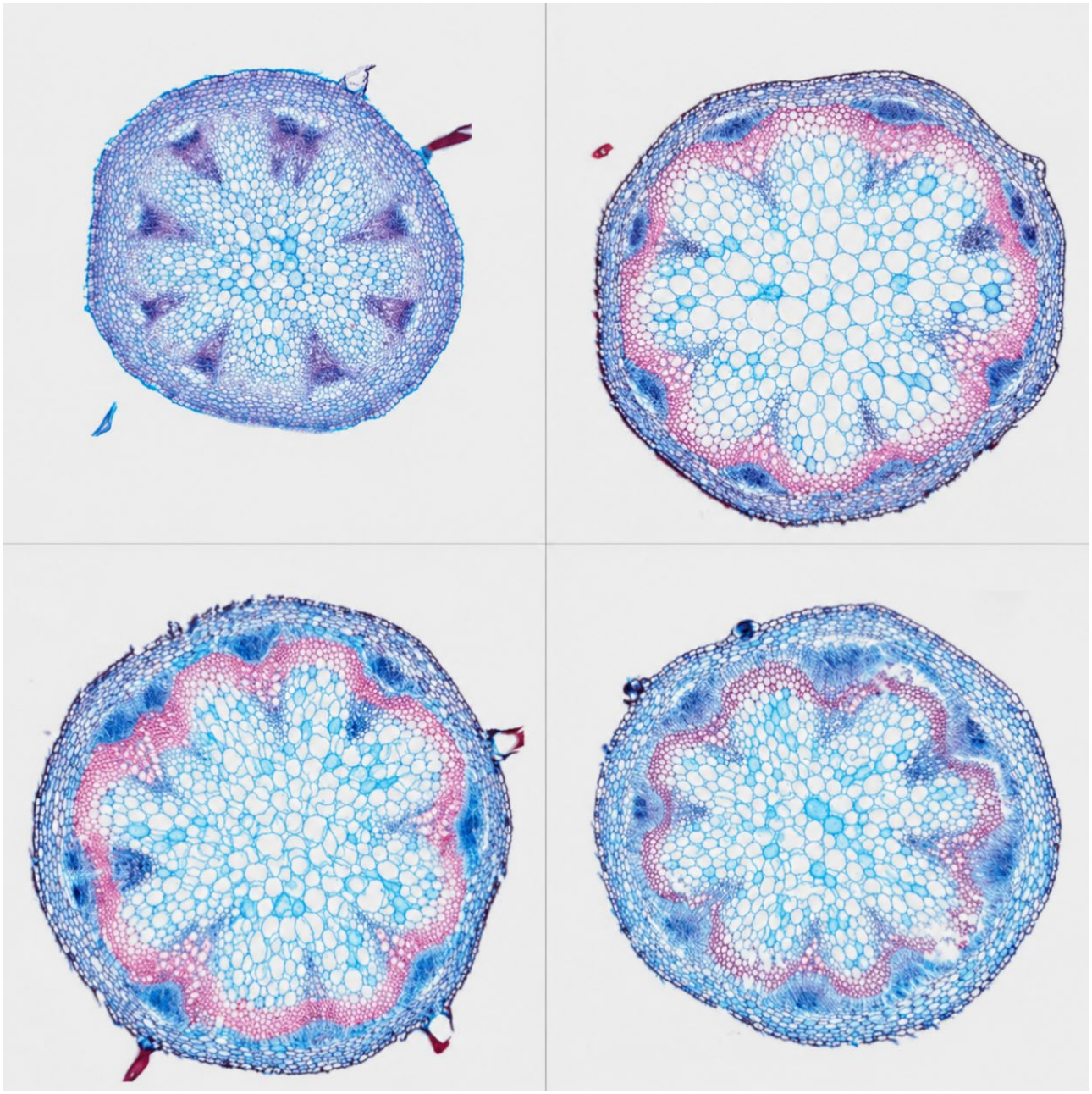


***Figure 3.10:*** *Light photomicrographs of basal stem cross-section of Arabidopsis* (Lee & Oh, 2025).

### *Biological Characteristics*

*Arabidopsis thaliana* is a dicotyledonous[28] angiosperm[29] belonging to the *Brassicaceae*[30] family. The plant group of angiosperms is one of the most diversified groups in terms of size,

[28] *Dicotyledons, or dicots, are defined as plants that have two embryonic leaves, or cotyledons. They include a variety of crops such as potatoes, beans, and fruits* (Finch, et al., 2023).

[29] *In botanical classification, a subdivision of the spermatophytes that includes plants with the highest degree of evolution; it comprises herbaceous or woody species, characterized by the presence, in the flower, of a closed ovary within which the ovules are found; the flowers are for the most part showy, more complete or complex than those of other plants, generally hermaphroditic and pentacyclic. Depending on whether the embryo possesses one or two cotyledons, angiosperms are divided into the two classes of mono- and dicotyledons* (Avetta, n.d.).

[30] *A family of plants (also called Cruciferae or crucifers) traditionally classified within the order Readales and included by modern cladistic analysis within the order Brassicales* (Treccani, n.d.).

morphology, habitat, and longevity. Their products are widely used in various industrial sectors, in the food and pharmaceutical sectors, in the timber industry, in fiber production, and even in biofuels (Shafi, et al., 2017). *A. thaliana* is a small annual plant, originally native to Eurasia, and now widespread in many of the temperate regions of the planet (Meinke, et al., 1998). It has a short life cycle, ranging from six to eight weeks, and small dimensions, from 20 to 50 cm in height. Its main components are the root system (I), which includes the primary root and lateral roots, the basal rosette (II), composed of leaves arranged radially close to the ground, the inflorescence stem (III), and it also bears small white flowers with four petals and elongated fruits called *siliques* (Meinke, et al., 1998). Thanks to its short life cycle and its very high seed production capacity, it is used as a model in a large part of studies on plant growth and development (Shafi, et al., 2017).

However, it is not the plant itself that provides the strategic and morphological reference for the project, but rather its cellular structure.

*Vascular Plants*

Vascular plants are defined as organisms endowed with specialized tissues for the transport of mineral salts, water, or various nutrients, and their evolution represents one of the most significant steps in the history of life on Earth, since it marked their presence on land and the consequent transformation of the planet. However, the conquest of the terrestrial environment was not only a physiological or genetic process, but also a profoundly structural and mechanical one. Plants, in fact, are sessile[31] organisms that cannot move in order to adapt to the environment; consequently, their evolution has been guided primarily by the ability to develop structural systems capable of resisting physical stresses, supporting vertical growth, ensuring mechanical stability, as well as implementing the most efficient strategies for sustenance and proliferation. For example, it is essential for plants to receive adequate quantities of light for their sustenance; consequently, the vertical development of the stem and the horizontal extension of branches and canopy prove extremely advantageous. This is the result of very long and complex evolutionary processes, enduring for millions of years, whose purpose is to enable the adaptation of plants to the surrounding environment and the overcoming of natural challenges (Kanahama, et al., 2023). In particular, the appearance of vascular systems, responsible for the transport of water and nutrients, has allowed these organisms to develop increasingly complex and varied structures and, in some cases, remarkable dimensions (Miyashima, et al., 2013).

Unlike animals, whose evolution has been dominated by mobility and dynamic interaction with the surrounding environment, plants are structural organisms. Animals move in search of food, shelter, or reproductive partners, whereas plants, being autotrophic and rooted in the substrate, construct their own architecture through growth processes controlled by the physics of biological materials and by the organization of cells (Niklas & Spatz, 2012). In this sense, the form of the plant is not merely the result of genetic programs but emerges from the interaction between the physical properties of cellular materials, the geometric organization of tissues, and intrinsic and extrinsic mechanical stresses. Plant morphology may therefore be interpreted

[31] *A sessile organism is an organism that lives fixed to a substrate and cannot move freely through space during its adult life* (Branch, 2001).

as the result of a complex system in which biological and mechanical principles operate simultaneously.

Animal development may be defined as determinate, whereas that of plants, by contrast, is indeterminate. This depends on the presence of meristems, namely regions composed of undifferentiated and highly proliferative cells, defined as plant stem cells, responsible for the formation of new tissues and therefore for the growth of the organism. These are essential for plant growth and for ensuring, over time, the orderly formation of new tissues and organs (Miyashima, et al., 2013).

There are various types of meristems, the apical meristems of the stem and root control primary growth, that is, the increase in length; in particular, the shoot apical meristem is described as a dome-shaped structure occupying the most apical region of the main and lateral axes and from whose activity new cells, tissues (such as vascular tissues), and plant organs such as leaves and buds derive (Beck, 2010). W. Hofmeister (1867) was the first to conclude that it is meristems, not individual cells, that control the growth and development of plants (Kutschera & Niklas, 2007). There are also lateral meristems, which instead determine the thickening of the plant axes. Among these, the most important is the vascular cambium, a meristematic tissue arranged in an almost cylindrical form around the axis of the plant, responsible for the continuous production of new cells that differentiate into vascular tissues (Miyashima, et al., 2013).

Xylem and phloem are the principal vascular tissues and may be distinguished as primary or secondary. In the first case, they develop during plant elongation and are produced by the apical meristems (primary growth). Secondary tissues are produced when the vascular cambium determines the thickening of the structure. Xylem is specialized in the transport of water and mineral salts absorbed by the roots toward the upper parts of the plant, such as the stem and leaves, and performs a structural function by contributing to the rigidity and support of the organism. Phloem, by contrast, is responsible for the transport of the products of photosynthesis from the leaves toward the other parts of the plant where these substances are used or stored, distributing nutrients throughout the organism (Beck, 2010).

*Cellular Structure*

At the cellular scale, a crucial difference between the animal and plant kingdoms is the presence of the cell wall. Unlike animal cells, which lack a rigid external envelope, plant cells are enclosed by a wall that defines their shape, strength, and mode of growth, while the internal content exerts upon it a decidedly high pressure, turgor, which contributes decisively to the mechanical stability of the tissue (Bacete, et al., 2022). The behavior and morphology of the cell wall therefore depend on the continuous interaction between internal pressure and wall resistance.

The presence of the cell wall is one of the most characteristic aspects of plant organisms. It completely encloses the protoplast (the cell content) and stably joins contiguous cells through common walls, preventing them, once division has been completed, from migrating or reorganizing themselves in space as occurs in animal cells. Consequently, plant tissues preserve a true structural memory of the cell divisions that generated them, in which the arrangement of cells in a cross section of a stem or root corresponds, in essence, to the geometric trace of the growth history of that organ. There are three different categories of cell

walls in vascular plants: The primary wall, the secondary wall, and the middle lamella. These differ from one another not only in chemical composition but also in their respective functions. From a biochemical and structural point of view, a typical cell wall is composed of three types of polysaccharides. First and foremost is cellulose, that is, a linear polymer composed of glucose units. It is organized into crystalline microfibrils that constitute the principal structural component of the cell wall. The microfibrils are interconnected by hemicellulose, a polysaccharide chain, and the whole is immersed in a soft and viscous matrix, similar to a gel, of pectin and other structural proteins (Cosgrove, 1993; Cosgrove, 2016; Zhang, et al., 2024).

From an anatomical point of view, most cell walls present a stratified structure, in which, after mitosis[32] and the formation of the middle lamella, the primary wall is formed, accompanying cell growth, and only subsequently is a secondary wall formed internally. The latter plays a particularly important role in determining the mechanical behavior of the cell, while the angular variation of the microfibrils between the layers gives the secondary wall a complex helical organization. In the secondary wall, the orientation of the microfibrils is more ordered and more closely correlated with the structural function of the cell than in the primary wall, where the microfibrils are less rigidly organized because they are deposited while the cell is still expanding (Preston, 1974; Beck, 2010).

This composite architecture is directly responsible for the mechanical properties of plant tissues. Fibrous cells, in particular, perform an essential support function by virtue of their flexibility and high tensile strength, allowing the bending of axes without rupture. Their importance is such that it has also determined technological and commercial uses, for example in the production of twine, ropes, mats, and plant textiles (Beck, 2010). Recent studies on different types of plant cells have highlighted heterogeneity in the mechanical response of the cell wall, a behavior comparable to that of composite materials. These works have outlined a stress-strain curve showing a biphasic trend of the cell wall. Initially, a linear behavior is evident, in which both the matrix and the fibers deform together. Once the yield point has been exceeded, which according to Cosgrove coincides with pressures between 0.1 and 0.3 MPa, the behavior becomes plastic and it is the matrix that continues to deform irreversibly while the fibers absorb the load. According to the latter, the addition of cellulose or hemicellulose would make the wall more resistant and would slow extension, although it would allow greater deformation before the loss of integrity (Spatz, et al., 1999; Cosgrove, 2000; Zhang, et al., 2024).

In order to understand why plant organisms, and in particular their cellular structure, constitute the morphological and structural reference of this thesis work, the study by O. Hamant, *Developmental Patterning by Mechanical Signals in Arabidopsis*, is particularly interesting. The latter focuses on the shoot apical meristem (SAM), responsible for the formation of leaves, flowers, and branches. In the study, this is defined as a pressurized vessel, comparable to an inflated shell stressed by internal pressure, demonstrating that the superficial layers of plant tissues are subjected to considerable pressures, deriving from the close interconnection between cells through the cell walls, upon which turgor pressure is exerted. The research explains that microtubules, tubular structures composed of the protein tubulin and an integral part of the cytoskeleton, align along the principal stress directions of the cell wall, establishing the position and direction of the cellulose microfibrils, which finally prove to be parallel both to the microtubules and to the directions of maximum stress. It is thus demonstrated, through mechanical models and microscopy, that microtubules influence the dynamics of cell growth

[32] *Mitosis is a tightly regulated phase of the cell cycle in which duplicated chromosomes condense and are accurately segregated by the mitotic spindle into two daughter nuclei* (Schatten, 2013).

and are directly responsible for the anisotropic behavior of the cell wall, making it more resistant in the direction parallel to the orientation of the microtubules and cellulose microfibrils. Therefore, in this context as well, clearly emerges the anisotropic behavior of the wall, highlighting how comparable it is to composite materials used in architecture or structural engineering (Hamant, et al., 2008).

The plant cell is often compared to a bicycle tire or to a balloon, that is, a pressure vessel in which the content stiffens the containing surfaces (Cosgrove, 2016; Ali, et al., 2023). Understanding turgor pressure is essential to understanding the structure of the cell and the dynamics of growth at the scale of the organism. The latter is often defined as the hydrostatic pressure imposed by the protoplast against the cell wall; it is generated by the inflow of water into the cell through the plasma membrane, which has the characteristic of being selectively permeable, and is due to osmotic processes. It plays a vital role in the various processes of the organism, such as growth and development, mechanical support, flowering, or stress response. It is important to note that turgor confers rigidity to plant cells, tissues, and organs, and rigidity is a measure of resistance to deformation. By exerting a thrust against the walls, pressure produces the expansion of tissues whose direction and magnitude are controlled by the orientation of the cellulose microfibrils in the cell walls. Consequently, the distribution of stresses and the deformations appear non-uniform. Turgor pressure can reach values up to 1.0–1.5 MPa (10–15 bar), remarkably high values when one considers the cellular scale and the thickness of the walls (Niklas & Spatz, 2012; Brulé, et al., 2016).

The tensile stress generated in the cross section of the cell wall is measured in $N/m^2$ or pascal (Pa). When stretched, the wall is subject to reversible deformation (elastic phase), that is, the increase in length along an axis and defined by the following formula: $\varepsilon = \Delta l/l$. During the expansion of the cell wall, the relevant deformation is the relative deformation in area and, if sufficiently small, it falls within the elastic phase and is defined by Hooke's law: $\sigma = E\varepsilon$, in which E represents the elastic modulus (Young's modulus) of the material. It is interesting to note the difference in values between plant and animal cells. Plant cells have values between $10^6$ Pa and $10^{10}$ Pa, clearly higher than in the animal case, in which the values do not exceed $10^5$ Pa. From the point of view of the properties of a material, the higher the value of E, the stiffer and more difficult the material is to deform. It is therefore understandable that plant cell walls can withstand decidedly higher mechanical stress compared with animal ones. However, these analyses, although they facilitate understanding, are reductive and simplistic. According to them, the cell wall is considered as a simple and homogeneous material, neglecting its composite nature (Zhang, et al., 2024).

The research by Xinyi Zhang et al., *The biomechanics of turgor pressure*, conducted on different parts of *Arabidopsis thaliana* (shoot apical meristem, pollen tube, and epidermal cells), highlights how cell geometry and the number of adjacent cells directly influence the relationship between turgor and wall stress. For example, in the pollen tube, it was observed that circumferential stress is double that in the longitudinal direction, underlining the role of cell geometry in the management of mechanical stresses. Considering that cells share their walls with adjacent ones, there is no single pressure value universally valid for all cells. Indeed, a cell with an internal pressure of up to 15 bar (1.5 MPa) may be adjacent to one with completely different pressure values (Niklas & Spatz, 2012; Zhang, et al., 2024).

The purpose of this analysis is to understand why the biological reference of this thesis work is plant cells, and particularly those of *Arabidopsis thaliana*. The structure designed here is a shell that must cope with high mechanical stress due to internal pressurization, just as occurs in

plant cells. Therefore, in the case of this thesis work as well, the morphology of the envelope, the material of which it is composed, and its structural organization are crucial for the achievement and maintenance of the equilibrium of forces and the consequent stability of the structure.

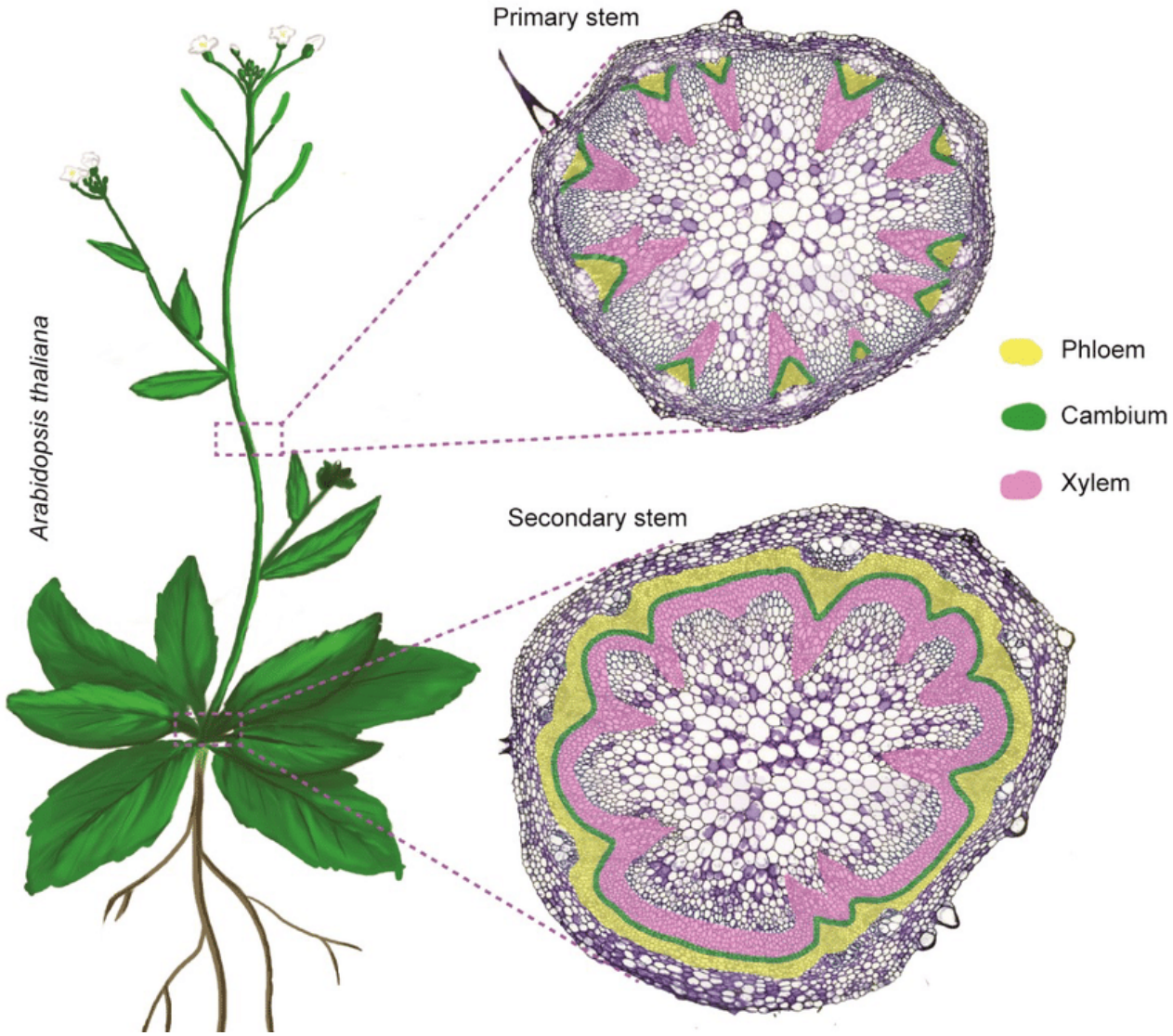



***Figure 3.11:*** *Schematic representation of primary and secondary stem growth in Arabidopsis. In the upper stem, cambium is limited to the vascular bundles, whereas near the base, interfascicular cambium develops between them, forming a continuous ring that produces xylem and phloem. The tissues are color-coded according to the legend* (Wallner, 2018).

*Cell Growth*

During growth, the cell increases its internal volume following water uptake and its wall expands until it reaches irreversible deformations. In order to grow, therefore, cells must simultaneously preserve mechanical integrity and expand their containing walls (Cosgrove, 2000). As described in the previous paragraph, cell wall growth passes through an initial elastic phase and a subsequent plastic phase, outlining a biphasic trend in the stress-strain curve. In the first case, by definition, elastic deformations are reversible and instantaneous upon the application of force; therefore, once the load is removed, the wall is able to absorb these deformations by returning to its initial configuration. When the yield point is exceeded, the plastic phase begins, where deformations are irreversible. The polymeric nature of the cell wall is responsible for the viscoelastic properties of the material; this means that, if we evaluate cell growth by considering the temporal scale, we will observe first a viscoelastic behavior and subsequently a viscoplastic one (Cosgrove, 2018).

Materials with viscoelastic mechanical properties display hybrid behaviors between elastic solids and viscous liquids. An elastic solid, upon the application of a force, deforms reversibly and immediately, and its behavior is described by Hooke's law. In the case of viscous liquids, they flow at a speed proportional to the applied force. According to Cosgrove, growing walls behave in a manner comparable to viscoelastic liquids, that is, they do not return to their original configuration once the loads are removed, whereas mature walls would be more similar to viscoelastic solids, since the morphological and dimensional conditions are re-established, almost completely, as soon as the loads are removed (Cosgrove, 1993).

In this respect, both the cell wall and turgor pressure play a crucial role. As analyzed previously, cell geometry and its wall influence the regulation of cell growth; however, it is known to the scientific community that it is turgor pressure that determines irreversible cell expansion and consequently the growth of the organism (Ali, et al., 2023). Rapidly growing cells have internal pressure values that vary according to species or growth conditions but are generally between 0.3 and 1 MPa (3–10 bar). At this point in the analysis, it appears clear that the wall is the only structural element able to contain the internal pressure, since the cytoplasmic membrane and the cytoskeleton are not capable of doing so. The wall's cross-sectional area is about one hundredth compared with the entire cell; therefore, according to Cosgrove, growing walls would withstand forces on the order of 100 MPa or 1000 bar, considering that Stress = Force / Area (Cosgrove, 1993).

When the cell must develop according to a preferential direction, the chemical composition and structural organization of the load-bearing walls are adapted so as to confer anisotropic mechanical properties (Ali & Traas, 2016). The local stiffness of the cell wall may therefore be interpreted as the outcome of a regulation of growth during development. Within this framework, hypocotyl elongation and the undulating pattern of pavement epidermal cells represent two exemplary cases useful for highlighting the heterogeneity of plant cell walls. In particular, the anisotropic elongation of the hypocotyl is traditionally traced back to the anisotropy of the cell wall, determined by the orientation of the cellulose fibers (Zhang, et al., 2024).

Considering cell wall expansion in a temporal dimension, we can highlight two phases with different time scales. It is important to note that these are not two consecutive phases, but rather two different temporal windows within the same growth process. The first, on a large scale, comprises the growth of the cell in its entirety, a relatively slow meristematic growth that

may last from hours to several days and that ends with the deposition of new material, determining thickening and stiffening of the wall. In this phase, the structure and conformation of the wall are modified as a consequence of expansion, variations in the deposition of wall materials, and the action of enzymes, outlining variations in the physical and biochemical properties of the wall, and corroborating the observations seen previously concerning the heterogeneity of the mechanical responses of the cell wall. The second growth phase, by contrast, is much shorter and lasts from a few seconds to a few hours at most. In this case, expansion is not constant over time; on the contrary, it shows continuous microvariations in speed with dynamic fluctuations, in some cases cyclic, or even irregular and in general complex. Cosgrove also clarifies the reason for the difference between the two scales; indeed, seconds or minutes are not sufficient for the wall composition to change radically through polymer synthesis and deposition, consequently the rapid variations in growth must depend above all on transient modifications of the wall environment, rather than on its complete structural reconstruction. The factors responsible for temporary changes in the wall environment are pH, reactive oxygen species (ROS), and redox potential, all factors that the cell can rapidly modulate through transport across the plasma membrane. In addition, Cosgrove explains that auxin, light, and other signals can modulate the growth rate very rapidly, even within minutes or seconds, and that precisely for this reason attention must be directed toward dynamic changes in the bonds between wall components. In other words, on the short time scale the cell does not rebuild the wall from scratch in order to consolidate the parts thinned during expansion, but rapidly modifies its mechanical state, making it temporarily more or less yielding (Cosgrove, 2000).

At this point, the role of expansins becomes important. Expansins are proteins presented as the principal agents responsible for causing stress relaxation in the wall (primary wall loosening agents), allowing water uptake and expansion. Moreover, the change in wall pH can control the rapidity and reversibility of wall responses to stresses, by activating or inactivating expansins. In conclusion, the cell rapidly modulates pH and other local wall conditions, changing the activity of expansins and of other loosening processes, causing the expansion rate to oscillate. It should finally be specified that the precise mechanism of expansin action remains uncertain; therefore, Cosgrove's research proposes a plausible interpretative framework, not a consolidated model (Cosgrove, 2000).

The analysis of the biological references, of plant cell growth and structure, provides the basis for the design strategy developed in the following chapters. The aim is not to literally reproduce the morphology of Arabidopsis thaliana, but to translate the principles of a biological organism into an architectural system. It is from these premises that a pressurized structure was developed with a geometry that actively manages the stress distribution according to a pre-established and efficient load path and whose material follows a differentiation strategy based on structural behavior. Consistent with what has been stated so far, the biological domain is a methodological reference, rather than a merely morphological one, and has guided the form-finding process discussed in the next chapter.

# CHAPTER 4 – The process

## 4.1 Shell Structures

Shell structures constitute one of the most fascinating and efficient structural typologies, widely observable both in nature and in human-made constructions. In the natural world, they can be found in numerous configurations, of both biological and abiotic[33] origin, such as air bubbles, skulls, carapaces, eggshells, cell walls, coconuts, and other hard-shelled fruits. In the anthropogenic world as well, examples are numerous and highly heterogeneous, confirming the versatility and intrinsic efficiency of this structural principle. Beyond architecture, a field in which various shell forms have been explored since antiquity, the transport sector and, more broadly, engineering have represented some of the most fertile areas for their practical development. Significant examples include automobile bodies, ship hulls, and aircraft fuselages (Petrova & Zheleva-Martins Viana, 2022).

Although no single, universally accepted definition exists, the various formulations agree in assigning a central role to geometry. The American Concrete Institute defines shells as "*Three-dimensional spatial structures composed of one or more curved slabs or folded plates whose thickness is small compared with other dimensions. Thin shells are characterized by their three-dimensional load-carrying behavior, which is determined by the geometry of their shape, the manner in which they are supported, and the nature of the applied load*." (American Concrete Institute, 2014). From this perspective, shells can be understood as thin structures in which thickness is significantly smaller than the other dimensions, and whose structural behavior depends to a decisive extent on form. As a result, geometry and structural efficiency are closely interdependent (Petrova & Zheleva-Martins Viana, 2022).

In *Hacia una Nueva Filosofía de las Estructuras*, Félix Candela described the behavior of shells by stating that "*External forces, loads, are transformed into direct or membrane stresses, that is, stresses which, at every point on the surface, are contained within its tangent plane, excluding the bending of the sheet and thus allowing the material to work in the most efficient possible way*" (Candela, 1962). When a load acts on the structure, first and foremost its self-weight, it tends to be redistributed primarily along the curved surface of the shell and transferred to the supports, from which it is then conveyed to foundations. The resulting stresses are mainly membrane stresses, namely compressive, tensile, and shear actions acting within the tangent plane of the surface. In this sense, curvature plays an essential role, since it provides the structure with geometric stiffness and promotes predominantly membrane behavior, limiting the onset of bending and torsional moments, which tend to occur especially near supports, edges, and geometric discontinuities.

The possibility of relying primarily on form for structural resistance makes shells particularly effective for spanning large distances while significantly reducing the need for internal supports. For this reason, this structural typology is frequently employed in works of considerable scale and complexity, such as stadiums, large exhibition pavilions, and airport terminals. Not surprisingly, shells may be interpreted as structures that resist through form or, to borrow an expression used by Pier Luigi Nervi, as the expression of an authentic "work by form." Nervi himself also recognized the broad presence in nature of analogous configurations, identifiable in crustaceans, insects, eggs, and plants. Nature, in fact, gives rise to systems in

[33] *Abiotic factors are defined as the non-living physical and chemical components of the environment that influence the growth of organisms, including humidity, light, temperature, substrate type, ventilation, and air pollution. These factors significantly impact biological processes and microbial colonization on various surfaces* (Ranalli, et al., 2009).

which the curvature of surfaces emerges as a recurring operative principle and in which stability derives largely from geometric configuration. Similarly, Eduardo Torroja argued that the most efficient structure is the one that bases its reliability first and foremost on form rather than on the performance of the material. Heinz Isler further observed that shell structures possess a distinctive capacity to express structural beauty (Isler, 1980), a concept also echoed by Vladimir Grigoryevich Shukhov (1853–1939), the Russian engineer and inventor, who maintained that aesthetic value implies robustness and solidity (Petrova & Zheleva-Martins Viana, 2022).

The essential elements of a shell structure are continuity and curvature, which define its form. Continuity may be understood in a material sense, as in the case of the fiberglass hull of a boat or a pressure vessel, which must constitute an almost continuous envelope in order to perform their function, even though they may be composed of different parts assembled through joints. In other cases, such as masonry domes and vaults, continuity is not material in the strict sense, since the structure is composed of distinct elements, but it is ensured at the structural level by the state of compression that keeps the blocks in mutual contact. In this sense, the fundamental character of the shell lies in its ability to behave as a structurally continuous surface, capable of transmitting forces along different directions according to the applied stresses (Calladine, 1983).

Form is therefore confirmed as the primary factor underlying the behavior of shells, always in close relation to the material, thickness, and support conditions. From this perspective, the reference to nature assumes central importance. As discussed in Chapter 3 – *Nature Inspires*, biological systems tend to maximize the effectiveness of their performance while minimizing the consumption of matter, energy, and work. Shells observable in nature are frequently doubly curved, that is, they exhibit an efficient configuration that can restrict the onset of bending moments, thereby ensuring stability and the preservation of form (Petrova & Zheleva-Martins Viana, 2022). The connection with the natural world, therefore, cannot be reduced to mere formal affinity, but extends more deeply to the underlying logics of behavior, adaptive strategies, and operative principles that govern their performance.

In light of the analysis conducted so far, shells are distinguished by a high degree of efficiency from the material, functional, constructive, and structural points of view. Their reduced thickness relative to the other dimensions allows for an economical use of material, while their load-bearing behavior, favorable strength-to-weight ratio, and considerable stiffness confirm their remarkable effectiveness, especially in large-span structures (Petrova & Zheleva-Martins Viana, 2022).

*Classification of shell structures*

The types of shell structures are numerous and may be categorized according to different criteria, although this is not a rigid classification, since the same type of shell may simultaneously fall into more than one category. The first distinction must be made on the basis of shell geometry, and in particular in relation to its Gaussian curvature (Farshad, 1992).

To define the geometry of a shell, it is necessary to know two fundamental aspects of it: the middle surface and the thickness. If one considers a generic point on its surface, identified as point A, one may imagine a tangent plane at that point and its perpendicular line, normal to the surface at that given point. Starting from this normal, one may imagine an infinite number of

planes passing through point A and containing it. The intersection of each of these planes with the surface generates a curve; these curves are called normal sections, and they make it possible to observe how the surface curves in different directions. Each normal section in fact has its own curvature and a corresponding radius of curvature. Among all the possible sections, the fundamental ones are the two principal sections, identifiable by the maximum and minimum curvature, which are denoted as K1 and K2. An important aspect is that these principal directions are always orthogonal to each other, and their product generates the so-called Gaussian curvature:

$$K = K1 \times K2$$

Through this quantity, it is possible to classify the surface and better understand its geometric behavior. When the value is positive ($K > 0$), the surface is synclastic and curves in the same direction along both principal directions, as in domes or spheres. When the value is negative ($K < 0$), the surface is anticlastic and curves in opposite directions, as in saddles or many tensile structures. When the value is 0 ($K = 0$) the surface is singly curved, as in cylinders or cones, and curvature occurs in only one direction. A related criterion concerns developability. Cylinders and cones can be flattened onto a plane without deformation, whereas doubly curved surfaces generally require cutting or stretching and are therefore non-developable (Farshad, 1992).

This distinction is also relevant from a structural point of view. Non-developable surfaces, precisely because they cannot easily be "laid out" onto a plane, often tend to resist deformation more effectively and are generally more stable and stronger than developable surfaces of similar dimensions (Farshad, 1992).

A further classification, particularly useful in the study and design of shells, finally distinguishes surfaces according to their mode of generation. In this sense, it is possible to identify:

• Surfaces of revolution, obtained by rotating a curve around an axis;

• Translation surfaces, generated by moving a curve along a given direction or along another profile;

• Ruled surfaces, obtained through the movement of a straight line in space.

This classification is particularly useful because it makes it possible to recognize not only the form of the shell, but also the geometric principle by which it can be generated and therefore studied or designed (Farshad, 1992).

It is also possible to provide a brief overview of the most common shell structures, some of them extremely ancient and used in various architectural typologies for centuries, others of more recent application.

*Hemispherical domes*

The hemispherical dome may be defined as a doubly curved shell with positive Gaussian curvature, that is, as a synclastic shell of revolution. It is one of the most emblematic and enduring architectural configurations in the history of architecture, widely employed in different periods and contexts, from the celebrated buildings of ancient Rome, such as the Pantheon, to Romanesque and Byzantine basilicas, and up to modern and contemporary architecture (Farshad, 1992; Vidya Vijay, et al., 2023). In many cases, the dome continues to assume a strong symbolic and representative value, characterizing institutional and monumental

buildings, such as parliaments, for example the United States Capitol and the Hungarian Parliament, as well as major Christian religious architectures, such as St. Peter's Basilica and the Panthéon in Paris.

*Barrel vaults*

The barrel vault is an architectural system formed by the succession of identical arches arranged in sequence, thus generating a continuous covering of semicylindrical form. Appreciated for its constructive clarity, structural robustness, and the expressive force of its geometry, this typology has a very ancient history. From the earliest applications of the arch among the Etruscans and the civilizations of the Near East, to its full establishment as a constructive principle in the Roman world (Swenson, 2026), the barrel vault has been used in a great variety of buildings, from the baths and basilicas of antiquity to Romanesque and Byzantine cathedrals, and even in some modern public architectures, such as contemporary stations and libraries (Vidya Vijay, et al., 2023).

*Hyperbolic paraboloids*

Hyperbolic paraboloids, also commonly referred to as *hypars* or saddle shells, constitute a specific category of architectural and structural forms characterized by an anticlastic doubly curved surface. Their geometric configuration in fact recalls the shape of a saddle, being defined by two opposite curvatures developed along mutually orthogonal directions, conventionally associated with the x and y axes. From a geometric point of view, the hyperbolic paraboloid also belongs to the family of ruled surfaces, since it can be generated by means of a set of straight lines appropriately arranged in space, a feature that has also favored its significant diffusion in the field of construction (Tak Lee, 1962).

*Gridshells*

Within the framework of shell structures, gridshells constitute a particular family of shell structures in which the surface continuity typical of traditional shells is replaced by a reticular configuration of linear elements, without abandoning the load-bearing principle based on form and curvature. More generally, a shell structure may be defined as a curved surface structure that derives its resistance primarily from geometry and that works through a combination of membrane actions and, secondarily, bending, generally being thin in the direction perpendicular to the surface (Steinar Hillersøy, et al., 2021; Manuello Bertetto, et al., 2024a; Manuello, 2020).

In this sense, gridshells are shell structures in every respect, since they share with them the behavior associated with double curvature and the ability to transfer loads through form, despite being composed of a grid rather than a continuous surface (Sanket G, et al., 2022; Manuello Bertetto, et al., 2024a; Manuello, 2020). This configuration makes them particularly interesting in the field of contemporary architecture, both for their efficiency in the use of material and for the expressive possibilities offered by the lightness of the structural mesh and the legibility of the constructive logic. Their construction may also be advantageous in terms of prefabrication, transport, and assembly, while the filigree character of the whole gives the structure a tectonic quality in which elements, joints, and materials make the static behavior of the system perceptible (Steinar Hillersøy, et al., 2021; Manuello Bertetto, et al., 2024b; Manuello, 2020).

Within this category, it is possible to distinguish two main types: bending-active gridshells, obtained through the elastic deformation of the elements, and discrete gridshells, instead composed of straight members assembled through joints specifically configured to resolve the overall geometry of the shell.

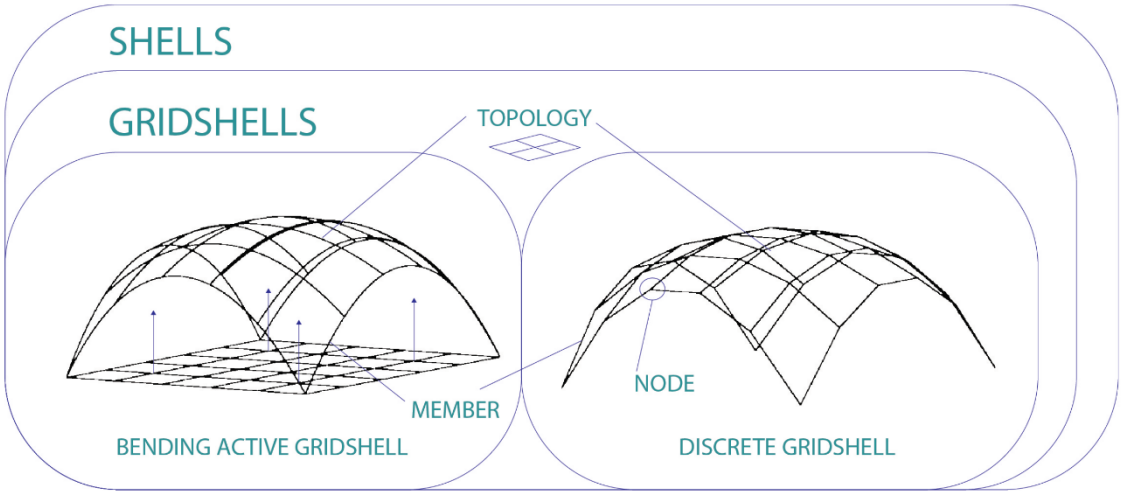



***Figure 4.1:*** *A diagram illustrating the classification of shell structure typologies* (Steinar Hillersøy, et al., 2021).

*Bending-active gridshells*

Bending-active gridshells are structures in which the elements are initially arranged in a planar configuration and subsequently raised until they reach the final doubly curved shell form (Steinar Hillersøy, et al., 2021).

The kinematic construction process is in fact one of the most characteristic methods for their realization and consists in progressively deforming a grid, generally rectangular or quadrangular, by lifting some of its parts until the desired three-dimensional configuration is achieved (Sanket G, et al., 2022). In these structures, the mesh is typically quadrilateral and may be organized in one or more layers in each direction, so as to allow curvature to form through the controlled bending of continuous members. Once the shape has been achieved, the elements are fixed in place to prevent further movement, generally through the tightening of the connections and the addition of diagonal bracing or cables, which are necessary to ensure shear stiffness in the plane of the grid (Steinar Hillersøy, et al., 2021). Timber is particularly well suited to this type of application because of its favorable bending properties, which is why many of the most well-known bending-active gridshells have been built with timber elements that were initially straight and subsequently curved in situ (Sanket G, et al., 2022).

The most emblematic example of this family is generally recognized as Frei Otto's Multihalle in Mannheim, which recurs several times within this research as a design reference and which demonstrated the formal and structural potential of a grid capable of acquiring resistance through elastic deformation and double curvature (Steinar Hillersøy, et al., 2021).

*Discrete gridshells*

Discrete gridshells, often also referred to as rigid gridshells, differ from the previous type because they do not derive their form from the continuous bending of the elements, but rather from the assembly of straight members connected to one another through joints. In this case, the geometry of the shell emerges from the configuration of the network and above all from the ability of the joints to resolve the geometric variations between the elements, such as plan angle, inclination, and torsion, according to the global form and the adopted topology. Unlike bending-active gridshells, in discrete gridshells the members are therefore composed of discrete elements extending from one joint to the next, and the behavior of the whole depends to a large extent on the geometric precision of the mesh and the mechanical quality of the connections. The most common topologies are quadrilateral and triangular, but the pattern of the network may assume many different configurations, defining the order of connectivity between elements and joints and directly affecting both the structural performance and the architectural expression of the system. From a constructive point of view, these structures generally employ steel or timber members that intersect according to a predetermined geometric pattern and are assembled through rigid joints, making it possible to realize complex curved surfaces even when straight elements are used. The joint, in particular, does not simply coincide with the theoretical point of intersection in the digital model, but constitutes an actual construction device that makes the connection between multiple members physically feasible and which, precisely because of the significant stresses to be transferred, is often made of metal even when the grid itself is composed of another material (Steinar Hillersøy, et al., 2021).

It follows that discrete gridshells represent a variation of the shell structure concept in which the continuity of the shell is not material but geometric and structural, since the overall continuous form is obtained through the ordered cooperation of discrete elements.

*Examples of shell structures*

Within this subsection, a brief series of case studies exemplifying contemporary shell structures is presented. However, it is important to emphasize that the shell principle has a much older and deeper history, intimately connected to the development of human building experience. From its earliest forms of adaptation to the environment, humankind has in fact observed, interpreted, and progressively assimilated spatial and structural configurations capable of enclosing and protecting with the minimum use of material. In this sense, the shell should not be understood exclusively as a twentieth-century engineering invention, but rather as a universal constructive principle that has been present for centuries in multiple fields of human activity, as well as a universal morphological configuration abundantly employed in the natural world.

Its most archaic manifestations can be found in ceramics, basketry, the earliest forms of dwelling, rural constructions such as barns and granaries, and funerary buildings, where curved, continuous, and thin surfaces already emerged as an intuitive response to needs of containment, protection, transport, and shelter. Long before the theoretical formalization of shell structures, humankind had therefore empirically understood the effectiveness of curvilinear and membranal forms, exploiting their ability to distribute stresses, improve stability, and optimize available resources. In light of this long genealogy, the case studies analyzed in this chapter do not represent the origin of the shell concept, but rather one of its most evolved and recent outcomes. They show how an ancient constructive principle, born

from intuitive and vernacular practices, has found in contemporary architecture and engineering an extraordinary opportunity for development (Petrova & Zheleva-Martins Viana, 2022).

Within the panorama of shell structures, the contribution of certain designers has been decisive both on the theoretical and on the constructive level. Among the most important are Buckminster Fuller (1895–1983), pioneer of the geodesic dome; Idelfonso Sánchez del Río Pisón (1898–1980), author of innovative modular corrugated shells; Eduardo Torroja (1899–1961), who brought the shell to an extraordinary level of structural and expressive maturity; Anton Tedesko (1903–1994), a key figure in the diffusion of thin shells in the United States; Oscar Niemeyer (1907–2012), who explored their potential in Brazil; Félix Candela (1910–1997), renowned for his extremely thin hyperbolic paraboloids; Eero Saarinen (1910–1961), interpreter of fluid and catenary forms; Kenzo Tange (1913–2005), author of large structures marked by strong monumental tension; Eladio Dieste (1917–2000), who demonstrated the possibilities of brick in doubly curved shells; Frei Otto (1925–2015), innovator of lightweight structures and membranes; and Heinz Isler (1926–2009), master of form-finding through physical models. More recently, these figures have been joined by Frank Gehry (1929), Norman Foster (1935), Nicholas Grimshaw (1939), and Santiago Calatrava (1951), who have continued to reinterpret the theme of the shell in contemporary design (Petrova & Zheleva-Martins Viana, 2022).

*Zeiss Planetarium (1923–24), Jena, Germany*

The Zeiss Planetarium in Jena is generally recognized as one of the earliest and most significant applications of the thin reinforced concrete shell. Built in Germany between 1923 and 1924, the building features a concrete dome with a diameter of 16 m and a thickness of only 3 cm, an exceptionally small value that makes it one of the most extraordinary examples of structural slenderness of its time. This minimal use of material made it possible to achieve a considerable reduction in overall weight, bringing it to approximately one thirtieth of that of a traditional dome of the same dimensions. The project was developed by Walter Bauersfeld, chief engineer at Carl Zeiss, with the contribution of structural engineer Franz Dischinger of Dyckerhoff & Widmann AG. The structure consisted of a steel rod framework clad in ferrocement, a configuration that emblematically anticipated the development of subsequent thin concrete shells (Petrova & Zheleva-Martins Viana, 2022).




***Figure 4.2:*** *Zeiss Planetarium.*

*Zarzuela hippodrome (1934–41) Madrid, Spain*

This is probably Eduardo Torroja's most iconic work, emblematic of his ability to combine structural audacity, formal lightness, and constructive innovation. The racecourse features three grandstands, the two lateral ones measuring 60 m in length and the central one 30 m, all topped by an extraordinarily slender and innovative roof. The latter, built with a variable thickness of only 5 cm at the tip and 14.5 cm at the supports, is striking for its extreme thinness and for the impression of almost impossible suspension that it succeeds in evoking. The roof consists of a continuous sequence of doubly curved shell sectors, with a geometry traceable to that of a hyperboloid, and develops into a bold 12.80 m cantilever (Cassinello, 2016).

"*They have asked me on various occasions how I conceived the design of the Hipódromo de la Zarzuela... And then the question arises: is the invention of a form particularly suited to the solution of a concrete problem purely a process of imagination, or is it the result of logical reasoning based on technical form? I do not believe it is either of these two things alone, but rather a mixture of both. Imagination alone could not arrive at such a design without the help of reason, nor could a deductive process, advancing through successive stages of refinement, be so logical and deterministic as to lead inevitably to such a design*." (Torroja, 1958).



***Figure 4.3:*** *Zarzuela hippodrome.*



***Figure 4.4:*** *Zarzuela hippodrome seen in a historical photograph.*

*Pavilion B of Torino Esposizioni (1947–54) Turin, Italy*

Nervi is considered one of the most influential designers of the twentieth century, as well as one of the most prolific and interesting figures in the context of shell structures, particularly in concrete. He is remembered above all for his patent of ferrocement, consisting of dense concrete in which a thin metal mesh arranged in layers and reinforced with bars was embedded. This made it possible to prefabricate very thin, lightweight, flexible, and economical slabs.

In 1947, the company *Nervi e Bartoli* was awarded the contract for the construction of Pavilion B, intended for the exhibition of the Turin automotive industry. The building, characterized by a rectangular plan terminated by an apse, features along its sides a series of inclined columns that contribute decisively to the definition of its aesthetic and structural character. The vaulted roof is composed of prefabricated corrugated ferrocement elements, assembled on a tubular framework, giving rise to a structural organism of great lightness and representational value. The result is the image of a rhythmic succession of arches, comparable to a load-bearing ribbing system, clad with thin and refined surfaces of prefabricated ferrocement. These arches connect to the inclined perimeter columns by means of fan-shaped elements, which accentuate the formal and structural continuity of the whole. In the apsidal semi-dome, on the other hand, the intrados is marked by a diamond pattern generated by the use of ferrocement tiles employed as permanent formwork, a solution that combines constructive value with decorative quality (Petrova & Zheleva-Martins Viana, 2022; Laboratorio Pier Luigi Nervi, n.d.).

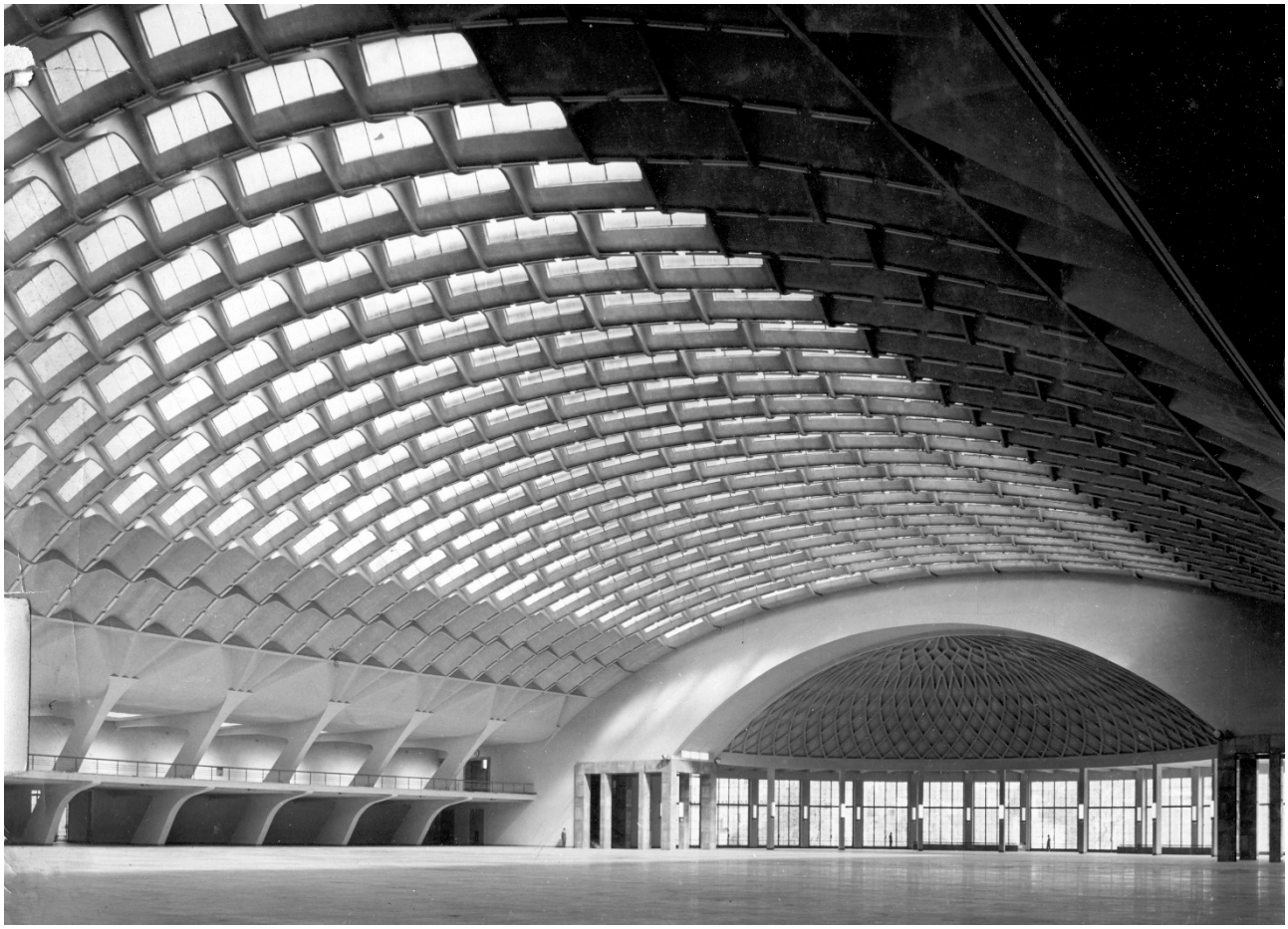


***Figure 4.5:*** *An interior view of Pavilion B.*



***Figure 4.6:*** *A more detailed view of the vault of Pavilion B.*

*Palazzetto dello Sport (1956–57) Rome, Italy*

The *Palazzetto dello Sport* in Rome was designed by Annibale Vitellozzi and Pier Luigi Nervi, who was specifically responsible for the roof, on the occasion of the 1960 Rome Olympic Games. The structure consists of a central volume 60 m in diameter surmounted by a dome, supported by inclined trestles set on an external circumference 78 m in diameter. The structure was built primarily with prefabricated elements, making it possible to reduce costs and accelerate construction time (Petrova & Zheleva-Martins Viana, 2022; Laboratorio Pier Luigi Nervi, n.d.).

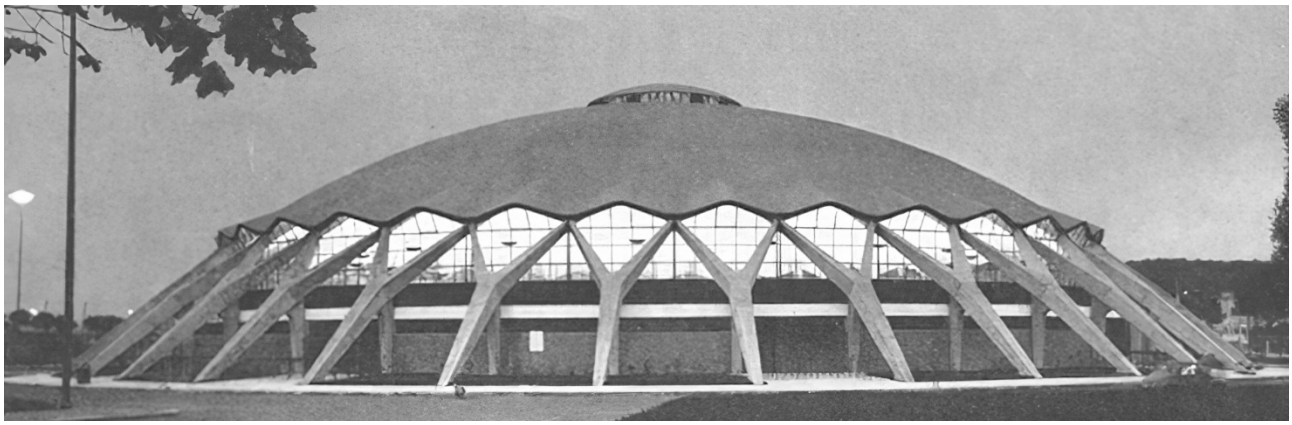


***Figure 4.7:*** *The Palazzetto dello Sport in elevation.*



***Figure 4.8:*** *The interior of the Palazzetto dello Sport.*

*Trans World Airlines (TWA) Flight Center at J.F.K. Airport, (1956-62) New York, U.S.A.*

Eero Saarinen's TWA Flight Center, designed in 1956 for JFK Airport, represents one of the most emblematic airport terminals of the twentieth century. Conceived as a unified and immediately recognizable organism, the project stands out for its plastic and dynamic configuration, based on four intersecting thin concrete shells capable of evoking the theme of flight and of contrasting with the more conventional orthogonality of the other airport terminals, which were mainly built in steel and glass. Saarinen in fact intended to transform the terminal into an expressive space, not static, but conceived as a place of movement, transition, and perceptual continuity (Davidson, 2019).

The architectural layout emerged from a careful study of flow organization and route efficiency. The large central hall, covered by curved concrete vaults, constituted the distributive core of the building, while a mezzanine accommodated lounges, bars, and restaurants, helping to define a unified environment in which furnishings and details also participated in the same formal language. From an engineering point of view, the passenger circulation system was particularly innovative. Saarinen designed fluid paths from the curb to the aircraft, with slight changes in level, gentle ramps, and connection tubes inclined toward the flight wings, thus integrating functional requirements with spatial quality. From a material and constructive point of view, the project is based primarily on the use of reinforced concrete, chosen not only for its structural performance but also for the possibility it offered to shape continuous, plastic, and highly expressive surfaces. The terminal thus presents itself as a coherent synthesis of form, structure, and function. However, precisely because of its strongly iconic nature, subsequent expansions proved more complex, as they became necessary due to the increase in air traffic and the introduction of larger aircraft (Davidson, 2019).



***Figure 4.9:*** *TWA elevation seen in a historical photograph.*

*Los Manantiales restaurant (1957-58) Mexico City, Mexico*

The roof of the main dining hall, designed by Félix Candela, consists of an octagonal groined vault resulting from the intersection of four hyperbolic paraboloids. The edge of each individual shell was defined through the intersection of the surfaces with a plane inclined outward (Burns, 1959). From the interpenetration of these four hyperbolic saddles emerges an eight-petaled roof, characterized by a span of approximately 32 m, a maximum height of 5.8 m, and an extraordinarily reduced thickness of only 4 cm (Luzuriaga, 2021).

Despite the apparent complexity of its double curvature, the roof was built through a construction process of surprising rationality, based on formwork arranged linearly along the generatrixes of the hypars alone. These timber elements were supported by a dense framework of uprights, runners, and wooden battens, assembled on site by skilled carpenters. A steel reinforcement mesh was then placed above the formwork, onto which the concrete was manually poured. Once the structure had reached the capacity to support itself under its own weight, the scaffolding and formwork boards were removed, revealing a shell of great plastic intensity, similar to a large seashell or a flower composed of eight petals (Luzuriaga, 2021).

The structural system was completed by a foundation system composed of 4 × 4 m square umbrella footings, conceived to receive and transfer the thrusts of the roof to the ground. To counteract lateral thrust, the eight footings were connected by a reinforced perimeter tie beam. Above each footing rose a concrete block from which the rib ascended with a progressive reduction in thickness, decreasing from 95 cm at the base to 7 cm at the top. Within these ribs, heavily reinforced V-shaped beams were also concealed, designed to collect the forces and channel them to the foundations (Del Cueto Ruiz-Funes, et al., 2024).

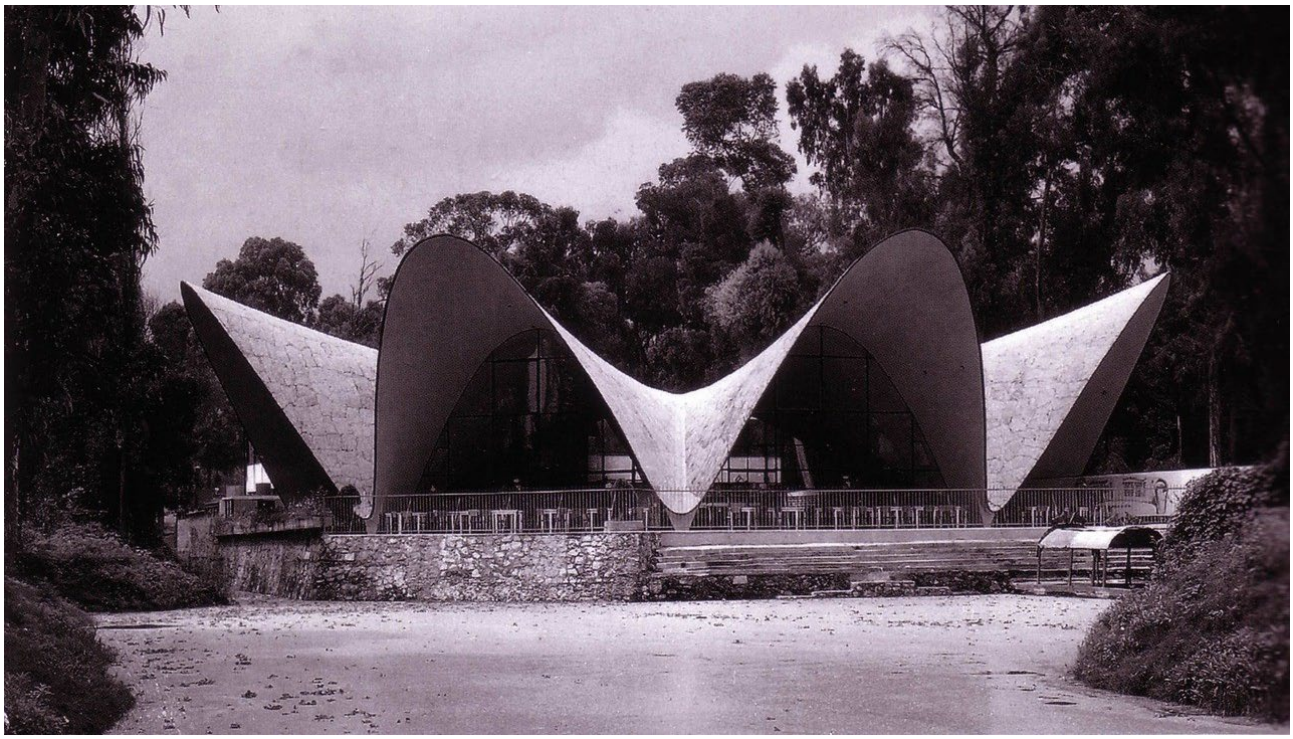


***Figure 4.10:*** *Los Manantiales restaurant.*

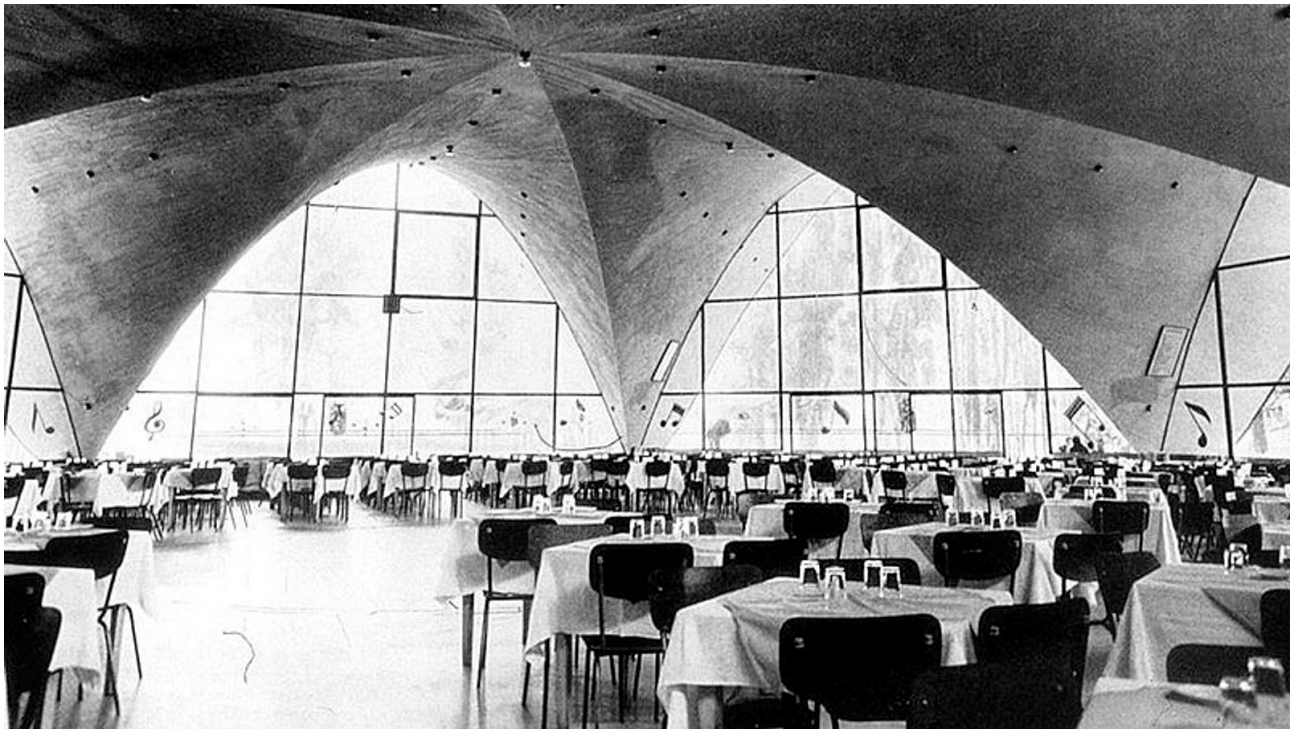


***Figure 4.11:*** *Interiors of Los Manantiales.*

*Multihalle (1970-74) Mannheim, Germany*

When, in 1970, it was decided to hold the 1975 *Bundesgartenschau* (Federal Garden Show) in Mannheim, Carl Mutschler & Partners were selected as architects and immediately involved Frei Otto, who was responsible for the design and the form-finding process behind the project. The Multihalle is undoubtedly one of Otto's most iconic and memorable creations, and it is the building most representative of the concept of the bending-active gridshell. The structure is composed of two exhibition halls connected by covered passageways. It has a maximum span of 60 m, a longitudinal extent of 85 m, and a maximum height of 20 m. The vast roof, characterized by a complex gridshell geometry, is composed of interwoven timber laths arranged in a structural mesh consisting of two to four overlapping layers. Each lath measures 5.5 cm and the spacing between them is 50 cm. The construction principle of bending-active gridshells such as this one requires that the network of laths be laid out flat on the ground and then raised until the doubly curved shell configuration is achieved, with the required morphological characteristics. The bolts at the joints were inserted but not tightened, since only once the final shape had been reached was it possible to stiffen the structure. A pair of 6 mm cables was also provided in order to ensure adequate stiffness (Liddell, 2015).

Behind these structures lies an extremely complex design process, which begins with form-finding, the subject explored further in Section 4.2 Form-finding. For Otto, the search for form was expressed above all through physical models, as a means by which the idea comes to life (Boller & D'Acunto, 2021; Weber, 2021).



***Figure 4.12:*** *The Multihalle in an aerial photograph.*



***Figure 4.13:*** *The interior of the Multihalle.*

*Roof of the Great Court, British Museum (1998-2000) London, United Kingdom*

The roof of the Great Court of the British Museum, completed in 2000 to a design by Foster + Partners, is a fitting example of a discrete gridshell made of steel members and glass panels arranged according to a triangular geometric pattern. The roof was conceived to make the large central courtyard an integral part of the museum route, generating a covered court of approximately 6,700 $m^2$, perforated at the center by a cylindrical volume surmounted by a dome, the Reading Room. The whole consists of 4,878 members, 1,566 nodes, and 3,312 triangular glazed panels, with a total weight close to 800 t. From an architectural point of view, the work arose from the need to establish a formal relationship between the volumes of the court and stands out for the visual lightness of the envelope, the continuity of the surface, and the triangular mesh. The design phase involved the use of the dynamic relaxation method, a form-finding method that will be analyzed in subsection 4.2, in order to optimize the position of the nodes, make the reticular pattern more regular, and control the dimensions of the glazed panels. Moreover, the roof does not transfer its loads onto the historic Reading Room, but rather onto 20 steel supports embedded in concrete and arranged around its volume (Williams, 2001; Foster + Partners, n.d.).



***Figure 4.14:*** *The Great Court seen in an aerial photograph.*



***Figure 4.15:*** *The Reading Room at the center of the Great Court.*

The set of case studies referred to here does not claim to offer an exhaustive overview of the universe of shell structures; rather, it aims to highlight, through a number of exemplary works, the extraordinary variety of outcomes that this system was able to produce throughout the twentieth century. From continuous concrete shells, from the pioneering experiments of the

Zeiss Planetarium to Torroja's extraordinary inventions, from Nervi's masterful applications of ferrocement to the visionary forms of Candela and Saarinen, and up to Frei Otto's gridshells and more recent examples such as the roof of the British Museum, it clearly emerges how the shell may be understood as a privileged point of encounter between architectural expression and structural efficiency. The choice of these examples therefore reflects the intention to demonstrate the potential of this typology in combining lightness, continuity, economy of material, and load-bearing capacity (Manuello Bertetto, et al., 2020; Adriaenssens, et al., 2025; Manuello, 2020). Despite the diversity of geographical contexts, dimensional scales, and geometric configurations, all the works considered in fact testify to how resistance may be entrusted above all to form and how, precisely from this principle, there arises that peculiar convergence between constructive necessity and extraordinary architectural quality that makes shells one of the highest expressions of architectural and engineering research.

From this perspective, the analysis of the case studies proves useful not only for understanding their historical development, but also for grasping their contemporary relevance and their enduring significance within the current architectural debate (Manuello Bertetto, et al., 2020; Manuello, 2020).

*Tensile Structures*

The transition from shell structures to tensile structures can be framed within the wider field of lightweight shell and spatial structures, which includes membranes, grid-shells, active-bending systems, shell roofs, tensegrity structures, pneumatic and inflatable structures, active and deployable structures, and bio-inspired structures (Manuello Bertetto, et al., 2020). Form also represents a fundamental parameter in tensile structures, that is, in those systems composed of membranes and/or cables whose structural effectiveness depends on the geometric configuration assumed in equilibrium and on the corresponding state of tension. In such structures, the load-bearing elements work predominantly in tension, according to a behavior that finds analogies in nature, for example in spider webs and soap films. In light of this, it is possible to provide an initial distinction, namely that between shell structures and tensile structures, while shell structures are generally defined as *form-passive* systems, tensile structures are defined as *form-active* systems (Petrova & Zheleva-Martins Viana, 2022; Boller & D'Acunto, 2021). Form-passive refers to systems in which the form does not change significantly as the loads vary. The geometry is substantially stable, and the structure continues to function without having to seek a new resistant configuration each time (Adriaenssens, et al., 2014). Form-active, on the other hand, refers to those structural systems in which the load-bearing capacity depends directly on the geometric form assumed in equilibrium; every variation in load entails a variation in geometry necessary to reach a new state of equilibrium (Quinn, et al., 2016).

Tensile structures, like shells, have ancient origins, dating back approximately to 20,000 BC (Milošević, et al., 2013). Their history is intertwined with that of various nomadic populations throughout the world, especially in the Maghreb, where these structures are still used today (Monjo-Carrió & Tejera, 2011). Their use has continued uninterrupted over the centuries; it is in fact well known that in Roman constructions, such as amphitheaters, retractable textile devices called *velaria* were used to protect spectators from the sun (Campioli, et al., 2007), as were *toldos*, fabrics stretched between facing buildings to provide shade on the streets below and still in use today in southern Spain. However, it is generally recognized that the principal

advocate of tensile structures was the German architect and engineer Frei Otto (1925-2015), whose work has already been discussed and will be examined several more times throughout the development of this chapter (Chilton, 2010).

These tensile systems represent spatial structures with an essential aesthetic and structural functioning; they are extremely light, both in weight and in visual perception (Manuello Bertetto, et al., 2020). As in shells, their structural effectiveness depends primarily on form. However, unlike shells, tensile membranes cannot resist compression and must therefore remain in a continuous state of tension. They typically weigh approximately 1 kg/m$^2$ and have a thickness of about 1 mm. In order to maintain the stability of the system, tensile structures must be subjected to tensile prestressing, so that the membrane remains tense at all its points. Prestressing usually ranges from 1% to 6% of the maximum tensile strength that the material can withstand. In addition, conventional design loads such as snow and wind must also be considered, with wind effects being particularly complex because they may act laterally, downward or upward on the surface (Forster & Mollaert, 2004; Milošević, et al., 2013).

If shells can respond to loads through in-plane tensile, compressive, and shear stress states, with bending contributions that are generally secondary and localized, tensile membrane structures instead require the load-bearing surface to remain in a state of tension. For this reason, membrane stresses must not assume compressive values, their ideal lower limit being zero (0 kN). Another relevant aspect of tensile structures is their high deformability, in relation to the material from which they are made, a characteristic that constitutes both an advantage and a critical issue of the system. When subjected to external forces, that is, applied loads, tensile structures may modify their formal configuration, which is why at the beginning of this subsection they were defined as form-active (Milošević, et al., 2013), meaning that they actively modify their shape in order to adapt to the imposed loading conditions and ensure the stability of the entire system.

Under external loads, elements working in pure tension are generally considered among the most efficient from a structural point of view, since they allow the entire resistant cross-section to be exploited in an almost uniform manner, thereby confirming tensile structures as the most efficient structural systems, especially in relation to self-weight, quantity of material employed, and covered surface area. By contrast, predominantly compressed elements are more exposed to instability phenomena, which in slender structures may occur long before the material strength is reached; in the case of thin shells, this may result in local or global buckling[34] phenomena. Beams also show lower efficiency, since bending induces tensile and compressive stresses distributed non-uniformly across the section, leading to a less effective use of material compared with systems that work predominantly in tension (Chilton, 2010).

As with shells, tensile structures may be classified according to different criteria: according to the load-bearing element, distinguishing between cable structures and membrane structures; according to the stabilization principle, distinguishing between prestressed membranes and pneumatic structures; according to the configuration of the supports; or according to the morphology of the surface (Milošević, et al., 2013; Chilton, 2010; Monjo-Carrió & Tejera, 2011). However, a first fundamental distinction may be introduced between cable-net structures and membrane structures. The first category includes interconnected cable nets that constitute the

[34] *Buckling is a structural instability phenomenon affecting members subjected to compression, in which the member or part of its cross-section undergoes a sudden deformation that may limit its load-bearing capacity before the material reaches its full strength* (Zhao, et al., 2005).

main load-bearing element, whereas the second represents a later development of such systems, in which the covering element, the membrane, also assumes a structural load-bearing function (Milošević, et al., 2013). The fundamental principle of membrane structures is that the fabric must maintain a sufficient state of tension in the two principal directions and, more generally, at every point of the surface; from this perspective, it is possible to introduce a further distinction. When stability is achieved through air pressure acting normally to the membrane, pneumatic structures are obtained, usually associated with synclastic forms. By contrast, tensile membrane structures are stabilized through prestressing applied at the perimeter and anchorage points, usually resulting in anticlastic configurations. Cable structures, instead, rely on linear elements such as cables and ropes, while the covering may remain separate from the load-bearing system (Monjo-Carrió & Tejera, 2011).

These structural models also find interesting analogies in nature, in particular spider webs for cable structures, insofar as they are made of thin and very lightweight threads that work almost exclusively in tension, and soap or air bubbles for membrane structures, since they demonstrate the ability of a thin surface to assume a configuration according to conditions of tensile equilibrium. In particular, the air bubble constitutes an especially effective analogy for pneumatic structures, whose stability is a consequence of internal pressurization.

These systems make it possible to achieve not only structural and aesthetic lightness and a limited use of material, but also great freedom in their morphology (Chilton, 2010) and covered spaces that are largely free from structural obstructions such as columns. Like shells, these systems are widely used for covering large surfaces and were often used in the past for the construction of stadiums, exhibition spaces, and pavilions.

It also emerges that the membrane material is decisive for the performance and efficiency of these systems. The materials employed in membrane structures may be traced back to two main macro-categories: coated fabrics and films. Among the former, the most widespread are polyester coated with polyvinyl chloride (PVC), appreciated for its favorable ratio between cost and durability; glass fiber coated with polytetrafluoroethylene (PTFE); glass fiber coated with silicone; and, in some cases, fabrics based on aramid fibers. It should also be considered that these materials are composite in nature, since they are made up of several layers, each of which performs a specific function. The textile substrate provides the principal mechanical resistance, the coating gives the material stability and ensures waterproofing, UV protection, and adequate fire performance, while the surface finish, which constitutes the outermost layer, contributes to overall durability by acting as a protective barrier against dirt and atmospheric agents (Monjo-Carrió & Tejera, 2011).

*Olympic Stadium of Munich (1968-1972) Munich, Germany*

The Olympic Stadium of Munich, built for the 1972 Games, represents one of the highest and most pioneering expressions of tensile architecture, as well as one of Frei Otto's most celebrated works. The intervention, which also extended to the swimming hall, the gymnastics hall, and the connecting pathways, covers a total surface area of approximately 74,000 $m^2$, giving shape to a unified, lightweight, and biomorphic artificial landscape. The doubly curved steel cable net forming the roof has a 75 × 75 cm mesh and an acrylic glass cladding that generates an undulating surface of extraordinary lightness and transparency. From an engineering point of view, the work marked a decisive transition from concrete shells, which had already radically expanded the possibilities of covering large spans with minimal

thicknesses, to an even more advanced system, capable of reaching greater spans with even smaller sections and with a visual lightness previously unimaginable. The structure, articulated into nine interconnected segments, was based on a highly sophisticated static system, in which 80 m-high steel pylons, suspended pylons, edge and stabilization cables, and a long radial tension cable measuring more than 300 m worked together to ensure the equilibrium of the whole without compromising the visibility of the stands with internal supports. The design process was characterized by physical models, so dear to Otto, which constituted a form-finding process of an empirical nature. The project was not only an architectural masterpiece, but a true experimental enterprise that definitively demonstrated the validity of tensile structures as a revolutionary evolution of shell structures and as a new frontier for long-span structures (Milošević, et al., 2013).



***Figure 4.16:*** *Aerial view of the Olympic Stadium in Munich.*

### 4.2 Form-finding

The design process through which the configuration of formally active structures and systems is determined is commonly referred to as form-finding or shape finding (Veenendaal & Block, 2012).

Adapting the definition proposed by Lewis, the process may be described as the search for the optimal form of a form-active structure, such that it is, or comes as close as possible to being, in a condition of static equilibrium (Lewis, 2003).

This formulation, although widely accepted, was criticized by Haber and Abel, who observed that in many cases even the stress state cannot be assigned a priori, since it is as unknown as the form itself. For this reason, they proposed interpreting the form-finding problem as a problem of initial equilibrium. Along similar lines are also more restrictive definitions, such as those proposed in later works by Bletzinger et al., in which form-finding is described as the search for a shape in force equilibrium within a given boundary and with respect to a given stress state (Veenendaal & Block, 2012).

In the analysis of the different types of shell structures developed in the preceding paragraphs, form emerges as the common denominator, since it constitutes the very condition of their structural effectiveness. However, it is not always possible to establish a priori which configuration is the most appropriate in relation to the acting forces, and it is precisely within this space of indeterminacy between geometry and mechanical behavior that form-finding is situated.

In cable structures and textile membranes, form is not defined a priori independently of static behavior but rather emerges from the search for an equilibrium configuration made possible by the tensile or prestressed state of the system. These are configurations that, in general, are not known in advance, cannot be reduced to simple mathematical functions, and therefore require the designer to undertake a genuine process of form-finding. It is precisely this dependence of geometry on the stress state that distinguishes these structures from other systems, such as those in concrete, non-funicular steel, or masonry, in which form is generally a parameter established upstream of the design process. In general terms, form-finding helps identify optimal structural forms capable of satisfying functional requirements and demands of strength and durability, while at the same time finding the configuration that responds most effectively to loads using the least amount of material, thereby optimizing its use and reducing construction costs (Manuello Bertetto, et al., 2020; Adriaenssens, et al., 2025; Manuello, 2020). This concern for efficiency is linked to the broader principle of lightness, which finds one of its deepest references in nature (Lewis, 2003).

In continuity with the concepts developed in Chapter 3, nature operates according to a logic of maximum effectiveness with minimum expenditure of matter, energy, and work, since every organism tends to optimize the available resources while responding adequately to the required performance demands. It is precisely this same principle of efficiency that underlies the behavior of shell structures, whose load-bearing capacity derives from form even before it derives from the quantity of material employed, which is why structures can achieve large spans with minimal envelope thicknesses. Hence their profound connection with the natural world: a convergence of principles in which economy of means, structural effectiveness, and architectural quality coincide.

Interest in natural structures has long involved biologists, mathematicians, and architects, precisely because in them form appears as the result of a refined balance between growth, matter, and stresses. In his book *On Growth and Form*, D'Arcy Thompson observed that shells increase in size without altering their general configuration, preserving constant similarity during growth. Their morphology may be described by means of the equiangular, or logarithmic, spiral, confirming that even the apparently freest natural forms actually obey rigorous geometric principles (Thompson, 1917).

Similarly, Mattheck's studies on the mechanics of tree growth showed how these organisms are highly optimized systems, characterized by minimum weight compatible with sufficient resistance to withstand the relevant load cases. Their growth process in fact ensures a substantially uniform distribution of stresses on the surface of the trunk and branches, offering an extremely significant model for the design of artificial structures (Mattheck, 1990).

The principle according to which form follows forces manifests itself particularly clearly in structures that transmit loads exclusively through axial or in-plane stresses, that is, in all those cases in which bending does not act as the dominant load-bearing mechanism. In such systems, form and forces determine one another reciprocally, since the geometric arrangement derives from the flow of stresses and, at the same time, conditions their distribution (Manuello Bertetto, et al., 2024a; Fallacara, et al., 2024; Manuello, 2020). The examples examined so far, such as continuous shells, gridshells, or tensile structures, may all be related to this principle (Manuello Bertetto, et al., 2020; Manuello, 2020). Among the best-known historical precedents of this form-finding process through physical models are Antoni Gaudí's hanging chains, Heinz Isler's hanging membranes, and Frei Otto's grid models, all capable of making structural equilibrium directly visible through matter and gravity. Although physical models retain an undeniable experimental fascination, since the 1960s form-finding has found its principal field of development in the digital context, accompanying the advent of the computer age and the introduction of multiple numerical methods. Nevertheless, after almost half a century of studies, the systematic comparison among the various methods remains far from straightforward, owing to the marked variety of nomenclatures, mathematical approaches, and notational conventions that characterize the different contributions (Veenendaal & Block, 2012).

*Pioneers of form-finding*

Within the field of form-finding, and particularly in its application to shell structures, the figures of Frei Otto (1925-2015), Heinz Isler (1926-2009), and Sergio Musmeci (1926-1981) occupy an outstanding pioneering position. Although their paths, cultural references, and the outcomes of their work differ, they shared the choice of making form-finding the foundation of their design and experimental approach (Boller & D'Acunto, 2021).

Robert Hooke (1635–1703) and Antoni Gaudí (1852–1926) represent two emblematic figures, respectively in the scientific and architectural fields, whose contribution laid some of the theoretical and operative foundations of modern form-finding. In the case of St. Paul's Cathedral in London, Sir Christopher Wren (1632-1703) devised a complex triple-dome solution capable of reconciling formal and structural requirements, defined by an external dome dominating the skyline, an internal dome, and a hidden intermediate structure, necessary to support the lantern and the roof (Boller & D'Acunto, 2021; Higgott, 2026). This approach stands in continuity with the insights of Robert Hooke, who understood that a rope

suspended at its ends is subjected exclusively to tension, but that once inverted it identifies the load-bearing principle of an arch working predominantly in compression. The latter is defined as a catenary arch and is self-supporting (Fallacara, et al., 2024). From this analogy between chain and arch derived one of the most fruitful ideas in the history of statics, namely the possibility of deriving structurally efficient forms directly from conditions of equilibrium. Building on these insights, Wren developed for St. Paul's a solution intended to achieve a more structurally efficient form, capable of ensuring stability and continuity in the transmission of forces. Gaudí, several centuries later, would bring this principle to a further level, making form-finding not merely a tool of verification, but the very foundation of the design process (Boller & D'Acunto, 2021; Higgott, 2026).



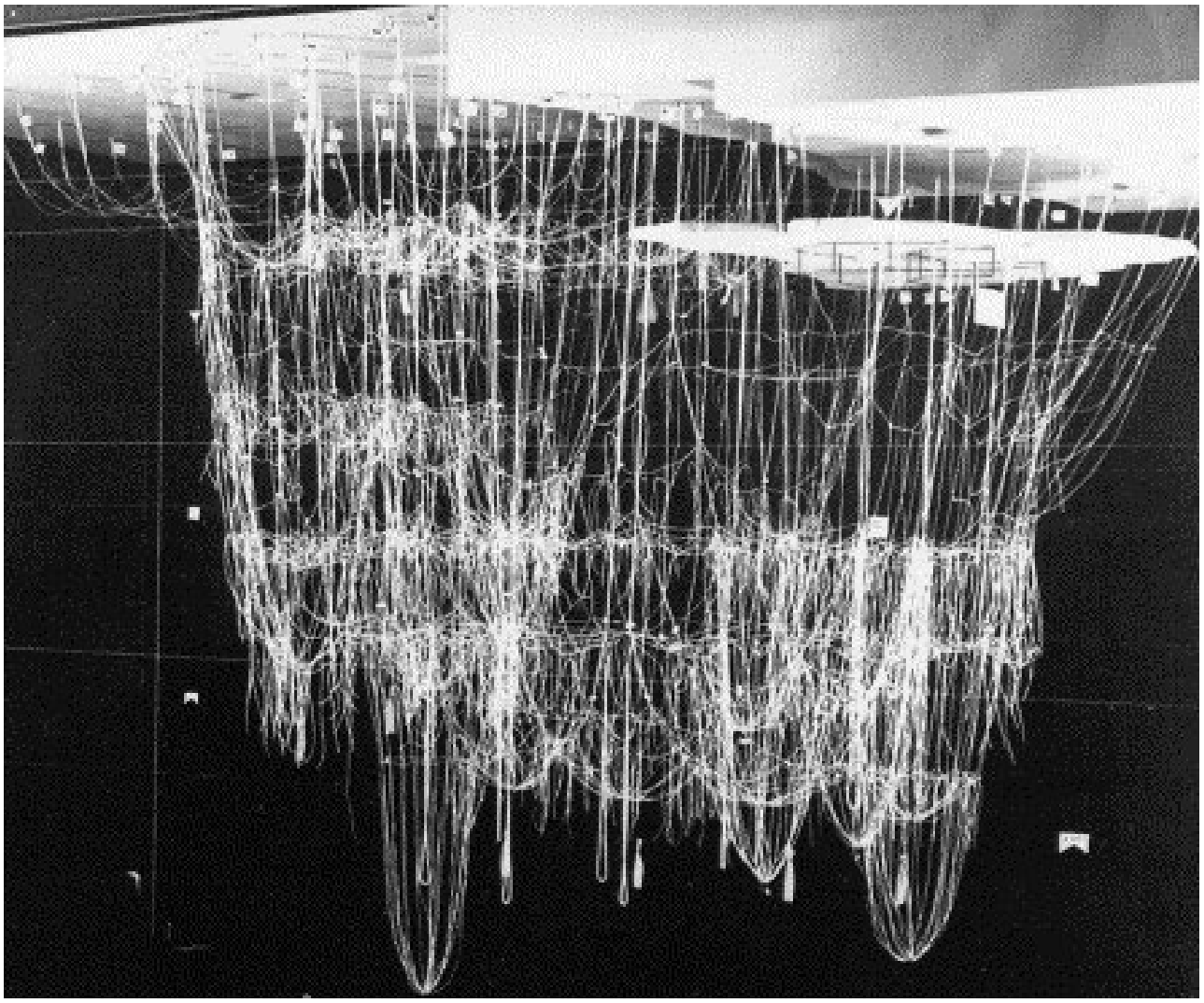
***Figure 4.17:*** *The section of the dome of St. Paul's in London shows its internal structure.*

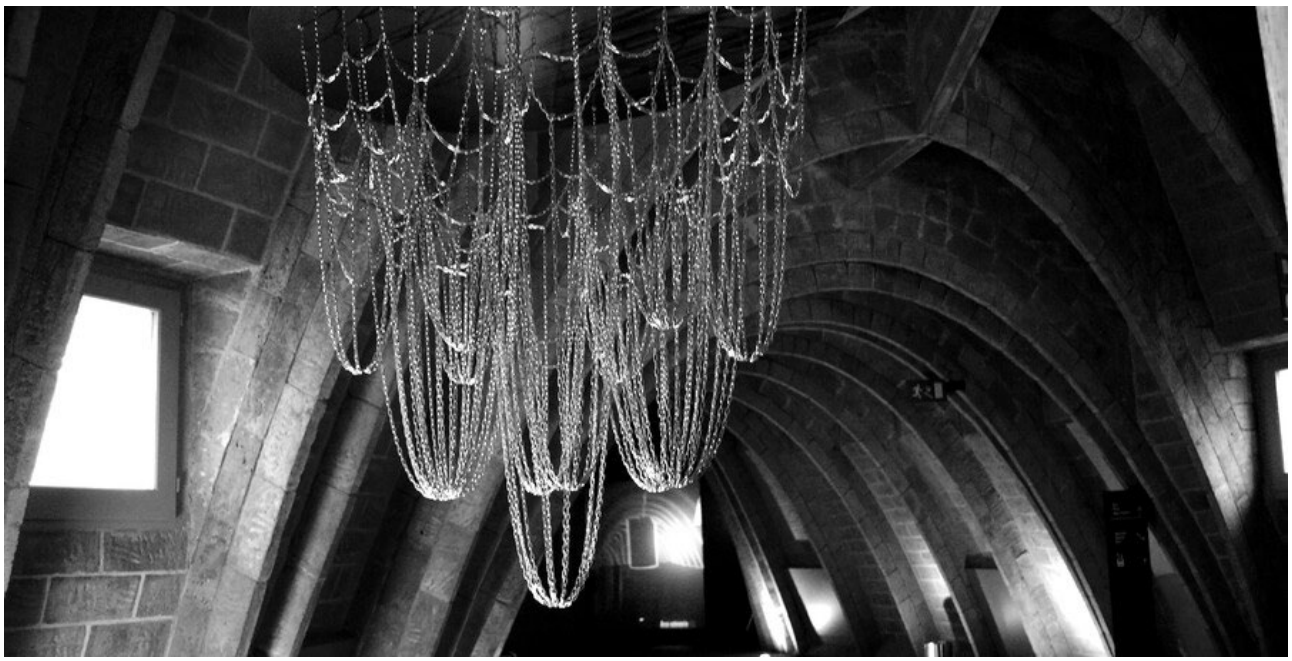
Antoni Gaudí made material experimentation and constructive verification an essential tool of the design process, studying the churches of the Sagrada Família and Colònia Güell through scale models with which he investigated, with extraordinary precision, the limits of structure

and matter (Burry, 2011). His conception of architecture did not separate stability from the other aspects of the work, but integrated layout, construction, ornamentation, and the figurative arts from the outset within a unified vision of the project. For Gaudí, structural design was not merely a final verification, but rather a generative component of the architectural idea, active from its very first formulations (Huerta, 2006); it is precisely for this reason that he is considered the first pioneer of form-finding.

One of the most emblematic tools of this approach was the hanging-chain model, which Gaudí used to prefigure the profile of arches and vaults, modifying the configuration of the chains by means of weights until he obtained an equilibrium form that could then be transferred, by inversion, into the construction (Chilton & Chuang, 2017; Fallacara, et al., 2024). These processes found concrete application especially in the studies for the church of Colònia Güell and, more generally, in the design research for the Sagrada Família, works in which analogical experimentation became a true instrument of formal and structural conception (Huerta, 2006; Burry, 2011). The value of these forms did not lie solely in their figurative outcome, but above all in the process that generated them, since their beauty derived from the coincidence of material logic, structural behavior, and geometric configuration (Chilton & Chuang, 2017).

This procedure found its theoretical foundation in the intuition formulated by Robert Hooke in the seventeenth century, according to which the line assumed by a suspended flexible element, once inverted, yields the ideal form of a rigid arch in equilibrium. From this analogy between chain and arch derived the adoption of catenary profiles, which Gaudí employed in an original way not only as an efficient static solution, but as a compositional principle capable of guiding the architectural project in its entirety. In this sense, his contribution appears particularly innovative, since it was not a matter of verifying a posteriori the stability of a form already imagined, but of conceiving from the outset an architecture generated through intrinsically stable forms (Huerta, 2006; Burry, 2011). It is precisely in this convergence between analogical experimentation, mechanical intuition, and architectural intention that Gaudí's work anticipates some of the fundamental principles of contemporary form-finding (Huerta, 2006; Burry, 2011; Chilton & Chuang, 2017).





***Figures 4.18 (above) and 4.19 (below):*** *The physical models made with chains for Gaudí's form-finding processes.*

The approaches to form-finding developed by Frei Otto, Heinz Isler, and Sergio Musmeci arise from an engagement with the physical phenomena of the natural world but are articulated according to profoundly different cultural and operational orientations (Neri, 2014; Boller & D'Acunto, 2021). Frei Otto interprets nature in a broad sense, as a set of biological, physical, and mechanical processes, and seeks to transfer their logics into architecture through scientific research. From this perspective, biology does not merely constitute a repertoire of images but becomes a true model for rethinking design and re-establishing a rigorous connection between nature and artifice, based on the direct observation of natural phenomena and their experimental reproduction. Consequently, form is not conceived as the arbitrary product of the designer, but rather as the outcome of a process that the designer must be capable of initiating, observing, and understanding (Boller & D'Acunto, 2021).

Within the Institute for Lightweight Structures in Stuttgart, the *Biologie und Bauen* group studies different disciplines, ranging from botany to zoology, and from biophysics to paleontology, in an attempt to revolutionize the conventional approach to design (Otto, 1984). For Otto, the physical experiment represents the methodological basis of all research, because it makes it possible to abstract a natural phenomenon, reproduce it under determined conditions, and materially verify the theoretical hypotheses developed by the group (Weber, 2021). It is therefore not surprising that he experimented with an extraordinary variety of materials and principles, from sand cones to tensile nets, from pneumatic membranes to soap films, making experimentation the privileged means through which to investigate structural behavior (Boller & D'Acunto, 2021). In particular, experiments with soap bubbles allowed him to explore the theme of minimal surfaces, confirming his interest in the physical processes that govern the formation of structures (Golański, 2023).

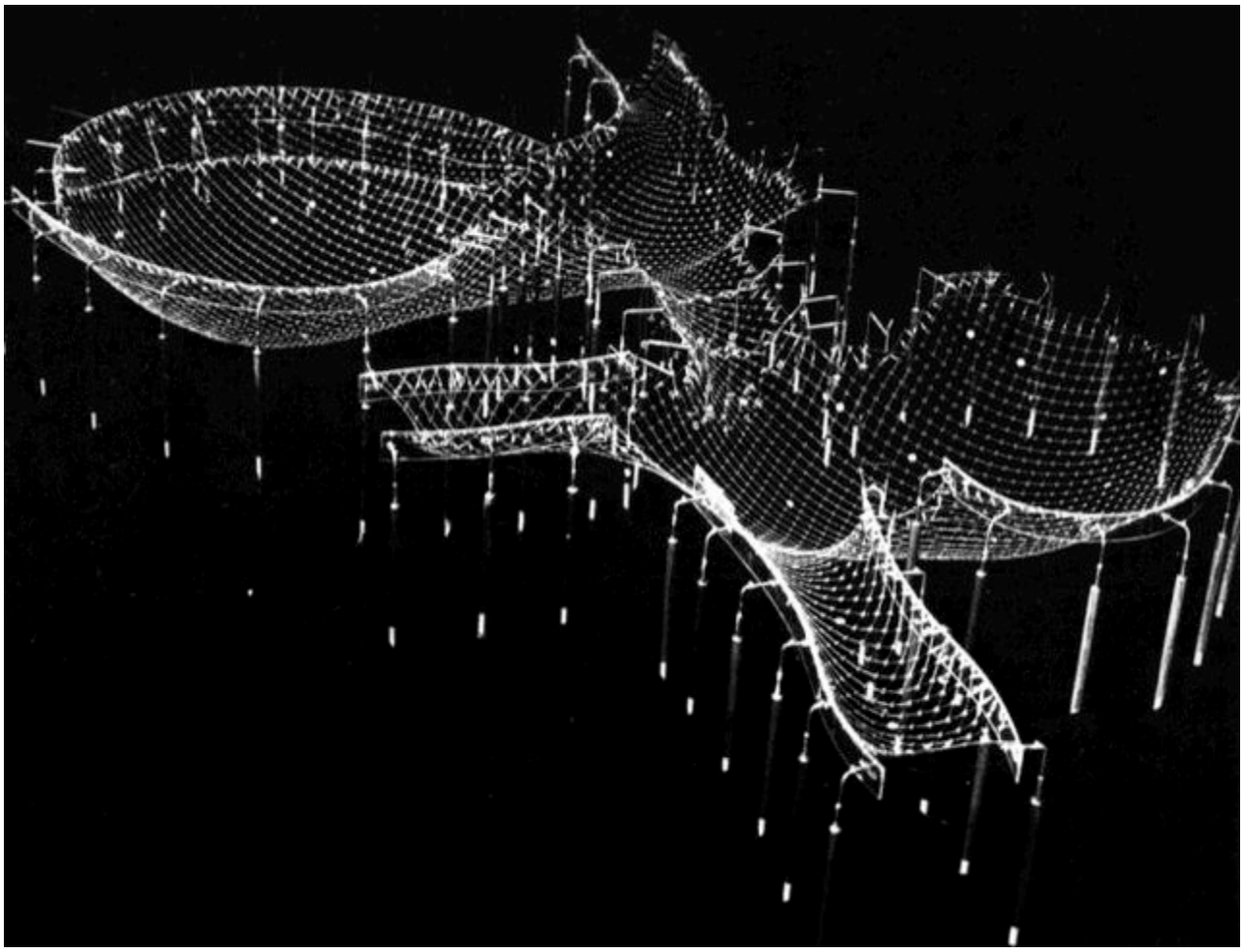


***Figure 4.20:*** *Physical form-finding model developed by Frei Otto for the Multihalle in Mannheim*.

Heinz Isler also recognized in the natural world a primary source of inspiration, but his relationship with it was less oriented toward the scientific explanation of processes and more closely tied to the capacity of natural forms to suggest structurally effective images. His visual sensitivity enabled him to grasp, in insects, plants, and fruits, those physical principles that could be translated into a formal model to follow (Chilton, 2000). From this derived the conviction that truly optimal structural forms, precisely because they are generated according to the processes and logics of nature, are inevitably also beautiful (Isler, 1980; Boller & D'Acunto, 2021). In the 1950s, Isler also came to distinguish form-finding methods into three broad categories—analytical, experimental, and free-form modeling methods—recognizing doubly curved shells as the most efficient configurations from a static, material, and spatial point of view. For him, the shell was not merely a load-bearing element, but at once structure and envelope, that is, an organism capable of unifying architectural function and structural behavior within a single coherent system (Golański, 2023).

Unlike Otto, who experimented across a wide range of systems, Isler concentrated his research almost exclusively on the reinforced concrete shell and developed a strongly experimental design method, extending from the conceptual phase to pre-construction measurement models (Isler, 1993). His new shell forms are free forms obtained mainly through hanging and pneumatic models, in which air pressure or gravity become the generating principles of geometry. In this sense, the pneumatic membrane refers to the behavior of a pressurized

surface, while the hanging membrane illustrates the logic of the catenary curve. Isler set up the experiment by selecting materials and boundary conditions but then allowed the form to evolve according to its own physical necessity, seeking not so much to impose a formal configuration as to allow the one most suited to the given constraints to emerge. The starting materials were deliberately simple (rubber membranes cut and stretched over wooden frames) and, once a promising configuration had been identified, he developed it further by means of solid plaster casts and geometric measurements at scale. The simplicity, economy, and rapidity of this procedure allowed him to test many variants, until the form emerged that best satisfied both structural and architectural requirements (Boller & D'Acunto, 2021).

Unlike Gaudí's explorations, which were more focused on defining the lines of thrust of ribs and columns through suspended chain models, Isler's experiments aimed directly at the search for the form of the surface, that is, a geometry made efficient by the law of gravity and capable of optimizing the behavior of the shell as a whole (Golański, 2023). In this approach, constructive logic and formal configuration coincide, in accordance with that principle of harmony between material, structure, and form that Eduardo Torroja identified as the very foundation of load-bearing design (Boller & D'Acunto, 2021; Golański, 2023).



***Figure 4.21:*** *Heinz Isler working with a fabric model.*

Sergio Musmeci, for his part, stands apart quite clearly from both Otto and Isler because of the analytical manner in which he looked at physical phenomena, seeking in their manifestations the universal laws governing their behavior. Although he shared with Otto a fascination for physical and mechanical processes in continuous transformation, he interpreted nature as a

set of mutually interrelated entities whose form reveals geometric and structural principles. In his view, the optimal configuration of a structure is the one that makes legible, through form itself, the flow of internal forces and their variation in relation to the properties of the material. For this reason, the “natural” form coincides with the best form, not because it outwardly imitates nature, but because it materializes the principle of static equilibrium (Boller & D’Acunto, 2021).

Musmeci’s background, rooted in Italian scientific culture and structural engineering, led him to make a decisive theoretical shift. Whereas classical theory assumes geometry as an initial datum and merely verifies structural behavior, he argued that the true unknown of the design process should be precisely form itself (Boller & D’Acunto, 2021). In this reversal of perspective, analytical methods cease to be mere tools of verification and become means of determining structural configuration and the use of material (D’Acunto & Ingold, 2016; Boller & D’Acunto, 2021). For this reason, unlike Otto and Isler, Musmeci did not use the physical model as the principal design tool, but rather above all as a support for making visible a mathematical theory from which the final form emerged (Boller & D’Acunto, 2021; Ingold, 2021). His search for integral structural forms clearly emerges in works and experiments such as the saddle supports of the Palazzo del Lavoro in Turin, the funnel-shaped roof of the church of *Villaggio del Sole* in Vicenza, and the *Basento Bridge*, in which the geometries far exceeded the ordinary constructive possibilities of their time (Musmeci, 1971; Golański, 2023).



***Figure 4.22:*** *Sergio Musmeci’s bridge over the Basento River under construction.*

Finally, the three designers occupy a crucial position in the transition from physical to digital form-finding methods, marking a turning point in the structural culture of the second half of the twentieth century (Boller & D'Acunto, 2021). Otto and Musmeci recognized in the newly introduced computers tools capable of radically expanding the possibilities of design, and as early as the 1970s Musmeci was already using ANSYS for static analysis, verifying a substantial convergence between analog and numerical results (Golański, 2023). Isler, by contrast, regarded the new computational means with greater skepticism, fearing that they might obscure the authentic understanding of a method which, in his view, had to remain anchored to the direct experience of the physical model and to practical knowledge of the behavior of forms (Boller & D'Acunto, 2021).

*Form-finding methods*

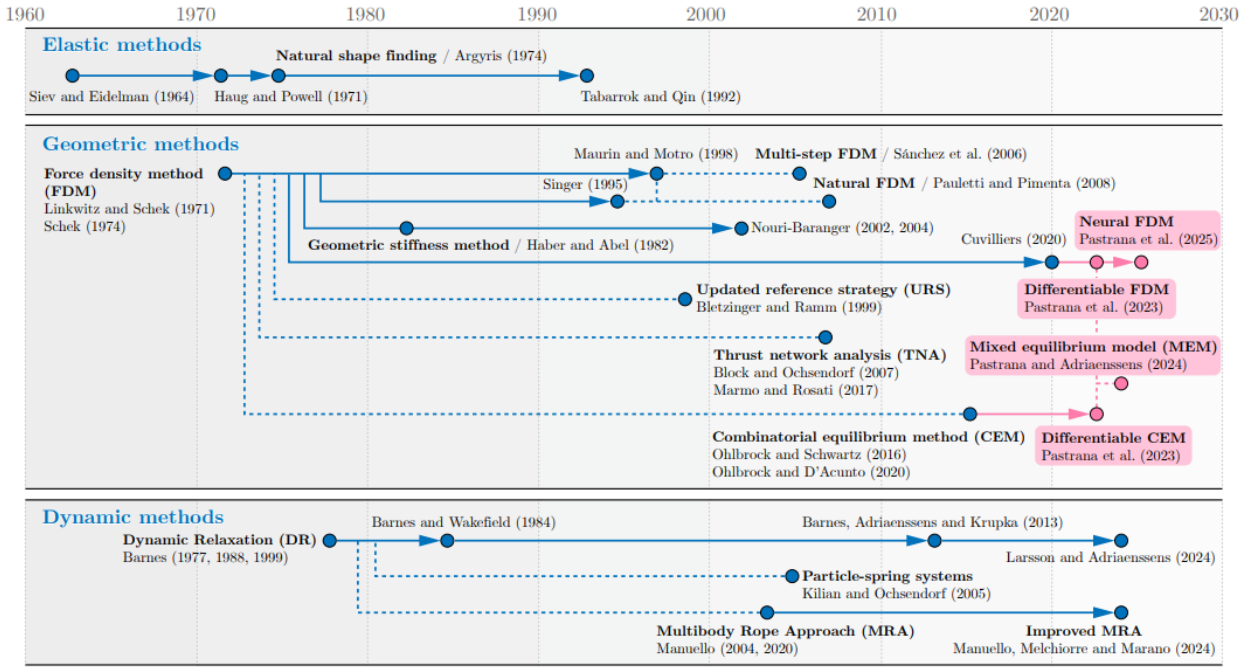



***Figure 4.23:*** *A genealogy of numerical form-finding methods* (Pastrana Jimenez, 2026).

The development of form-finding evolved from the physical models of Gaudí and Isler to numerical methods, which became central from the 1960s onward with the spread of computational analysis and with the major experiments on cable-net roofs and lightweight membranes (Linkwitz, 1999; Veenendaal & Block, 2012; Pastrana Jimenez, 2026). Literature on the subject converges in distinguishing three groups of methods: *Elastic methods*, or methods based on the stiffness matrix; *Geometric methods*; and *Dynamic methods*. Figure 4.23 shows a chronological overview of the development of the various methods, from the early approaches of the 1960s and 1970s to progressively more specialized and recent techniques (Veenendaal & Block, 2012; Pastrana Jimenez, 2026). Recent research has also extended this trajectory by coupling form-finding procedures with multi-objective optimization algorithms, allowing structural efficiency, constructability, material consumption, and production waste to be considered simultaneously during the conceptual design phase (Melchiorre, et al., 2025; Manuello, 2020).

Elastic methods, among the first to be formulated, derive directly from structural analysis and use the standard elastic and geometric stiffness matrices to iteratively correct an initial configuration that is not in equilibrium. This family includes the works of Siev and Eidelman (1964), Haug and Powell (1971), Argyris (1974), and, later, Tabarrok and Qin (1992). Precisely because of their connection with nonlinear analysis, they generally require the introduction of material properties, even though they deal with a problem that is primarily geometric (Veenendaal & Block, 2012; Haber & Abel, 1982).

Geometric methods, by contrast, are based on the idea that the form-finding problem can be addressed independently of the material used, by prescribing relationships between form and force rather than constitutive properties, and they find their classical reference in the Force Density Method (FDM). Here, the force/length ratio, that is, the force density, becomes the key quantity that makes it possible to reformulate the equilibrium problem in linear terms and to obtain coherent funicular forms with great rapidity (Haber & Abel, 1982; Linkwitz, 1999; Veenendaal & Block, 2012).

From this approach derive its principal extensions, such as the Geometric Stiffness Method of Haber and Abel (1982), the Updated Reference Strategy (URS) of Bletzinger and Ramm (1999), and the Natural FDM of Pauletti and Pimenta (2008), which share the objective of maintaining the numerical efficiency of geometric methods even in nonlinear formulations, by appropriately updating the reference configuration and prescribing forces or geometric stiffnesses rather than force densities in the strict sense (Veenendaal & Block, 2012).

Within the more recent genealogy of the same family (Geometric methods) are also Thrust Network Analysis (TNA) and the Combinatorial Equilibrium Method (CEM). The former is particularly suited to compressive systems, such as shells and reticulated vaults, because it separates horizontal and vertical equilibrium while keeping the plan projection fixed under vertical loads, whereas the latter is designed for mixed tension-compression systems, such as bridges, towers, or tensegrity structures, and calculates equilibrium sequentially for groups or layers of vertices, proving robust when load transfer follows a clear hierarchy (Pastrana Jimenez, 2026).

Finally, Dynamic methods address the problem by allowing a configuration initially out of equilibrium to evolve toward a stationary state equivalent to static equilibrium, and the paradigmatic case is Barnes's Dynamic Relaxation (1977), in which residual forces are transformed into nodal velocities and accelerations, with the use of fictitious masses and damping to stabilize convergence. This line also includes subsequent developments such as the particle-spring systems of Kilian and Ochsendorf (2005) and, in the more recent genealogy shown in the figure, the Multibody Rope Approach of Manuello (2004) and the Improved MRA of Manuello, Melchiorre, and Marano (2024) (Linkwitz, 1999; Veenendaal & Block, 2012; Manuello Bertetto, et al., 2024a; Fallacara, et al., 2024; Pastrana Jimenez, 2026; Manuello, 2020).

Overall, all these methods pursue the same objective, namely to find a funicular geometry capable of transferring loads predominantly through axial forces, but they do so with different assumptions and tools. Elastic methods materialize the problem, Geometric methods linearize it through more compact equilibrium quantities, and Dynamic methods solve it as an evolution toward a stationary state, while the more recent contributions highlighted in Figure 4.23, such as Differentiable FDM, Differentiable CEM, the Mixed Equilibrium Model (MEM), and Neural FDM, show how this tradition is now evolving toward hybrid models that combine mechanics,

optimization, and machine learning without abandoning the conceptual core of classical form-finding (Veenendaal & Block, 2012; Pastrana Jimenez, 2026).

### 4.3 The first form-finding process

Following the theoretical framework outlined so far, this section and the next will explain the form-finding process that determined the final configuration of the structure examined in this thesis. For the purposes of the design development, it proved necessary to articulate the procedure into two distinct yet closely sequential phases. The present section examines the first of these.

The geometric modeling and the subsequent structural study were developed through Rhino and Grasshopper, with the support of their related plug-ins. In this context, the first form-finding phase was entrusted to Kangaroo Physics, a Grasshopper plug-in that makes it possible to simulate the physical behavior of the system and identify its equilibrium configurations.

The process began with the generation of a planar square-based mesh measuring 10 × 10 m and subdivided into ten divisions per side. At this stage, this dimensioning was adopted conventionally and does not constitute a determining parameter for the purposes of the present investigation. It was nevertheless chosen while taking into account possible future developments of the research, oriented toward the study of the spatial organization and internal distribution of the habitation module. From this perspective, the structure may subsequently be investigated at a greater level of detail, as a possible habitat for multiple crew members, including differentiated spaces such as living quarters, workspaces, multifunctional common areas, recreational spaces, areas for physical activity, and a greenhouse intended for the cultivation of fresh food, in coherence with long-duration mission scenarios or permanent human presence.

The first form-finding phase was therefore set up by means of a set of specific Kangaroo components. The Show component, shown in Figure 4.24, enables real-time visualization of the deformation of the mesh during the evolution of the process.




***Figure 4.24:*** *Component "Show".*

The Edge Length component, Figure 4.25, was instead used to assign the edges of the mesh a target length and a given degree of stiffness, thus giving the surface a behavior comparable to that of a deformable network. In this way, the mesh becomes suitable for undergoing controlled geometric transformations within the form-finding process.

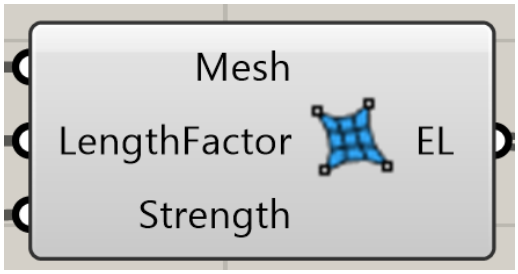



***Figure 4.25:*** *Component "Edge Lengths".*

A central role is played by the Load component, visible in Figure 4.26, used to simulate the action of a vertical load acting downward. The corresponding Force Vector input was connected to the Unit Z vector oriented along the negative direction of the Z axis, so as to reproduce the effect of gravity.

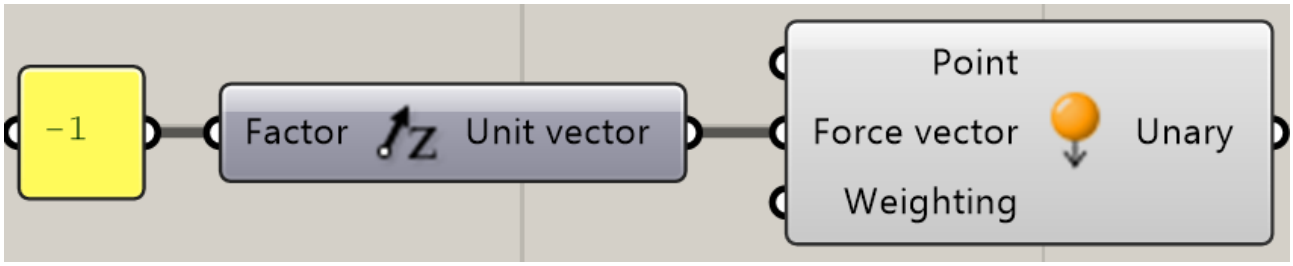



***Figure 4.26:*** *Component "Load" and "Unit Z".*

The Anchor component, Figure 4.27, was instead used to define the point constraints of the mesh and to control its boundary behavior during the simulation.

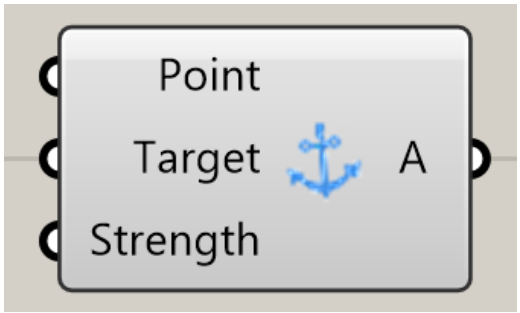



***Figure 4.27:*** *Component "Anchor".*

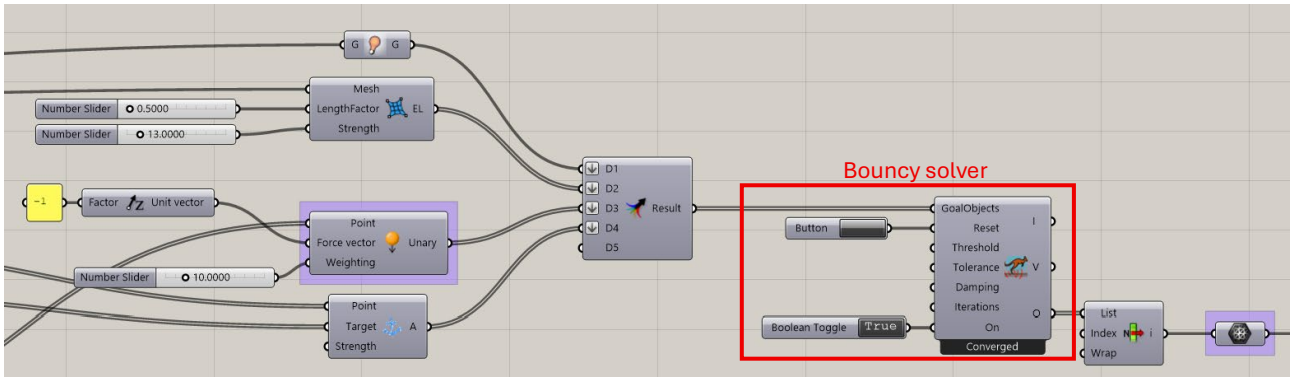



***Figure 4.28:*** *Grasshopper definition for the first form-finding stage, with the "Bouncy Solver" component highlighted in red.*

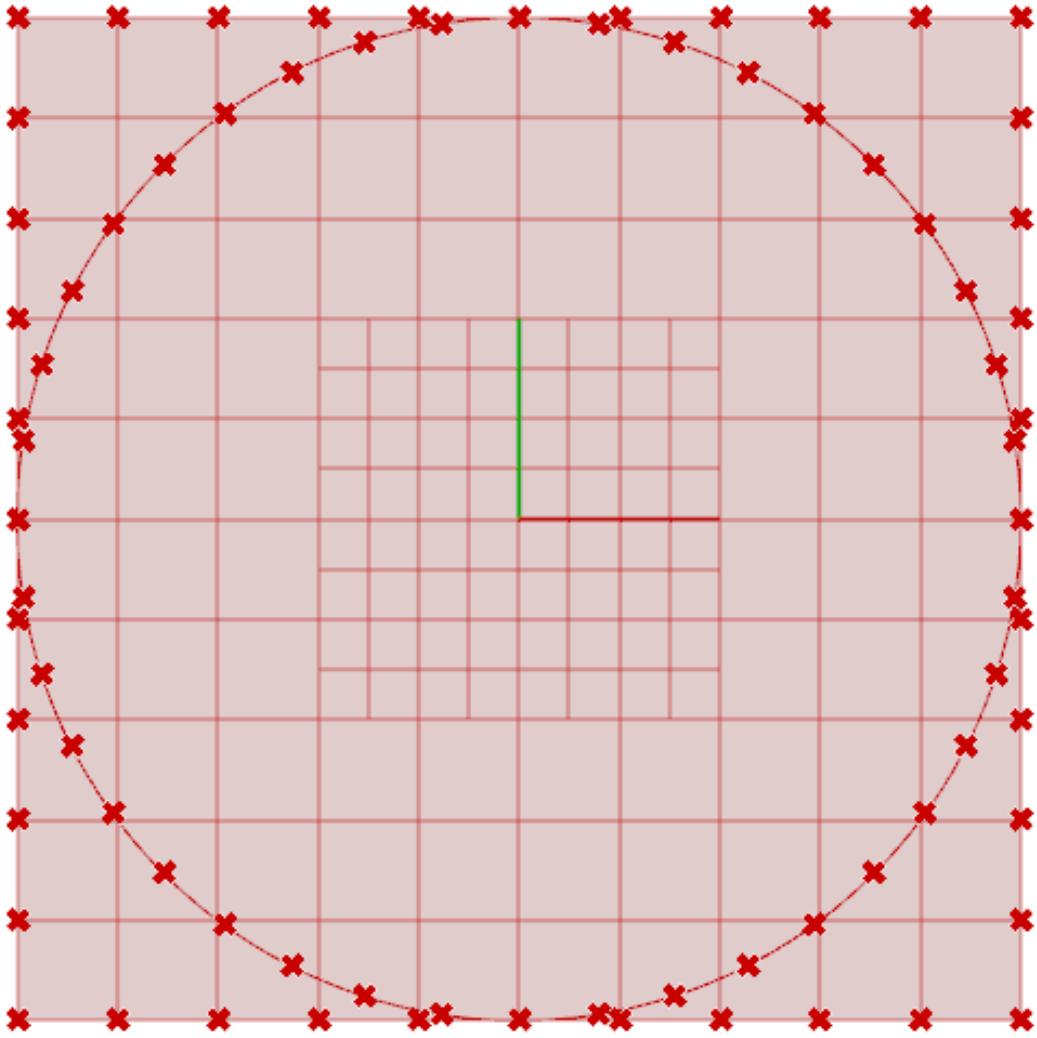


***Figure 4.29:*** *The initial square mesh and the inscribed circumference that defines the perimeter of the structure.*

All the Goal objects thus defined were finally connected to the Bouncy Solver, Kangaroo's dynamic solver, which makes it possible to observe iteratively the evolution of the mesh until an equilibrium configuration is reached.

Although the procedure began from a square mesh, this choice responded exclusively to the need for operational simplicity and parametric control. The basic configuration of the structure was in fact subsequently brought back to a circular plan, considered more efficient from a structural point of view in the presence of internal pressurization. A circular base in fact allows a more uniform distribution of stresses along the perimeter, limiting the localized stress concentrations that would instead be more pronounced at the corners of a square configuration. To this end, a circle inscribed within the initial mesh was generated, and from it discrete points were derived along the circumference, subsequently assumed as the target positions of the perimeter nodes of the square mesh. During the simulation, the boundary nodes are therefore progressively drawn toward the corresponding points on the circumference, transforming the originally square boundary into a coplanar circular edge.

Under the combined action of the vertical load and the boundary constraints, the mesh progressively deforms downward, seeking an equilibrium configuration under its self-weight. The result of this first phase may be interpreted as a gravitational funicular form, that is, a configuration that tends to organize itself according to a geometrically efficient arrangement with respect to the action of its own weight. The resulting geometry therefore defines the essential form of the structure and may be described, in general terms, as a dome with a funicular profile, derived from a process of equilibrium under gravity.

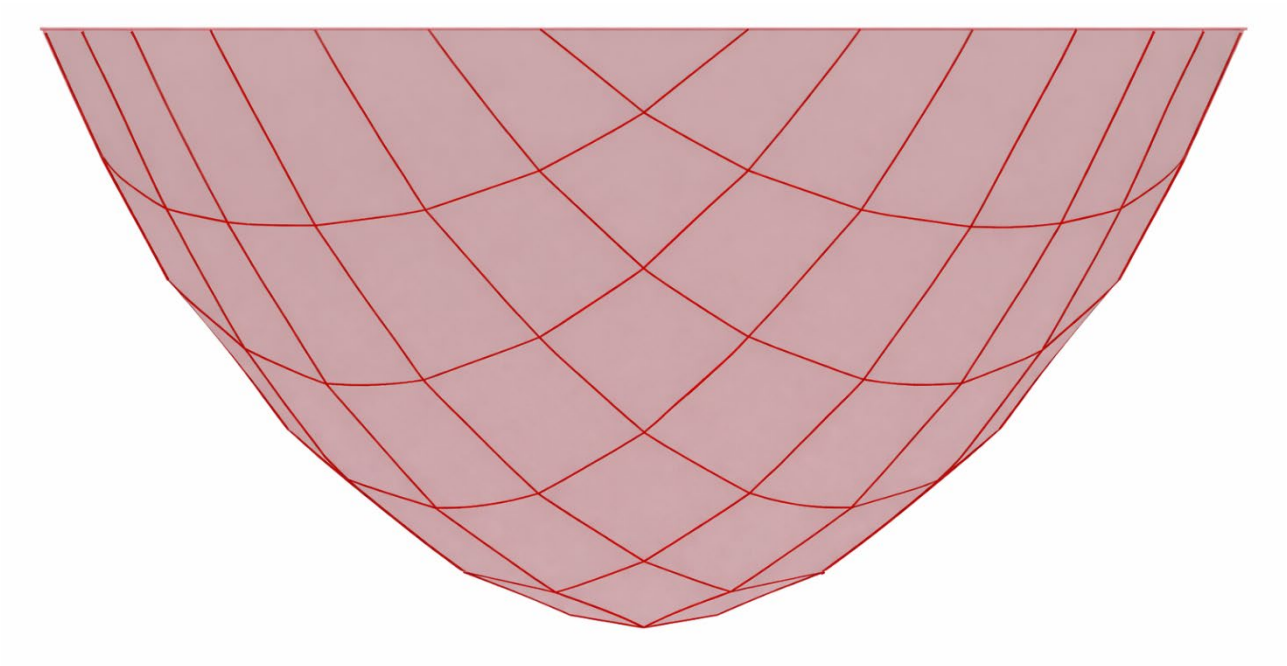


***Figure 4.30:*** *The result of the first form-finding stage.*

This procedure digitally evokes the physical principles underlying the experimental models developed by Antoni Gaudí, Frei Otto, and Heinz Isler. In all these cases, the objective is to identify a form capable of responding efficiently to gravitational action, reducing the presence

of bending and favoring a predominantly axial or membrane behavior. A flexible rope suspended at its ends and subjected only to its own weight, in fact assumes a catenary configuration and works ideally in tension. Once inverted, the same curve defines a funicular arch that, under the same loading condition, works ideally in compression. It is precisely this principle that constitutes the theoretical foundation of the first form-finding phase described here.

### 4.4 The second form-finding process

Having obtained the spatial equilibrium configuration under the action of gravity following the first form-finding process, the work proceeded with a second phase aimed at investigating the effects of internal pressurization on the definition of the structural form. This process was explored through a second Grasshopper plug-in, Karamba3D. Although this tool was primarily developed as a structural analysis instrument based on the Finite Element Analysis method (FEA), it proved particularly suitable for this second stage of the process, as it makes it possible to determine and describe the behavior of the structure with greater mechanical rigor. In this second phase, therefore, form-finding is no longer understood merely as the search for a stable geometric configuration, but as a process guided by the structural response of the system under a physically determined action, namely the internal pressure necessary for human life inside the habitat.

Starting from the mesh derived from the first phase, the first step consisted in assigning a cross-section to the surface by means of the corresponding Cross-section component. As shown in Figure 4.31 below, this component makes it possible to define various section parameters, such as material and thickness, through the Material and Height (cm) inputs. In the present case, the Shell Const typology was adopted, that is, a constant-thickness section, consistent with the continuous shell nature of the model. At this preliminary stage, material and thickness are to be understood in an exploratory sense, and not yet as definitive design data.

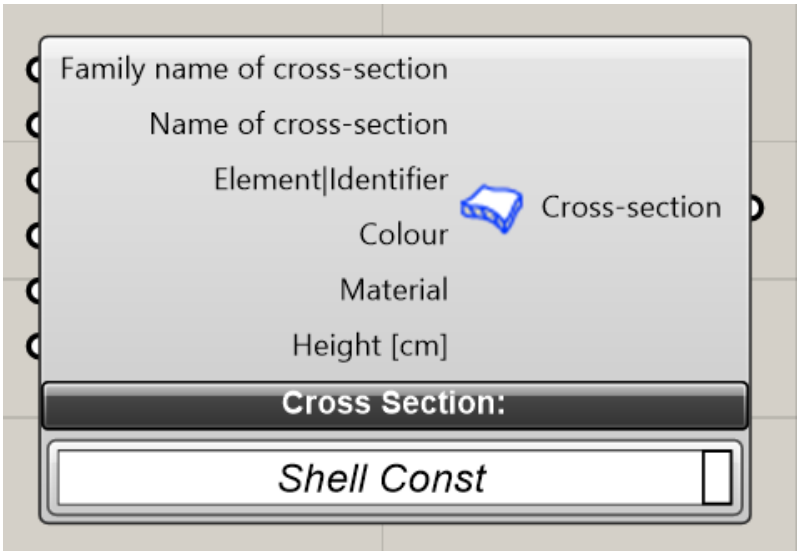



***Figure 4.31:*** *Component "Cross-section".*

The cross-section was subsequently associated with the Create Surface Element component, here used in the MToShell variant. This component, visible in Figure 4.32, serves to convert the geometric mesh into a set of finite surface elements that can be analyzed by Karamba3D as a continuous shell. The component in fact receives the mesh and the cross-section as inputs, returning the corresponding structural elements. In this way, the surface generated in the first form-finding phase is reinterpreted no longer as a simple geometric entity, but as a continuous structural organism discretized into shell elements.

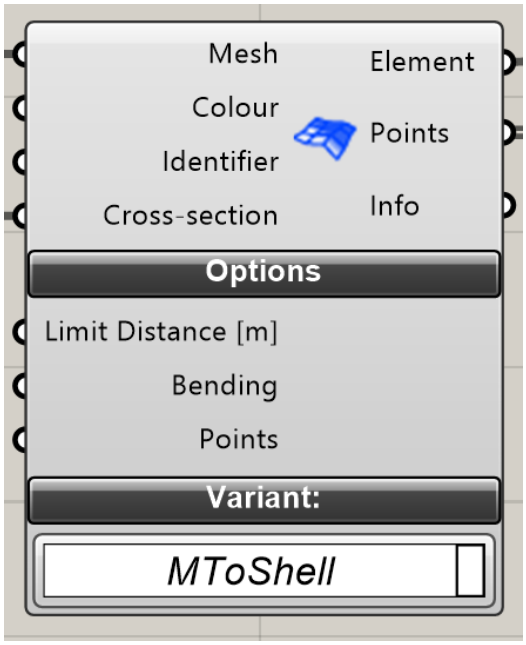



***Figure 4.32:*** *Component "Create Surface Element" in the MToShell configuration.*

From a geometric point of view, it is important to emphasize that the initial mesh, originally consisting of a regular subdivision of perfectly equal squares, undergoes a substantial transformation during the first form-finding phase. The gravitational deformation that leads to the dome configuration causes the original square cells to become a network of irregular quadrilateral faces distributed over a curved surface. The lines that were initially straight are thus transformed into a pattern of spatial curves intersecting on the surface of the dome, as shown in Figure 4.33. This geometric transformation is decisive, since it defines the morphological support on which the second phase of form-finding acts.

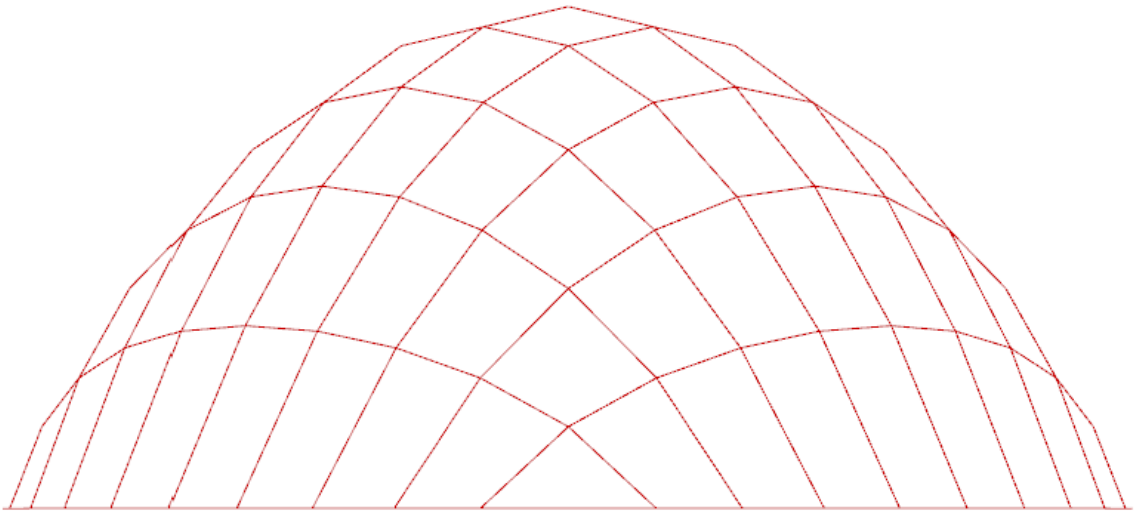


***Figure 4.33:*** *The grid network of the shell.*

For the definition of the constraints, a strategy was adopted that was not limited to the base circumference of the dome but extended to the entire network of edges delimiting the quadrilateral faces. This network was decomposed into a series of points, which were subsequently associated with the Support component, as shown in Figure 4.34. In this context, the constraints at the base of the model should be understood as the actual structural supports of the system, while the ones located along the edges of the faces serve as form-generation constraints used during the computational process.

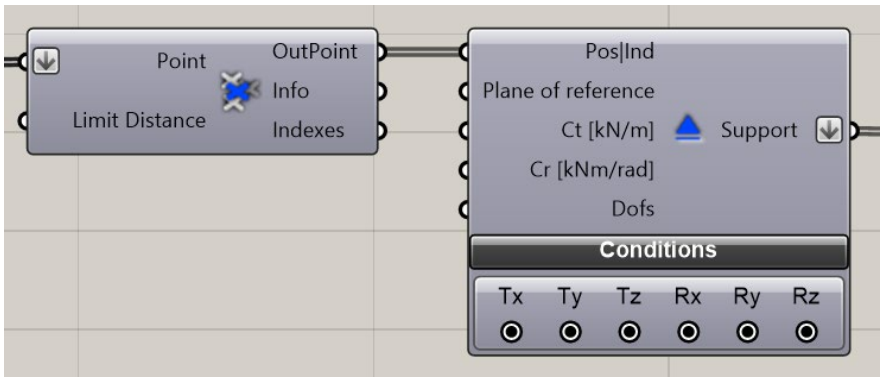



***Figure 4.34:*** *Component "Support".*

At this stage of the process, the system is subdivided into two components: The quadrilateral faces of the mesh and their mutually adjacent edges. This strategy proved effective for the application of internal pressurization and for the definition of the supports.

The pressurization action was then introduced by means of the Loads component, modeling the load as *MeshLoad Const*, that is, a constant load applied uniformly to the mesh and

associated with a dedicated Load Case (LC0). As shown in Figure 4.35, the component receives as inputs the load vector, the mesh, and the Load case, while the *Local to mesh* option makes it possible to refer the load to the local system of the shell elements. This step is fundamental: Rather than a generic global vector along the Z axis, it is precisely the local reference to the mesh that ensures that the load acts orthogonally to each face, that is, along its normal, regardless of its inclination in space. The magnitude of the vector is equal to 101 kN/m$^2$, approximately corresponding to standard terrestrial atmospheric pressure. This value was deliberately adopted as a severe and conservative case, in order to simulate an internal condition compatible with a long-term habitable environment and, at the same time, mechanically demanding for the structural system.

At this stage, the vector defining the pressure was intentionally inverted by means of the *Reverse* component in Grasshopper, visible in Figure 4.35. This choice should not be understood as a literal reproduction of internal pressure, but rather as a morphogenetic strategy aimed at generating the desired configuration of the surface modules. The inversion of the vector in fact induces the formation of surface modules concave toward the interior, comparable to a succession of small shells; in section, as shown in Figure 4.39, they may be read as arches. In this way, the deformation of the surfaces does not assume a merely aesthetic value but becomes a tool for directing the flow of stresses toward the edges of the individual faces and, above all, toward the interfaces between adjacent elements, which thus take on a primary role in the transfer of forces.

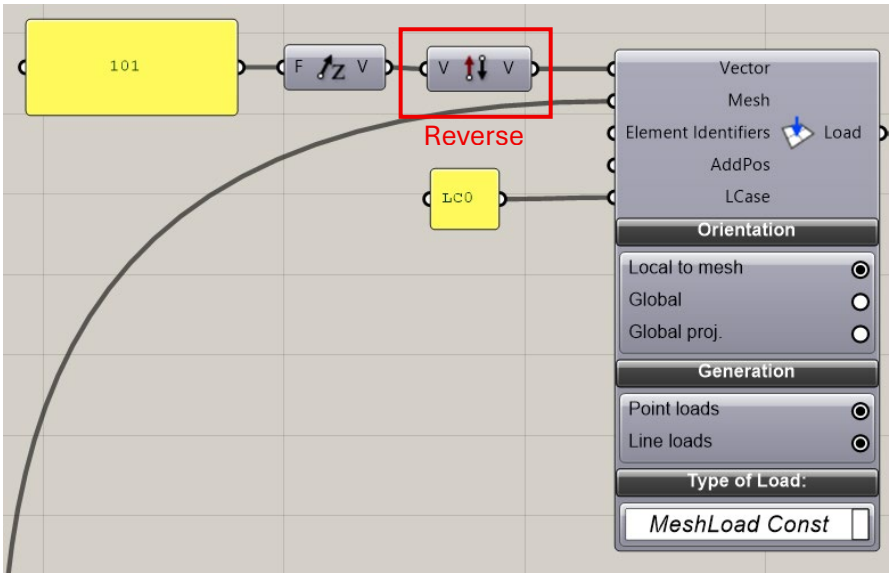



***Figure 4.35:*** *Component "Loads".*

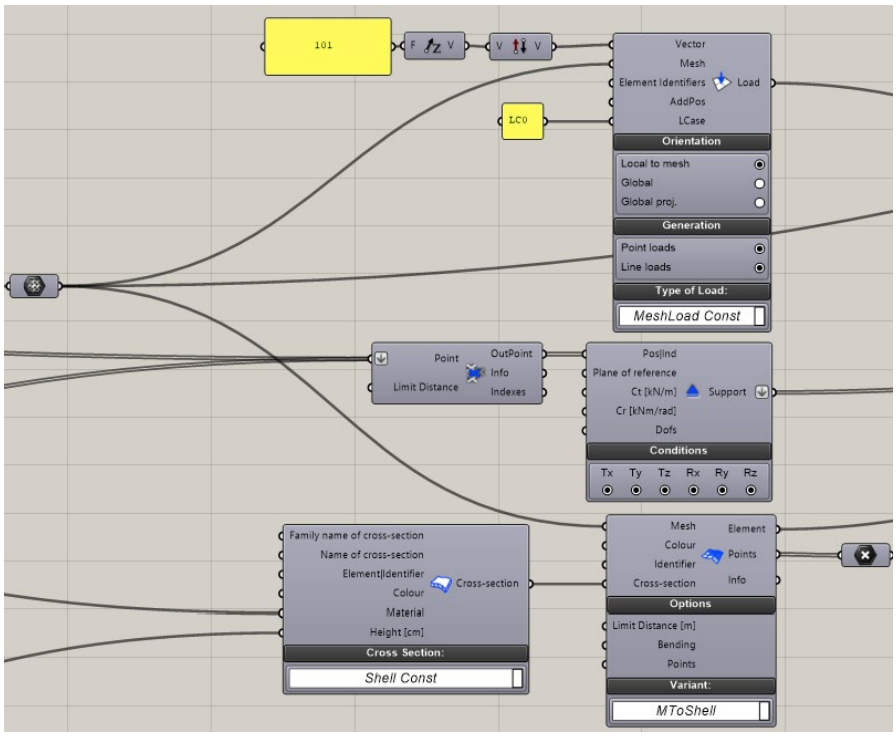



***Figure 4.36:*** *Grasshopper definition for the second form-finding stage.*

The most structurally significant aspect of this second stage therefore lies in the choice to apply pressure exclusively to the quadrilateral faces, while keeping the edges of the mesh as constrained lines. This strategy makes it possible to control the mechanical behavior of the system intentionally. Each face, free to deform within a restrained perimeter, assumes a curvilinear configuration comparable to pressurized lobes, which promotes a predominantly membrane response. The deformations thus generated are to be interpreted as a mechanical reorganization of the entire surface. The curvature assumed by each element in fact makes the transmission of stresses within its plane more efficient, while the edges and their corresponding intersection nodes are configured as privileged locations for the collection, concentration, and redistribution of stresses.

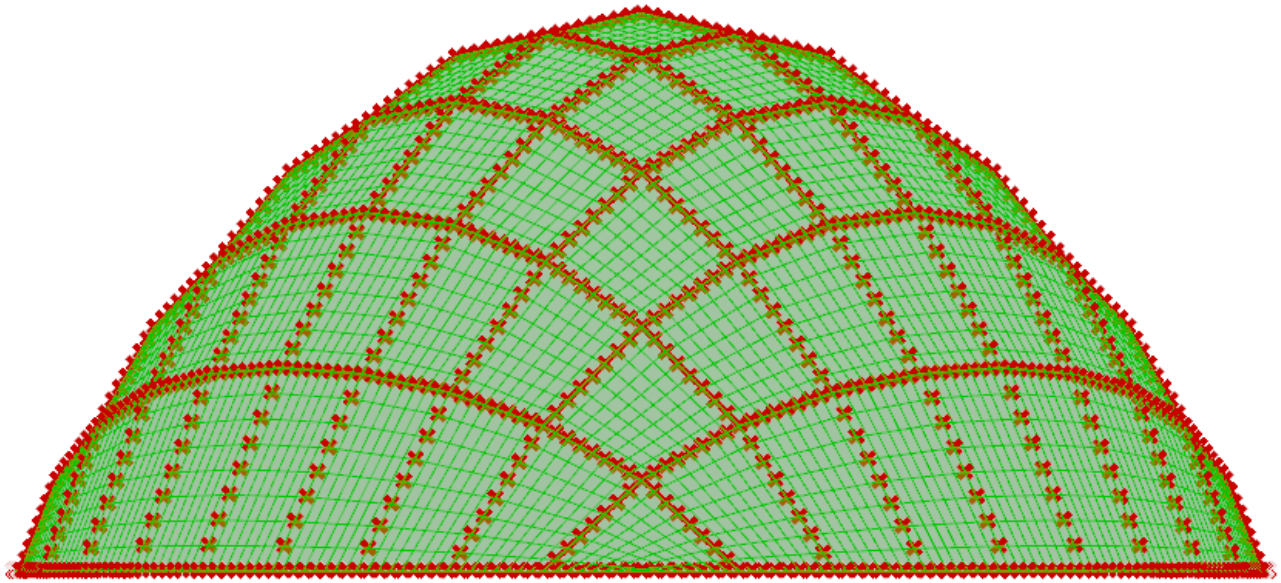


***Figure 4.37:*** *The structural subdivision between the mesh (in green) and the edges, highlighting the support points (in red) along the perimeters of the faces.*

This results in a clear differentiation of structural roles, as shown in Figure 4.37 above. On the one hand, the curved surfaces work as membrane-resistant fields; on the other, the network of interfaces performs the function of a containing and load-transferring framework. The system, therefore, does not distribute forces uniformly and indiscriminately over the entire shell, but organizes them along discrete lines, which may be interpreted as privileged structural bands and, in a subsequent phase of the project, may become the subject of structural analysis and specific reinforcement.

The mechanical behavior of the structure will be investigated in greater depth in Chapter 6.

The result of this second form-finding process is illustrated in Figures 4.38 and 4.39, which represent the elevation view and the sectional view of the structure, respectively. The first figure allows us to visualize the formal configuration of the lobes on the surface of the shell, while Figure 4.39 allows us to grasp their organization on the intrados of the structure and to understand how the forces are distributed along the interfaces.



***Figure 4.38:*** *The structure seen in elevation after the second form-finding stage.*

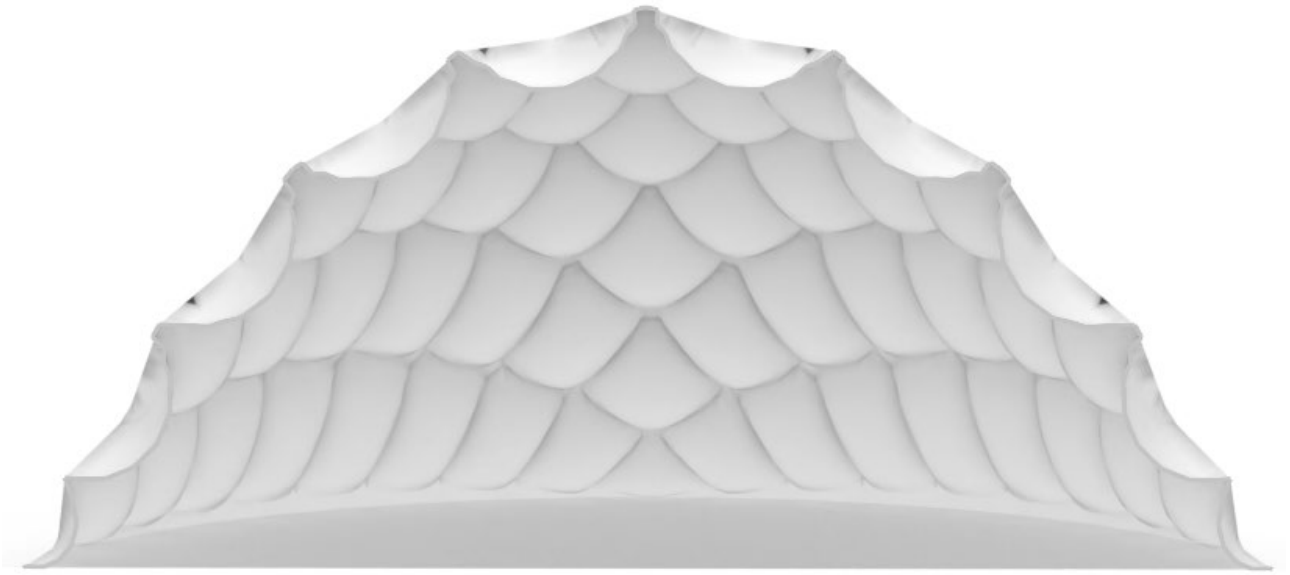


***Figure 4.39:*** *A cross-section view of the structure.*

The next step concerned the definition of an outer shell, mirroring the inner one and conceived with a threefold purpose: to enhance the radiation shielding of the interior spaces by adding shielding mass to the system; to help counterbalance the effects of internal pressurization through its own weight; and to generate interstitial spaces intended to accommodate life-support systems. The outer shell was modeled by following the same process adopted for the inner one, starting from an identical planar square mesh and subjecting it to the same form-finding steps, so as to maintain geometric continuity, morphological coherence, and uniformity of structural language. The only difference introduced concerned the inversion of the direction of the pressure vector during the second stage of form-finding, which generated mirrored lobes,

concave outward, geometrically corresponding to those of the inner shell and connected along their respective edge lines.

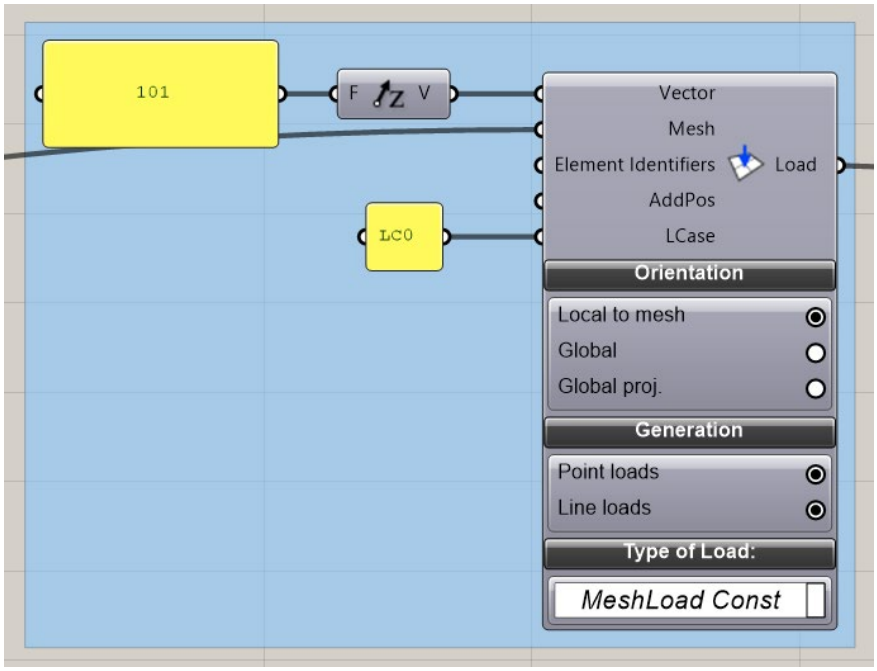



***Figure 4.40:*** *The "Loads" component used for the second form-finding process of the outer shell. As can be observed here, the "Reverse" component is not present, thus generating lobes mirrored to those of the inner shell.*

The introduction of the second shell thus transforms the system into a collaborative double-shell configuration. Whereas the inner shell responds to pressurization primarily through membrane stresses, channeling them toward the edges and nodes of the mesh, the outer shell, thanks to its opposite curvature and its own weight, performs an equilibrating and stabilizing function. The lines of connection between the lobes of the two surfaces therefore become the main locations for the collection and redistribution of forces, defining a more legible structural hierarchy in which the interfaces between the modules are configured as privileged load-bearing surfaces and potential locations for local reinforcement.

At this point the connection with the biological reference becomes explicit. The geometry obtained at the end of the form-finding process does not simply imitate the morphology of Arabidopsis thaliana cells but transfers one of their fundamental principles into an architectural and structural language. As stated in Chapter 3, plant cells' internal pressure acts against the cell walls, generating a state of tension that actively contributes to the stability, growth, and definition of the cell. Similarly, in the proposed structure, internal pressure is not merely considered as a load to be resisted, but rather as a generative factor capable of shaping the shell into an efficient morphological configuration.

In this way, the resulting lobed surfaces may be interpreted as a translation of cellular tissues, where each module behaves as an individual pressure-responsive unit connected to the adjacent ones through a network of interfaces. These collect and redistribute stresses, recalling the functional differentiation of biological tissues. The reference to Arabidopsis thaliana is both mimetic and methodological, taking inspiration from its shape and from the processes that define it.

The whole form-finding process developed in this chapter therefore establishes the conceptual core of the proposed lunar habitat. The first stage defines a funicular configuration, driven by gravity, while the second introduces internal pressurization as an active shaping load. The resulting model encloses the main themes discussed in previous chapters, such as the need for protection from the lunar environment, the use of geometry as a structural tool and the biomimetic translation of biological principles into an architectural system. At this stage, the structure is not yet at its final configuration but is rather the morphological basis upon which the subsequent analyses are carried out.



***Figure 4.41:*** *The outer shell seen in elevation.*

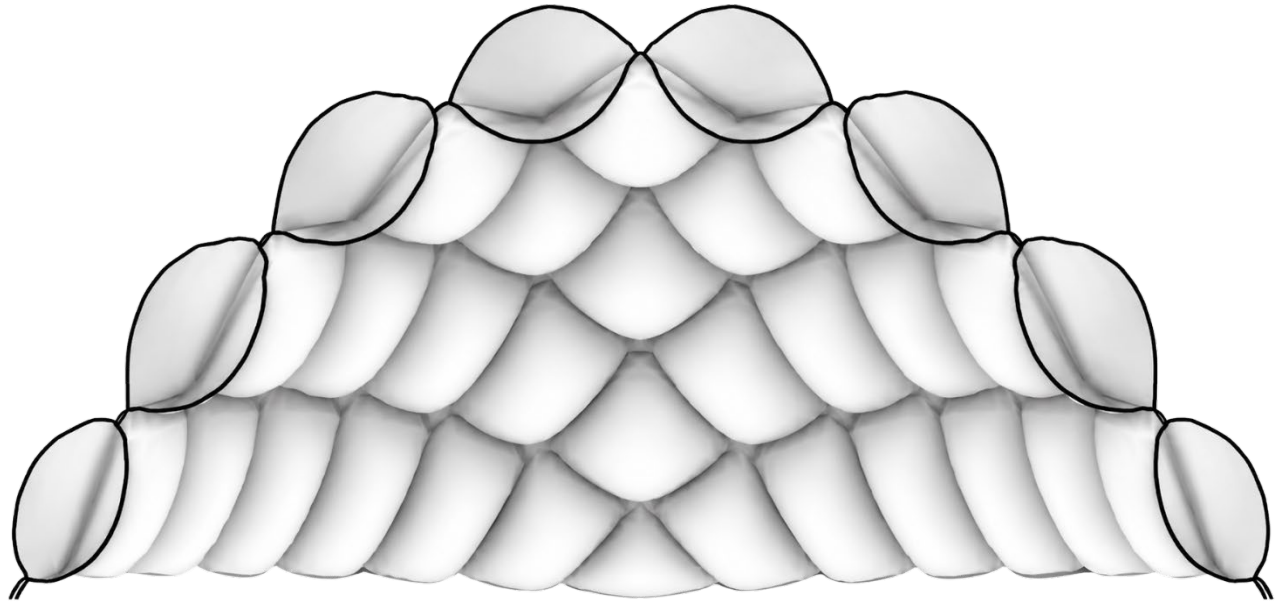


***Figure 4.42:*** *The structure, complete with inner and outer shell, seen in cross-section.*

# CHAPTER 5 – Resource-Based Design Strategies

## 5.1 In-Situ Resource Utilization (ISRU)

In the context of human exploration of the Moon and Mars, the theme of In-Situ Resource Utilization (ISRU) emerges as a settlement strategy that includes the identification, extraction, processing, transformation, and use of resources available directly on the celestial body, with the aim of reducing dependence on terrestrial resupply and progressively making long-duration missions and permanent presence sustainable. From this perspective, ISRU concerns not only essential resources such as water and oxygen, but also energy supply, propellants, construction materials, manufacturing, life support, and settlement logistics (Arnhof, et al., 2022; Zhang, et al., 2023; NASA, 2023c)[35].

Building on these premises, the exploitation of indigenous resources is central to this research, as it has determined a series of design choices, such as the construction material and the design of the structure.

The centrality of ISRU derives first and foremost from issues of mass, cost, and risk. Transporting from Earth everything required for a permanent human settlement on the Moon or Mars entails an enormous logistical penalty, which increases with the duration of the mission and with the distance from the planet of origin. For this reason, the literature on the subject emphasizes that the sustainability of exploration will depend not only on the efficiency of launch systems or the frequency of resupply, but on the ability to support the habitat and its crew using local resources, converting what is available in-situ into essential goods for survival, energy production, and construction. NASA itself presents ISRU as a key condition for deep space exploration, while ESA explicitly links it to a sustainable return to the Moon, based on partnerships, local infrastructure, and the transformation of site materials into useful resources (ESA, 2019; NASA, 2023c; Zhang, et al., 2023).

In the review article *Overview of the Lunar In Situ Resource Utilization Techniques for Future Lunar Missions*, Zhang et al. observe that lunar exploration is progressively moving from a phase of mere scientific understanding to a phase of utilization, and that future missions will tend to shift from short-term stays to long-term residence, with particular attention to resource-rich areas, such as the lunar south pole. According to this scenario, the Moon can function as a technological and infrastructural platform for even more distant missions, including Mars (NASA, 2023c; Zhang, et al., 2023).

From a strategic point of view, the priorities of ISRU are quite clear: Water, oxygen, energy, and construction materials are the first elements to be guaranteed, as they constitute the essential requirements for establishing a human presence in extraterrestrial contexts. The research by Zhang et al. identifies four major categories of lunar resources: (1) Mineral resources, (2) water resources, (3) volatiles, and (4) solar energy. The research also highlights that the main objectives of lunar ISRU include the in-situ supply of materials required for life support, the in-situ construction and manufacturing of habitats and infrastructure, the production of propellants, and support for Moon-based scientific research (Zhang, et al., 2023).

With regard to water resources, the permanently shadowed regions of the lunar poles constitute the most promising reservoir, with the total mass of water in the first surface meter of the PSRs (Permanently Shadowed Regions) estimated at around $2.9 \times 10^{12}$ kg (Crawford,

[35] *The citation refers to the source: Overview, In-Situ Resource Utilization* (NASA, 2023c).

2015), while the Apollo samples show much lower water contents (Li & Milliken, 2014). Regarding water, literature distinguishes between two main strategies. The first consists of the thermal extraction of ice through systems that use sunlight directed by mirrors or heated drills, in order to sublimate or evaporate the ice and collect the vapor through cold traps. The second consists of the production of water through the hydrogen reduction of regolith, particularly ilmenite ($FeTiO_3$), a solution considered highly promising because it can also be applied outside polar areas and is therefore less constrained by the geographical distribution of ice. The prototypes developed within ESA and NASA contexts have already demonstrated the feasibility of this approach, although yields remain limited and unresolved issues persist regarding energy consumption, excavation, and mining activities. In terms of settlement scenarios, the first strategy appears more suitable for polar bases, while the second has a broader relevance, and its further development could expand settlement horizons by not limiting human presence solely to polar areas (NASA, 2023c; Zhang, et al., 2023).

Oxygen represents another major strategic supply chain. In addition to being obtainable from water, it can be extracted directly from regolith through processes such as hydrogen reduction, molten regolith electrolysis (MRE), molten salt electrolysis (MSE), and vacuum thermal decomposition. Among these, molten regolith electrolysis is particularly interesting because it allows oxygen and metals to be obtained simultaneously, without additional electrolytes, although it requires very high temperatures and highly resistant electrode materials. This is a promising approach because it closely connects the life-support supply chain with that of manufacturing; from this perspective, oxygen extraction produces a vital consumable while also generating metallic by-products that can be reintegrated into construction and production processes (Zhang, et al., 2023).

*Regolith*

When discussing extraterrestrial habitats, and especially those built by exploiting in-situ resources, the issue of regolith must inevitably be addressed. The entire surface of the Moon is covered by regolith, and its mineral composition, close to that of terrestrial basalts, makes it a raw material potentially suitable for in-situ construction. Zhang et al. emphasize that the construction of a lunar base is one of the fields in which ISRU appears most practicable, but also most dependent on the extreme environmental conditions of the lunar context, particularly high vacuum, low gravity, severe thermal fluctuations, and energy limitations. For this very reason, terrestrial construction methods cannot simply be transferred into space but must be reconsidered starting from the nature of the lunar soil and from the ways in which it can be transformed into a building component (Zhang, et al., 2023).

The construction strategies currently most widely studied can be traced back to three families: Additive manufacturing with mixtures or binders, sintering techniques, and extrusion printing of regolith-based inks. The first group includes *contour crafting*, which uses a liquid binder and materials such as sulfur concrete, and the *D-Shape system*, also developed within the ESA context to produce protective shells using regolith as a raw material. Both methods show considerable potential, but also significant limitations in the lunar environment, especially about material pumping, the use of liquids in vacuum, and the need to transport significant parts of the system from Earth (Zhang, et al., 2023).

Sintering techniques, however, appear particularly promising, as they directly exploit the mineral nature of regolith. Microwave sintering has been proposed as an alternative to radiative

furnaces and offers advantages such as high efficiency, relatively uniform heating, and good energy availability. Solar sintering, on the other hand, exploits an energy resource available in-situ and makes it possible to produce bricks, interlocking components, and small structural elements, although with a lower processing depth and longer times compared to microwaves (Zhang, et al., 2023).

This line of research is also connected to the reflections presented in *Turning Dust to Gold: Building a Future on the Moon and Mars*, by Haym Benaroya, who, in the seventh chapter of his book, addresses ISRU within the broader framework of autonomous construction and the transformation of regolith into a true building material. In particular, the text refers both to the topic of *cast regolith*, or *cast basalt*, which could be produced by melting regolith and cooling it slowly in order to obtain a crystallized material with very high compressive strength but brittle behavior in tension, and to that of *lunar concrete*, including sulfur-based concrete, designed to operate without water and to reach useful strengths in short times. From this perspective, the possibility of casting or sintering prefabricated elements shows a certain relevance to the theme of this research (Benaroya, 2010). This theme is consistent with structural studies on lunar habitats, in which regolith-based concrete shells have been investigated as possible structural systems for pressurized lunar habitats, especially when combined with Earth-supplied tensile reinforcement capable of resisting pressurization-induced tensile stresses and contributing to micrometeoroid protection (Sumini, et al., 2018).

*Automated construction processes*

Benaroya also insists that extraterrestrial construction cannot be separated from automation. The idea of sending teams of autonomous robots to the Moon, capable of preparing the site, levelling or sintering the ground, processing the regolith, and fabricating a layered structure in the 6–12 months preceding the astronauts' arrival, is not presented as a mere suggestion, but as a direct response to the constraints of mass, energy, safety, and EVA time. The logic of ISRU concerns the entire construction process and all aspects of the habitat, from its construction to its use and maintenance. In this regard, local material becomes useful only if there is a technical chain that extends from mining to processing, from transformation to placement, through to maintenance and the possible self-repair of the system (Benaroya, 2010). From a design-evaluation perspective, multi-objective studies on lunar habitat structures similarly show that regolith-based construction must be evaluated not only as a material substitution strategy, but as part of a broader trade-off involving transported mass, local material processing, crew protection, radiation shielding and micrometeorite resistance (Sumini, et al., 2018).

The role of robotics also appears central in the Moon Village project. Arnhof et al. show that the reference studies envisage habitat construction being managed entirely through robotics, with the initial infrastructure, such as landing pads and traffic routes, being built with extremely limited human collaboration. Human interaction in the construction and maintenance process must be reduced to the minimum necessary, and this requires the integration, already at the design stage, of principles of modularity, repairability, standardization, and recycling, from the structural scale down to that of the individual component (Arnhof, et al., 2022).

The Moon Village project proposes a useful reference framework for the present research. In the initial phase, still uncrewed, ISRU is expected to support energy production, extraction tests, the construction of the landing pad, shelters for equipment, and the first infrastructures;

in the subsequent phases, activity extends to the production of water and oxygen for propellant and life support, radiation shielding, the construction of roads and support volumes, and eventually to more advanced scenarios involving waste recycling, metal refining, and the production of fibers and ceramic or glassy materials (Arnhof, et al., 2022).

The first step in the development of these perspectives is certainly represented by robotic precursor missions, capable of constructing fundamental infrastructure before the arrival of the crew. This requires the extraction and handling of ISRU resources, site preparation, construction site management and all its components, as well as the positioning of prefabricated components brought from Earth and integrated into the structure on site. All of this requires a highly coordinated operational chain.

The research, *Robotic Construction & Prototyping of a 3D-Printed Mars Surface Habitat*, by Yashar et al. revealed an important distinction between automated construction and autonomous construction. An automated sequence performs pre-programmed operations, as in the case of the robotic arm; an autonomous sequence, instead, should be able to perceive the environment, recognize anomalies, adapt the process in real time, modify the printing path, avoid collisions, correct placement errors, and decide when to request human support. The study indeed emphasizes that future developments will need to focus on the integration of robotics, sensors, real-time control, dynamic BIM, and 4D construction sequences (Yashar, et al., 2019).

In perspective, extraterrestrial construction will therefore require robots capable of working in a coordinated manner according to multilevel logics. Machines for site preparation, systems for resource extraction and transport, mobile 3D printers, robotic arms for the insertion of components, and inspection robots for maintenance (Sumini & Mueller, 2017). After the arrival of the crew, robotics would continue to operate in a collaborative mode, supporting inspection, maintenance, repair, and management of the mechanical and electrical systems integrated into the structure. Autonomous construction should therefore not be understood as a replacement for humans, but as the progressive reduction of their direct operational involvement, through a hybrid model in which automation, local autonomy, remote supervision, and human-robot collaboration contribute to the construction of habitats (Yashar, et al., 2019).

In the context of the present research, automation is treated as a necessary condition for the construction process of the habitat. The lobed modules are indeed designed as geometric and structural units, conceived to be robotically fabricated and subsequently positioned and connected through automated procedures. Although the development of a definite construction protocol is beyond the scope of this thesis, the strategy assumes that complex extraterrestrial structures will require a coordinated chain of automated operations.

*Energy as enabling infrastructure*

The design of such habitats cannot be separated from the definition of a highly reliable and autonomous energy system, capable of operating under extreme environmental conditions. In a lunar or Martian settlement, energy is in fact a primary condition for crew survival and for the operational continuity of the mission. Electrical loads include, first and foremost, the extraction and manipulation of resources, the construction of the first settlement structures, life-support and environmental control systems, responsible for thermal regulation, pressure

management, regeneration of the breathable atmosphere, and the treatment of water and waste. Alongside these are communication systems with Earth and with other surface units, scientific instrumentation, sensors for monitoring the state of the habitat, fault detection and diagnosis devices, charging stations for rovers and electric vehicles, and loads related to the astronauts' daily life, such as lighting, food preparation, and food storage. Energy demand varies according to crew size, mission phase, and habitat location. In the study *Microgrids for Extraterrestrial Habitats: A Review of Technologies, Needs, and Challenges*, Chebbo et al. estimate that, for a lunar base of six people, the average energy demand is approximately 35 kW, around 5–10 kW per crew member, not including high-consumption industrial activities, such as possible ISRU plants. Some loads, such as life support, communications, and monitoring, must be powered continuously, while others, such as laboratories, vehicle charging, water recovery, and domestic activities, follow more variable profiles linked to the crew's operational rhythms. In uncrewed missions, on the other hand, priority is given above all to robotic systems, sensors, and minimal environmental control functions. Within this framework, space microgrids must integrate generation, storage, distribution, and control sources according to a redundant and adaptive logic (Chebbo, et al., 2025).

Energy planning estimates were also provided by Arnhof et al. regarding the research on the Moon Village, although in this case the organizational structure of the mission is clearly defined and includes numerous ISRU plants. Already in Phase 0, limited to testing and site preparation, energy demands on the order of 54 kW are hypothesized. In Phase 1, with the first production of propellant and water, the demand rises to approximately 165 kW. In Phase 2, with the arrival of the crew and the expansion of activities, an energy demand of approximately 363 kW is estimated (Arnhof, et al., 2022).

Solar energy represents a mature and safe solution, with a high power-to-mass ratio and long lifetime, but it is strongly conditioned by available irradiance, panel orientation, dust accumulation, day-night cycles, and distance from the Sun. In the lunar case, for example, the duration of the night requires storage systems capable of ensuring continuity for more than two weeks. Nuclear fission reactors, especially in compact configurations with *Stirling* or *Brayton* converters, instead offer stable production independent of insolation, making them particularly suitable for long-duration missions or poorly illuminated sites, but they require specific solutions for shielding, physical separation from the habitat, thermal management, and radiological safety. Fuel cells and batteries, on the other hand, complete the system as generation and storage devices. Regenerative cells, based on the cyclical conversion between hydrogen, oxygen, water, and electricity, could reduce mass compared to large batteries, but they still have limited technological maturity; lithium-ion batteries, now widely used, ensure good performance but remain vulnerable to low temperatures, overheating, and thermal runaway (Chebbo, et al., 2025).

***Table 5.1:*** *Typologies of energy production sources, advantages and disadvantages* (Chebbo, et al., 2025).

| Generation Technology | Advantages | Disadvantages |
|---|---|---|
| Solar PV | • Higher technology readiness level<br>• Higher specific power (power-to-mass ratio)<br>• Safe technology and can be installed near the human base<br>• Long lifetime | • Limited to daytime operation<br>• Larger size to achieve high power levels<br>• May require frequent cleaning due to dust accumulation<br>• Higher degradation factors due to space environmental conditions |
| Nuclear fission reactor based on Stirling converter | • Smaller physical size<br>• Highly reliable, resilient, and stable<br>• Capable of continuous operation (location and time independent) | • Radiation concerns require physical separation between the reactor and base camp<br>• Lower power-to-mass ratio<br>• Lower technology readiness level<br>• Lower designed operational lifetime (≈10 years) |
| Primary fuel cells | • Lower power-to-mass ratio | • Lower technology readiness level<br>• Lower designed operational lifetime |

The entire energy distribution system must be designed to withstand dust, vacuum, ultraviolet and particle radiation, plasma, thermal cycles, micrometeorites, and material degradation, which may compromise photovoltaic panels, cables, semiconductors, batteries, radiators, and nuclear components. For this reason, the microgrid of an extraterrestrial habitat must be conceived as a critical, autonomous infrastructure monitored in real time, based on modularity, standardization, accessibility, remote diagnostics, predictive maintenance, and load prioritization. The ability to detect anomalies, reconfigure energy distribution, and keep vital systems active even in the event of failure therefore becomes essential to ensuring safety and operational continuity in environments where direct human intervention is limited and every component must be selected by considering not only performance, but also mass, durability, maintainability, and environmental vulnerability (Chebbo, et al., 2025).

*Biocomposites*

Within this panorama, there are also alternative approaches, which do not primarily aim at the transformation of regolith but rather at the production of biological materials in-situ. The ESA ACT report, *Growing Fungi Structures in Space* proposes, for example, the construction of building and architectural elements made of fungal biocomposites as a possible alternative to reduce the costs of locating, extracting, and handling indigenous resources, by transporting minimal quantities of mycelium from Earth and allowing it to grow on organic substrates cultivated in-situ. Despite the theoretical advantage of a low initial mass requirement, biodegradability, and the possibility of integrating them into a *cradle-to-cradle* cycle, the report itself acknowledges important limitations, such as the need for a highly controlled growth environment and uncertainty regarding the final properties of the material (Wösten, et al., 2018).

At the current level of technological maturity, the use of biomaterials appears more plausible as a complementary or internal layer than as the primary envelope of a pressurized extraterrestrial habitat. The reason is that, in the specific case of an architectural envelope

designed to respond to internal pressurization, shielding, and structural stability, regolith remains today the candidate most directly studied and most consistent with ISRU supply chains that are already mature or in the process of maturing. It is available in large quantities, can function as shielding mass, can be sintered or transformed into components, and can be integrated into a construction logic that combines robotics, additive manufacturing, and thermo-mineral processing. In this sense, research on biomaterials is useful above all as a conceptual comparison, because it shows that ISRU is not necessarily only "mineral-based", but that, on the contrary, the in-situ production of biological systems is possible and necessary, also in the context of biocomposite materials (Wösten, et al., 2018; Zhang, et al., 2023).

It appears increasingly evident that ISRU cannot be restricted solely to the issue of construction materials but is instead a system of operational processes and functional logics intimately connected to energy supply, resource extraction and transformation, subsistence, life-support systems, radiation shielding, and transport.

ISRU is widely regarded as one of the most promising strategies for reducing dependence on terrestrial resupply and, despite the multidisciplinary efforts that still need to be undertaken, for supporting the progressive development of long-duration or permanent extraterrestrial settlements (Petrov, et al., 2019; Vock, 2025).

### 5.2 Construction material

The present section investigates the theme of the construction material more closely and introduces the experimental campaign, developed starting from the purchase of Martian and lunar regolith simulants.

Although the thesis focuses on the design of a lunar habitat, the investigation of Martian simulants has been included in order to broaden the field of research towards scenarios of human exploration of deep space. As previously stated, the Moon is not considered an ultimate objective, but rather a first strategic step towards human deep-space exploration missions and stable presence in extraterrestrial contexts, Mars first and foremost. At present, the experimentation is in its initial phase, which concerns the preparation of specimens using sand rather than actual Martian regolith simulants, with the aim of defining the components of the mixture, verifying their quantitative ratios, controlling setting and early-age hardening conditions, and analyzing the mechanical response of the material through flexural and compressive tests. This first phase therefore assumes an exploratory and methodological value, as it makes it possible to calibrate the mixture, understand its initial behavior, and correctly set up the subsequent experimental tests.

The next step involves the use of actual Martian regolith simulants and the refinement of the mixture and its properties, in order to then test the mechanical response of the material and draw the necessary design considerations in relation to construction technique, automated construction processes, architectural aspects, and design.

Ultimately, the experimental campaign will focus on the lunar regolith simulant, also including the verification of consolidation processes through microwave sintering.

The experimental campaign fits fully within the framework of this thesis, while at the same time broadening its perspective by investigating material and construction solutions that may potentially be adaptable to different extraterrestrial contexts and to future developments in

research on inhabiting extreme environments. Although this represents one of the fields of research still in evolution and numerous aspects require further investigation and in-depth analysis, it makes it possible to outline the future directions of development of the project, aimed at defining the main aspects of the structure in an increasingly complete way.

*Selected regolith simulants*

The first step in setting up this experimental process was the selection and purchase of regolith simulants. First, the technical specifications of the products were analyzed, as well as the literature concerning extraterrestrial structures made of regolith and related to the ISRU logic, in order to select the products most suitable for this operational scenario.

The limited quantity of extraterrestrial samples returned to Earth does not allow extensive experimental tests to be conducted for the validation of ISRU processes and technologies. For this reason, research relies on regolith simulants produced from terrestrial materials, designed to reproduce as accurately as possible the characteristics of real regolith. Consequently, the greater the fidelity of the simulant, the more reliable the experimental evaluations related to the processes of extraction, processing, construction, and material handling become (Long-Fox & Britt, 2023).

The simulants selected for the experimental campaign belong to the line developed by *Exolith Lab*, a laboratory established at the University of Central Florida for the production of high-fidelity planetary simulants. Their design is based on compositional accuracy and on the control of particle geometry, including grain size, shape, and particle size distribution (PSD). These parameters are particularly relevant because they influence the physical, mechanical, thermal, electromagnetic and chemical behavior of regolith. For this reason, the fidelity of a simulant depends on its ability to reproduce both mineralogical composition and granulometric characteristics of the reference planetary material, while also considering practical constraints such as cost, safety and the availability of terrestrial raw materials (Long-Fox & Britt, 2023).

The lunar simulant to be investigated in the experimental campaign is *LMS-1 Lunar Mare Simulant*.

From a geological point of view, the lunar surface can be traced back to two main regions: The highlands and the basaltic maria. The Apollo missions made it possible to collect samples from both, as well as from transition areas between the two provinces. In these contact zones, the compositions of the regolith show intermediate characteristics, attributable to impact ejecta and subsequent surface mixing. The variety of lunar compositions therefore makes it necessary to develop specific simulants, capable of reproducing different geological contexts and supporting the testing of technologies suited to diversified operational scenarios (Long-Fox & Britt, 2023).

Exolith Lab produces two main lunar simulants, LHS-1, designed to approximate the regolith of the lunar highlands, and LMS-1, intended to simulate the regolith of the basaltic maria. Both have a maximum particle size of approximately 1000 μm (Long-Fox & Britt, 2023).

***Table 5.2:*** *General characteristics of lunar simulant.*

| | **LMS-1** |
|---|---|
| Simulant Name: | LMS-1 Mare Simulant |
| Simulant Type: | General purpose |
| Reference Material: | Average lunar maria |
| Uncompressed Bulk Density: | 1.65 g/cm$^3$ |
| Median Particle Size: | 138.86 µm |
| Particle Size Range: | <0.04 µm – 1000 µm |

*Supplier-reported data adapted from Space Resource Technologies / Exolith Lab datasheets. These values should be understood as supplier-reported reference data for the selected simulants and may vary according to production batch, source material, and processing conditions.*

The grain-size distribution and geomechanical properties of LHS-1 and LMS-1 are consistent with reference lunar samples from highlands and maria, respectively, as well as with previously developed simulants. This correspondence is particularly relevant for ISRU applications, since processes such as sintering, molten regolith electrolysis and other high-temperature treatments depend on both chemical composition and particle distribution. Although terrestrial simulants cannot perfectly reproduce real lunar regolith, the mineralogical and geochemical fidelity of LHS-1 and LMS-1makes them suitable reference material for developing and testing technologies intended for lunar applications (Long-Fox & Britt, 2023; Long-Fox, et al., 2023).

From a compositional point of view, LMS-1 has a more diversified composition than LHS-1, with significant proportions of pyroxene (32.8%), glass-rich basalt (32%), and anorthosite (19.8%).

***Table 5.3:*** *Mineralogy (As mixed).*

| **Component** | **Wt. %** |
|---|---|
| Bronzite | 32.8 |
| Glass-rich Basalt | 32.0 |
| Anorthosite | 19.8 |
| Olivine | 11.1 |
| Ilmenite | 4.3 |

*Supplier-reported data adapted from Space Resource Technologies / Exolith Lab datasheets. These values should be understood as supplier-reported reference data for the selected simulants and may vary according to production batch, source material, and processing conditions.*

***Table 5.4:*** *Bulk Chemistry (Measured by XRF).*

| **Oxide** | **Wt. %** |
|---|---|
| $SiO_2$ | 48.22 |
| $TiO_2$ | 2.70 |
| $Al_2O_3$ | 12.40 |
| FeO | 8.79 |
| MnO | 0.06 |
| MgO | 15.97 |
| CaO | 7.65 |
| $Na_2O$ | 1.73 |
| $K_2O$ | 0.42 |

| Oxide | Wt. % |
|---|---|
| $P_2O_5$ | 0.23 |
| LOI | 0.56 |
| Total | 98.87 |

*Supplier-reported data adapted from Space Resource Technologies / Exolith Lab datasheets. These values should be understood as supplier-reported reference data for the selected simulants and may vary according to production batch, source material, and processing conditions.*

Density represents one of the fundamental parameters for describing the behavior of a granular material; in this context, it is useful for rover mobility, foundation stability, the construction of roads and landing platforms, as well as for the operation of excavation devices, and for the collection and processing of regolith. LMS-1 shows good correspondence with mare regolith, especially at higher relative densities (Long-Fox, et al., 2023). Particle size and particle size distribution significantly affect mechanical, thermal, and electrical properties, as well as the ability to retain volatiles. In the case of LMS-1, the particle size distribution is consistent with that of key lunar mare regolith samples for the fraction below 1000 μm. However, the greater mineralogical complexity of the source material requires a more articulated processing procedure, which introduces a certain variability comparable to that found in natural regolith (Long-Fox, et al., 2023).

Overall, the measured properties indicate that LHS-1 and LMS-1 constitute simulants suitable for studies and experimentation. They can therefore be used as reference materials for research and development activities related to lunar ISRU, infrastructure design, and regolith handling (Long-Fox, et al., 2023).

The Martian regolith simulants adopted in this experimental phase are *MGS-1 Mars Global Simulant* and *JEZ-1 Mars Jezero Delta Simulant*.

***Table 5.5:*** *General characteristics of Martian simulants.*

| | MGS-1 | JEZ-1 |
|---|---|---|
| Simulant Name: | MGS-1 Mars Global Simulant | JEZ-1 Jezero Delta Simulant |
| Simulant Type: | General purpose | General purpose |
| Reference Material: | Rocknest soil | Jezero Delta |
| Uncompressed Bulk Density: | 1.33 g/cm$^3$ | 1.37 g/cm$^3$ |
| Median Particle Size: | 70.51 μm | 43.01 μm |
| Particle Size Range: | >0.04 μm – 1000 μm | <0.04 μm – 1000 μm |

*Supplier-reported data adapted from Space Resource Technologies / Exolith Lab datasheets. These values should be understood as supplier-reported reference data for the selected simulants and may vary according to production batch, source material, and processing conditions.*

***Table 5.6:*** *Mineralogy (As mixed).*

| Component | MGS - 1 Wt. % | JEZ - 1 Wt. % |
|---|---|---|
| Olivine | 13.7 | 32.0 |
| Anorthosite | 27.1 | 16.0 |
| Glass-rich basalt | 22.9 | 13.5 |
| Bronzite | 20.3 | 12.0 |
| Mg-carbonate | - | 11.0 |
| Smectite | - | 6.0 |
| Mg-sulfate | 4.0 | 2.4 |
| Ferrihydrite | 3.5 | 2.1 |
| Hydrated silica | 3.0 | 1.8 |
| Magnetite | 1.9 | 1.1 |
| Anhydrite | 1.7 | 1.0 |
| Fe-carbonate | 1.4 | 0.8 |
| Hematite | 0.5 | 0.3 |

*Supplier-reported data adapted from Space Resource Technologies / Exolith Lab datasheets. These values should be understood as supplier-reported reference data for the selected simulants and may vary according to production batch, source material, and processing conditions.*

***Table 5.7:*** *Bulk Chemistry (Measured by XRF).*

| Oxide | MGS – 1 Wt. % | JEZ – 1 Wt. % |
|---|---|---|
| $SiO_2$ | 43.90 | 38.57 |
| $Al_2O_3$ | 12.84 | 7.87 |
| CaO | 7.91 | 5.39 |
| $Na_2O$ | 1.49 | 0.96 |
| $Fe_2O_3$ | - | 8.34 |
| $K_2O$ | 0.29 | 0.35 |
| MgO | 14.81 | 26.96 |
| MnO | 0.11 | 0.10 |
| $P_2O_5$ | 0.17 | 0.10 |
| $TiO_2$ | 0.46 | 0.29 |
| LOI | 4.90 | 8.79 |
| Total | 97.48 | 97.73 |

*Supplier-reported data adapted from Space Resource Technologies / Exolith Lab datasheets. These values should be understood as supplier-reported reference data for the selected simulants and may vary according to production batch, source material, and processing conditions.*

Martian regolith results from the combined action of impact, aeolian, fluvial, and volcanic processes, while remote analyses indicate the presence of a predominantly basaltic crust. Since fine dust particles can be transported over large areas by atmospheric and mechanical processes, the *Rocknest* soil analyzed in *Gale Crater* represents one of the main references for the average composition of the Martian surface (Long-Fox, et al., 2023). On this basis, Exolith Lab developed MGS-1 as a global Martian regolith simulant, intended for geochemical and geomechanical tests related to exploration systems, ISRU technologies, and infrastructure development on Mars (Long-Fox & Britt, 2023).

JEZ-1 was instead developed from the MGS-1 matrix through the addition of specific mineral phases, in order to approximate the expected mineralogy of *Jezero Crater*, a site characterized by geomorphological and mineralogical evidence related to past fluvial and lacustrine processes. While MGS-1 is dominated by silicate and basaltic components, including anorthosite, glass-rich basalt, bronzite, and olivine, JEZ-1 presents a more differentiated composition, with a higher olivine content and the presence of magnesium carbonates and smectite. These compositional differences are also reflected in their particle-size distribution: MGS-1 has a median particle size of approximately 70.51 μm, whereas JEZ-1 is finer, with a median particle size of 43.01 μm (Long-Fox & Britt, 2023).

Together, MGS-1 and JEZ-1 provide two differentiated experimental references for investigating how distinct Martian-like mineralogical and granulometric compositions may affect mixture workability, consistency, and mechanical response (Long-Fox & Britt, 2023). Their use in the following phases of the campaign will make it possible to compare the behavior of simulant-based mixtures with the preliminary sand-based formulation and to refine the quantitative ratios of the components in relation to the specific response of the selected simulants, as part of the methodology developed in this thesis.

### 5.3 Preliminary experimental campaign

The first phase of the experimental campaign was conceived as a preliminary methodological step, rather than as a direct reproduction of the final regolith-based construction material. Although the overall research is primarily oriented toward the development of a lunar habitat, this stage of the campaign focuses on a material formulation intended for possible Martian applications, with the aim of establishing and calibrating an experimental protocol before introducing planetary simulants.

At this stage, a sand-based gypsum mixture was adopted as a simplified and easily controllable granular reference system. The purpose was not to reproduce the mineralogical, chemical or thermal behavior of the Martian regolith, but to define the preparation procedure, assess workability and casting behavior, control setting and early-age hardening, and prepare a repeatable protocol for subsequent mechanical testing. In this sense, the preliminary mixture served as an experimental baseline, allowing the main variables of the process to be identified and refined.

The mixture was therefore calibrated by adjusting the ratio between the granular fraction, water, gypsum binder, superplasticizer and gypsum set retarder. Following a series of preliminary trials, a formulation suitable for this first experimental phase was identified. The selected mixture should not be understood as an optimized material solution, but as a workable compromise between casting feasibility, setting time, expected mechanical response and the need to limit the amount of water and additives. This strategy was considered relevant from a methodological point of view since both parameters would become critical in later ISRU-oriented solutions. Water availability, extraction and management represent major constraints in extraterrestrial environments, while chemical additives would either have to be transported from Earth or produced through future in-situ supply chains. At the same time, water and additives dosage may significantly affect the mechanical response of the material, influencing workability, porosity, drying behavior and strength development.

The first trials investigated water/gypsum ratios between 0.3 and 0.4. However, these values immediately proved insufficient to ensure adequate workability and casting behavior. Subsequent formulations were therefore developed by progressively increasing the water content until a water/gypsum ratio of 0.6 was reached. This value provided a more suitable balance between fluidity, handling and the need to avoid an excessive amount of water in the mixture. Regarding the additives, the gypsum set retarder proved effective even in limited quantities, corresponding to approximately 1.33% of the water mass. This dosage made it possible to extend the workability time of the mixture, allowing the mixing, casting and compaction operations to be carried out within a timeframe compatible with the preparation of the specimens. By contrast, the action of the superplasticizer did not appear decisive in this preliminary phase. Despite its addition, the mixture still showed limited fluidity at the end of mixing, and casting remained partially difficult, probably suggesting the need to increase its amount in the mixture. Nevertheless, both the water content and the amount of superplasticizer were intentionally limited. In this case, this choice was related to the necessity of considering water availability, extraction and management in future applications, as well as the possible influence of water content on mechanical performance. In the second case, the reduction of the additives was linked to the need to limit the use of components that would not be immediately available in-situ and would therefore depend on terrestrial supply or on future ISRU-based production chains.

The formulation adopted for the preliminary campaign was defined by a water/gypsum ratio of 0.6 and sand/gypsum ratio of 3.0. The superplasticizer was dosed at 1% of the gypsum mass, corresponding to 2 g per 200 g of binder, while the gypsum set retarder was dosed at 1.6 g. This formulation represents the reference mixture for the first phase of testing and provides the basis for the subsequent operational steps.

***Table 5.8:*** *Mixture components, their dosage and ratios.*

| Component | Quantity | Ratios |
|---|---|---|
| Sand | 600 g | Sand/gypsum = 3.0 |
| Water | 120 g | Water/gypsum = 0.6 |
| Gypsum | 200 g | - |
| Superplasticizer | 2 g | Superplasticizer /gypsum = 0.01 |
| Gypsum set retarder | 1.6 g | Retarder/water = 0.0133 |
| **Total** | **923.6 g** | **-** |

After the dosage of components had been defined, the mixing stage followed. First, all the liquid constituents, namely water, superplasticizer, and gypsum set retarder, were combined. The gypsum binder was then added to the liquid phase and mixed at low speed for approximately 30 seconds, alternating clockwise and counterclockwise movements. The sand fraction was later incorporated into the other components and mixed for a further 30 seconds at the same speed. Thereafter, the mixing speed was increased for an additional 30 seconds, reaching a total initial mixing time of 90 seconds. The mixture was then left to rest for 90 seconds, followed by a final 60 seconds high-speed mixing phase, aimed at improving homogeneity before casting.

The fresh mixture was then cast into 80 x 20 x 20 mm molds in two successive stages. First, the molds were filled approximately halfway using a spatula, after which light manual compaction was carried out by gently tapping the mold on the work surface. The molds were then

completely filled, followed by a second tapping phase to reduce entrapped air. Finally, the upper surface of the specimens was levelled with a spatula to improve their regularity.



***Figure 5.1:*** *Specimens produced for mechanical testing.*

At the end of the forming phase, the specimens were placed in a glovebox maintained at approximately 100% relative humidity, in order to limit uncontrolled drying and ensure comparable environmental conditions during setting and early-age hardening.

The next phase of the campaign involved the mechanical testing of the preliminary specimens through flexural and compressive tests. The aim was to assess the evolution of the mechanical performance over time and to identify the most appropriate testing and hardening intervals for the following phases of the experimental campaign. For this purpose, a testing schedule was defined in which specimens were stored in the glovebox for 1, 4, 7, 14 and 30 days, before being subjected to different pre-test conditioning intervals.

The testing campaign was defined by also considering the time elapsed after the specimens' removal from the glovebox. The ones stored in the glovebox for 1 and 4 days were removed approximately 1 hour before testing, in order to limit uncontrolled exposure to ambient laboratory conditions while allowing the specimens to stabilize before the mechanical tests. For the 7-days specimens, a more detailed comparison was carried out by testing the samples after 1, 5, 8, 24 and 48 hours of exposure to ambient laboratory conditions. The specimens tested after 14 and 30 days were instead kept outside the glovebox for 24 hours before testing. This made it possible to evaluate the possible influence of the time spent outside the controlled humid environment on the mechanical response.

***Table 5.9:*** *Summary of mean mechanical test results.*

| Series | Controlled humid storage time | Ambient pre-test conditioning time | Mean compressive strength [MPa] | Mean flexural strength [MPa] |
|---|---|---|---|---|
| 1 | 1 day | 1 h | 2.76 | - |
| 2 | 4 days | 1 h | 3.38 | 0.98 |
| 3 | 7 days | 1 h | 3.41 | 0.99 |
| 4 | 7 days | 5 h | 3.01 | 0.98 |
| 5 | 7 days | 8 h | 3.07 | 0.92 |
| 6 | 7 days | 24 h | 3.94 | 0.92 |
| 7 | 7 days | 48 h | 9.21 | 3.72 |
| 8 | 14 days | 24 h | 8.24 | 3.52 |
| 9 | 30 days | 24 h | 8.10 | 3.73 |

*For each testing series, the mean flexural strength was calculated from two prismatic specimens. After the flexural tests, the resulting halves were used for compression testing, providing four compression measurements from which the mean compressive strength was calculated.*

Table 5.9 summarizes the mean values obtained from the preliminary mechanical tests carried out on the sand-based gypsum specimens. The results show that the mechanical response is influenced not only by the controlled humid storage time, but also by the ambient pre-test conditioning time after the removal from the glovebox. For this reason, the values cannot be interpreted exclusively as a function of specimens' age but must be related to the combined effect of the storage under controlled humidity conditions and the subsequent phase of exposure to the ambient laboratory environment.

From the first testing series, it is possible to observe an initial increase in compressive strength between the specimens of series 1 and 2, respectively left in controlled humid storage conditions for 1 and 4 days and with a pre-test conditioning time of 1 hour for both cases. The mean compressive strength increased from 2.76 MPa to 3.38 MPa, indicating the early development of mechanical performance during the first days after preparation. However, the comparison with series 3, tested after 7 days of controlled humid storage time and only 1 hour of pre-test conditioning time, shows a very limited increase in mechanical response; showing a mean compressive strength of 3.41 MPa and 0.99 MPa of mean flexural strength. These data suggest that, under controlled humid storage conditions and with short exposure to ambient conditions, the increase in strength between 1, 4 and 7 days remains modest.

A more significant variation emerges when the specimens with a 7-days storage time are compared according to their ambient pre-test conditioning time. The specimens tested after 1, 5, 8 and 24 hours outside the glovebox show compressive values ranging between 3.01 MPa and 3.94 MPa, while the flexural values remain relatively stable, between 0.92 and 0.99 MPa. These results suggest that a short-term exposure to ambient laboratory conditions produces only limited variations in the measured mechanical response. By contrast, the specimens

tested after 48 hours of conditioning time show a substantial increase in both mean compressive and flexural strength, reaching respectively 9.21 MPa and 3.72 MPa. This discontinuity suggests that prolonged exposure to ambient conditions, and therefore partial drying after controlled humid storage, has had a decisive influence on the measured strength of the preliminary material.

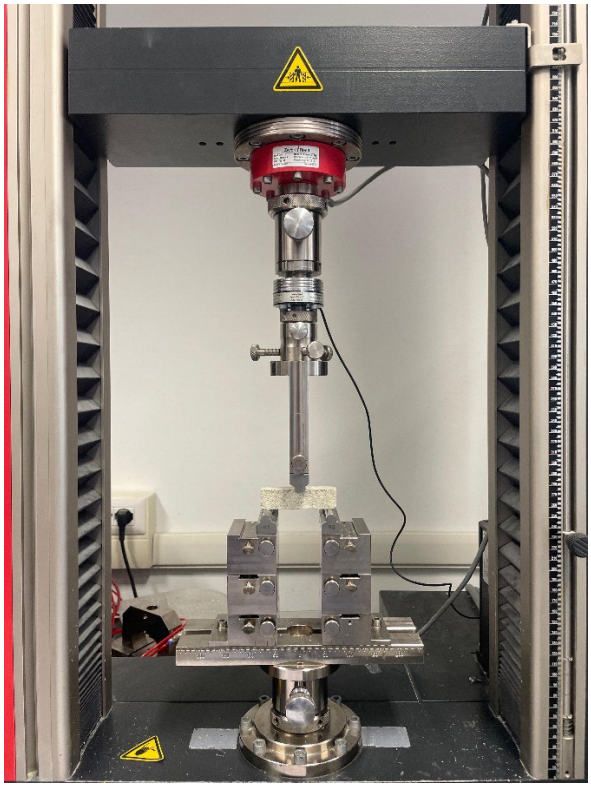


***Figure 5.2:*** *Flexural testing setup for one of the prismatic specimens. The sample is positioned on two supports inside the testing machine, while the central loading head applies a vertical force to evaluate the material's bending resistance.*

Overall, the exploratory results highlight the sensitivity of the material to the environmental conditions before testing. The highest mechanical values were obtained in two specific conditions. Series 7, stored for 7 days under controlled humidity and then exposed to ambient conditions for 48 hours, reached the highest mean compressive strength, equal to 9.21 MPa, and a mean flexural value of 3.72 MPa. In parallel, series 9, stored for 30 days in the glovebox and subjected to 24 hours of ambient pre-test conditioning time, reached 8.10 MPa in compression and the highest mean flexural strength of 3.73 MPa.

This comparison suggests a possible interaction between storage under controlled humidity and ambient pre-test conditioning time. In particular, when the specimens remained in the glovebox for 7 days, a longer exposure to ambient conditions appeared necessary to obtain satisfactory strength values. Conversely, when the specimens remained longer under controlled humidity conditions as for series 9, 24 hours of exposure to ambient conditions were sufficient to reach comparable values. Therefore, the most favorable mechanical performance appears to result from a balance between humid storage and subsequent exposure to ambient laboratory conditions, rather than from storage duration alone.

Although the preliminary phase does not yet involve Martian regolith simulants, it establishes the methodological basis for their introduction. The following stage of the campaign will involve actual simulants, while maintaining the same preparation, casting, conditioning and testing

procedure adopted in this first preparatory phase. In this way it will be possible to evaluate how the introduction of planetary simulants affects the fresh-state behavior of the mixture, including workability, casting capacity, compaction as well as its hardened state response under flexural and compressive loads.

In parallel, the lunar-oriented branch of the experimental campaign will be developed through the use of lunar regolith simulants and the investigation of microwave sintering as a dry consolidation process more directly aligned with the construction strategy proposed in this research. In this context, the preliminary campaign does not yet validate the final construction material but defines a controlled experimental protocol through which material formulation, conditioning procedure, mechanical response and future ISRU-based construction techniques can be progressively connected.

### 5.4 Radiation shielding and life-support system

As discussed in the first chapter[36], radiation exposure represents one of the main environmental constraints for human missions on the lunar surface and becomes even more critical in the case of long-duration or permanent extraterrestrial habitats. Within this research, the issue of radiation protection is therefore addressed not only as a passive shielding problem but as part of a broader multifunctional strategy involving material mass, biological systems and life-support functions.

Following the second form-finding process, the structure assumes a geometry close to the final one, illustrated in the following chapter, which is configured as a double shell composed of interconnected lobed modules. The interstitial space between the two regolith “skins” of the lobe was considered suitable for hosting technical systems intended for radiation protection and life support. According to this logic, the design proposal envisages a hybrid strategy based on two main elements: Photobioreactors for the cultivation of microalgae, and a mycelium-based layer conceived as an additional shielding component. The former performs a multiple function, as they combine the shielding contribution of water and polyethylene with the possibility of cultivating biomass, contributing to $CO_2$ absorption, oxygen production, and the generation of a food resource potentially available in-situ. Mycelium, placed alongside this system, is instead assumed as an additional component for radiation protection, based on the promising results reported in the literature regarding its shielding behavior.

*Photobioreactors*

The integration of photobioreactors within the project was inspired by the *COSMICA project*, developed by *Alta Scuola Politecnica* as a modular system for the cultivation of microalgae in extreme environments and specifically conceived in relation to lunar exploration. In the context of long-duration missions, the high cost of terrestrial resupply makes bioregenerative systems particularly relevant, since microalgae photobioreactors can contribute to closed-loop life-support processes by producing oxygen, removing $CO_2$ from the confined environment, and generating nutritionally valuable biomass (Renzulli, et al., 2024).

Among the microorganisms considered, *Arthrospira platensis*, commonly known as Spirulina, plays a central role due to its photosynthetic activity, high nutritional value, and relatively

[36] *Chapter 1, Section 1.5.*

simple cultivation requirements. It grows under controlled conditions characterized by temperatures between 30 and 35 °C, alkaline pH between 9 and 11, high $CO_2$ availability, and a photoperiod of approximately 18 hours of light and 6 hours of darkness. However, microalgae cultivation also presents critical issues, including limited biomass productivity, harvesting difficulties, system complexity, contamination control, and the need for continuous monitoring and automation (Renzulli, et al., 2024).

For this reason, the COSMICA project focused on optimizing lighting, gas-liquid exchanges, contamination control, process simplification, and spatial efficiency within a closed photobioreactor system. Compared with open cultivation systems, photobioreactors allow more precise control of growth conditions and reduce exposure to contamination; however, they require careful fluid-dynamic design to avoid stagnation and cellular aggregation within the culture medium. In particular, the hydraulic system assumes a fundamental role, since it distributes water, nutrients, and $CO_2$, keeps the culture medium in motion, limits biomass sedimentation and contributes to the regulation of temperature and pH (Renzulli, et al., 2024).

The COSMICA research also addressed the management of communication between adjacent bags and the collection of biomass, introducing electronic valves to limit the spread of contamination and a turbidity sensor to detect possible anomalies. Biomass harvesting was integrated into a 3D-printed basin equipped with a filtering system, in order to simplify maintenance and the operational cycle of the module. Fluid-dynamic analyses conducted under both terrestrial and lunar gravity showed that reduced lunar gravity slows the motion of aeration bubbles and decreases recirculation efficiency, although the central regions of the bag remain involved in the flow, suggesting the possibility of further optimization (Renzulli, et al., 2024).

In addition to its bioregenerative function, COSMICA was evaluated as a complementary radiation shielding system, due to the presence of polymeric containment bags filled with a predominantly aqueous culture medium. Water and hydrogen-rich polymeric materials are relevant for radiation attenuation, and the simulations showed a limited reduction in daily absorbed dose, equal to 0.47%, but a more significant reduction in equivalent dose, equal to approximately 34.01%. A second simulation including lunar albedo returned a total dose of 0.1993 mGy/day, with 32.29% attributable to albedo, and showed equivalent dose reductions of 26.28% according to the ICRP60[37] model and 18.78% according to NASA-Q[38]. These results indicate that photobioreactors may contribute to radiation mitigation, although they cannot replace dedicated shielding systems and should therefore be understood as integrative devices within a broader multilayer protection strategy (Renzulli, et al., 2024).

Overall, the COSMICA project demonstrates the potential of a circular, modular, adaptive, and multifunctional system capable of contributing simultaneously to oxygen production, $CO_2$ management, biomass generation, water recirculation, and complementary radiation shielding (Renzulli, et al., 2024). Building on these findings, the integration of photobioreactors

[37] *ICRP60 refers to the radiation protection model introduced by the International Commission on Radiological Protection in Publication 60, in which absorbed dose is converted into equivalent dose through radiation weighting factors* (International Commission on Radiological Protection, 1991).

[38] *NASA-Q refers to the NASA quality factor model, which evaluates the biological effectiveness of space radiation mainly as a function of the linear energy transfer (LET) of charged particles* (Cucinotta, et al., 2011).

within the interstitial layer of the shell is understood in this thesis as a way to transform the envelope into an active environmental control layer. In this scenario, photobioreactors may contribute to radiation mitigation, $CO_2$ absorption, oxygen generation, water recirculation and the production of nutritionally valuable biomass. The approach should therefore be understood as integrative rather than substitutive. Photobioreactors do not replace dedicated radiation shielding or primary life-support systems but reinforce them as part of a wider multilayer strategy (Isolan, et al., 2024).

*Fungi and mycelium in radiation shielding*

A further component of the shielding system is constituted by mycelium, which is of particular interest not only because of its biological and cultivable nature, but also because recent literature shows that fungal biomass, melanized materials, and fungal-based biocomposites can offer a concrete contribution to radiation attenuation in the space environment (Shunk, et al., 2021; Cordero, et al., 2025).

Fungal mycelium constitutes the vegetative phase of filamentous fungi and is formed by a network of thin microscopic elements, *hyphae*, which develop and intertwine until they generate a compact and strongly connected structure. Thanks to this morphological organization, materials derived from mycelium possess characteristics of considerable interest, such as lightness, structural cohesion, and broad adaptability to processing and modelling procedures. Currently, numerous studies are exploring its applications in various fields, including fashion, packaging, decorative elements, construction, the food and pharmaceutical sectors, as well as aerospace and space architecture. Similarly to fungal melanin, mycelium can also be cultivated and transformed with limited use of resources, an aspect that makes its possible production directly in an extraterrestrial environment particularly interesting, reducing dependence on the transport of materials from Earth. The association between mycelium and melanin therefore opens promising perspectives for research, although their actual performance and resistance under space conditions still require further investigation (Cordero, et al., 2025).

The study by Cordero et al. analyses biocomposites based on PLA (polylactic acid) and fungal or melanized components, exposed for approximately six months in LEO[39] on the ISS. The comparison between pure PLA, PLA enriched with fungal melanin (PLA-FunMel), synthetic melanin (PLA-SynMel) or animal melanin (PLA-AniMel), and PLA-coated compressed mycelium (PLA-CMy) showed that the response of the samples depended on both composition and exposure orientation, either towards the zenith or towards the orbital wake of the ISS. The PVC layers placed beneath the samples were used as indicators of radiation damage (Cordero, et al., 2025).

The results indicate that PLA-FunMel underwent a much lower mass loss than pure PLA, suggesting that fungal melanin may improve the stability of the material in an orbital environment. By contrast, PLA-coated compressed mycelium showed the highest mass loss, probably due to its fibrous and hygroscopic nature. However, the samples maintained their overall shape and nevertheless demonstrated shielding capabilities against UV-A and UV-C radiation, confirming the protective potential of fungal or melanized components (Cordero, et al., 2025).

[39] *Low Earth Orbit (LEO).*

Further preliminary support comes from the study by Shunk et al., *A Self-Replicating Radiation-Shield for Human Deep-Space Exploration: Radiotrophic Fungi can Attenuate Ionizing Radiation aboard the International Space Station*, which tested the melanized and radiotrophic fungus *Cladosporium sphaerospermum* aboard the ISS. The fungus was cultivated for 30 days in LEO, showing the ability to grow in orbit and, above all, faster growth compared to terrestrial controls, a result interpreted by the authors as compatible with the hypothesis that ionizing radiation may contribute to the metabolism of melanized fungi (Shunk, et al., 2021).

The shielding effect was initially limited, with an average radiation reduction of 0.5% in the first 24 hours but increased with biomass growth up to approximately 4.34 ± 0.5%. Despite the very limited thickness of the fungal mat, equal to 1.67 mm, the experiment detected measurable attenuation, confirming that even a thin biological layer can contribute to radiation protection (Shunk, et al., 2021).

The simulations conducted by the authors, based on biomass containing approximately 8.6% melanin, also indicate that melanized fungal biomass has a higher attenuation coefficient than non-melanized biomass. This confirms the role of melanin in increasing the shielding capacity of the biological material (Shunk, et al., 2021).

***Table 5.10:*** *Comparison of radiation attenuating capacity of in-situ resources on Mars and the Moon with melanized composites. Adapted from:* (Zhang, et al., 2020; Shunk, et al., 2021).

| **Material and literature source for molecular formula and density** | **Mass Attenuation Coefficient '$\mu/\rho$'[cm$^2$/g] at 150 MeV** | **Linear Attenuation Coefficient '$\mu$' [cm-1] at relative material density** | **Required thickness [cm] to reduce Martian radiation levels by ~ 97%** | **Required thickness [cm] to reduce lunar radiation levels from 500 mSv/year* to 6.2 mSv/year**** |
|---|---|---|---|---|
| Water | 0.0149 | 0.0149 | 367 | 444 |
| Martian regolith | 0.0268 | 0.0407 | 128 | 155 |
| Martian regolith + melanin (equimolar mixture) | 0.0288 | 0.0518 | 106 | 128 |
| Non-melanized fungus | 0.0141 | 0.0155 | 351 | 424 |
| Melanized fungus | 0.0213 | 0.0234 | 232 | 281 |

**Values of radiation levels on the Lunar surface are taken from "First measurements of the radiation dose on the lunar surface"* (Zhang, et al., 2020).

*** Values of radiation levels on Earth surface are taken from "A Self-Replicating Radiation-Shield for Human Deep-Space Exploration: Radiotrophic Fungi can Attenuate Ionizing Radiation aboard the International Space Station"* (Shunk, et al., 2021).

The table above is extracted from the research, however, since the study focuses on Martian values, a final column was added to include lunar radiation levels, estimated at around 500 mSv/year[40]. It highlights how the shielding effectiveness of the materials considered varies

[40] *The measurements carried out by Zhang et al. through the Lunar Lander Neutrons and Dosimetry experiment aboard the Chang'E 4 lander indicate an average dose equivalent on the lunar surface of 1369 μSv/day, corresponding to approximately 500 mSv/year. The radiation field is mainly composed of galactic cosmic rays, solar particle events, and a secondary*

significantly in relation to their respective attenuation coefficients and, consequently, to the thicknesses required to reduce radiation exposure to values close to those on Earth. The comparison between the Martian and lunar scenarios shows that the most favorable results are associated with composite materials containing melanin, which demonstrate a greater attenuation capacity than both non-melanized biological materials and water. In particular, the composite of Martian regolith and melanized fungal biomass appears to be the most efficient solution among those reported in the table, requiring the smallest thicknesses in both the Martian case (106 cm) and the lunar case (128 cm). Martian regolith alone also shows significant performance, but with thicknesses that are still greater than those of the composite containing melanized fungal biomass (128 and 155 cm). Particularly relevant is the comparison between non-melanized and melanized fungi, as it makes it possible to directly understand the contribution of melanin to radiation shielding. Overall, the data suggest that the most promising strategy for radiation protection does not lie in the isolated use of a single material, but rather in the integration of different components within composite and multilayer systems (Shunk, et al., 2021).

*Computational design of the interstitial layer*

This section of the research investigates the first preliminary design of the containment bags conceived to host the aqueous cultivation of microalgae and the mycelium-based layer, together with a first hypothesis for the piping network required for the proper functioning of the system. Even though the design is still at a preliminary conceptual stage, the aim of this section is to describe both the methodological workflow and the design logic.

The cultivation of Spirulina microalgae and the integration of a mycelium-based layer require controlled environmental conditions, water and air circulation, and a specific spatial organization within the architectural envelope. For this reason, the interstitial space between the inner and outer shell layers was interpreted as an active technical zone intended to host the components of the radiation shielding and life-support system. In particular, photobioreactors and mycelium are conceived to be located in containment bags inserted within the regolith-based layers of each lobed module. The bags' geometry was therefore developed according to a form-finding logic similar to the one used for the structural lobes that contain them. The workflow started from the tessellation of the shell, which made it possible to subdivide the overall surface into individual lobed modules. Once the modules had been isolated, the geometry of the containment bags was generated in relation to the available internal volume of each lobe.

This tessellation process also has a broader design relevance. By subdividing the shell into discrete modular components, it becomes possible to investigate, in future developments of the research, the interlocking logic between adjacent elements, the sequence of assembly, and the definition of a coherent construction strategy. In this sense, the computational subdivision of the shell does not only serve the modeling of the biological and technical systems but also supports the development of the overall modular logic of the habitat.

*component of neutral particles, consisting of neutrons and gamma radiation generated by the interaction of primary radiation with the lunar soil* (Zhang, et al., 2020).

The workflow was developed in Grasshopper, with *Raven* used as a support tool for setting up and troubleshooting specific parametric operations. Rather than replacing the design process, the tool was used to assist the construction of project-specific scripts, particularly in relation to mesh tessellation, face selection, and the generation of containment geometries. To make this support more effective, project-specific profiles were configured for specific tasks, allowing the workflow to be organized around recurring operations such as the interpretation of the input geometry, the management of quadrangular faces, and the selection of suitable modeling procedures.

The first operational step consisted in tessellating the mesh into the individual quadrangular faces defined by the structural grid. The expected result was a subdivision faithful to the original geometry, allowing the independent management of each face. In this way, the shell was transformed into a system of discrete elements consistent with the actual form of the structure and therefore usable for subsequent phases of analysis, modeling, and construction development.

Once this step had been defined, it became possible to manage the faces individually, select a variable number of them simultaneously, and generate the containment geometries intended for the active interstitial layer. This stage was developed using Kangaroo, simulating pressure acting on the selected faces in order to obtain inflated geometries capable of adapting to the internal space of the lobed modules. The resulting bags recall the morphology of the structural lobes and are conceived to fit within them without altering the main structural configuration of the shell.

A further design aspect concerned the preliminary definition of the piping network, which represents an essential component for the functioning of the photobioreactor system and, more generally, of the active interstitial layer. The network was conceived as a distribution grid following the development of the shell and reaching each lobe in order to supply the containment bags with water, nutrients, and $CO_2$, support the recirculation of the culture medium, and integrate lighting, monitoring, and sensor systems.

Although its path follows the geometric logic of the structure, the piping network does not coincide with the structural grid of the shell. In the adopted module geometry, the inner and outer surfaces meet along localized perimeter connection regions, leaving interstitial cavities between adjacent lobes. The piping network was therefore designed to exploit these cavities as preferential routes for the passage of technical systems, avoiding the need to perforate the lobes and simplifying the construction process. As shown in the corresponding diagrams, this preliminary network defines the main distribution path, to which secondary branches may be added in future developments in order to serve additional subsystems.

Although the technical details still require further development, the proposed configuration suggests a multilayer strategy in which the two outermost regolith-based layers provide an initial passive shielding contribution through their mass, while the interstitial space hosts two distinct biological and technical systems: photobioreactor bags and a mycelium-based layer. Radiation protection is therefore not entrusted to a single material, but to a stratified system in which regolith-based mass, the aqueous medium contained in the photobioreactors, and mycelium jointly contribute to the safety and multifunctionality of the habitat.

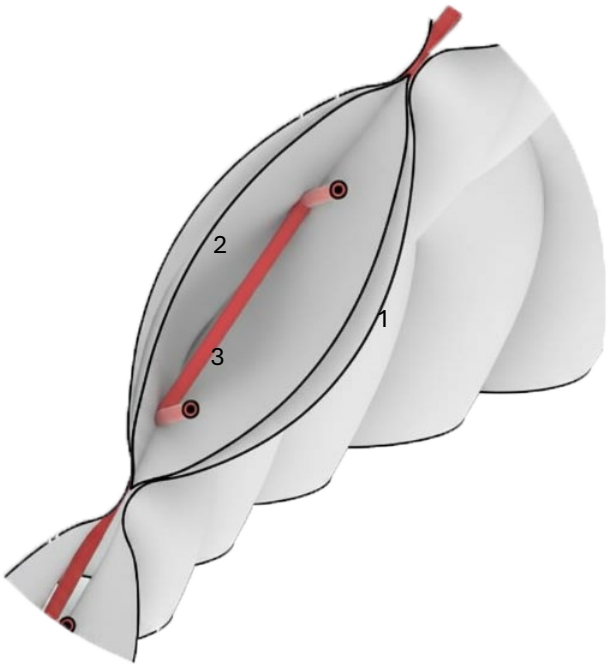



***Figure 5.3:*** *Detail view in cross-section depicting a single lobed module (1), the internal bag conceived for photobioreactors and mycelium (2) and, in red, the piping network (3). The image represents the concept of the interstitial system.*

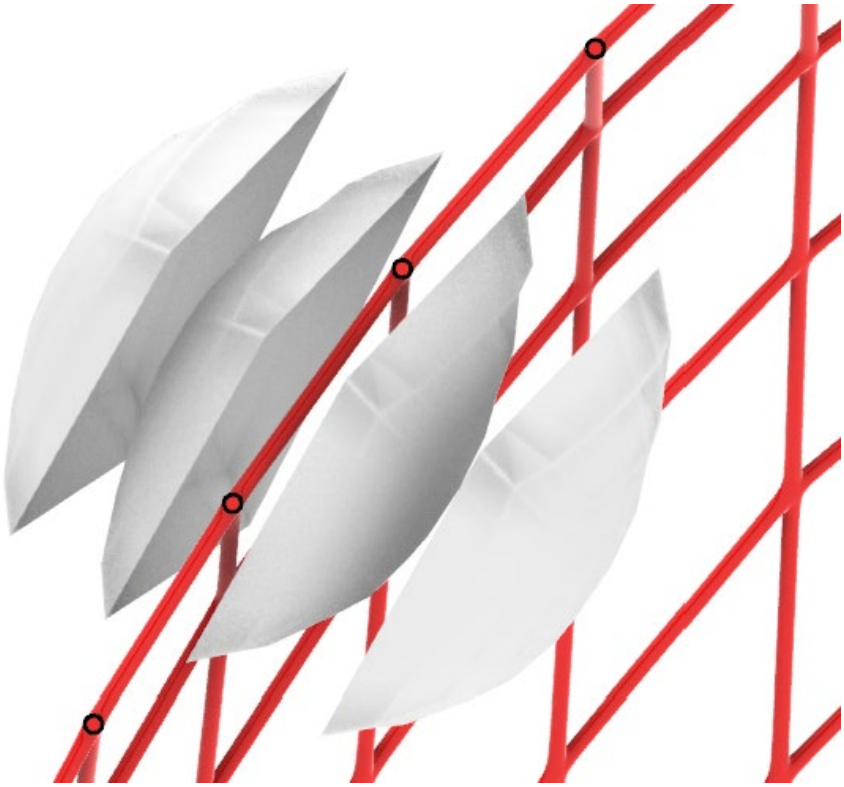


***Figure 5.4:*** *Exploded conceptual view of a lobed module, showing the layers of the lobe and of the internal bag, as well as the piping network. The red elements represent the conceptual arrangement of the piping system, while the exploded configuration highlights the spatial relationship between the shell geometry and the inner pouch.*

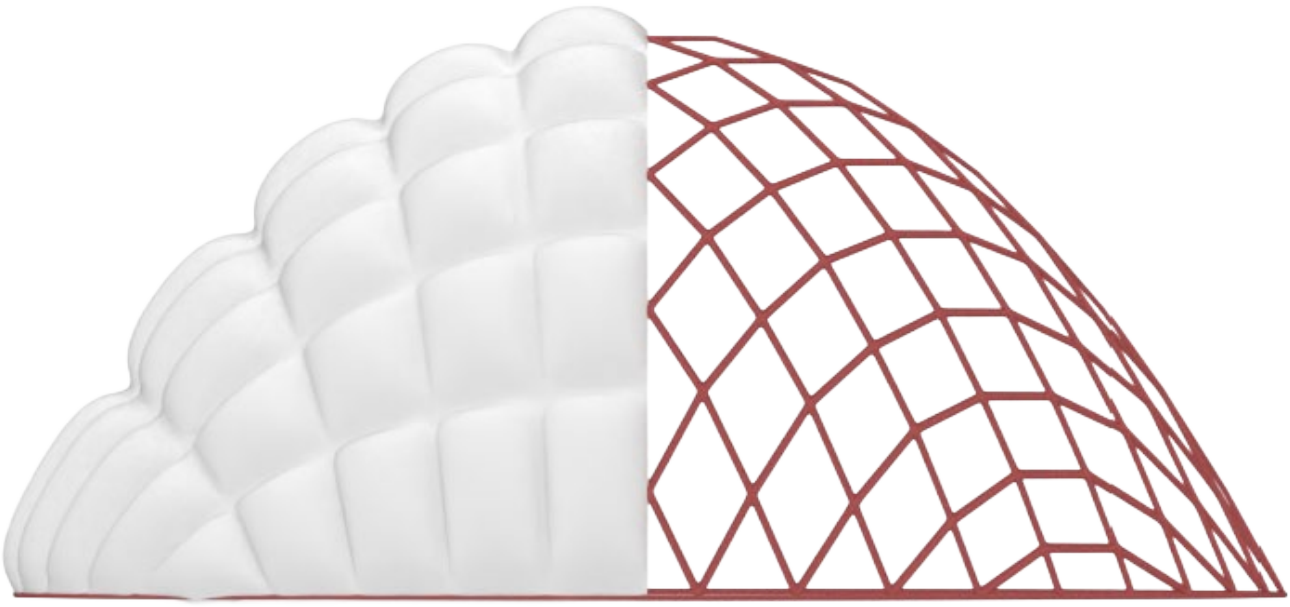


***Figure 5.5:*** *Diagram showing the spatial relationship between the lobed modules and the interstitial piping network. One half of the structure illustrates the arrangement of the lobes, while the other half shows the interstitial piping network in red, making visible how the two systems relate to one another within the overall shell configuration.*

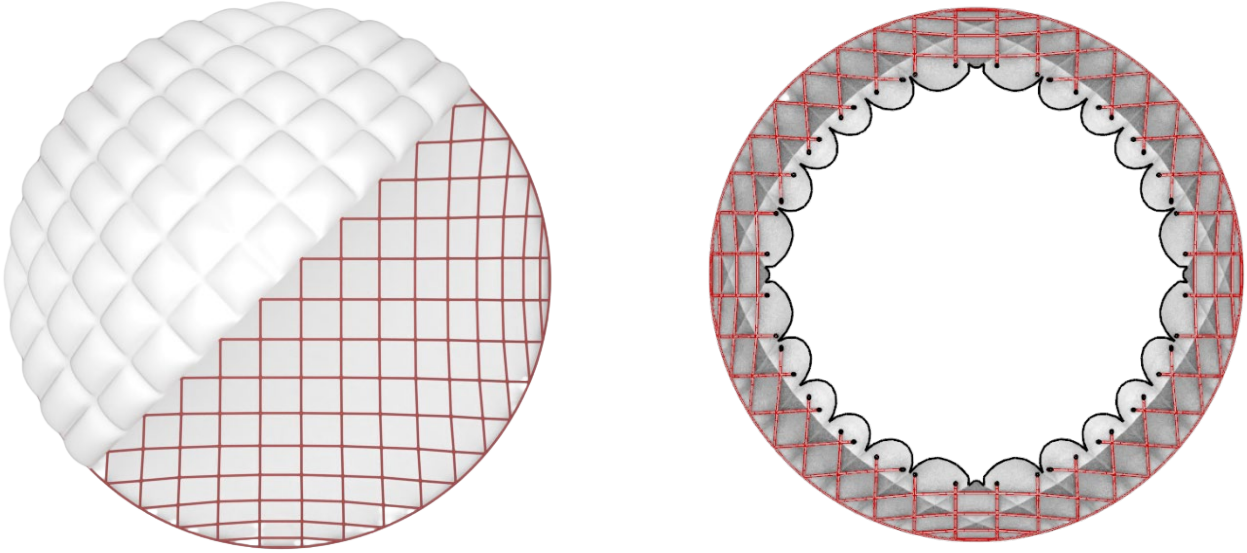


***Figure 5.6 (left):*** *Top view of the conceptual shell configuration. One half of the structure shows the arrangement of the lobed modules, while the other half omits them in order to reveal the distribution of the interstitial piping network and clarify its spatial relationship with the lobed geometry.*

***Figure 5.7 (right):*** *Horizontal section of the inner shell showing the relationship between the lobed geometry and the piping network. As in the previous concept, the aim is to clarify the spatial distribution of the piping system in relation to the lobes.*

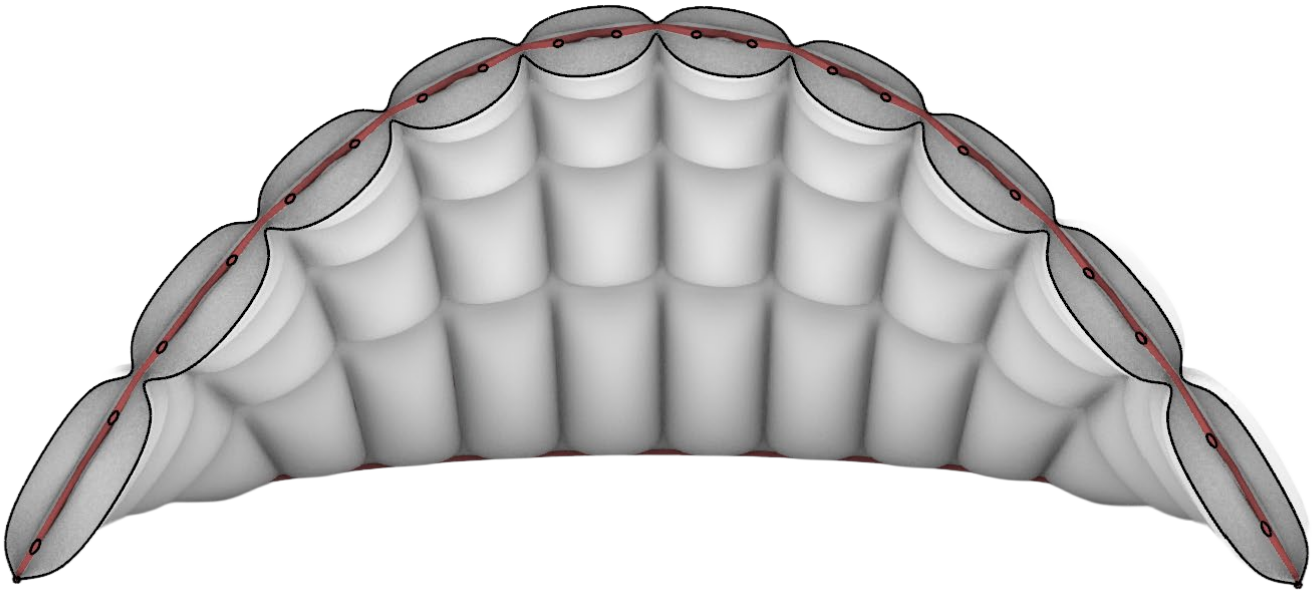


***Figure 5.8:*** *Conceptual cross-section showing the arrangement of the piping network in relation to the lobed modules. The image illustrates how the piping system is distributed along the shell section and how it spatially relates to the geometry of the lobes within the overall structural concept.*

# CHAPTER 6 – Structural analysis

## 6.1 Load definition

This chapter presents a preliminary structural analysis aimed at critically assessing the adopted design strategies and verifying their consistency with the expected mechanical behavior. It is important to emphasize that the model should not be intended as the final configuration of the structure, since some structural, constructional and material-related aspects require further investigation and verification. The analysis presented in this chapter should therefore be understood as an initial assessment of the shell's structural behavior, intended to identify the main criticalities, determine which aspects require further refinement or integration and guide the progressive development of the model during the subsequent stages of the research.

The structural analysis was conducted in Karamba3D and represents the final computational stage of the design workflow developed to generate and assess the proposed structural system. At this stage, the reference geometry corresponds to the mesh obtained from the second form-finding stage, in which the shell is articulated into a network of double-curvature lobes. The first step of the analysis consists in defining the loading actions considered in the reference scenario.

Although the inner and outer shells are conceived as interconnected components of a single construction system, the computational model was developed through two parallel branches of the Grasshopper script. The complete structure is intended to be assembled from prefabricated lobed modules, each representing a construction unit composed of two mirrored curved surfaces, one belonging to the inner shell and the other to the outer one. The use of separate script branches made it possible to generate and investigate the two layers independently, allowing the individual structural response of each shell and the influence of their opposite curvatures to be examined separately. At this stage, the analytical models therefore do not reproduce the mechanical interaction between the layers or the transfer of forces through their connecting elements. Since the present work constitutes the initial phase of a broader research process, a subsequent stage will investigate the structural behavior of the two shells as a single interconnected and assembled system. The development of a coupled model of the structure therefore represents one of the principal directions for the future continuation of this research.

The following sections first define the main modelling assumptions and loading actions and then examine the structural response of the system in relation to material properties, geometric configuration, boundary and loading conditions. The results are subsequently discussed in order to identify the principal limitations of the current model and to outline the investigations required in the next stages of the research.

The reference load configuration includes lunar self-weight, the internal pressure differential and the equivalent dead loads associated with the radiation shielding and life-support systems, including the weight transferred by the outer shell on the inner one. Thermal actions were temporarily excluded from the present model. Consequently, the results discussed in this chapter do not account for stresses induced by the severe temperature variations and thermal gradients that may affect a lunar habitat such as the one discussed in this thesis.

Lunar self-weight was introduced through the Karamba3D *Gravity* component shown in Figure 6.1. The gravitational action was approximated as 1/6 of terrestrial gravity. The vector was

oriented along the negative global Z-axis and scaled by a factor of 0.162. Under the SI convention adopted by Karamba3D, this corresponds to an effective gravitational acceleration of approximately 1.62 m/s$^2$, providing a representation of lunar gravity. The action was assigned to load case LC0. Although lunar self-weight was expected to be secondary to the internal pressure differential, it was retained to provide a more accurate representation of the actual loading conditions on the Moon.

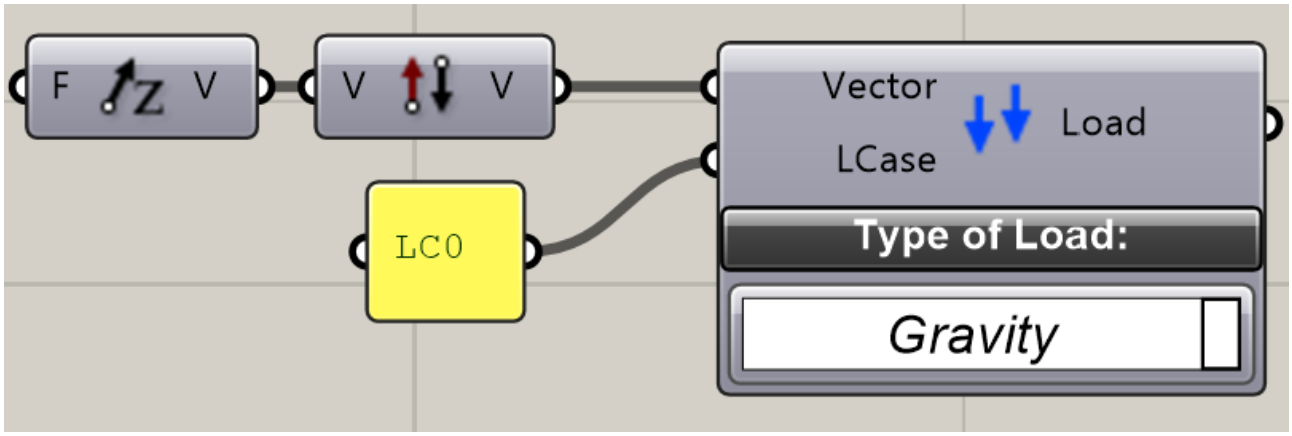



***Figure 6.1:*** *Component "Gravity".*

As discussed in Chapter 4[41], the internal pressure differential was expected to represent the governing loading action. A value of 101 kN/m$^2$, 1.01 bar or 1 atm, was adopted in the structural model.

The pressure load was applied according to the same geometric principle adopted during the second form-finding stage. In those circumstances, pressure acted as a generative input for the definition of the lobed geometry, while in the present analysis, the same action was introduced as a structural load in order to assess the mechanical response of the resulting shell. This action was modelled as a constant mesh load uniformly distributed over the shell surface. Its magnitude was set to 101 kN/m$^2$, according to the component input units adopted by Karamba3D, and its direction was defined as normal to each face of the mesh. The "*Local to mesh*" orientation was selected so that the load vector would be interpreted according to the local coordinate system of the model rather than the global axes of Rhino. Consequently, the local Z-component of the vector acts perpendicular to the corresponding faces. This required the mesh normals to be consistently oriented so that the pressure acted from the interior toward the exterior of the shell. The pressure load was assigned to LC0 so that it would act simultaneously with lunar self-weight and the other actions included in the reference load case.

[41] *Chapter 4, Section 4.4.*

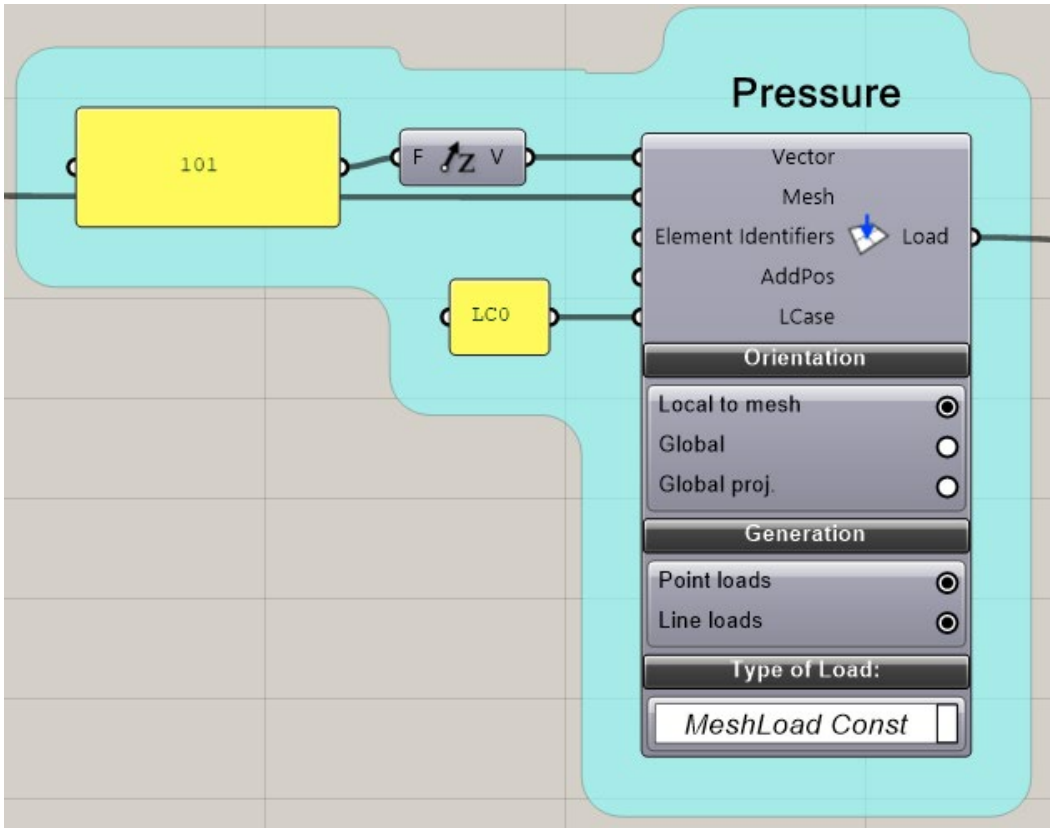



***Figure 6.2:*** *Definition of the internal pressure differential as a constant mesh load locally oriented to the shell faces and assigned to load case LC0.*

The final loading contribution considered in the model consists of the equivalent dead loads associated with the interstitial system and the weight transferred by the outer shell on the inner one. The interstitial system includes photobioreactors, the aqueous microalgae culture, the mycelium-based layer and the containment bags. In the preliminary structural model, these contributions were assumed to be supported by the inner shell and were therefore represented as an additional distributed load acting on its surface.

The mass of each component was estimated separately from its density and assumed occupied volume. The total volume of the interstitial cavities was preliminarily estimated at approximately 500 $m^3$ on the basis of the current preliminary dimensions of the structure, characterized by a circular base with a radius of 10 m and an overall height of approximately 9 m. This value was used as an assumed geometric reference for estimating the mass of the components accommodated within the interstitial layer. The volume and mass of the outer shell were calculated separately from its geometric configuration and assigned material density.

The lunar weight of each component was calculated by multiplying its estimated mass by the lunar gravitational acceleration, assumed to be approximately 1.62 $m/s^2$. The individual contributions were then summed to obtain the total vertical force acting on the inner shell. For implementation in the preliminary Karamba3D model, the resulting force was converted into an equivalent uniformly distributed surface load by dividing it by the actual area of the inner shell. The same procedure was used to estimate the load associated with the weight of the outer shell transferred to the inner layer. Among the additional contributions considered, the

outer shell represents the largest component of the estimated dead loads. The combined contribution of the interstitial system and the transferred weight of the outer shell layer was represented by an equivalent distributed load of approximately 16 kN/m$^2$. Unlike the internal pressure, this additional load was oriented according to the global coordinate system, as shown in Figure 6.3. The vector was defined along the negative global Z-axis, consistently with the gravitational nature of the action, and was assigned to load case LC0.

The conversion of the different contributions into a uniformly distributed load represents a modelling simplification. In the assembled system, the weight of the outer shell and the interstitial components would be transferred to the inner layer through their supports and connecting elements and could therefore generate localized rather than perfectly uniform actions. The value obtained through the calculations should consequently be interpreted as an initial estimate rather than as a definitive design load. It includes only the component currently defined in the model and is intended to assess their potential influence on the global response of the structure. The estimate will require further refinements as the geometry, technological systems, supports and connections of the components are developed in greater detail.

The equivalent additional loads combination was applied to the inner shell only. According to the preliminary load path assumption adopted in the analysis, the interstitial components are primarily supported by the inner layer. The outer-shell model therefore includes its own self-weight through the Gravity component, but it does not include the additional equivalent load assigned to the inner shell. This assumption will need to be reassessed in the future developments of the model, since the detailed configuration of the supports and connection system may redistribute part of the interstitial loads according to a path different than the one predicted.

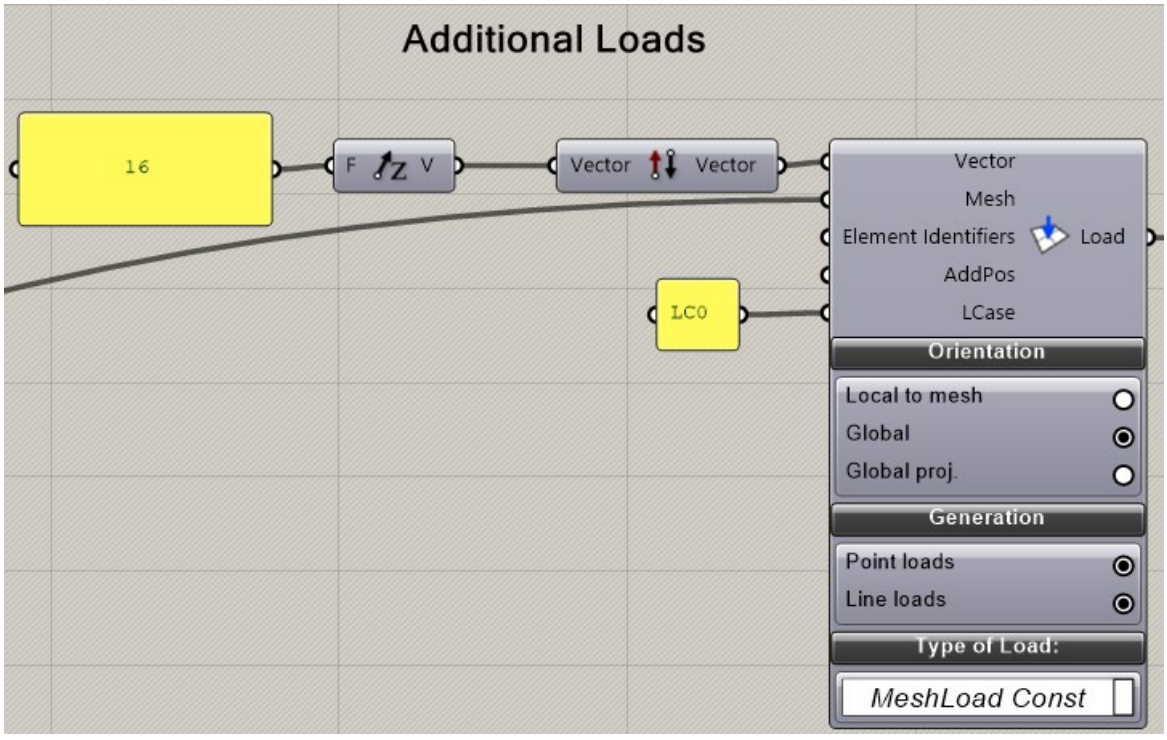


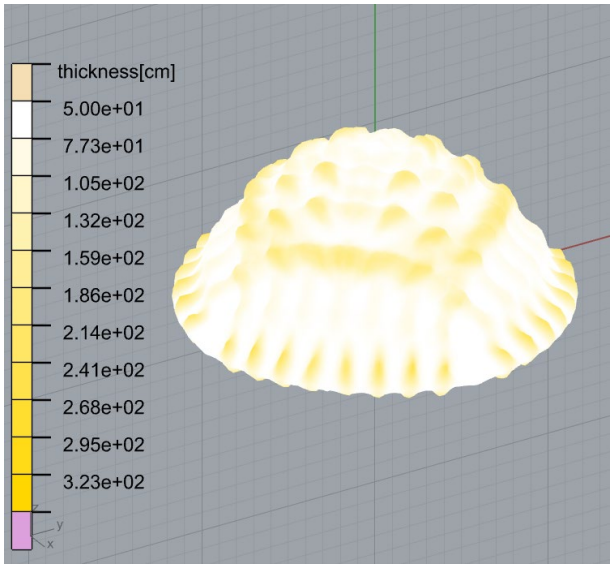

***Figure 6.3:*** *Definition of the equivalent additional dead load as a uniformly distributed mesh load oriented along the negative global Z-axis and assigned to load case LC0.*

### 6.2 Cross-section optimization and geometric smoothing

Once the loading actions had been defined, a first structural analysis of the uniform-thickness model was carried out in Karamba3D. The results revealed high material utilization values in some regions of the shell, highlighting the need to refine the initial configuration characterized by a uniform thickness. A cross-section optimization procedure was therefore introduced to reduce the utilization levels by locally adapting the section to structural demand. This strategy was applied independently to the inner and outer shell models and involved a broad admissible thickness range of 0.05 – 5 m, allowing the algorithm to associate different local sections in a way more consistent with the structural requirements of the system.

As shown in Figures 6.4 and 6.5, the greatest thicknesses are concentrated in the areas where adjacent lobes meet, corresponding to the grid junctions of the computational model. The inner shell (Figure 6.4) shows values that vary from 0.5 m to approximately 3.23 m, whereas the outer shell (Figure 6.5) ranges from roughly 0.5 m to 2.51 m. In both cases the lobed surfaces showed the thinnest sections of the model. Although the optimization algorithm did not use the full admissible range, this broad interval was adopted as a conservative measure, since it was observed that narrowing it led to an increase in the stress/strength ratio values. Another consideration that led to a broad range of values associated with the cross-sections was the necessity to have appropriate thickness to shield the crew from radiation and the overall external environment.

The range was refined through successive iterations, comparing the resulting stress/strength ratio values, displacements and morphology of the structure. The purpose was to identify a preliminary balance between structural performance and material demand rather than to obtain a definitive dimensioning of the shell.



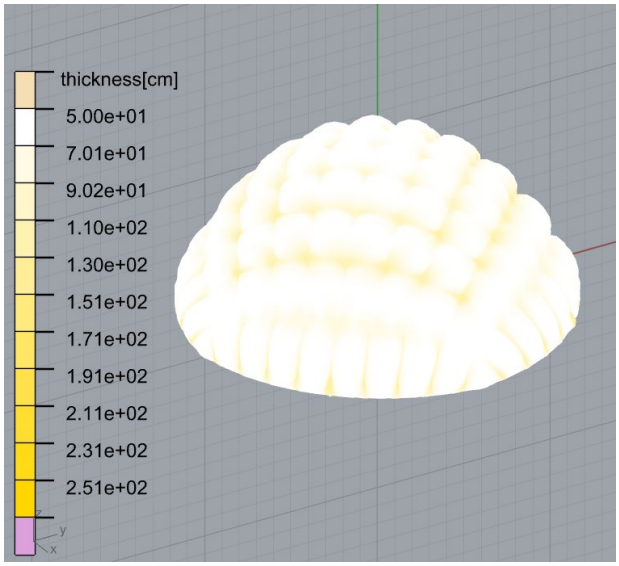




***Figure 6.4 (left) and 6.5 (right):*** *The figures show the thickness distribution of both the inner and outer shell. The greatest values of thickness are located in the regions of connection between the lobed modules.*

The cross-section optimization strategy identified the regions subjected to the greatest stress and assigned them greater thicknesses, while reducing the material usage in lightly stressed areas. This produced a material distribution that responds more directly to the calculated

structural demand, and to strategies of material saving. However, the result should be interpreted as a preliminary numerical optimization based on material properties, boundary conditions and loading assumptions adopted in the current model.

The differentiated thickness distribution led to a more efficient configuration, in which matter is distributed according to a performance-based hierarchy. In this sense, the optimization also reinforces the value of biological inspiration within the research. As discussed in Chapter 3, in many natural systems matter is organized according to principles of adaptation, structural efficiency, and resource saving. This strategy therefore fits within this same logic, in which matter is concentrated where it is structurally necessary and reduced where stresses are less relevant. In conclusion, the biological reference concerns not only the morphology of the shell, but also the selective and performance-oriented organization of its material.

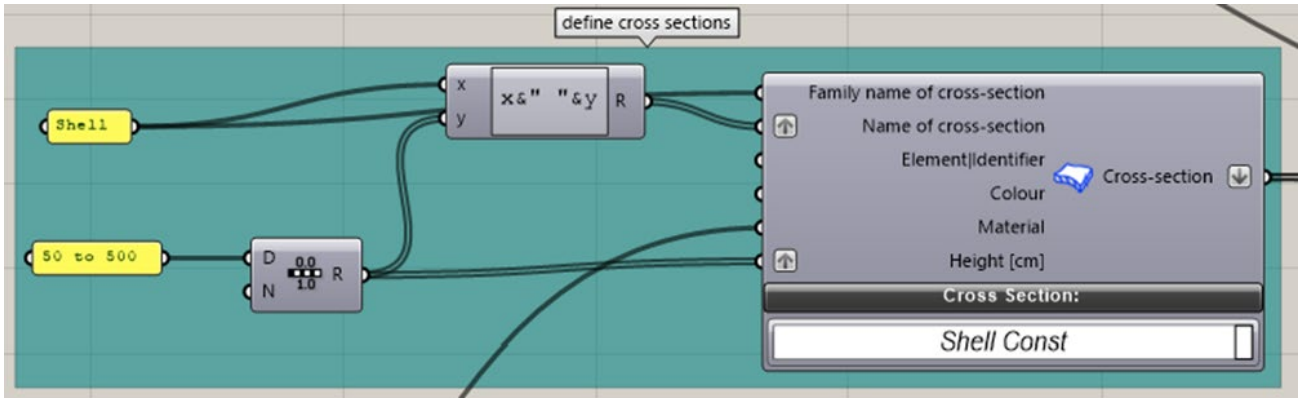



***Figure 6.6:*** *Components used for cross-section optimization.*

Following cross-section optimization, the resulting geometry was refined in Grasshopper using *Weaverbird's Laplacian Smoothing* component. This operation was introduced as a geometric post-processing step rather than as an additional stage of structural optimization. The thickness distribution generated by the optimization process produced abrupt concentrations of material in some areas of the shell. Although these irregularities directly reflected the stress distribution, they were not considered satisfactory from a formal and perceptual perspective. Smoothing was therefore used to improve the geometric continuity of the surface and preserve the aesthetic value of the structure.

### 6.3 Results of the structural analysis

Once the loading conditions had been defined, the structural response of each shell was assessed separately. Karamba3D was used to evaluate the mechanical behavior of the models through three main parameters: *Stress/Strength Ratio*, *Displacement*, and *Equivalent Stress*. These benchmarks provide complementary information on the degree of stress in relation to the material strength, the magnitude and distribution of displacements and the stresses throughout the structure.

The first parameter to be investigated was stress/strength ratio, expressed as a percentage. This value represents the ratio between the stresses locally developed within the shell and the resistant capacity of the material.

At this stage of the analysis, a methodological clarification is required. As discussed in Chapter 5[42], the design strategy envisages the use of microwave-sintered lunar regolith as the primary construction material, in accordance with an in-situ resource utilization approach. However, the definition of a material in Karamba3D requires a complete set of mechanical properties, either selected from the available material library or introduced through a custom material model.

As the experimental campaign on the regolith-based material is still at an early stage and has not yet provided a complete and validated set of mechanical properties for numerical modelling, and since the experimental activities involving lunar regolith simulants and microwave sintering have not yet begun, C20/25 concrete was provisionally adopted as the reference material for the preliminary structural analysis. However, this choice does not imply mechanical equivalence between concrete and sintered lunar regolith. Rather, it provides a preparatory benchmark for investigating the influence of geometry, loading conditions and thickness distribution on the response of a quasi-brittle material characterized by a marked difference between its compressive and tensile strengths.

C20/25 represents an ordinary, moderate-strength class of structural concrete. Its adoption should not, however, be interpreted as inherently conservative, since the calculated response depends on the complete set of assigned mechanical properties and on the selected strength criterion. The results presented in this section should therefore be regarded as preliminary and primarily comparative. Once validated experimental data become available, the reference material will be replaced by a custom material model more closely aligned with the measured properties of the regolith-based material, allowing a more accurate structural analysis.

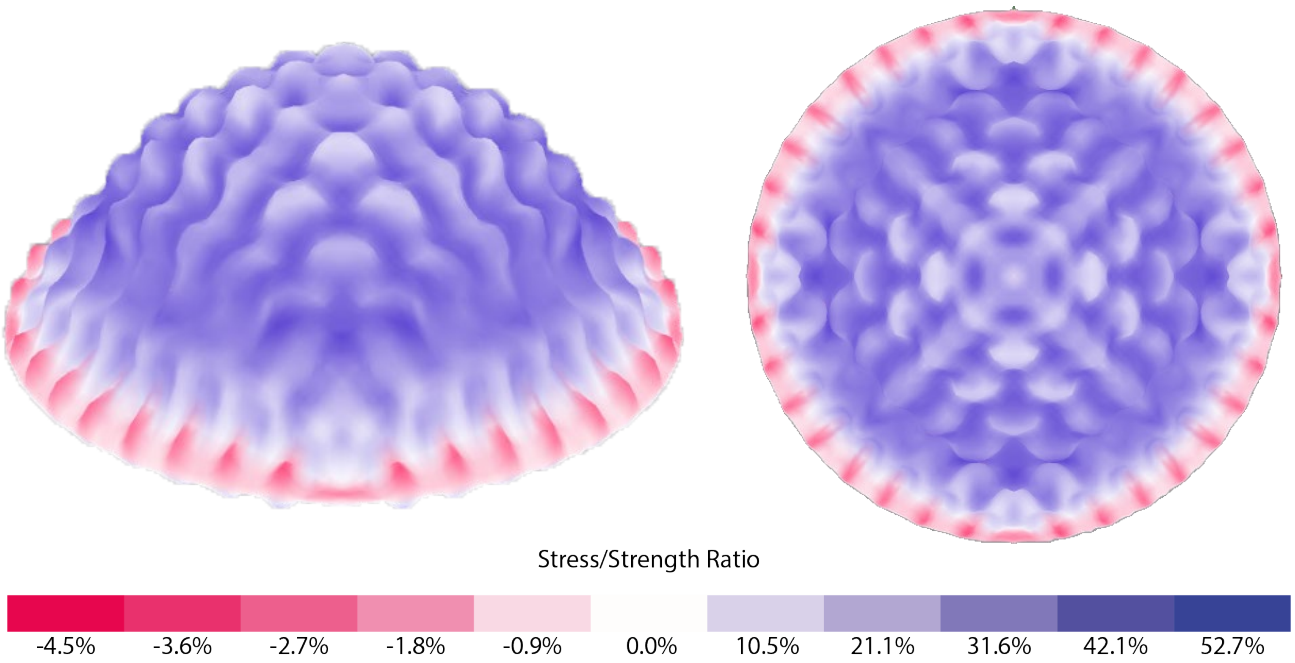



***Figure 6.7:*** *Stress/strength Ratio of the inner shell.*

[42] *Chapter 5, section 5.2 – Construction material.*

Figure 6.7 shows the stress/strength ratio of the inner shell, expressed as the ratio between the local stress and the corresponding strength assigned to the reference material. This output makes it possible to identify the most highly stressed regions of the structure and to evaluate how the stress demand is spatially related to the geometric configuration of the shell. According to the sign and color convention adopted for the visualization, red tones correspond to negative values associated with a prevailing compressive response, white tones indicate values close to zero, and the blue tones correspond to positive values associated with a prevailing tensile response. Each color shade is associated with a numerical value that indicates the percentage of the assigned material strength reached by the calculated stress demand. The values returned by the analysis vary according to the magnitude and distribution of the applied loads, the cross-section assigned to the shell, and the mechanical properties of the reference material. For the purpose of interpreting the results, two aspects are particularly relevant: The spatial distribution of tensile and compressive regions across the surface and whether the calculated values of stress/strength ratio remain below the nominal threshold of 100%.

From the point of view of stress distribution, the inner shell shows a response that is coherent with its geometric configuration and with the applied loads. A large portion of the surface presents positive values, represented by the blue tones of the legend, indicating that the tensile response is the governing condition. This is consistent with the effect of internal pressurization, which tends to generate tensile stress demand within the shell. The results are also consistent with the functional logic of the lobed geometry. The concave surfaces of the lobes appear to contribute to the redistribution of stress demand across the shell, with higher values concentrated in the interlobar regions and lower values located in the lobed surfaces. As can be observed from the figure, these regions show a prevalence of tensile stresses, represented by the most intense shades of blue. Within this range highlighted by the legend, the stress/strength ratio increases progressively and reaches a maximum value of 52.7%, corresponding to slightly more than half of the nominal strength assigned to the reference material. The values remain below the limit of 100%; therefore, within the assumptions of the model, no region of the shell reaches the strength limit associated with the material. At the same time, the distribution of values clearly indicates that tensile demand represents the most critical condition for the structure.

The interlobar regions are also significant because they receive the gravitational loads associated with the outer shell and the other additional loads. The introduction of such loads, however, did not substantially alter the overall stress pattern. A slight reduction in the maximum ratio values was observed as the add loads increased; this result may be explained by the compressive contribution of the vertical loads, which partially counteracts the tensile demand generated by internal pressure. This interpretation should be regarded as preliminary and depends on whether the geometry and thickness distribution were kept unchanged during the analysis.

By contrast, the shell works only marginally in compression. The maximum compressive utilization reported in the legend is approximately 4.5%, indicating that compression is not the governing condition in this model. The areas characterized by red tones are mainly located along the annular region at the base. This result is consistent with the behavior of a pressurized shell constrained along its perimeter, where the internal actions of the curved surface are transferred to the supports. The edge therefore represents a structurally sensitive zone, where

local stress concentrations, ring effects and localized compressive responses occur as a consequence of the boundary conditions.

Overall, the stress/strength ratio values of the inner shell support the design strategy adopted during the form-finding process. The results suggest that the lobed configuration is capable of organizing the stress demand in a spatially differentiated and efficient way, concentrating the highest tensile stresses within the interlobar regions rather than distributing them uniformly across the entire surface. Compression plays only a minor role in the structural response; however, this does not necessarily imply that the shell is globally overdesigned, since the thickness distribution is mainly governed by tensile demand and localized stress concentrations. At this preliminary stage, the results are promising, but they should be interpreted within the assumptions of the model, including the provisional reference material, the assigned boundary conditions, the environmental factors and the additional loads assumed. In conclusion, the interlobar regions emerge as the most suitable areas for the future integration of targeted reinforcement systems aimed at improving the tensile response of the structure.

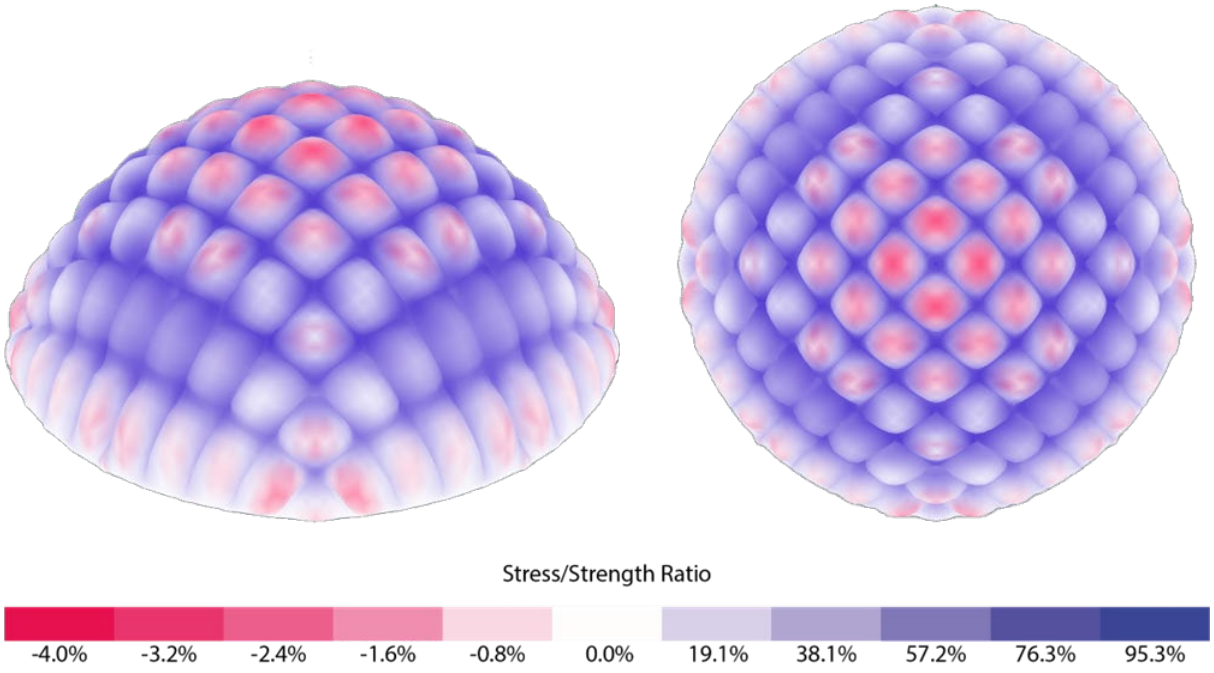



***Figure 6.8:*** *Stress/strength ratio of the outer shell.*

The structural response of the outer shell was then investigated through a separate yet parallel structural analysis. Although the two layers are conceived as parts of a single integrated structural system, they were analyzed separately for computational simplification. In the actual configuration, the internal pressure would act directly on the inner shell, while only part of the resulting actions would be transferred to the outer shell through the connection regions between the two layers. Since this transfer mechanism was not explicitly modelled, the full internal pressure was also applied to the outer shell as a deliberately demanding but simplified loading scenario. This assumption can be considered conservative with the overall magnitude of the pressure assigned to the outer shell, since the actual layer would be expected to receive

only part of the actions induced by internal pressurization. The resulting values should therefore be interpreted as a *worst-case evaluation* of the global response of the outer geometry, rather than as an accurate representation of the expected response of the joined system.

As in the inner shell, the highest values of tensile stress/strength ratio are primarily concentrated within the interlobar regions. Compared with the inner shell, compressive values extend into a larger number of localized areas across the upper lobed surfaces, while the compressive zone at the base is less extensive. The maximum values are approximately 4%, indicating that compression is not the governing condition of the outer shell. This result does not, by itself, demonstrate that the corresponding portions of the shell are structurally redundant or entirely overdesigned, but they may be considered during future refinements of the cross-section distribution. More extensive regions characterized by values close to zero can also be identified and are represented by the white tones of the legend. In these areas, the calculated stress demand remains low relative to the corresponding strength assigned to the reference material.

The most significant difference compared with the inner shell concerns the maximum tensile value, since in the most highly stressed interlobar regions, the calculated tensile demand reaches 95.3%. Although this value remains below the nominal threshold of 100%, it indicates only a limited residual margin within the assumptions of the model. The result identifies the tensile interlobar regions as critical areas requiring further verification, possible refinement of the computational model and future integration of specific reinforcements. The higher values of tensile stress may be attributed primarily to the deliberately demanding loading assumption adopted for the outer shell and to the reversed orientation of its curvature. Compared with the concave lobes, the outer-shell geometry is less favorable when directly subjected to the same outward pressure. The result may also be influenced by the optimized cross-section distribution and by the absence of structural interaction with the inner layer in the separate models.

The analysis therefore suggests that the outer geometry, when considered independently and subjected to the full internal pressure, exhibits a more demanding structural response than the inner shell. A separate and more detailed analysis would be required to determine which portion of these loads is actually transferred to the inner shell through the connecting elements.

The analysis was subsequently extended to the *Displacement* and *Equivalent Stress* parameters. The displacement output represents the magnitude of the resultant displacement of the shell, expressed in centimeters.

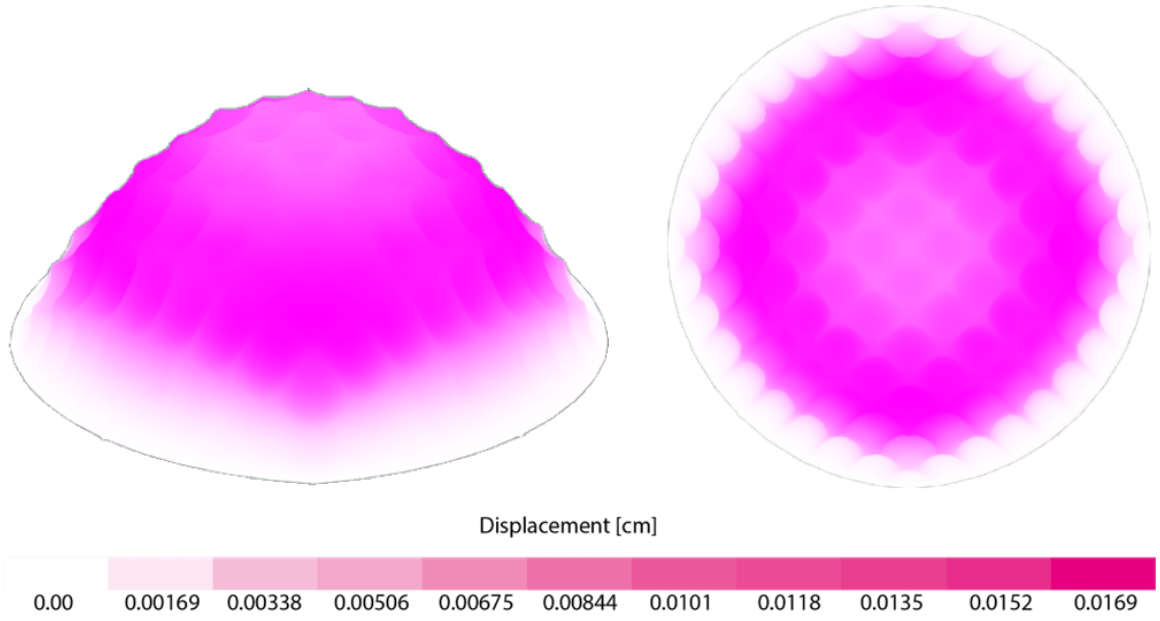



***Figure 6.9:*** *Displacement of the inner shell.*

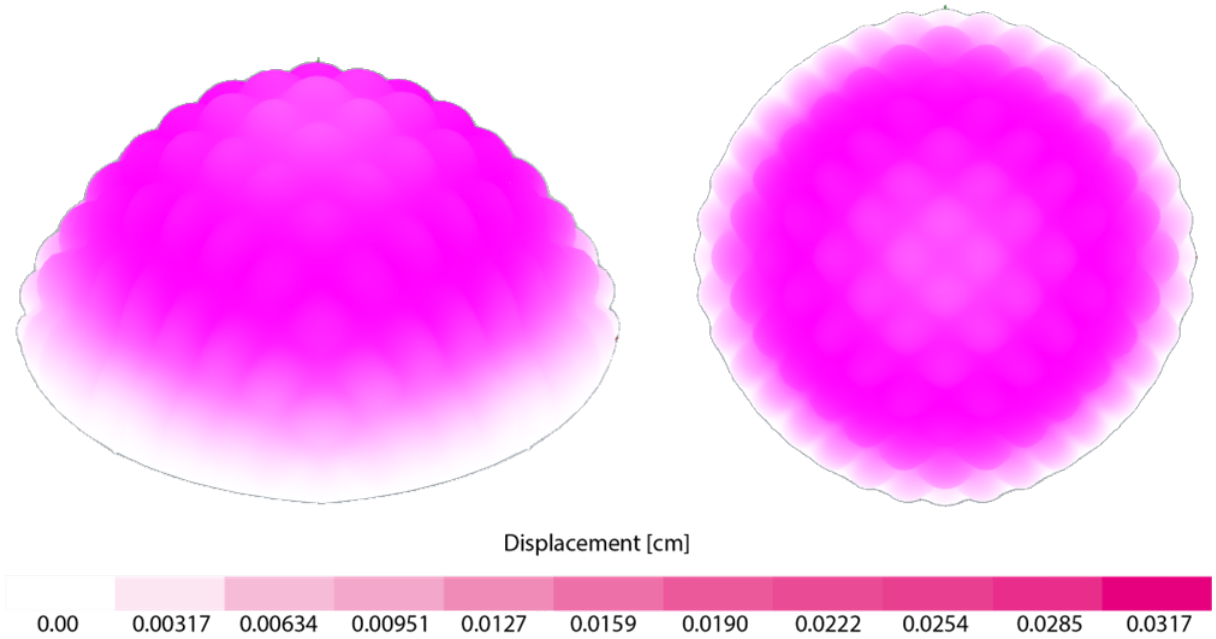



***Figure 6.10:*** *Displacement of the outer shell.*

Figures 6.9 and 6.10 show the displacement distribution of the inner and outer shells, respectively. The maximum values reported in the legends are 0.0169 cm, corresponding to approximately 0.169 mm for the inner shell, and 0.0317 cm for the outer shell, corresponding to approximately 0.317 mm. The maximum displacement of the outer shell is therefore roughly 1.9 times that of the inner one, although both values remain very limited compared to the overall dimensions of the structure. In both models, the minimum displacement values occur along the lower annular region, represented by the lightest tones of the legends. This

distribution is a direct consequence of the imposed boundary conditions, since the point supports located along the base restrain the movement of the structure. By contrast, the portions located farther from the restrained perimeter exhibit progressively larger displacement values.

Under the considered boundary conditions, both models therefore exhibit high global stiffness. However, the limited magnitude of the displacements should not be understood as a complete verification of structural stability. This parameter would require separate and further analyses, which are expected to be carried out in future developments of the research.

The last parameter considered within the structural analysis is the one defined as Equivalent Stress, namely a synthetic parameter that Karamba3D uses to summarize a complex stress state into a single numerical value. In a shell element, the local stress state may result from the combined contribution of in-plane membrane forces and bending moments, producing tensile and compressive stresses through the thickness of the element. Equivalent Stress expresses this combined condition through a single comparative value, making it possible to evaluate its spatial distribution and compare the results obtained in relation to different regions and geometries.

Unlike the Stress/Strength Ratio parameter, which is expressed in percentage terms, Equivalent Stress expresses a stress state and therefore uses kN/cm$^2$ as its unit of measurement.

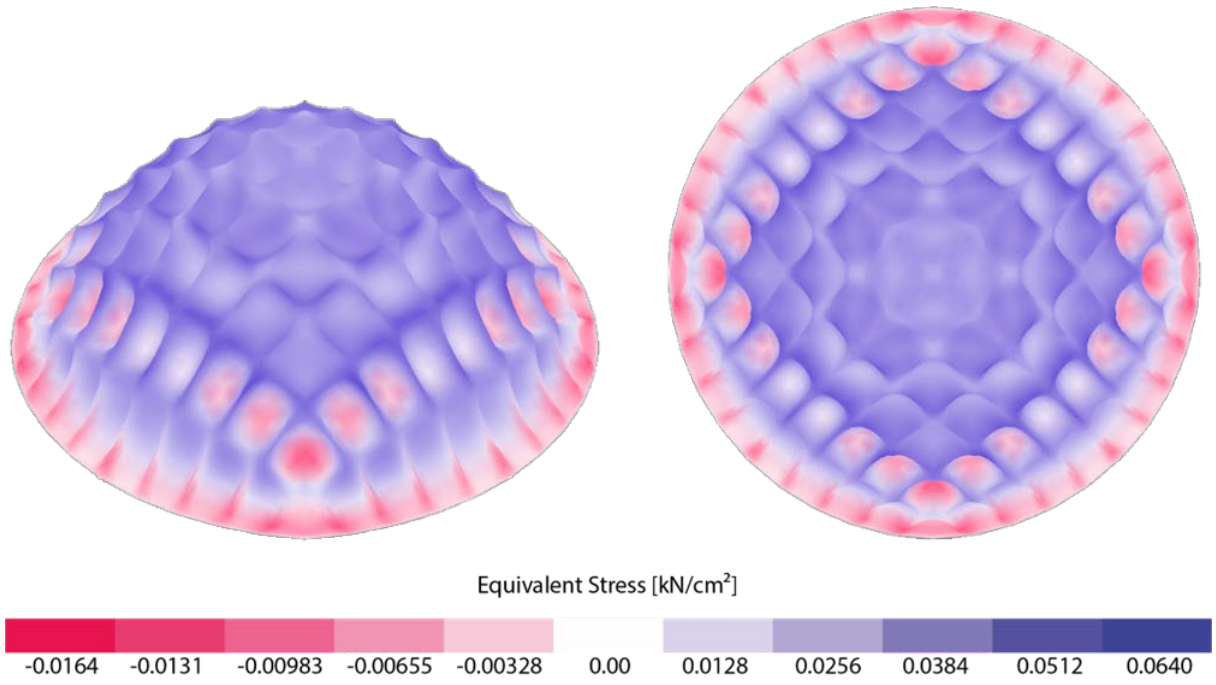



***Figure 6.11:*** *Equivalent stress of the inner shell.*

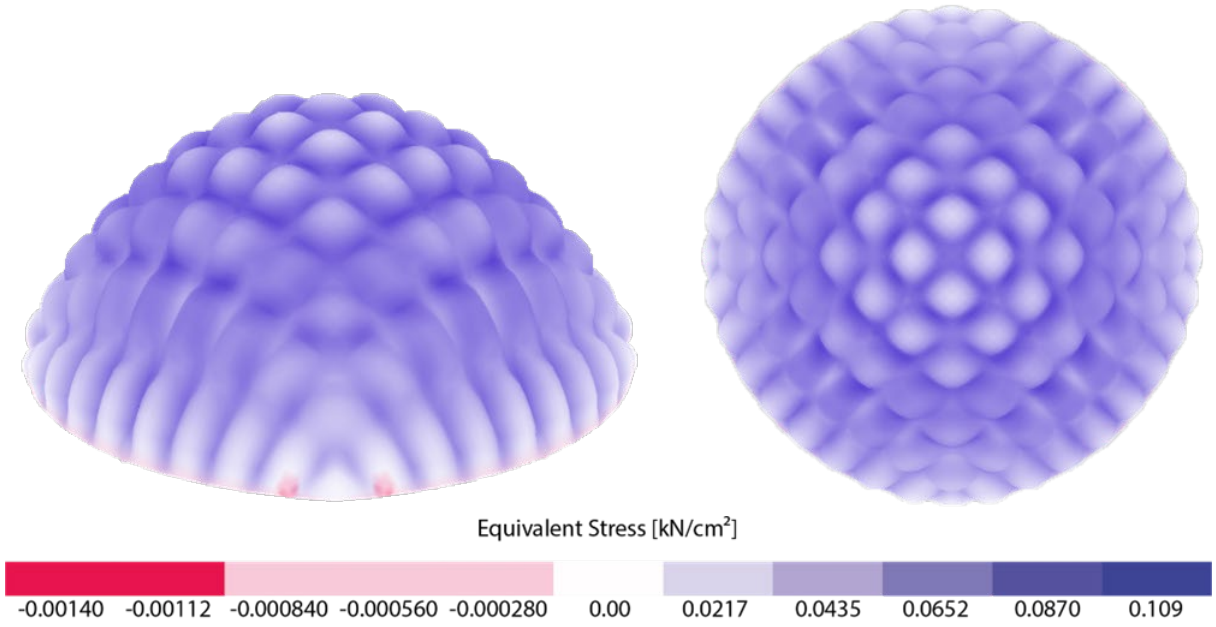



***Figure 6.12:*** *Equivalent stress of the outer shell.*

Figure 6.11 shows the equivalent stress distribution of the inner shell. The values range from approximately -0.0164 kN/cm$^2$ to +0.064 kN/cm$^2$, corresponding to -0.164 MPa and +0.64 MPa respectively. Under the same color convention adopted in the previous scenarios, negative values are associated with a compressive response, whereas positive values with a tensile response. The map shows a spatially differentiated stress distribution closely related to the lobed morphology. Most of the surface is characterized by blue tones, indicating that the tensile response is predominant in this case as well. This stress distribution is compatible with the in-plane tensile action expected in a shell subjected to internal pressure. The compressive regions, represented by red tones, are concentrated mainly along the restrained basal zone and within localized portions of some lobes. In these areas, compressive values range from 0.03 to 0.16 MPa approximately. The restrained perimeter limits the free deformation of the shell and may therefore generate localized stress concentrations and changes in the prevailing stress state. The spatial correlation between the stress distribution and the lobed morphology suggests that local curvature influences the redistribution of the structural demand. Consequently, the geometry appears to contribute to the mechanical response in an efficient way, rather than serving a purely formal purpose.

Figure 6.12 shows the distribution of stresses in the outer shell. The values range from approximately -0.0014 kN/cm$^2$ to +0.109 kN/cm$^2$, corresponding to -0.014 MPa to +1.09 MPa respectively. The map is predominantly characterized by blue tones, associated with mostly tensile stresses. Localized lighter regions occur around some lobe centers and geometric transition areas, while the regions characterized by a compressive response appear mainly near the lower restrained edge. These localized negative values do not represent the prevailing response of the outer layer. Rather, they constitute local effects plausibly associated with the boundary conditions and with variations in stiffness near the restrained perimeter. Overall, the outer shell model is therefore governed by a widespread tensile response, whereas compression remains marginal and localized.

Compared with the inner shell, the outer one exhibits less extensive compressive regions and higher maximum positive values of equivalent stress. This difference may be associated both with the reversed curvature of the outer geometric configuration and with the deliberately demanding assumption of applying internal pressure directly to its surface. The concave lobes of the inner shell are more favorably oriented with respect to the direction of the applied pressure, while the convex curvature of the outer shell model produces a more demanding response under the same equivalent loading condition.

These results should nevertheless be interpreted in relation to the intended double-shell system. In the proposed structural configuration, the outer shell would not be directly subjected to a uniformly distributed internal pressure. Instead, it would receive part of the actions induced by pressure, absorbed and redistributed by the inner shell through the connection regions of the two layers. The separate outer-shell model does not literally reproduce this load transfer mechanism and should therefore be regarded as a demanding assessment of the outer geometry and as a computational simplification, rather than as a direct representation of the structural system.

A final comparison was subsequently developed between the lobed configuration and a geometrically simpler continuous shell. The same reference material, load combination, boundary conditions, strength criterion and cross-section range were adopted. The continuous shell underwent the same cross-section optimization process, calculated according to its stress distribution. The purpose of this comparison was to assess whether the lobed configuration provides structural advantages over a regular continuous geometry, despite its greater geometric complexity and potentially higher fabrication demands. However, this comparison, as well as the overall structural analysis, should be considered as preliminary.

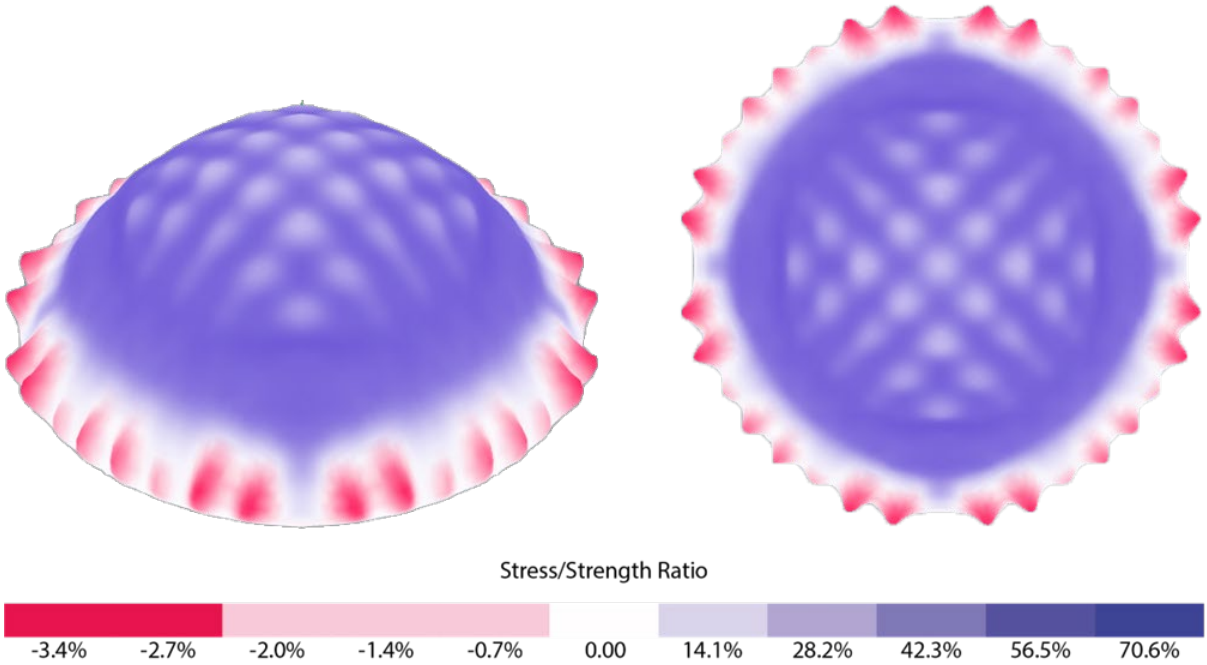



***Figure 6.13:*** *Stress/strength ratio of a continuous shell, used for comparison.*

Figure 6.13 shows the stress/strength ratio distribution of the continuous reference shell. Compared with the inner lobed shell, this configuration displays a less articulated alternation between tensile and compressive regions. Negative values are confined mainly to the lower annular region. By contrast, positive values, associated with a mostly tensile response, govern most of the surface. The irregular perimeter profile visible in the figure results from the cross-section optimization and geometrically coincides with localized compressive regions.

The maximum positive value of stress/strength ratio reaches 70.6%, compared with 52.7% in the inner lobed shell. Under the same boundary conditions the continuous geometry therefore develops a higher peak tensile demand. In addition to this increase in the maximum value, tensile stress extends over a broader and more continuous area of the surface. The comparison therefore suggests that the continuous configuration distributes tensile stress more uniformly, while the lobed geometry concentrates the highest values within interlobar regions, showing a more efficient distribution of forces.

The continuous shell is geometrically simpler and may offer advantages in terms of fabrication times and costs. However, the preliminary analysis suggests that it may require reinforcements to be distributed over a larger portion of the surface. In a lunar construction scenario, this could increase the logistical and material burden if reinforcement systems had to be transported from Earth or produced locally through ISRU processes that are not yet available at construction scale. On the other hand, the lobed configuration appears to localize the highest tensile demand primarily within the interlobar network, allowing the reinforcement system to be concentrated in more specific regions.

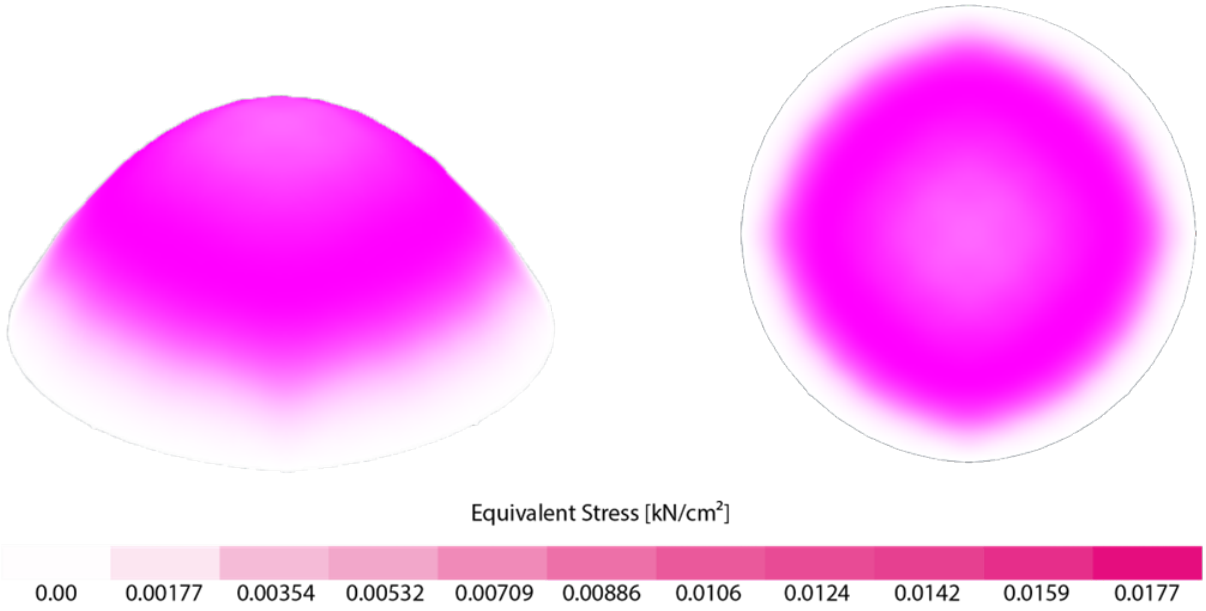



***Figure 6.14:*** *Displacement of a continuous shell.*

Figure 6.14 shows the displacement distribution of the shell. The model does not reveal anomalous local concentrations. The lowest displacement values occur along the supports at the base, while progressively higher values develop toward the central and upper portions of the dome. Moreover, the highest value (0.177 mm) is comparable to that observed in the inner shell (0.169 mm) and lower than observed in the outer layer (0.317 mm). Overall, as observed

in the previous cases, the displacement remains very small relative to the dimensions of the structure, indicating high global stiffness under the loading conditions considered.

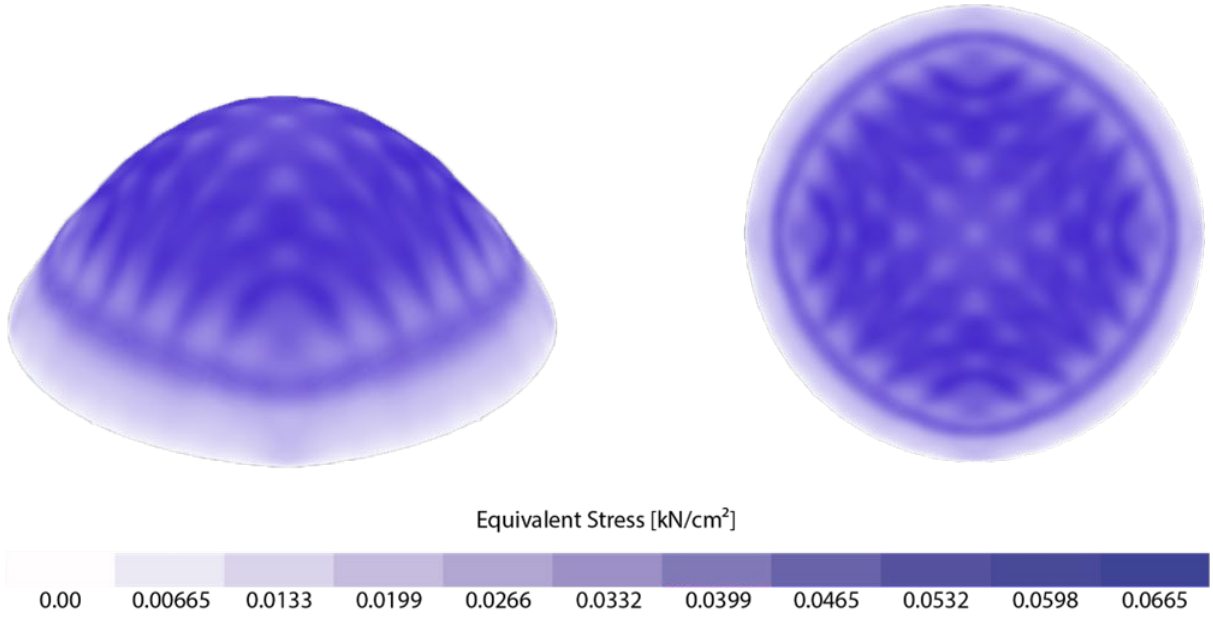



***Figure 6.15:*** *Equivalent stress of a continuous shell.*

Figure 6.15 shows the values and distribution of equivalent stress. The maximum value is 0.0665 kN/cm$^2$ or 0.665 MPa. According to the adopted sign and color convention, no negative values are present in the model, implying a negligible component of compressive stress. The lowest values of the scale are associated with the annular zone of the structure, while a consistent portion of the surface is characterized by the higher ones.

Immediately above the basal region, an annular band of high stress values can be identified. Its position appears compatible with the development of hoop tension caused by the tendency of the structure to expand rapidly when subjected to internal pressure. The response of the upper part of the structure seems to confirm this condition, since tensile stress spreads uniformly. The maximum value of approximately 0.665 MPa is close to the one obtained by the inner shell, of about 0.64 MPa. The principal difference between the two configurations, however, lies less in the numerical value itself than in the spatial distribution of forces. In the continuous shell, tensile stress affects a broader and more uniform portion of the surface, whereas the lobed geometry produces a differentiated pattern in which tensile stress is mostly concentrated along the interlobar network.

Overall, regarding the lobed geometry, the preliminary structural analysis seems to provide encouraging results, suggesting its validity as a structurally beneficial design choice rather than as a merely aesthetic one. The comparison with the continuous shell further strengthens this interpretation, since it would require a more extensive reinforcement system, with implications for material use, construction complexity and transportation.

Geometric complexity therefore emerges not simply as a formal consequence of the design process but as a means of structural control. The surface subdivision into lobes enables the form to respond more efficiently to the applied loads, to the mechanical limitations of the

reference material and to the aim of reducing additional reinforcements. Within the framework of the structural analysis, the investigated parameters indicate an overall stable and promising response. Nevertheless, the conclusions about the mechanical behavior of the structure should be understood as preliminary, since further investigations are required to assess the most highly stressed areas, the interlobar regions and possible local failure mechanisms. Under the loading, material and boundary conditions considered in this study, the lobed shell appears to offer a more favorable structural response than the continuous shell. Its principal advantage lies more in the spatial distribution of stresses than in a substantial reduction of its maximum value. In conclusion, the lobed configuration seems to promote a more targeted distribution of material and reinforcement, an aspect that appears consistent with the logistical and construction constraints of a lunar habitat. This potential should nevertheless be verified through a quantitative comparison of material volume, structural mass, and reinforcement requirements.

Finally, figures from 6.16 to 6.19 illustrate the developed geometric configuration of the double-shell structural system through an external view, a top view, a horizontal section and a vertical cross-section. The images show a relationship between the inner and outer layers, whose opposing curvatures generate a continuous system of interstitial cavities. These volumes form the intermediate functional layer that accommodates the shielding and life-support systems. The vertical section also reveals the variable thickness distribution resulting from the cross-section optimization process.



***Figure 6.16:*** *The shell in its final configuration.*

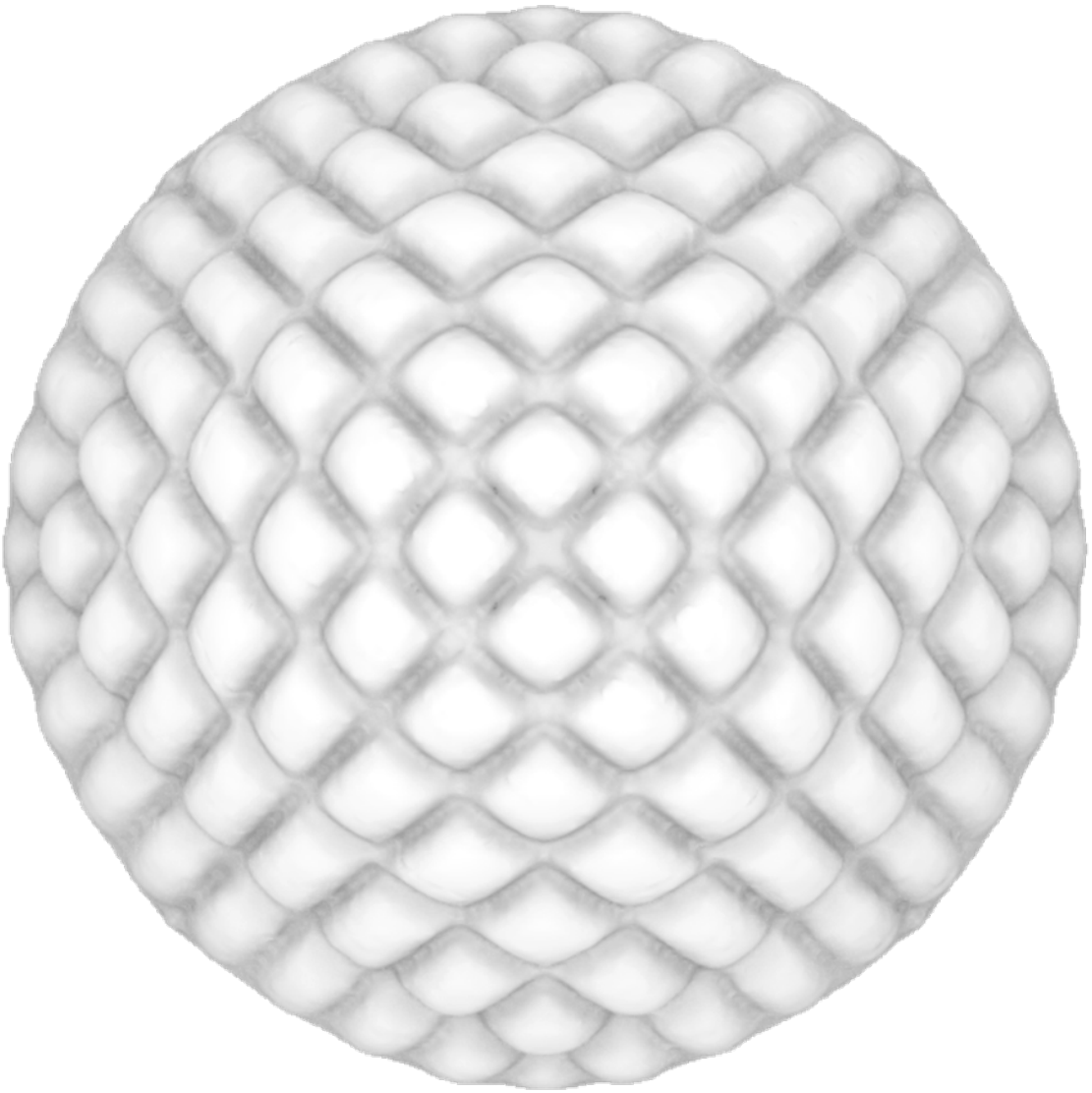


***Figure 6.17:*** *Top view of the shell.*

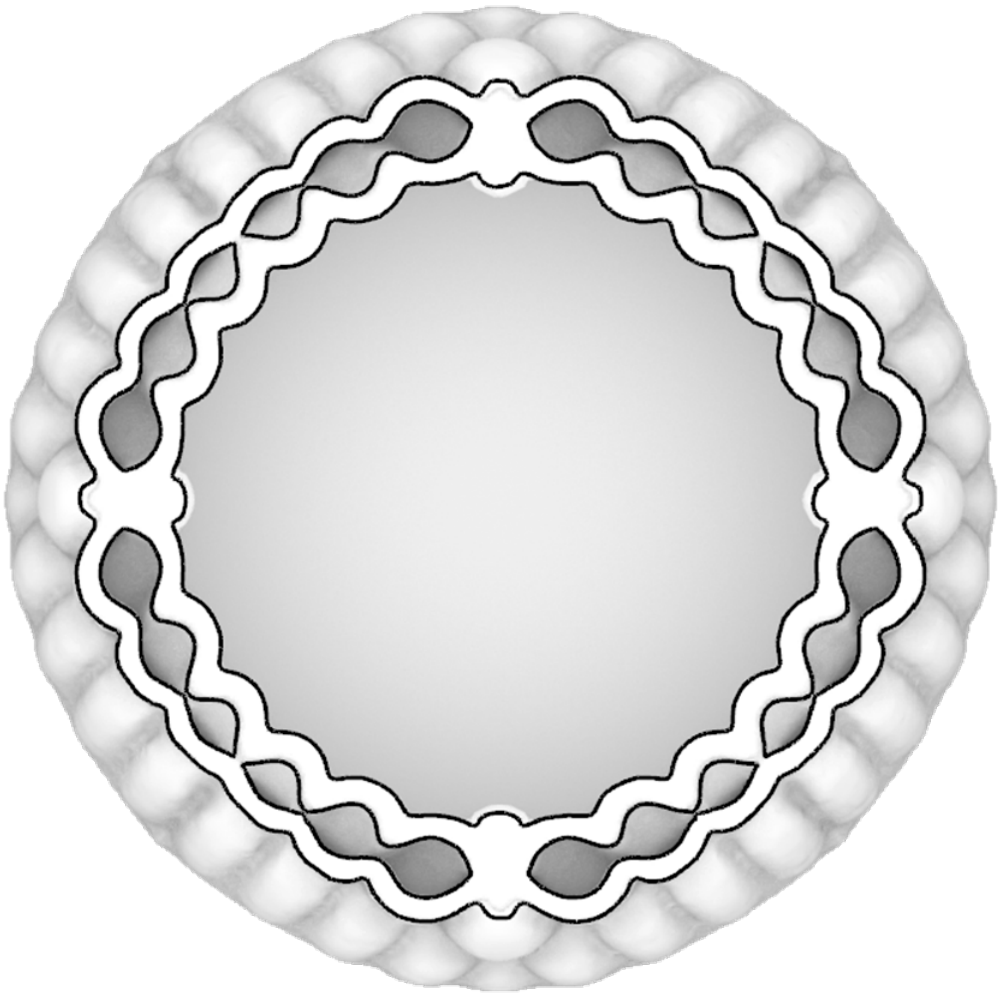


***Figure 6.18:*** *Horizontal section of the shell.*

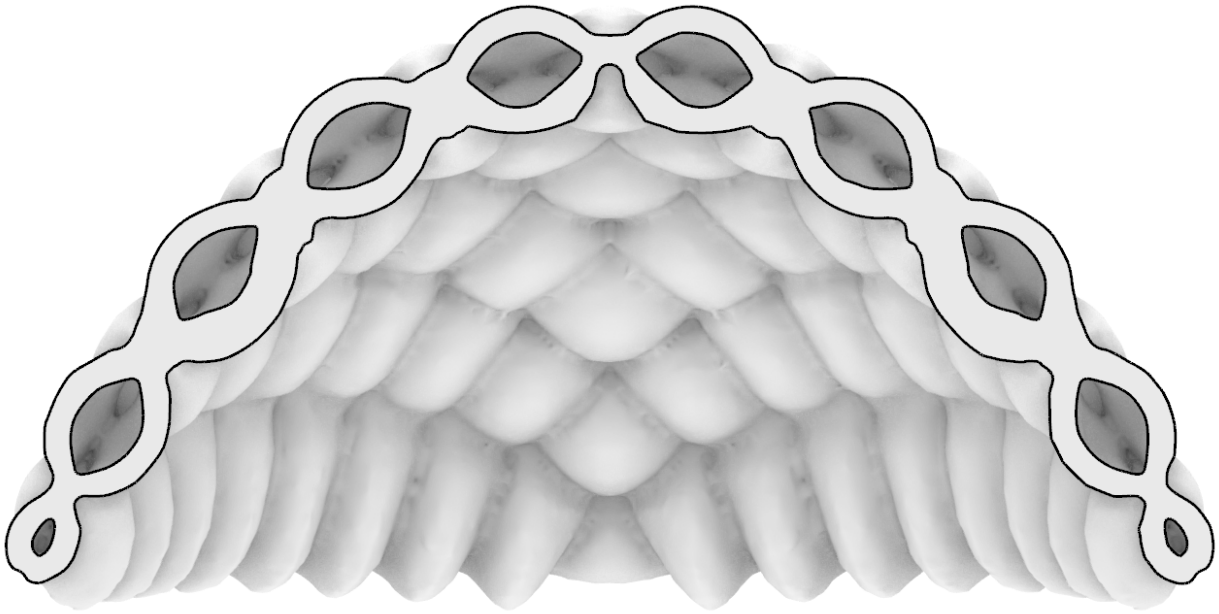


***Figure 6.19:*** *Cross-section of the shell.*

## Conclusions

This thesis investigated how biological principles, computational form-finding, structural differentiation, and in-situ resource utilization may be combined within the design of a pressurized habitat for future lunar settlements. The research originated from a fundamental contradiction in extraterrestrial construction: a lunar habitat must resist the considerable tensile stresses generated by internal pressurization, while the locally available mineral resources are more naturally suited to the production of ceramic-like materials whose mechanical behavior is generally more favorable in compression than in tension. Rather than addressing this conflict exclusively through the introduction of increasingly resistant materials or extensive reinforcement systems transported from Earth, the study explored whether geometry itself could become an active instrument for controlling the structural response. Within the fields of space architecture, biomimetic design and computational structural research, the scientific value of the work therefore lies in proposing a strategy in which form, loads, material distribution, construction resources and environmental parameters are developed as mutually dependent parts of the same system.

The principal original contribution of the thesis lies in the translation of the biological reference into a generative design method rather than into a merely morphological analogy. The research focused on the relationship among cellular geometry, resistant walls, shared interfaces, material differentiation, and turgor pressure. In plant tissues, internal pressure is not only an action that the cell wall must withstand, but it also contributes directly to cellular rigidity, growth and morphological definition. This principle was transferred to the structural scale by considering the internal pressure of the habitat not exclusively as an adverse load, but also as a shaping factor capable of contributing to the definition of the structural geometry. The resulting correspondence between the biological and architectural systems is therefore both morphological and methodological. Each lobe behaves as a pressure-responsive surface, while the interfaces between adjacent lobes form a continuous network in which stresses are collected and redistributed. In this sense, the research demonstrates how biomimetics can contribute to space architecture not through the literal reproduction of a natural organism, but through the reinterpretation of the physical and organizational principles that govern its behavior.

This conceptual framework was translated into a computational workflow articulated through two sequential form-finding stages. The first stage generated a gravitational funicular configuration from an initially planar mesh. Under the combined action of a vertical load and controlled boundary constraints, the mesh reached an equilibrium geometry characterized by a dome-like configuration. The second stage introduced the internal pressure required for human habitability as a further form-generating action. Pressure was applied to the individual quadrangular faces while their perimeter edges were maintained as constrained lines, producing a system of double-curvature lobes connected through a clearly recognizable interlobar network. This procedure established a differentiation of structural roles: the curved surfaces operate primarily as membrane-resistant fields, whereas the edges act as preferential regions for the collection and transmission of forces. A second, mirrored surface was subsequently generated to form an outer shell with opposite curvature. The resulting double-shell configuration creates a continuous system of interstitial cavities and extends the structural concept into a broader architectural and environmental strategy.

The computational process was followed by cross-section optimization and a preliminary finite-element assessment in Karamba3D. The optimization showed that material demand is

not distributed uniformly across the structure. The greatest thicknesses are concentrated around the grid network of the computational model, namely the regions where adjacent lobes meet, whereas the central portions of the lobed surfaces remain comparatively thinner. This result is consistent with the structural hierarchy anticipated during the form-finding process and supports the hypothesis that a differentiated material system may be developed in which greater structural capacity is assigned only to the areas where it is most necessary. The subsequent smoothing operation improved the geometric continuity of the optimized surfaces without replacing or contradicting the structural logic from which their variable thickness had been derived.

The preliminary structural results provide encouraging evidence regarding the validity of the lobed configuration. Under the adopted combination of lunar gravity, internal pressure, and additional loads associated with the outer shell and the interstitial systems, the inner shell reached a maximum stress/strength ratio of approximately 52.7%, while maintaining extremely limited displacements in relation to the overall dimensions of the habitat. The comparison with a geometrically simpler continuous shell is particularly significant. Under equivalent assumptions, the continuous configuration reached a higher maximum utilization of approximately 70.6% and developed tensile stresses over a broader and more homogeneous portion of its surface. By contrast, the lobed geometry produced a more differentiated stress pattern, concentrating the highest tensile demand along the interlobar network. The main advantage of the proposed geometry therefore does not consist simply in reducing the absolute maximum stress, but in controlling where the most demanding structural conditions occur. This offers the possibility of concentrating reinforcement and higher-performance materials within a limited network rather than distributing them across the entire envelope, with potentially important consequences for construction mass, resource use, and dependence on components supplied from Earth.

The response of the independently modeled outer shell was more demanding, reaching a tensile utilization close to the nominal capacity of the provisional reference material in the most highly stressed interlobar regions. This result should not be interpreted as a failure of the double-shell concept, but as the identification of one of the principal critical areas requiring further development. The outer shell was deliberately analyzed under the full internal pressure and without accounting for the mechanical interaction, load redistribution, and support provided by the inner layer and their connecting elements. The current model therefore represents a severe and simplified assessment of the outer geometry rather than the actual behavior of the assembled system. Nevertheless, the analysis is scientifically useful precisely because it reveals where the assumptions of the present model become most influential and where future structural refinement must be concentrated.

A further contribution of the research concerns the relationship between computational design and the development of construction materials based on extraterrestrial resources. The proposed shell is conceived primarily through regolith-based materials, potentially consolidated by processes such as microwave sintering and locally reinforced in the regions of greatest tensile demand. The experimental campaign initiated within the thesis does not yet validate the final lunar construction material, since its current phase employed sand-based gypsum specimens to establish and calibrate the preparation, casting, conditioning, and mechanical testing procedures. However, the tests provided relevant methodological results. They demonstrated that the measured compressive and flexural strengths depend not only on the duration of controlled humid storage but also on the subsequent conditioning time under

ambient laboratory conditions. The highest mean values, reaching approximately 9.21 MPa in compression and 3.73 MPa in flexure under the most favorable investigated conditions, indicate that the adopted protocol is capable of distinguishing the influence of preparation and conditioning parameters. The scientific achievement of this preliminary campaign therefore lies less in the absolute values obtained than in the definition of a repeatable experimental basis through which actual Martian and lunar simulants, fiber-reinforcement strategies, and dry consolidation processes can subsequently be assessed.

The double-shell configuration also made it possible to broaden the investigation beyond structural resistance. The interstitial layer generated between the opposing lobed surfaces was interpreted as an active component capable of accommodating photobioreactors, a mycelium-based layer, containment systems, and a preliminary distribution network. This strategy transforms the envelope from a passive separation between interior and exterior into a multifunctional system. The regolith-based skins contribute mass for passive shielding, while the aqueous medium and polymeric components of the photobioreactors may provide a complementary contribution to radiation attenuation. At the same time, the cultivation of microalgae may support $CO_2$ absorption, oxygen production, water recirculation, and the generation of nutritionally valuable biomass. Mycelium was introduced as an additional biological component whose potential for radiation mitigation and in-situ cultivation deserves further investigation. These systems are not proposed as substitutes for dedicated radiation protection or primary life-support equipment. Their value lies instead in their possible integration into a multilayer strategy in which the same architectural volume performs structural, protective, environmental, and biological functions. This multifunctional interpretation represents another significant aspect of the research, as it connects the geometric organization of the shell with the progressive reduction of dependence on terrestrial resupply.

The results must nevertheless be understood in relation to the initial stage of the research. The thesis does not present a fully engineered lunar habitat ready for construction, nor does it claim to resolve all the structural, technological, biological, and operational questions associated with long-duration human presence on the Moon. Its contribution is instead to establish a coherent and testable research framework, to produce a geometrically and structurally informed configuration, to identify its principal potential advantages, and to define the critical issues that must guide subsequent investigations. Within this scope, the results are promising. The two-stage form-finding process produced a structurally legible lobed geometry; the optimization confirmed a differentiated distribution of material; the structural comparison indicated a more targeted organization of tensile stresses than in the continuous reference shell; the material campaign established a controlled experimental protocol; and the double-shell system created an architectural space capable of integrating structural and environmental functions.

The first and most important future development concerns the construction of a coupled structural model in which the inner and outer shells are analyzed as parts of a single assembled system. This model will need to include the geometry and stiffness of the connecting elements, the actual transmission of pressure-induced forces between the layers, and the localized load paths generated by the interstitial systems. The preliminary assumption that the weight of the outer shell and of the biological and technical components acts as a uniformly distributed load on the inner layer must be replaced by a more accurate representation of supports, connections, and local load transfer. Particular attention will have to be devoted to the highly

stressed interlobar regions, the basal restraint system, the junctions between modules and the possible reinforcement of the outer shell. However, this development should be accompanied by deeper and more accurate structural analyses.

Thermal effects constitute another essential field of investigation. The present structural model does not include the severe temperature variations and thermal gradients characteristic of the lunar environment. Future simulations must therefore evaluate the interaction among temperature cycles, differential expansion, variable material properties, structural restraints, and the connections between the two shells. The long-term behavior of the structure should also be investigated in relation to micrometeoroid impacts, radiation-induced material degradation, lunar dust and the durability of seals and interfaces. These analyses will be necessary to move from a preliminary assessment of static behavior toward a more complete evaluation of safety, resilience, redundancy, and service life.

In parallel, the experimental campaign must progress from the current preparatory phase to the use of the selected Martian and lunar regolith simulants. For the lunar branch, a central objective will be the verification of microwave sintering as a dry consolidation technique and the characterization of the resulting material in terms of density, elastic modulus, compressive and tensile strength, flexural behavior, fracture resistance, thermal properties, and variability. The investigation should also assess the effectiveness of basalt, glass, carbon, or other compatible fibers, especially in relation to the localized tensile demand identified along the interlobar network. Once a sufficiently complete and validated dataset has been obtained, the provisional material currently used in Karamba3D can be replaced by a custom material model based on the experimental data obtained. This will allow the geometry, cross-section distribution, and reinforcement strategy to be recalibrated on a physically more representative basis.

The modular and constructional logic must likewise be developed beyond its current geometric definition. Future research should establish the dimensions and subdivision of the prefabricated lobed components, the interlocking system between adjacent modules, the sequence of robotic fabrication and assembly, allowable construction tolerances, and the methods required to ensure structural continuity and pressure containment. The relationship among the shell, foundations, lunar terrain, access points and airlocks will require specific design solutions.

The active interstitial layer constitutes an additional and substantial research trajectory. The photobioreactor system will require detailed fluid-dynamic analysis under lunar gravity, together with the design of circulation, gas exchange, lighting, monitoring, harvesting, contamination control, maintenance, and redundancy systems. Its actual contribution to radiation mitigation must be evaluated through radiation-transport simulations applied to the specific geometry and material stratification of the proposed shell. Similarly, the mycelium-based component must be experimentally characterized in relation to growth conditions, water and nutrient requirements, containment, sterilization, compatibility with the other layers, mechanical behavior and shielding effectiveness. The piping network currently developed as a preliminary distribution grid must be extended to include secondary branches, valves, sensors, maintenance access, and emergency isolation strategies. Only through these studies will it be possible to determine the effective contribution of the interstitial layer to life support, radiation protection, and resource circularity.

Finally, the habitat must be developed as an inhabited architectural environment. The current dimensions and morphology provide a basis for subsequent investigations into internal spatial organization, crew capacity, circulation, privacy, work and research areas, physical exercise, communal spaces, food production and emergency functions. The form-finding and structural systems should therefore be connected to human factors, operational scenarios, site selection, mission duration and the progressive growth of a lunar settlement. This step will make it possible to assess whether the modular logic can support not only structural and technological adaptation, but also the spatial evolution required by different phases of exploration and permanence.

The research is therefore not concluded. On the contrary, its present results define a clear trajectory from a geometric prototype to an assembled and inhabitable system. The principal achievement of the thesis is not the claim of having produced a definitive lunar habitat, but the demonstration that a coherent relationship can be established among biological organization, form-finding strategies, structural differentiation, local material use and multifunctional environmental systems. Within the assumptions of this initial phase, the proposed configuration has shown sufficient structural consistency and design potential to justify further investigation. It identifies both promising advantages and specific criticalities, transforming them into an articulated research program. In this sense, the work provides a scientific basis from which the proposed bioinspired double-shell system may be progressively refined, experimentally validated and evaluated as a possible contribution to the development of more autonomous, resource-conscious, and resilient extraterrestrial architectures.

# Bibliography


Adams, J. H. et al., 2007. The ionizing radiation environment on the moon. *Advances in Space Research,* Volume 40, p. 338–341.

Adriaenssens, S., Block, P., Veenendaal, D. & Williams, C., 2014. *Shell Structures for Architecture: Form Finding and Optimization*. Abingdon: Routledge.

Adriaenssens, S., Manuello Bertetto, A. & Marmo, F., 2025. Special issue: analysis and design of shell and spatial structures. *Meccanica,* Volume 60, p. 497–498.

Ali, O., Cheddadi, I., Landrein, B. & Long, Y., 2023. Revisiting the relationship between turgor pressure and plant cell growth. *New Phytologist*.

Ali, O. & Traas, J., 2016. Force-driven polymerization and turgor-induced wall expansion. *Trends in Plant Science*.

American Concrete Institute, 2014. *Building Code Requirements for Concrete Thin Shells (ACI 318.2-14) and Commentary on Building Code Requirements for Concrete Thin Shells (ACI 318.2R-14),* Farmington Hills, MI: American Concrete Institute.

Arnhof, M. et al., 2022. *Implementation of In-situ Resource Utilization for the Development of a Moon Village.* St. Paul, Minnesota, USA, s.n.

Avetta, C., n.d. *Angiosperme*. [Online]
Available at: https://www.treccani.it/enciclopedia/angiosperme_(Enciclopedia-Italiana)/
[Accessed March 2026].

Bacete, L. et al., 2022. THESEUS1 modulates cell wall stiffness and abscisic acid production in Arabidopsis thaliana. *Proceedings of the National Academy of Sciences of the United States of America (PNAS)*.

Barry, C., 2026. *The Moon's Atmosphere*. [Online]
Available at: https://science.nasa.gov/moon/lunar-atmosphere/
[Accessed 24 May 2026].

Beck, C. B., 2010. *An introduction to plant structure and development: Plant anatomy for the twenty-first century.* s.l.:Cambridge University Press.

Benaroya, H., 2010. *Turning Dust to Gold: Building a Future on the Moon and Mars*. I ed. Chichester, UK: Springer, published in association with Praxis Publishing.

Benaroya, H., 2018. *Building Habitats on the Moon: Engineering Approaches to Lunar Settlements*. Cham: Springer International Publishing.

Bhushan, B., 2016. *Biomimetics: Bioinspired hierarchical-structured surfaces for green science and technology.* II ed. s.l.:Springer International Publishing.

Bhushan, B. & Jung, Y. C., 2010. Natural and biomimetic artificial surfaces for superhydrophobicity, self-cleaning, low adhesion, and drag reduction. *Progress in Materials Science*.

Boller, G. & D'Acunto, P., 2021. *Structural design via form finding: Comparing Frei Otto, Heinz Isler and Sergio Musmeci*. Leiden, CRC Press/Balkema.

Bouley, S. et al., 2012. Power and duration of impact flashes on the Moon: Implication for the cause of radiation. *Icarus,* Volume 218, p. 115–124.

Branch, G. M., 2001. Rocky Shores. In: J. H. Steele, ed. *Encyclopedia of Ocean Sciences*. San Diego: Academic Press, p. 2427–2434.

Brulé, V., Rafsanjani, A., Pasini, D. & Western, T. L., 2016. Hierarchies of plant stiffness. *Plant Science*.

Burke, J. D., 2026. *Moon*. [Online]
Available at: https://www.britannica.com/place/Moon/Effects-of-impacts-and-volcanism
[Accessed 24 May 2026].

Burns, J. T., 1959. Mexican Architecture: New Forms, Imitation, or Evocation?. *Progressive Architecture,* 40(12), pp. 69-73.

Burry, M., 2011. Geometry Working Beyond Effect. *Architectural Design,* 81(4), pp. 80-89.

Caiazzo, A. et al., 2026. Structures for extraterrestrial habitat: A review. *Acta Astronautica,* Volume 238, p. 471–493.

Calladine, C. R., 1983. *Theory of Shell Structures*. I ed. Cambridge: Cambridge University Press.

Campioli, A., Mangiarotti, A. & Zanelli, A., 2007. *Learning From the Past to Renew Ephemeral Architecture in the Italian Context*. Milan, CLUP.

Candela, F., 1962. *Hacia una nueva filosofía de las estructuras*. Buenos Aires: Ediciones 3.

Cappelli, M., 2008. *Fasce di Van Allen*. [Online]
Available at: https://www.treccani.it/enciclopedia/fasce-di-van-allen_(Enciclopedia-della-Scienza-e-della-Tecnica)/
[Accessed March 2026].

Cassinello, P., 2016. *Museo Eduardo Torroja*. Madrid: Fundación Eduardo Torroja.

Chakraborty, T. et al., 2024. On the reachability and genesis of water ice on the Moon. *ISPRS Journal of Photogrammetry and Remote Sensing,* Volume 211, p. 392–405.

Chebbo, L. et al., 2025. Microgrids for Extraterrestrial Habitats: A Review of Technologies, Needs, and Challenges. *IEEE Access,* Volume 13, pp. 1-22.

Chilton, C., 2000. *Heinz Isler (Engineer's Contribution to Contemporary Architecture)*. London: Thomas Telford.

Chilton, J., 2010. Tensile structures – textiles for architecture and design. In: G. Pohl, ed. *Textiles, Polymers and Composites for Buildings*. Cambridge: Woodhead Publishing, pp. 229-257.

Chilton, J. & Chuang, C.-C., 2017. Rooted in Nature: Aesthetics, Geometry and Structure in the Shells of Heinz Isler. *Nexus Network Journal,* Volume 19, pp. 763-785.

CNSA & Roscosmos, 2021. *International Lunar Research Station: Guide for Partnership,* s.l.: China National Space Administration (CNSA) / State Space Corporation “Roscosmos”.

Cohen, M. M., 2002. *Selected Precepts in Lunar Architecture*. Houston, International Astronautical Federation / International Academy of Astronautics.

Cohen, M. M., 2003. *Mobile Lunar and Planetary Bases*. Long Beach, American Institute of Aeronautics and Astronautics.

Cohen, M. M. & Benaroya, H., 2009. Lunar-Base Structures. In: S. A. Howe & B. Sherwood, eds. *Out of This World: The New Field of Space Architecture*. Reston, Virginia: American Institute of Aeronautics and Astronautics, Inc., pp. 179-203.

Cordero, R. J. et al., 2025. Radiation protection and structural stability of fungal melanin polylactic acid biocomposites in low Earth orbit. *Proceedings of the National Academy of Sciences of the United States of America,* 122(18), pp. 1-8.

Cosgrove, D. J., 1993. Wall extensibility: Its nature, measurement and relationship to plant cell growth. *New Phytologist*.

Cosgrove, D. J., 2000. Expansive growth of plant cell walls. *Plant Physiology and Biochemistry.*.

Cosgrove, D. J., 2016. Plant cell wall extensibility: Connecting plant cell growth with cell wall structure, mechanics, and the action of wall-modifying enzymes. *Journal of Experimental Botany*.

Cosgrove, D. J., 2018. Diffuse growth of plant cell walls. *Plant Physiology*.

Cowley, A. et al., 2016. An ISRU-Based Architecture for Human Habitats on Mars: The "Lava Hive" Concept. *Acta Futura,* Volume 10, p. 109–119.

Crawford, I. A., 2015. Lunar Resources: A Review. *Progress in Physical Geography: Earth and Environment,* 39(2), pp. 137-167.

Crawford, I. A. & Joy, K. H., 2014. Lunar exploration: Opening a window into the history and evolution of the inner Solar System. *Philosophical Transactions of the Royal Society A: Mathematical, Physical and Engineering Sciences,* 372(2024).

Cucinotta, F. A., Kim, M.-H. Y. & Chappell, L. J., 2011. *Space Radiation Cancer Risk Projections and Uncertainties – 2010,* Houston: NASA.

D'Acunto, P. & Ingold, L., 2016. *The Approach of Sergio Musmeci to Structural Folding*. Tokyo, International Association for Shell and Spatial Structures (IASS).

Dachev, T. P. et al., 2011. An overview of RADOM results for earth and moon radiation environment on Chandrayaan-1 satellite. *Advances in Space Research,* Volume 48, p. 779–791.

Davidson, C., 2019. Up and Away at JFK. *Log,* Issue 46, pp. 130-138.

de la Fuente, H., Raboin, J. L., Spexarth, G. R. & Valle, G. D., 2000. *TransHab: NASA's Large-Scale Inflatable Spacecraft*. Atlanta, American Institute of Aeronautics and Astronautics.

Del Cueto Ruiz-Funes, J. I., López, A. & Mendoza Ramos, M., 2024. *Restoration and repair of Félix Candela's most celebrated shell: 'Los Manantiales' Restaurant*. Zurich, International Association for Shell and Spatial Structures (IASS).

Denisov, D. et al., 2011. Assessment of the radiation environment on the Moon. *Acta Astronautica,* 68(9–10), p. 1440–1447.

Di Feo, M., 2016. *Automi, realtà virtuale e formiche: Un'analisi della complessità del fenomeno bellico spaziale*. Florence: Firenze University Press.

Dobynde, M. I. & Guo, J., 2021. Radiation Environment at the Surface and Subsurface of the Moon: Model Development and Validation. *Journal of Geophysical Research: Planets,* Volume 126, pp. 1-12.

Dribi, Y. & Ounoughi, N., 2024. Enhancing Shielding Efficiency against Galactic Cosmic Radiation: Secondary Neutron Optimization. *Research Square,* pp. 1-20.

ESA, 2019. *In-Situ Resource Utilisation*. [Online]
Available at:
https://www.esa.int/Science_Exploration/Human_and_Robotic_Exploration/Exploration/In-Situ_Resource_Utilisation
[Accessed 05 May 2026].

ESA, 2020. *Moon Village: Conceptual Design of a Lunar Habitat,* Noordwijk: European Space Agency, Concurrent Design Facility.

Fallacara, G. et al., 2024. Reinterpretation of catenary vaulted spaces: Construction of a prototype and structural evaluation through Multibody Rope Approach. *Structures,* Volume 66, pp. 1-10.

Farrell, W. M. et al., 2023. The Dust, Atmosphere, and Plasma at the Moon. *Reviews in Mineralogy and Geochemistry,* 89(1), p. 563–609.

Farshad, M., 1992. *Design and Analysis of Shell Structures.* Dordrecht: Kluwer Academic Publishers.

Finch, S., Samuel, A. & Lane, G. P., 2023. *Lockhart and Wiseman' s Crop Husbandry Including Grassland*. X éd. s.l.:Woodhead Publishing.

Forster, B. & Mollaert, M., 2004. *The European Design Guide for Tensile Surface Structures.* Brussels: TensiNet.

Foster + Partners, n.d. *Great Court at the British Museum.* [Online]
Available at: https://www.fosterandpartners.com/projects/great-court-at-the-british-museum
[Accessed 7 April 2026].

Gaddis, L. R. et al., 2003. Compositional analyses of lunar pyroclastic deposits. *Icarus,* 161(2), p. 262–280.

Gasparini, A. & Wasser, M., 2026. *Water & Ices on the Moon.* [Online]
Available at: https://science.nasa.gov/moon/moon-water-and-ices/
[Accessed 24 May 2026].

Golański, M., 2023. Analogue and Computational Form-Finding Techniques in Shell Structures Design. *Architecturae et Artibus,* 15(4), pp. 9-18.

Gollins, N. et al., 2021. *First Steps Towards a Moon Village: Assessing the Feasibility of a Small Modular Lunar Habitat.* St Petersburg, International Astronautical Federation.

Gorkavyi, N., 2023. Origin of the Moon and Lunar Water. *Earth and Planetary Science,* 2(2), p. 86–99.

Gruber, P., 2011. *Biomimetics in architecture: Architecture of life and buildings.* s.l.:Springer-Verlag.

Haber, R. B. & Abel, J. F., 1982. Initial equilibrium solution methods for cable reinforced membranes. Part I-Formulations. *Computer Methods in Applied Mechanics and Engineering,* Volume 30, pp. 263-284.

Hamant, O. et al., 2008. Developmental patterning by mechanical signals in Arabidopsis. *Science.*

Hashemi Farzaneh, H. & Lindemann, U., 2019. *A practical guide to bio-inspired design*. s.l.:Springer Vieweg.

Häuplik-Meusburger, S., 2011. *Architecture for Astronauts: An Activity-based Approach*. I ed. s.l.:Springer.

Häuplik-Meusburger, S. & Bannova, O., 2016. *Space Architecture Education for Engineers and Architects: Designing and Planning Beyond Earth*. Cham: Springer International Publishing Switzerland.

Hauri, E. H., Saal, A. E., Rutherford, M. J. & Van Orman, J. A., 2015. Water in the Moon's interior: Truth and consequences. *Earth and Planetary Science Letters,* Volume 409, p. 252–264.

Hayne, P. O. et al., 2015. Evidence for exposed water ice in the Moon's south polar regions from Lunar Reconnaissance Orbiter ultraviolet albedo and temperature measurements. *Icarus,* Volume 255, p. 58–69.

Heiken, G. H., Vaniman, D. T. & French, B. M., 1991. *Lunar Sourcebook: A User's Guide to the Moon.* Cambridge: Cambridge University Press.

Heim, M., Römer, L. & Scheibel, T., 2010. Hierarchical structures made of proteins. The complex architecture of spider webs and their constituent silk proteins. *Chemical Society Reviews,* 39(1), p. 156–164.

Higgott, G., 2026. *Designs for the Dome, c. 1685–1710*. [Online]
Available at: https://www.stpauls.co.uk/5-designs-for-dome-c-1685-1710
[Accessed May 2026].

Huerta, S., 2006. Structural Design in the Work of Gaudi. *Architectural Science Review,* 49(4), pp. 324-339.

Ingold, L., 2021. The model as a concept: the origins of the design methods of Sergio Musmeci. In: B. Addis, ed. *Physical Models: Their Historical and Current Use in Civil and Building Engineering Design*. Berlin: Ernst & Sohn Verlag GmbH & Co. KG, p. 587–611.

International Commission on Radiological Protection, 1991. 1990 Recommendations of the International Commission on Radiological Protection. *Annals of the ICRP,* 21(1-3), pp. 1-211.

Isler, H., 1980. *Structural beauty of shells*. Wien, IABSE.

Isler, H., 1993. Generating shell shapes by physical experiments. *Journal of the International Association for Shell and Spatial Structures,* 34(1), pp. 53-63.

Isolan, L., Sumini, V. & Sumini, M., 2024. Monte Carlo analysis of dosimetric issues in space exploration. *Radiation Physics and Chemistry,* Volume 221, pp. 1-14.

Jaumann, R. et al., 2012. Geology, geochemistry, and geophysics of the Moon: Status of current understanding. *Planetary and Space Science,* 74(1), pp. 15-41.

Johnson, R. D. & Holbrow, C., 1977. *Space Settlements: A Design Study.* Washington, D.C.: National Aeronautics and Space Administration, Scientific and Technical Information Office.

Kalapodis, N., Kampas, G. & Ktenidou, O.-J., 2020. A review towards the design of extraterrestrial structures: From regolith to human outposts. *Acta Astronautica,* Volume 175, p. 540–569.

Kanahama, T., Tsugawa, S. & Sato, M., 2023. Rigidity control mechanism by turgor pressure in plants. *Scientific Reports*.

Kennedy, K., 2009. Vernacular of Space Architecture. In: S. A. Howe & B. Sherwood, eds. *Out of This World: The New Field of Space Architecture.* Reston, Virginia: American Institute of Aeronautics and Astronautics, Inc., pp. 7-21.

Kennedy, K. J., 2023. *Kriss J. Kennedy: Architect | Space Architect*. s.l.:s.n.

Kessler, P. & Johnson, J. E., 2024. *Evolution to Sustainable Lunar Habitation – Fall 2024 Project,* s.l.: NASA Strategy and Architecture Office, Lunar Architecture Team.

Knippers, J., Nickel, K. G. & Speck, T., 2016. *Biomimetic research for architecture and building construction: Biological design and integrative structures.* s.l.:Springer International Publishing.

Kutschera, U. & Niklas, K. J., 2007. The epidermal-growth-control theory of stem elongation: An old and a new perspective. *Journal of Plant Physiology*.

Laboratorio Pier Luigi Nervi, n.d. *Salone B, Palazzo di Torino Esposizioni, Torino, 1947-1954*. [Online]
Available at: https://www.laboratorionervi.polimi.it/portfolio/salone-b-palazzo-di-torino-esposizioni-torino-1947-1954/
[Accessed 6 April 2026].

Lee, S. & Oh, M.-M., 2025. Electrocultivation of Arabidopsis thaliana increases water and mineral absorption, electric charge and auxin accumulation, enhancing growth and development. *Bioelectrochemistry,* Volume 163, p. 1–11.

Lewis, W. J., 2003. *Tension Structures: Form and Behaviour.* London: Thomas Telford.

Liddell, I., 2015. Frei Otto and the development of gridshells. *Case Studies in Structural Engineering,* Volume 4, pp. 39-49.

Linkwitz, K., 1999. About formfinding of double-curved structures. *Engineering Structures,* 21(8), pp. 709-718.

Lin, S., Wang, X. & Chen, N., 2025. Direct solar radiation distribution and driving mechanisms on planetary surfaces – Moon, Mars, Ceres, and Mercury. *Icarus,* Volume 429, pp. 1-14.

Li, S. & Milliken, R. E., 2014. *Quantitative Mapping of Hydration in Lunar Pyroclastic Deposits: Insights into Water from the Lunar Interior.* Woodlands, Texas, USA, Lunar and Planetary Institute.

Liu, L.-g., 2022. Water on/in Mars and the Moon. *Terrestrial, Atmospheric and Oceanic Sciences,* Volume 33, pp. 1-6.

Loff, S. A., 2015. *Apollo 11 Mission Overview.* [Online]
Available at: https://www.nasa.gov/history/apollo-11-mission-overview/
[Accessed May 2026].

Long-Fox, J. M. & Britt, D. T., 2023. Characterization of Planetary Regolith Simulants for the Research and Development of Space Resource Technologies. *Frontiers in Space Technologies,* Volume 4, pp. 1-16.

Long-Fox, J. M. et al., 2023. Geomechanical Properties of Lunar Regolith Simulants LHS-1 and LMS-1. *Advances in Space Research,* 71(12), pp. 5400-5412.

Luzuriaga, M., 2021. *Replicating Candela's Los Manantiales.* Lisbon, CRC Press, pp. 382-391.

Manuello Bertetto, A., Gabriele, S., Marmo, F. & Micheletti, A., 2020. Shell and spatial structures: Between new developments and historical aspects. *Curved and Layered Structures,* Volume 7, p. 186–187.

Manuello Bertetto, A., Melchiorre, J. & Marano, G. C., 2024a. Improved multi-body rope approach for free-form gridshell structures using equal-length element strategy. *Automation in Construction,* Volume 161, pp. 1-24.

Manuello Bertetto, A., Melchiorre, J. & Marano, G. C., 2024b. *Improved Multibody Rope Approach for Free-Form Gridshells Shape and Construction*. Zurich, Switzerland, International Association for Shell and Spatial Structures (IASS).

Manuello, A., 2020. Multi-body rope approach for grid shells: Form-finding and imperfection sensitivity. *Engineering Structures,* Volume 221, p. 111029.

Mattheck, C., 1990. Why They Grow, How They Grow: The Mechanics of Trees. *Arboricultural Journal,* 14(1), pp. 1-17.

Meinke, D. W. et al., 1998. Arabidopsis thaliana: A model plant for genome analysis. *Science.*

Melchiorre, J., Manuello Bertetto, A., Adriaenssens, S. & Marano, G. C., 2025. Form-finding and metaheuristic multiobjective optimization methodology for sustainable gridshells with reduced construction complexity and waste. *Automation in Construction,* Volume 177, pp. 1-19.

Meyers, M. . A. & Chawla, K. K., 2008. *Mechanical behavior of materials*. II éd. s.l.:Cambridge University Press.

Meyers, M. A. et al., 2011. Biological materials: A materials science approach. *Journal of the Mechanical Behavior of Biomedical Materials,* 4(5), p. 626–657.

Meyers, M. A. et al., 2006. Structural biological composites: An overview. *JOM,* 58(7), pp. 35-41.

Milošević, V., Igić, T. & Kostić, D., 2013. Tensile Structures as the Most Advanced Lightweight Structures. *Facta Universitatis, Series: Architecture and Civil Engineering,* 11(3), pp. 269-284.

Miyashima, S., Sebastian, J., Lee, J.-Y. & Helariutta, Y., 2013. Stem cell function during plant vascular development. *The EMBO Journal*.

Monjo-Carrió, J. & Tejera, J., 2011. The use of textile materials for architectural membrane. In: R. Fangueiro, ed. *Fibrous and Composite Materials for Civil Engineering Applications.* Cambridge: Woodhead Publishing, pp. 325-387.

Mora, C. et al., 2011. How many species are there on Earth and in the ocean?. *PLoS Biology*.

Musmeci, S., 1971. *La statica e le strutture.* I ed. Rome: Cremonese.

NASA OCHMO, 2025. *Design for Ionizing Radiation Protection,* s.l.: National Aeronautics and Space Administration (NASA).

NASA, 2009a. *Apollo 12: The Pinpoint Mission*. [Online]
Available at: https://www.nasa.gov/missions/apollo/apollo-12-the-pinpoint-mission/
[Accessed May 2026].

NASA, 2009b. *Apollo 14: Mission Details.* [Online]
Available at: https://www.nasa.gov/missions/apollo/apollo-14-mission-details/
[Accessed May 2026].

NASA, 2009c. *Apollo 15: Mission Details.* [Online]
Available at: https://www.nasa.gov/missions/apollo/apollo-15-mission-details/
[Accessed May 2026].

NASA, 2011. *Apollo 17: Mission Details.* [Online]
Available at: https://www.nasa.gov/missions/apollo/apollo-17-mission-details/
[Accessed May 2026].

NASA, 2023a. *Clementine.* [Online]
Available at: https://science.nasa.gov/mission/clementine/
[Accessed May 2026].

NASA, 2023b. *CRaTER: Exploring Space Radiation at the Moon,* s.l.: National Aeronautics and Space Administration.

NASA, 2023c. *Overview: In-Situ Resource Utilization*. [Online]
Available at: https://www.nasa.gov/overview-in-situ-resource-utilization/
[Accessed 05 May 2026].

NASA, 2024a. *LCROSS.* [Online]
Available at: https://science.nasa.gov/mission/lcross/
[Accessed May 2026].

NASA, 2024b. *GRAIL (Ebb and Flow)*. [Online]
Available at: https://science.nasa.gov/mission/grail/
[Accessed May 2026].

NASA, 2025. *Moon to Mars Architecture Definition Document,* s.l.: National Aeronautics and Space Administration.

NASA, 2026a. *Moon Exploration*. [Online]
Available at: https://science.nasa.gov/moon/exploration/
[Accessed May 2026].

NASA, 2026b. *The Apollo Program*. [Online]
Available at: https://www.nasa.gov/the-apollo-program/
[Accessed May 2026].

NASA, 2026c. *Lunar Prospector*. [Online]
Available at: https://science.nasa.gov/mission/lunar-prospector/
[Accessed May 2026].

NASA, 2026d. *Lunar Reconnaissance Orbiter*. [Online]
Available at: https://science.nasa.gov/mission/lro/
[Accessed May 2026].

NASA, 2026e. *THEMIS-ARTEMIS*. [Online]
Available at: https://science.nasa.gov/mission/themis-artemis/
[Accessed May 2026].

NASA, 2026f. *Artemis I*. [Online]
Available at: https://www.nasa.gov/mission/artemis-i/
[Accessed May 2026].

NASA, 2026g. *Artemis III*. [Online]
Available at: https://www.nasa.gov/mission/artemis-iii/
[Accessed May 2026].

NASA, 2026h. *Artemis IV*. [Online]
Available at: https://www.nasa.gov/mission/artemis-iv/
[Accessed May 2026].

Neinhuis, C. & Barthlott, W., 1997. Characterization and distribution of water-repellent, self-cleaning plant surfaces. *Annals of Botany*.

Neri, G., 2014. *Capolavori in miniatura. Pier Luigi Nervi e la modellazione strutturale*. Mendrisio: Mendrisio Academy Press / Silvana Editoriale.

Niklas, K. J. & Spatz, H.-C., 2012. *Plant physics*. s.l.:University of Chicago Press.

Nir, S. & Reches, M., 2016. Bio-inspired antifouling approaches: the quest towards non-toxic and non-biocidal materials. *Current Opinion in Biotechnology,* Volume 39, p. 48–55.

Otto, F., 1984. Die Forschungsgruppe Biologie und Bauen. In: B. Burkhardt & H. Klotz, eds. *Schriften und Reden: 1951–1983*. Braunschweig/Wiesbaden: Friedr. Vieweg & Sohn, pp. 170-174.

Parkinson, A. E. et al., 2023. Detecting and characterizing the abundance and form of water-ice in permanently-shadowed regions of the Moon using a three-band lidar system. *Icarus,* Volume 400, pp. 1-27.

Pastrana Jimenez, A. R., 2026. *Differentiable form-finding for structural design*. Princeton: Princeton University.

Pataranutaporn, P. et al., 2021. *SpaceCHI: Designing Human-Computer Interaction Systems for Space Exploration*. New York, NY, USA, Association for Computing Machinery / ACM.

Petrova, M. N. & Zheleva-Martins Viana, D., 2022. Shells as a Universal Structural Type in Nature and Design. In: M. Noguchi, ed. *Prefabricated Construction for Sustainability and Mass Customization*. London: IntechOpen, pp. 1-23.

Petrov, G. I. et al., 2019. *Moon Village Reference Masterplan and Habitat Design*. Boston, Massachusetts, USA, Skidmore, Owings & Merrill LLP.

Preston, R. D., 1974. *Aspects of the cell wall: The physical biology of plant cell walls*. s.l.:Chapman and Hall.

Primrose, S. B., 2020. *Biomimetics: Nature-inspired design and innovation*. s.l.:Wiley-Blackwell.

Quinn, G. et al., 2016. *Calibrated and Interactive Modelling of Form-Active Hybrid Structures*. Tokyo, International Association for Shell and Spatial Structures (IASS).

Ranalli, G., Zanardini, E. & Sorlini, C., 2009. Biodeterioration – Including Cultural Heritage. In: M. Schaechter, ed. *Encyclopedia of Microbiology.* Oxford, UK: Academic Press, p. 191–205.

Reiss, P., 2024. Exploring the lunar water cycle. *Proceedings of the National Academy of Sciences,* 121(52), pp. 1-9.

Reitz, G., Berger, T. & Matthiae, D., 2012. Radiation exposure in the moon environment. *Planetary and Space Science,* Volume 74, p. 78–83.

Renzulli, L. et al., 2024. *COSMICA Project: Advancing astronaut survival and well-being through Microalgae-Based Design*. Milan, Italy, International Astronautical Congress (IAC).

Ripley, R. L. & Bhushan, B., 2016. Bioarchitecture: Bioinspired art and architecture—a perspective. *Philosophical Transactions of the Royal Society A: Mathematical, Physical and Engineering Sciences*.

Rizzo, A. et al., 2023. Foundations of radiological protection in space: The integrated multidisciplinary approach for next manned missions in deep space. *The European Physical Journal Plus,* Volume 138, pp. 1-12.

Sah, D., 2025. *The History of Space Exploration from ancient understanding to modern era,* s.l.: St. Xavier's College, Maitighar – Department of Physics.

Sanket G, . P., Milind R, N. & Vaibhav. A., K., 2022. A Review Paper on Behavior of Gridshell Structure. *International Research Journal of Engineering and Technology (IRJET),* 9(4), p. 1042–1044.

Schatten, H., 2013. Mitosis. In: S. Maloy & K. Hughes, eds. *Brenner's Encyclopedia of Genetics*. San Diego, USA: Academic Press, p. 448–451.

Shafi, A., Mir, M. A. & Zahoor, I., 2017. Understanding the anatomical organisation of Arabidopsis thaliana using scanning electron, confocal and bright field microscopy. *International Journal for Science and Advance Research in Technology (IJSART)*.

Sherwood, B., 2009. What is space architecture?. In: S. A. Howe & B. Sherwood, eds. *Out of this world: the new field of space architecture.* Reston, Virginia: American Institute of Aeronautics and Astronautics, Inc., pp. 3-6.

Shunk, G. K., Gomez, X. R. & Averesch, N. J. H., 2021. A Self-Replicating Radiation-Shield for Human Deep-Space Exploration: Radiotrophic Fungi can Attenuate Ionizing Radiation aboard the International Space Station. *bioRxiv,* pp. 1-16.

Simonsen, L. C. & Slaba, T. C., 2025. *Galactic Cosmic Radiation Shielding: Science on the Lunar Surface,* s.l.: National Aeronautics and Space Administration.

Sossi, P. A., Nakajima, M. & Khan, A., 2025. Composition, Structure and Origin of the Moon. In: *Treatise on Geochemistry.* s.l.:Elsevier, p. 417–479.

Spatz, H., Köhler, L. & Niklas, K. J., 1999. Mechanical behaviour of plant tissues: Composite materials or structures?. *The Journal of Experimental Biology*.

Steinar Hillersøy, D., Bendik, M. & Anders, R., 2021. Gridshells in Recent Research—A Systematic Mapping Study. *Applied Sciences,* 11(24), p. 11731.

Stern, S. A., 1999. The lunar atmosphere: History, status, current problems, and context. *Reviews of Geophysics,* 37(4), p. 453–491.

Sumini, V. & Mueller, C. T., 2017. Structural Challenges for Space Architecture. *STRUCTURE magazine,* 24(12), pp. 42-45.

Sumini, V. et al., 2018. *Multiobjective Optimization for Structural Design of Lunar Habitats*. Cleveland, Ohio, USA, American Society of Civil Engineers / ASCE.

Sun, J., Bhushan, B. & Tong, J., 2013. Structural coloration in nature. *RSC Advances*.

Swenson, A., 2026. *Roman achievements*. [Online]
Available at: https://www.britannica.com/technology/construction/Roman-achievements
[Accessed 6 April 2026].

Tak Lee, S., 1962. *The Buckling Load of Hyperbolic Paraboloid Shells*. Cambridge: s.n.

Tero, A. et al., 2010. Rules for Biologically Inspired Adaptive Network Design. *Science,* 327(5964), p. 439–442.

Thompson, D. W., 1917. *On Growth and Form*. I ed. Cambridge: Cambridge University Press.

Tiu, J., Belli, R. & Lohbauer, U., 2023. A step toward bio-inspired dental composites. *Biomaterial Investigations in Dentistry,* 10(1), pp. 1-7.

Torroja, E., 1958. *Las estructuras de Eduardo Torroja*. I ed. New York: F.W. Dodge Corporation.

Treccani, n.d. *Brassicacee*. [Online]
Available at: https://www.treccani.it/enciclopedia/brassicacee/
[Accessed March 2026].

Treccani, n.d. *Librazione*. [Online]
Available at: https://www.treccani.it/enciclopedia/librazione/
[Accessed March 2026].

Uri, J., 2022. *Apollo 16 Launches to the Moon*. [Online]
Available at: https://www.nasa.gov/history/apollo-16-launches-to-the-moon/
[Accessed May 2026].

Veenendaal, D. & Block, P., 2012. An overview and comparison of structural form finding methods for general networks. *International Journal of Solids and Structures,* Volume 49, p. 3741–3753.

Vidmachenko, A. P., 2026b. Physical characteristics and relief of the surface of the Moon. In: *Features of volcanic activity on the Moon*. Boston, USA: Primedia eLaunch, pp. 29-49.

Vidmachenko, A. P., 2026. General characteristics of the Moon and features of its internal structure. In: *Features of volcanic activity on the Moon*. Boston, USA: Primedia eLaunch, pp. 9-28.

Vidya Vijay, K. P., Pooja, S. M. & Shivakumar, G. S., 2023. Exploring the Design, Analysis, and Applications of Shell Structures. *International Journal of Engineering Research & Technology (IJERT),* 12(11).

Vock, A. L., 2025. *Additive Manufacturing for Lunar Settlements: Challenges, Applications, and Future Design Prospects,* Milan: Politecnico di Milano.

Vogel, T., 2026b. *Moon Composition & Structure*. [Online]
Available at: https://science.nasa.gov/moon/composition/
[Accessed 24 May 2026].

Vogel, T., 2026. *Moon Formation*. [Online]
Available at: https://science.nasa.gov/moon/formation/
[Accessed May 2026].

Wallner, E.-S., 2018. *Early events in phloem formation: Exploring the molecular network of SMXL3/4/5,* Heidelberg, Germany: Ruprecht-Karls-Universität Heidelberg.

Wang, H. et al., 2026. Revealing lunar regolith evolution through nanoscale morphological features. *Geoscience Frontiers,* Issue 102310.

Warner, C., 2026. *NASA Strengthens Artemis: Adds Mission, Refines Overall Architecture*. [Online]
Available at: https://www.nasa.gov/directorates/esdmd/nasa-strengthens-artemis-adds-mission-refines-overall-architecture/
[Accessed May 2026].

Weber, C., 2021. Physical modelling at the University of Stuttgart. In: B. Addis, ed. *Physical Models: Their historical and current use in civil and building engineering design*. Berlin: Ernst & Sohn Verlag GmbH & Co. KG, pp. 415-439.

Williams, C. J. K., 2001. *The analytic and numerical definition of the geometry of the British Museum Great Court Roof.* Geelong, Deakin University.

Wösten, H. A. B., Krijgsheld, P., Montalti, M. & Läkk, H., 2018. *Growing Fungi Structures in Space,* Noordwijk, The Netherlands: European Space Agency, Advanced Concepts Team.

Yashar, M. et al., 2019. *Robotic Construction & Prototyping of a 3D-Printed Mars Surface Habitat*. Washington D.C., USA, International Astronautical Federation (IAF).

Zhang, H. et al., 2024. Heterogeneity in mechanical properties of plant cell walls. *Plants*.

Zhang, P. et al., 2023. Overview of the Lunar In Situ Resource Utilization Techniques for Future Lunar Missions. *Space: Science & Technology,* Volume 3, pp. 1-18.

Zhang, S. et al., 2020. First Measurements of the Radiation Dose on the Lunar Surface. *Science Advances,* Volume 6, pp. 1-5.

Zhao, X.-L., Wilkinson, T. J. & Hancock, G. J., 2005. Members Subjected to Compression. In: *Cold-Formed Tubular Members and Connections: Structural Behaviour and Design*. Kidlington, UK: Elsevier, p. 67–89.